INTERACTION OF PALMATINE WITH DNA BY SPECTROSCOPIC AND MOLECULAR MODELING TECHNIQUES

A THESIS

Submitted in partial fulfilment of the requirements for the award of the degree of

DOCTOR OF PHILOSOPHY

in

BIOTECHNOLOGY

by

KUSHUMA BISHT

DEPARTMENT OF BIOTECHNOLOGY
INDIAN INSTITUTE OF TECHNOLOGY ROORKEE
ROORKEE - 247 667 (INDIA)

JULY, 2009

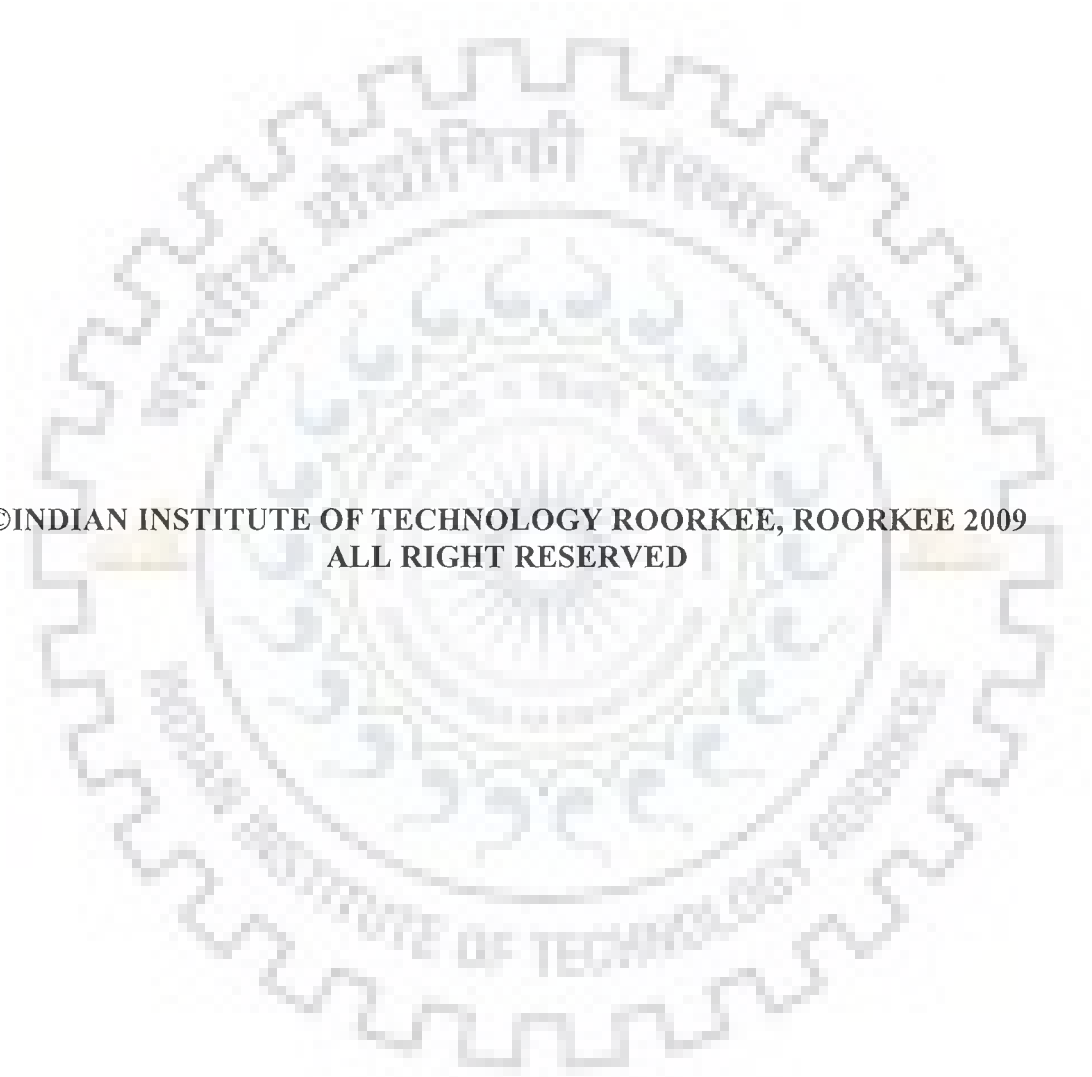

INDIAN INSTITUTE OF TECHNOLOGY ROORKEE
ROORKEE

CANDIDATE'S DECLARATION

I hereby certify that the work which is being presented in the thesis entitled **INTERACTION OF PALMATINE WITH DNA BY SPECTROSCOPIC AND MOLECULAR MODELING TECHNIQUES** in partial fulfilment of the requirements for the award of the Degree of Doctor of Philosophy and submitted in the Department of Biotechnology of the Indian Institute of Technology Roorkee, Roorkee is an authentic record of my own work carried out during a period from July 2004 to July 2009 under the supervision of Prof. Ritu Barthwal, Professor & Head, Department of Biotechnology, Indian Institute of Technology Roorkee, Roorkee, India.

The matter embodied in this thesis has not been submitted by me for the award of any other degree of this or any other Institute.

Kushuma Bisht

(KUSHUMA BISHT)

This is to certify that the above statement made by the candidate is correct to the best of my knowledge.

Ritu Barthwal

(Ritu Barthwal)
Supervisor

Date: 31/07/09

The Ph.D. Viva-Voce examination of **Ms. Kushuma Bisht**, Research Scholar, has been held on .....

Signature of Supervisor

Signature of External Examiner

ACKNOWLEDGEMENT

Today when I am intended to attain another milestone of my life in the form of this thesis, it will be simple to name all those people that helped me to get this done, but it will be tough to thank them appropriately. I would like to thank God for blessing me the company of such nice people around me.

First and foremost, I would like to record my sincere gratitude to my supervisor, Prof. Ritu Barthwal for her inspiring guidance, valuable suggestions, constant motivation and timely discussions from the very early stage of this research. This thesis grew out of a series of dialogue only because of her, who shared with me a lot of her expertise and research insight. I am very much gratified to her for developing the scientific temperament in me and providing me a healthy, professional and free working atmosphere as a result, research life became smooth and rewarding for me.

I am grateful to Dr.A.N.Tripathi for taking intense interest in this study as well as providing his valuable suggestion.

I would also like to acknowledge my labmates, Amit, Lata, Asif, Dr. Maya and Dr. Sulaxana for their cooperation and pleasant company in the lab. Special thanks to Lata for helping me to submit in time. I wish her a bright and joyful life. At this moment I would like to thanks Amit for sharing all my doubts and provided strength and courage in moments of despair.

No words and no language is ever adequate to express my heart felt admiration for my respected parents Mr. Trilok Singh Bisht and Mrs. Devki Devi who have always supported, encouraged and believed in me, in my all endeavors. They gently offered unconditional love, support and strength at each turn of the road. Particular thanks to my loving sisters Janki and Ushu and my brother Dinesh for their affection and moral boost-up whenever needed. They made me felt cheerful and joyful with their smile and humor during hectic and difficult hours. I am grateful to my in-laws whose faith on me has always inspired me in this venture

This thesis would have been a distant dream without care and support of my husband Sandeep Negi. He has been a pillar of support during the stressful periods, a great listener and has always been available for me. His enduring support at each bend and turn and wonderful sense of humor helped me to see the positive sides of even the most difficult moments.

"Friends are god's way of taking care of us" it's true because of my special friends, Ms. Priya Kapur and Mrs. Priyanka lal. Things wouldn't have been the same without them. I am thanking both for the good times, days filled with pleasure, fond

memories and the feelings that I will always treasure. I thank god for blessing me the company of wonderful friends like them.

Special thanks are due to my friends Mrs. Sreela Dey, Mrs Santosh Kaushik, Ms. Anjali Sardana, Ms. Pallavi Dwivedi, Mrs. Deepti Kushal Singh, Mrs. Dhanpati Rana, Mrs. Prerana Gupta, Jyoti shah and Mrs. Shilpa Pal who made my Roorkee days fun, colorful and unforgettable. I am grateful for all the emotional support, comraderie, and entertainment and caring they provided.

And to the rest, I extremely thankful to those people, whose names have been unknowingly left, thank you very much for your prayers. It really helped a lot. I apologize and believe, they will be always with me as they were there in the time of need.

Last but not the least; I would like to thank Council of Scientific & Industrial Research (CSIR) for providing financial support for my research work.

(Kushuma bisht)

Abstract

Palmatine belongs to the class of quaternary protoberberine alkaloid that has been utilized in Ayurvedic and Chinese traditional medicines since long time. It is found in the roots, rhizomes and stem bark of many species of berberidaceae, fumaraceae, menispermacea and other plant families. It exhibits a wide range of pharmacological effects including antimicrobial, antimalarial, anti-inflammatory, antipyretic, hepatoprotective and vasodilatory activity. The cytotoxic activity of palmatine to HL-60 leukemic cells has also been well documented. Palmatine has been reported to be effective against experimental tumors by inhibiting the activity of reverse transcriptase and was also found to exert sedative effect by decreasing the levels of catecholamines in rat brains. It acts as photosensitizer by generating singlet oxygen.

The molecular basis for designing DNA binding drugs with improved specificity and affinity stems from the ability to identify the structural elements of the drug and DNA which are responsible for the specificity of the binding and the stabilization of the drug–DNA complex. An analytical technique to elucidate the mode of drug-DNA interaction could be essential for the design of new drugs. Nuclear Magnetic Resonance (NMR) spectroscopy, Absorption spectroscopy, Fluorescence Spectroscopy, and restrained Molecular Dynamics (rMD) are some of the analytical techniques which have been used in this study to investigate conformation of drug, DNA and drug-DNA complexes.

The Ph.D. thesis work has been reported in the form of six chapters.

Chapter 1 contains introduction of the subject, a comprehensive review of the literature and scope of thesis.

Chapter 2 deals with the materials and methods used. The detailed Nuclear Magnetic Resonance spectroscopy techniques used, that is, - 1D NMR, Double Quantum Filtered Correlation Spectroscopy (DQF-COSY), ^{1}H - ^{1}H Nuclear Overhauser Enhancement Spectroscopy (NOESY) for the proton assignment; ^{1}H - ^{31}P Heteronuclear Multiple Bond Correlation Spectroscopy (HMBC), ^{31}P - ^{31}P NOESY and Diffusion Ordered Spectroscopy (DOSY) studies are discussed. The strategies used for restrained energy minimization, restrained Molecular Dynamics (rMD) simulations and quantum mechanical calculations involving GIAO method (for chemical shift calculation) and DFT method (for optimization) are discussed. Absorption and Fluorescence spectroscopy and Time-Correlated Single-Photon Counting methods (TCSPC) used to investigate drug-DNA interaction are also discussed.

Chapter 3 deals with the structural and electronic properties of palmatine using density functional theory (DFT) employing B3LYP exchange correlation. The geometries of these molecules have been fully optimized at B3LYP/6-311G** level. The chemical shift of ^{1}H and ^{13}C resonances phase Nuclear Magnetic Resonance (NMR) spectra of these molecules have been calculated in gaseous and solvent phase using the Gauge–invariant atomic model (GIAO) method as implemented in Gaussian 98 and 03. A restrained Molecular Dynamics approach was used to obtain the optimized solution structure of the drug. Comparison of the calculated NMR chemical shifts with the experimental values revealed that DFT methods produce good results for both proton and carbon chemical shifts. The importance of the basis sets with

solvent effect to the calculated NMR parameters has been discussed. It has been found that calculated structure and chemical shifts in solvent phase predicted with B3LYP/6-311G** were in good agreement with the present experimental data and measured values reported earlier.

Chapter 4 deals with the study of palmatine interaction with DNA using Absorption and Fluorescence spectroscopic techniques. Several DNA and oligonucleotides were used in this study to elucidate the sequence binding affinity of these drugs. Titration of these drugs with increasing amount of DNA showed that palmatine binds more effectively to AT rich sequences then to GC rich sequences Percentage hypochromicity, binding constant, extinction coefficient of bound palmatine, fluorescence-enhancement and relative fluorescence obtained from absorption and fluorescence spectroscopy were used to study the binding affinity.

Chapter 5 deals with ^{31}P, ^{1}H NMR and rMD studies on binding of palmatine with DNA sequence d–$(CGATCG)_2$. The following experiments were performed on the palmatine-DNA complex - ^{1}H and ^{31}P NMR titration studies at various drug (D)/DNA duplex (N) ratios up to 2.0 at 283 K, 298 K in 90% H_2O and 10% D_2O, temperature dependence of ^{31}P and ^{1}H NMR of the palmatine-DNA complex having D/N = 1.0 and 2.0 in the range of 278 - 328 K; 2D ^{31}P - ^{31}P exchange spectra of drug-DNA complex by phase sensitive NOESY; DOSY experiments of the palmatine-DNA complex and uncomplexed palmatine, rMD studies on the solution structure of palmatine - d-$(CGATCG)_2$ complex using inter-proton distance restraints obtained from 2D NOESY. Results revealed that the addition of palmatine to the oligonucleotide did not induce significant chemical shift variation of the phosphate signals in the ^{31}P NMR spectra. Absence of large downfield shift in ^{31}P NMR spectra

suggest that there is no characteristic unwinding of the DNA helix due to change in backbone torsional angle ζ , C3'–O3'–P–O5' from gauche⁻ to trans as observed with intercalators. Since, only one set of resonances are observed for the complexes at different D/N ratios for free hexamer and hexamer bound to palmatine, it is expected that ^{31}P signals from the bound DNA are in fast exchange with the corresponding signals from free DNA to be followed individually on NMR time scale. The proton resonances of palmatine were broad even at low values of drug/DNA (D/N = 0.2) and move upfield with respect to the free drug. An upfield shift of ~0.09-0.31 ppm was found for the drugs protons on binding with DNA up to D/N ratio of 2.0. Maximum upfield shift in the drug protons was found to be for H24 and H28. Thermal melting of imino shows that the drug is stabilizing the DNA. The thermal melting temperature of the palmatine-hexamer was found to be 298 ± 2 K which is 5 K higher than that observed for uncomplexed d-$(CGATCG)_2$. The presence of all sequential NOE connectivities in the NOESY spectra at D/N = 2.0, as expected in standard B–DNA geometry confirmed that the DNA duplex is intact with apparently no opening of base pairs to accommodate drug chromophore as generally observed on intercalation. 2D NOESY experiment allowed the detection of several contacts between the protons of palmatine molecule and those of the double helix, specifically with protons of the CG base pairs at the terminal end. The drug protons H(36,37, 38), H(41,42,43) and H(46,47,48) shows intermolecular contacts with G6H1', C1H1' and C1H6 of the hexamer d-$(CGATCG)_2$. H(36,37,38) and H(41,42,43) give close contacts with G6H8. Similarly, H10 proton show intermolecular peaks with C1H6 and C1H5. Zero intermolecular NOEs are found for imino residues and with protons of the central minor groove region of the hexamer. The result suggests that the drug is binding

externally to the hexamer sequence in a specific orientation which gives rise to the observed NOEs. In contrast to the previous NMR characterized minor groove complex, the resonances of DNA protons located outside the minor groove binding site appear perturbed. The analysis of DNA chemical shift perturbation induced by palmatine suggests that the extremity of the hexamer is the site of binding.

Chapter 6 summarizes the results obtained and their implications in understanding the molecular basis of action of palmatine.

CONTENTS

LIST OF PUBLICATIONS

Published in refereed international journal

A.N. Tripathi, **K. Bisht**, P.P.Thankanchan and R. Barthwal. Quantum chemical and Nuclear Magnetic Resonance spectral studies on molecular properties and electronic structure of palmatine. Journal of molecular structure, 878, 139-148, (2008)

To be communicated:

1. **Bisht K** and Barthwal R. Studies on the binding of palmatine to DNA by spectroscopic and fluorescence techniques.
2. **Bisht K** and Barthwal R. Structure determination of palmatine-d$(CGATCG)_2$ complex using phosphorus-31, proton Nuclear Magnetic Resonance and restrained molecular dynamics techniques
3. **Bisht K,** Saxena R and Barthwal R. Palmatine binding studies with promoter site sequence d-$(CCAATTGG)_2$ using Nuclear Magnetic Resonance and molecular modeling technique.

Papers in International/National Conference

1. Chauhan L, **Bisht K**, Barthwal S K, and Barthwal R (2005). NMR based solution structure of antitumor drug Berberine. *XXI International Conference on Magnetic Resonance in Biological Systems, Hyderabad, Andhra Pradesh, INDIA (XXIst ICMRBS-2005)* January 16 – 21

2. National Symposium on Biophysics: Trends in Biomedical Research IBS 2007, Department of NMR and MRI facility AIIMS, New Delhi India, 13-15 February 2007, entitled "Quantum chemical and nuclear magnetic resonance spectral studies on molecular properties and electronic structure of palmatine. : A.N. Tripathi, **Kushuma Bisht**, P.P. Thankanchan and Ritu Barthwal. (2007). pg no. 183 Abs. no.120.

3. **Bisht K**, and Barthwal R (2009). Interaction of protoberberine alkaloid palmatine with DNA by spectroscopic and molecular modeling techniques" 6th Asian biophysics Assocciation (ABA) Symposium, 27th Hong Kong society of neuroscience Annual meeting, at Hong Kong university of Science and technology, Hong Kong, January 11-15.

Chapter 1

Introduction

1.1 GENERAL

Transcription and replication are vital to cell survival and proliferation as well as for smooth functioning of all body processes. DNA starts transcribing or replicating only when it receives a signal, which is often in the form of a regulatory protein binding to a particular region of the DNA. Regulatory proteins that can repress or stimulate the flow of genetic information through DNA or RNA control the gene expression throughout a cell's lifetime. Small molecules can also alter the activities of nucleic acids, and regulate gene expression by disrupting protein-DNA interactions in vivo [Dervan, 1986]. In designing novel chemotherapeutic agents, one of the major strategies is to develop novel DNA binding ligands that influence crucial cellular processes such as DNA topology, replication, transcription, and DNA repair [Chaires, 1998; Panousis and Phillips, 1994]. Systematic modifications of clinically effective chemotherapeutic agents have the potential for positively influencing their activity and delivery. For these reasons, nucleic acids have been a primary target for binding or chemical modification by several classes of molecules. If the binding specificity and strength of this regulatory protein can be mimicked by a small molecule, then DNA function can be artificially modulated, inhibited or activated by binding this molecule instead of the protein. Thus, this synthetic/natural small molecule can act as a drug when activation or inhibition of DNA function is required to cure or control a disease. These molecules can be isolated from natural sources or synthetically

prepared. The chemical functionality of small molecules can be much more diverse than that found in proteins, and the structural simplicity of such molecules, combined with facile synthesis, has accelerated work directed toward understanding the relationships between molecular structure and DNA recognition [Dervan, 1986; White, 1998].

By investigating natural DNA binding molecules, we can expand our ability to probe DNA and develop new approaches for DNA-targeting chemotherapeutics. Structural tools such as X-ray crystallography and NMR spectroscopy, coupled with molecular modeling techniques and theoretical studies have considerable impact in advancing our understanding of the structural selectivity and the molecular basis for drug-DNA interactions and may also provide a key to more rational drug design

1.2 MODE OF ACTION OF ANTICANCER DRUGS

Drugs bind to DNA both covalently as well as non-covalently:

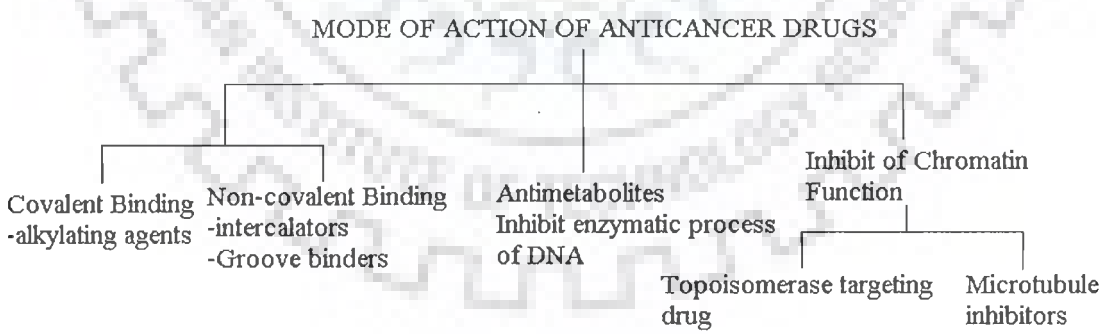

.

1.2.1 Covalent DNA binding Drugs

1.2.1.1 Polyfunctional alkylating agents

These drugs interfere with DNA function by chemically modifying specific nucleotides. There are two types of alkylating agents: mono–functional (one reactive group) which cause single–strand breaks in DNA or damage bases and bi–functional (two reactive groups) which form cross–links. A large number of first generations of anti– cancer drugs were designed to combine a simple alkylating function. Their common feature is that they form an initial physical complex with DNA before covalently bonding to it. Many of them have also shown selective anti–tumor activity, this can be attributed to DNA binding specificity or to preferential metabolic activation by tumour cells. The mechanism of action of these anticancer agents is by alkyl group transfer and they cause alkylation of DNA at N7 or N2 position of guanine (other sites as well) and interaction may involve single strands or both strands. Anthramycin is an anti–tumor antibiotic that binds covalently to N–2 of guanine located in the minor groove of DNA. It has a preference of purine–G–purine sequences with bonding to the middle G. Cisplatin is a transition metal complex cis–diamine–dichloro–platinum and clinically used as anticancer drug. The effect of the drug is due to the ability to platinate the N–7 of guanine on the major groove site of DNA double helix. This chemical modification of platinum atom, cross–links two adjacent guanines on the same DNA strands, interferes with the mobility of DNA polymerases Other interactions involve the reaction of these drugs with amino, hydroxyl and phosphate groups of other cellular constituents. These drugs usually form a reactive intermediate ethyleneimonium ion.

Poly functional alkylating drugs offer resistance against cancer by increased ability to repair DNA defects, decreased cellular permeability to the drug, increased

glutathione synthesis, which inactivates alkylating agents through conjugation reactions. Mitomycin C is a well characterized anti–tumor antibiotic, which forms a covalent interaction with DNA after enzymatic reductive activation of its quinone to alkylate DNA. The activated antibiotic forms a cross–linking structure between guanine bases on adjacent strands of DNA thereby inhibiting single strand formation which is essential for m–RNA transcription and DNA replication. Covalent binding in DNA is irreversible and invariably leads to complete inhibition of DNA processes and subsequent cell death.

1.2.2 Noncovalent DNA Binding Drugs

1.2.2.1 Groove binding molecules

The major and minor groove differs significantly in electrostatic potential, hydrogen bonding characteristics, steric effects and hydration. Typically minor groove binding molecules have several simple aromatic rings connected by bond with torsional freedom. This creates compounds, which with the appropriate twist, can fit into the helical curve of the minor groove with displacement of water from the groove and forming van der Waals contacts with the helical chains which define the walls of the groove. Additional specificity in the binding comes from contacts between the bound molecule and the edges of the base pairs on the 'floor' of the groove. Thus, the aromatic rings of many groove binding molecules form close contact with AH2 protons in the minor grooves of DNA. Pullman and coworkers have shown that the negative electrostatic potential is greater in the A.T minor groove than G.C rich regions, and this provides an additional important source for A.T specific minor groove binding of cations. Additionally, these drugs can form hydrogen bonds to bases, typically to N3 of adenine and O2 of thymine. Most minor groove binding

drugs bind to A/T rich sequences. This preference in addition to the designed propensity for the electronegative pockets of A.T sequences is probably due to better van der Waals contacts between the ligand and groove walls in this region, since A/T regions are narrower than G/C groove regions and also because of the steric hindrance in the latter, presented by the C2 amino group of the guanine base. Examples of minor groove binding drugs are netropsin and distamycin. However, a few synthetic polyamides like lexitropsins and imidazole-pyrrole polyamides have been designed which have specificity for G-C and C-G regions in the grooves.

1.2.2.2 Intercalators

Intercalators are drugs, usually with aromatic rings, that inserts between adjacent, stacked base pairs. In the early 1960, Lerman conducted a number of physical studies on the interaction of DNA with planar aromatic cations and concluded that planar aromatic molecules could bind to DNA by process, which he termed as intercalation. These are clinically useful anticancer antibiotics, which are primarily derived from *Streptomyces peucetius*. These antibiotics act by intercalating between base pairs of DNA causing lengthening of the double helix and a decrease in the helical twist on unwinding, inducing topoisomerse II mediated strand scission. These drugs prevents the religation of cleaved DNA thereby making the ternary complex stable either by increasing the rate of forward reaction i.e, more rate of DNA clevage or by decreasing the rate of backward reaction i.e, slow rate of religation. These structural modifications can lead to functional changes, often to the inhibition of transcription and replication and DNA repair processes, which makes intercalators potent mutagens.Thus synthesis of DNA and RNA is blocked. They also alter membrane fluidity and ion transport. One potential mechanism is based on the ability

of these agents to participate in electron-transfer processes, with the subsequent generation of free radicals. The first crystal structure with a monointercalator and oligonucleotide was obtained by Wang and co-workers [Wang et al, 1987] for a complex of antibiotic daunomycin and $d(CGTACG)_2$. Synthetic bisintercalators have two covalently linked intercalated ring systems with connecting chains of variable length. The synthesis of this multiple ring compounds was partially stimulated by the idea that the medicinal activity of intercalating drugs could be enhanced by the significantly higher DNA binding

1.2.3 Antimetabolites

1.2.3.1 Inhibit enzymatic process in nucleic acid synthesis

Purine antagonists like mercaptopurine (purinethol) act by hypoxanthine-guanine phosphoribosyl transferase (HGPRT) to form 6-thioinosinic acid, which inhibits enzymes involved in purine metabolism. Thioguanine acts as inhibitor of purine nucleotide pathway enzyme which decreases intracellular concentration of guanine nucleotides and inhibit glycoprotein synthesis, finally blocking DNA/RNA synthesis.

1.2.4 Inhibition of chromatin function

1.2.4.1 Topoisomerase targeting drugs

Chromosomal DNA is extensively twisted and topoisomerases permit selected regions of DNA to untangle so as to allow transcription and replication. These enzymes temporarily break DNA, allowing for topological changes, and then reseal the breaks. Topoisomerase targeting drugs like etoposide stabilizes the topoisomerase II–DNA complex preventing it from making a topological change. This results in an

irreversible double strand break, which is lethal to cells in S and G2 phases. Six anti–neoplastic drugs targeting topoisomerase II, i.e., doxorubicin, daunorubicin, idarubicin, mitoxantrone, etoposide and teniposide are currently approved for clinical use in the United States. Synthetic topoisomerase inhibitory analogs are also studied [Singh, et al., 1992].

DNA topoisomerase II is a ubiquitous enzyme that is essential for the survival of all eukaryotic organisms and plays critical roles in virtually every aspect of DNA metabolism. The enzyme unknots and untangles DNA by passing an intact helix through a transient double–stranded break that it generates in a separate helix. Beyond its physiological functions, topoisomerase II is the target for some of the most active and widely prescribed anticancer drugs currently utilized for the treatment of human cancers. DNA is an extremely important target for drug action, with a wide range of biological activities (anti-tumor, antiviral and antimicrobial) arising from the ability of compounds to bind sequence specifically to DNA and interfere with DNA topoisomerases or with transcription binding factor [Lancelot & Paquet, 2003]. These antibiotics act by intercalating between base pairs of DNA causing lengthening of the double helix and a decrease in the helical twist on unwinding, inducing mediated strand scission. These drugs act in an insidious fashion and kill cells by increasing levels of covalent topoisomerase II–cleaved DNA complexes that are normally fleeting intermediates in the catalytic cycle of the enzyme. The anti–tumor topoisomerase II inhibitors presently used in the clinic, poison the enzyme by stabilizing cleavable complexes, presumably by increasing the rate of forwards reaction i.e. more rate of DNA cleavage or by decreasing the rate of backward reaction i.e. slow rate of religation of cleaved DNA. Thus synthesis of DNA and RNA is blocked.

1.2.4.2 Microtubule Inhibitors

Microtubules are protein polymers involved in cellular movement and morphology. Microtubules occur in equilibrium between polymerized and free tubulin dimmers. Inhibitor drugs disrupt this equilibrium. Vinca alkaloids (vinblastine, vincristine) are examples of this type of drugs. Non-covalent binding is reversible and is typically preferred over covalent adduct formation keeping the drug metabolism and toxic side effects in mind. However, the high binding strength of covalent binders is a major advantage.

1.3 FORCES INVOLVED IN DRUG-DNA INTERACTION

The binding of drug to DNA involves different energy contributions. These include energy from any conformational changes, from the entropic cost of forming a bimolecular complex, from the hydrophobic transfer process, from the polyelectrolyte effect, and from the formation of non-covalent molecular interactions (e.g. hydrogen bonds and van der Waals interactions) within the complex. A few of these forces play an important role in stabilizing the intercalation of drug in drug-DNA complex are as follows:

1.3.1 Hydrogen Bonding

The phosphate group, sugar, bases in nucleic acids and hydrophilic groups in anthracycline drug participate in hydrogen bonding with water. Since all linear hydrogen bonds have similar free energies, they make little net contribution to the favorable free energy change when drug and nucleic acid interact in solution. In contrast, the formation of poorly aligned hydrogen bonds or absence of some of them on the complex formation carries a 4 KJ mol^{-1} free energy penalty. Thus hydrogen

bonds are one of the most important means of making sequence specific interaction of nucleic acid with drug.

1.3.2 Electrostatic Forces: Salt Bridges

Salt bridges are electrostatic interactions between groups of opposite charge. They typically provide about 40 KJ mol^{-1} of stabilization per salt bridge. In drug-DNA complex, they are formed between the ionized phosphates of nucleic acid and positively charged groups of drug. Salt bridges are influenced by the concentration of salt in the solution. Strength of salt bridge decreases with the increase in concentration of the salt. They are much stronger when there are no water molecules between the ionized groups because water has a high dielectric constant. These are relatively long-range forces.

1.3.3 Entropic Forces: The Hydrophobic Effect

The hydrophobic effect is due to the behavior of water at an interface. Any molecule in water creates a sharply curved interface and so orders a layer of water molecules around itself. When molecules aggregate, the ordered water molecules at the interface are released and become part of the disordered bulk water, thus stabilizing the aggregate by increasing the entropy of the system. Polar surfaces, where the enthalpy loss tends to offset the entropy gain or de-solvation are less likely to aggregate than non-polar ones. Molecules of water left at the interface between the drug and the nucleic acid obviously decrease the entropy of the system. Therefore the surface of the non-planar aromatic chromophore of drug tends to be exactly complementary so that no unnecessary water molecules remain when the complex forms.

1.3.4 Base Stacking: Dispersion Forces

Base stacking is caused by two kinds of interaction: the hydrophobic effect mentioned above and dispersion forces. Molecules with no net dipole moment can attract each other by a transient dipole-induced dipole interaction. Such dispersion forces decreases with the inverse sixth power of the distance separating the two dipoles, and so are very sensitive to the thermal motion of the molecules involved. Despite their extreme distance dependence, dispersion forces are clearly important in maintaining the structure of double stranded nucleic acids because they help to cause base stacking. Besides they allow aromatic ring of the drug to intercalate between bases and stabilize it by base stacking.

1.4 STRUCTURE OF NUCLEIC ACIDS

DNA (deoxyribonucleic acid) and RNA (ribonucleic acid) are polymers of nucleotides linked in a chain through phosphodiester bonds. Each nucleotide consists of three distinct chemical groups, a nitrogenous base, a five-carbon sugar, and a phosphate group.

1.4.1 Nucleotide Bases

1.4.1.1 Purines: Adenine and Guanine

Two different heterocyclic aromatic bases with a purine ring (composed of carbon and nitrogen) are found in DNA (Fig. 1.1a). Adenine has an amino group ($-NH_2$) on the C6 position of the purine ring. Guanine has an amino group at the C2 position and a carbonyl group at the C6 position. Besides these, minor bases like inosine, 7–methyl guanosine, etc. are also found as components of nucleic acids.

1.4.1.2 Pyrimidines: Thymine, Cytosine and Uracil

Thymine contains a methyl group at the C5 position with the carbonyl group at C4 and C2 positions. Cytosine contains a hydrogen atom at the C5 position and an amino group at C4 (Fig. 1.1b). In RNA thymine is replaced by uracil.

1.4.2 Sugar Ring

Ribose sugar is found in all RNA molecules while a slightly different sugar, β-D-2-deoxyribose is found in DNA. This is a derivative of β–D–ribose in which the hydroxyl (–) the 2' position is replaced by hydrogen (–OH) (Fig. 1.2). The sugar moiety of DNA is one of the more flexible and dynamic parts of the molecule. The sugar base combination is called nucleoside unit. A nucleotide is a nucleoside phosphorylated at one of the free sugar hydroxyls.

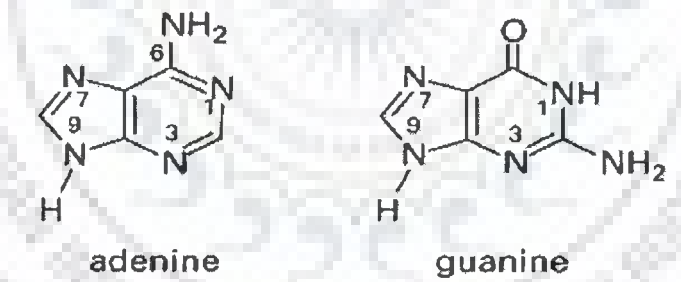

(a) Purines

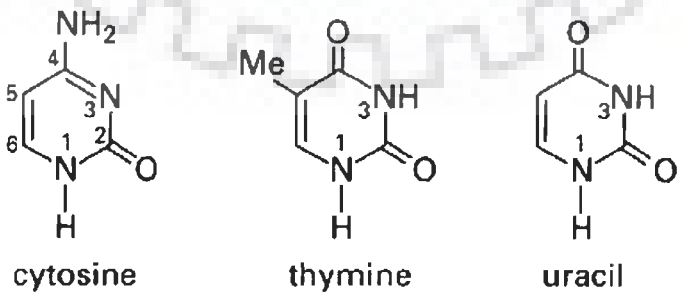

(b) Pyrimidines

Fig. 1.1: (a) Structural formulae of purines and (b) pyrimidines.

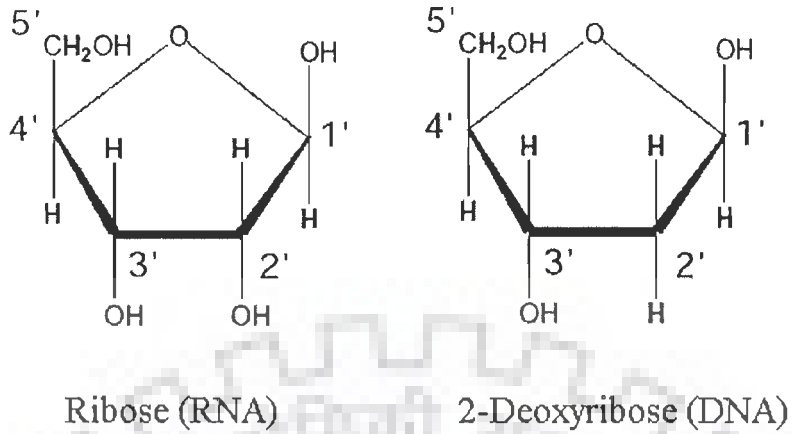

Fig. 1.2: Five membered furanose ring of deoxyribose and ribose sugar

1.4.3 Conformation of sugar phosphate backbone and furanose sugar ring

The conformation of the sugar- phosphate backbone, following the sequential numbering of atoms P –O5'–C5' –C4'etc., is defined by torsional angles α, β, γ, δ, ε and ζ. Angles υ_0, υ_1, υ_2, υ_3 and υ_4 decide the geometry of sugar ring (Fig. 1.3 and Fig. 1.4). The different families of DNA structures are characterized by the values of these torsion angles.

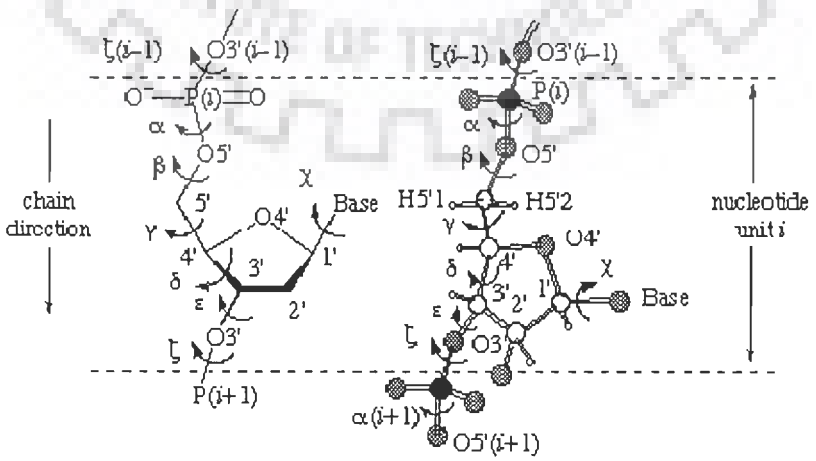

Fig. 1.3: Section of a polynucleotide backbone showing the atom numbering and the notation for torsion angles

The sugar ring occupies a pivotal position in the nucleotide unit because it is part of both the backbone and the side chain. In order to provide a complete description of the ring conformation, it is necessary to specify the endocyclic torsion angles for the ring as well as the bond lengths and bond angles. The ribose sugar geometry is defined by the following five endocyclic torsion angles: O4'-C1', C1'-C2', C2'-C3', C3'-C4' and C4'-O4' are denoted by the symbols, respectively. The sequence of atoms used to define each backbone torsion angle is shown in e.g. $\upsilon_0, \upsilon_1, \upsilon_2, \upsilon_3, \upsilon_4$ refers to the torsion angle of the sequence of atoms C4'-O4'-C1'-C2', etc (Fig. 1.4).

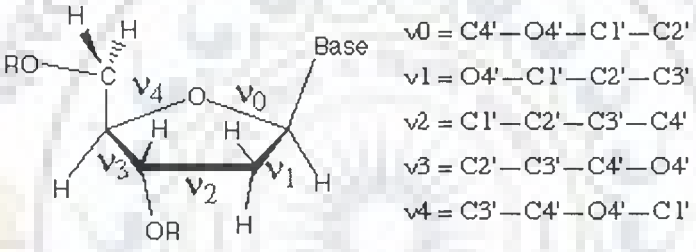

Fig. 1.4.: Endocyclic torsional angles in the sugar ring

The magnitudes of such angles are all interrelated and, therefore, the geometry of the ribose ring can be defined from two parameters: the pseudorotation phase angle (P) and the pucker amplitude. The ribose ring is not a planar and usually presents C2'-endo (South) or C3'-endo (North) conformation. For the sugar pucker conformation, homonuclear $^3J_{H-H}$ coupling constant serve as the most direct determinant. These constants can be measured in a qualitative way from 2D ^{1}H-^{1}H TOCSY, 2D ^{1}H-^{13}C TOCSY-HMQC or 2D ^{1}H-^{13}C TOCSY-HSQC experiments:

- Very weak $J_{H1'-H2'}$ and strong $J_{H3'-H4'}$ cross-peaks correspond to *pure N-type conformation* (preferred conformation in RNA).

- Strong $J_{H1'-H2'}$ and weak $J_{H3'-H4'}$ cross-peaks correspond to *pure S-type conformation.*
- $J_{H2'-H3'}$ is similar in both states.
- Intermediate intensities indicate equilibrium between N and S states.

1.4.3.1 Sugar pucker

The five-membered ring is generally non planar and its conformation is designated as follows. If four atoms lie in the pane, this plane is chosen as reference plane and the conformation is designated as envelope (E) and if they do not, the reference plane is then that of the three atoms that are closest to the five-atom, least-squares plane, and the conformation is described as twist (T).

a) The present *E* and *T* notations for puckered forms of the sugar ring confirm to those recommended for the conformational nomenclature of five and six-membered rings of monosaccharide and their derivatives.

b) The *E/T* notation has superseded the *endo/exo* description in which atoms now designated by superscripts were called *endo*, and those now designated by subscripts were called *exo*. They are shown by both systems of designation (Fig. 1.5). Examples: C3'-*endo*/C2'-*exo* has become ${}^{3}T_{2}$ and C3'-*endo* has become ${}^{3}E$.

c) Symmetrical twist conformations, in which both atoms exhibit equal displacements with respect to the five-atom plane are denoted by placing the superscript and subscript on the same side of the letter *T*, e.g. ${}_{2}{}^{3}T$, ${}_{4}{}^{3}T$, etc.

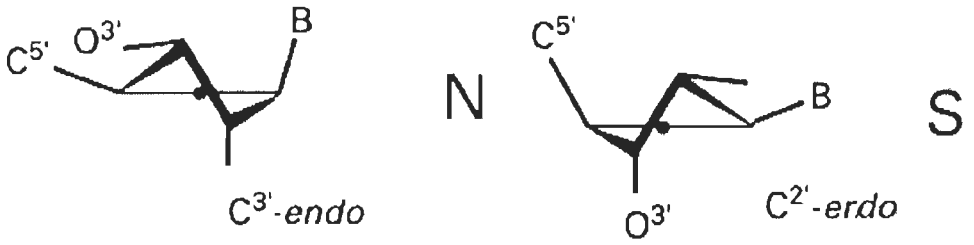

N-puckered
P=0º–18º

Ribose: $^{3}J_{H1'-H2'} \approx 1$ Hz
Deoxyribose: $^{3}J_{H1'-H2'} \approx 1.8$ Hz

S-puckered
P=144º–162º

Ribose: $^{3}J_{H1'-H2'} \approx 7.9$ Hz
Deoxyribose: $^{3}J_{H1'-H2'} \approx 10$ Hz

Fig. 1.5: Preferred conformation of sugar pucker C2' endo and C3' endo of sugar

1.4.3.2 Pseudo rotation cycle

Sugar conformation can only be approximately defined by sugar pucker if intermediate twist modes are considered and hence inadequate. In furanose ring maximum pucker rotates virtually without any potential energy barriers, giving rise to infinite number of conformations. Each conformation of the furanose ring can be unequivocally described by two pseudorotational parameters: the phase angle of pseudorotation, *P*, and the degree of pucker, Ψ_{max}. In nucleotides, the pseudorotation phase angle P is calculated from the endocyclic sugar torsion angles according to Altona C. and Sundaralingam M.

$$\tan P = \frac{(\nu_4 + \nu_1) - (\nu_3 + \nu_0)}{2.\nu_2 (\sin 36° + \sin 72°)}$$

Given the phase angle P, the five torsional angles are related by:

$$\nu_j = \nu_{max}. \text{Cos} (P + j.\psi)$$

Where j = 0 to 4 and ψ = 720° / 5 = 144°. The maximum torsion angle, ν_{max} is derived by setting j = 0. $\nu_{Max} = \nu_0$ / Cos P

At every phase angle P, the sum of the positive torsional angles is equal to the sum of the negative torsional angles, i.e. the sum of the five angles is zero.

$$\nu_0 + \nu_1 + \nu_2 + \nu_3 + \nu_4 = 0$$

Standard conformation (P=0°) is defined with a maximally positive C1'-C2'-C3'-C4' torsion angle [i.e. the symmetrical ${}_2{}^3T$ form], and P has value 0-360° (Fig.1.6). Conformations in the upper or northern half of the circle (P = 0±90°) are denoted N and those in the southern half of the circle (P = 180±90°) are denoted S conformation. It is seen that the symmetrical twist (T) conformations arise at even multiples of 18° of P and the symmetrical envelope (E) conformations arise at odd multiples of 18° of P. The symbols 'r' and 'd' represent the usual range of P values for N and S conformations of ribo- (r) and 2'-deoxyribo- (d) furanose rings of β-D-nucleosides and nucleotides. In B- DNA two ranges of psedorotation phase angles are preferred C3' – endo at 0° ≤ P ≤ 36° (N conformer) and C2' endo at 144° ≤ P ≤ 180° (S- conformer).

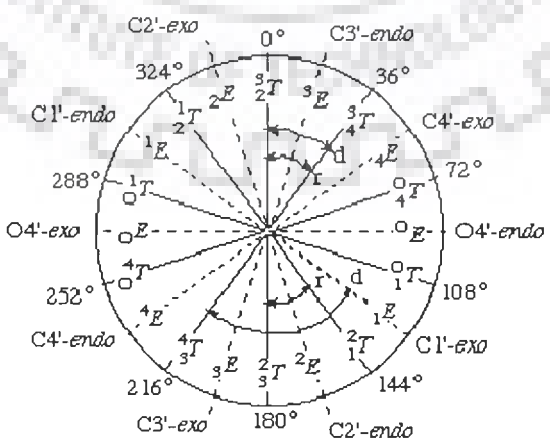

Fig. 1.6: Pseudorotation cycle of furanose ring in nucleosides (Altona and Sundarlingam)

1.4.3.3 N-Glycosidic Bond rotation (χ_{CN})

The torsion angle about the N-glycosidic bond (N-C1') that links the base to the sugar is denoted by the symbol χ_{CN}. The sequence of atoms chosen to define this angle is O4'-C1'-N9-C4 for purine and O4'-C1'-N1-C2 for pyrimidine derivatives. Thus when $\chi = 0^{o}$ the O4'-C1' bond is eclipsed with the N9-C4 bond for purine and the N1-C2 bond for pyrimidine derivatives. Relative to the sugar moiety, the base can adopt two main orientations, called anti and syn. In anti, the six membered rings in purines and O2 in pyrimidines is pointing away from the sugar, and in syn it is over or towards the sugar. High anti is a variant of anti, in which the bond C1'–C2' is nearly eclipsed with N1-C6 in pyrimidine or N9-C8 in purine nucleosides. The term high anti actually denotes a torsion angle lower than anti (Fig. 1.7).

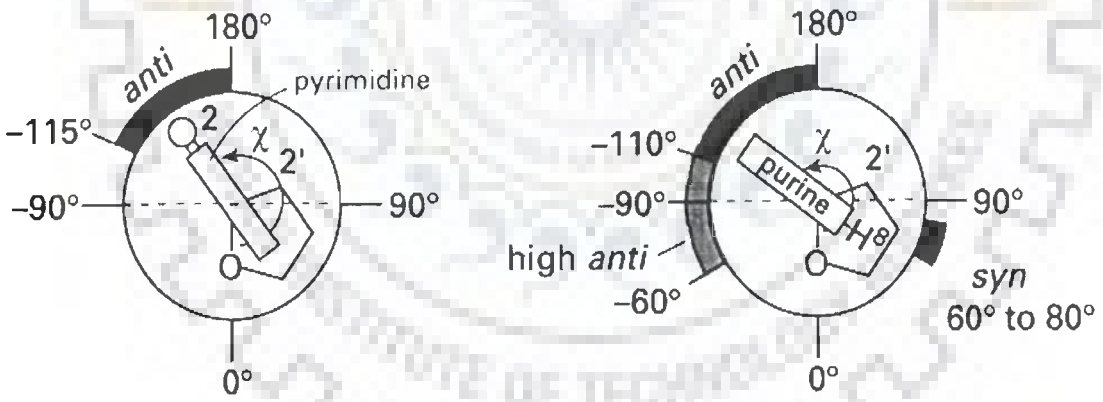

Fig. 1.7: Anti high, anti and syn orientations about the glycosidic.

1.5 NUCLEIC ACID FUNCTION

The main function of nucleic acids is to store and transmit genetic information and use that information to direct the synthesis of new protein. DNA is the permanent storage place for genetic information in the nucleus of a cell. DNA controls the

synthesis of RNA. RNA transmits genetic information from DNA to the protein synthesizers in the cell. RNA is also responsible for directing the production of the new protein by transmitting the genetic information to the protein building structures. The sequence of nucleotides information nucleic acids molecules (mainly DNA) makes up a code that stores and transmits the direction required for assembling all types of proteins. DNA serves two central roles. First, it maintains the genetic information and is replicated to pass this information to each new cell. Second, it contains the code which is translated into RNA which is then transcribed into proteins. This has become known as the central dogma of molecular biology (Fig.1.8).

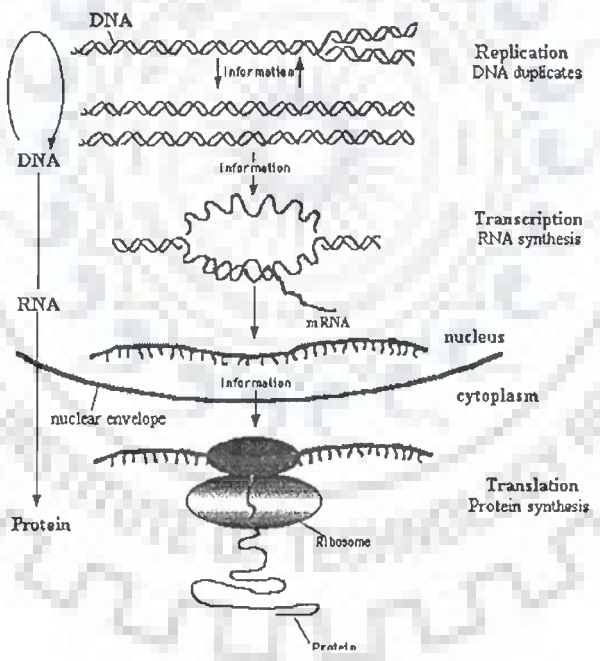

Fig. 1.8 The "Central Dogma of Molecular Biology" depicting the key cellular processes of DNA replication and translation

Individual nucleotides provide the building blocks of nucleic acids and carry out a variety of biological functions. Many nucleotides transport chemical energy in the form of phosphate groups or electrons from one reaction system to another. Others

carry metabolites such as acetyl groups between reactions. Other nucleotides in cyclic form are important in cell regulation.

1.6 NMR SPECTROSCOPY, UV-VISIBLE AND FLUORESCENCE SPECTROSCOPY INVOLVED IN DRUG –DNA INTERACTION

NMR spectroscopy has enjoyed many advances recently, and the pace of development shows no signs of slowing. These advances are allowing NMR to help solve important problems in the field of drug discovery. NMR spectroscopy is now being used to determine protein structures, to monitor ligand-receptor binding, to study diffusion, to analyze mixtures using LC-NMR, to analyze solid-phase synthesis resins and to determine the structures of organic small molecules. It is not only limited to the solution only, its use in lyotropic crystals and Liquid crsytals is a very important for some kind of systems from ancient time [Khetrapal and Diehl, 1975; Kunwar, 1991]. Biomolecular NMR spectroscopy has expanded dramatically in recent years and is now a powerful tool for the study of structure, dynamics, and interactions of biomolecules. NMR spectroscopy is already well-established as an efficient method for ligand screening. A number of recently developed techniques show promise as aids in structure-based drug design. An advantage of the method is that all these interactions can be studied in solution-time-consuming crystallization is not necessary. Being in solution form, even structural and biochemical changes in intact cells (in vivo NMR) can be monitored. Nuclear Magnetic Resonance (NMR) spectroscopy uses radiation to induce nuclear spin state changes which are unique for different atoms and their local environment. From the 1D and 2D NMR spectrum acquired on solid or liquid samples, the structure of molecules can be deduced. NMR can observe static as well as dynamic interactions between molecules. It requires that

the sample to be dissolved in a deuterated solvent. The most commonly used resonances in NMR studies are ^{1}H, ^{13}C, ^{31}P and ^{15}N. ^{1}H NMR gives rise to a series of absorption lines in the region 0-15 ppm. A larger spectral dispersion of chemical shifts is observed in ^{13}C NMR. In ^{15}N NMR, chemical shifts are sensitive to primary structure as well as molecular conformation. But it has low sensitivity due to low natural abundance (0.36%) which causes difficulties in its detection hence offers limited applications of ^{15}N NMR. ^{31}P NMR has developed as a powerful probe of the structure and dynamics of DNA due to existence of spin ½, 100% natural abundance, moderate relaxation times, wide range of chemical shifts and non-interference from solvent peaks. In ^{31}P NMR, chemical shifts are sensitive to molecular conformation of the phosphate group. Thus it becomes very informative in case of nucleic acid structure elucidation since backbone of DNA and RNA contains phosphorus nuclei. NMR spectroscopy can provide both qualitative and quantitative information. This information can benefit numerous disciplines in drug discovery, including natural products research, synthetic medicinal chemistry, metabolism studies, drug production, quality control, rational drug design and combinatorial chemistry. This focuses on how they might be of value in removing some of the current "bottlenecks" in structure-based drug discovery.

Fluorescence spectroscopy provides structural information on the basis of emission and excitation wavelength. The fluorophore has different emission and excitation wavelengths which gives different spectra ranging from 200-800nm. UV-Vis spectroscopy uses the wavelengths of light in the spectrum ranges of 120 to 800 nm. DNA typically absorbs in the region of 160 to 300 nm due to the electronic transitions regions of the bases. These techniques are conducted in solution and are simple to conduct, but average the results across molecules in different states. New

anticancer drug can be screened, by these methods, for example specific designed peptides interaction study with different oncogenes provides sufficient knowledge about their mode of action [Aklank Jain and Rajeswari, 2003; Jain et al., 2005].

1.7 MOLECULAR MODELING STUDY INVOLVED IN DRUG-DNA INTERACTIONS

Molecular modeling is a broad term that encompasses ab initio quantum mechanical calculations, semi-empirical calculations, and empirical calculations (charge-dependent molecular mechanics force fields). These techniques can be used to study the three-dimensional structure, dynamics, and properties of a molecule of interest. Molecular modeling can identify and define the possible key details of the molecular interaction and, using the graphics/computational approach, decide on optimal structural modifications likely to enhance either general binding affinity or recognition of a particular nucleotide-binding site. A number of studies have revealed the converse, with the discovery that particular patterns of chemical modification on a given drug (e.g., doxorubicin) can result in both low biological activity and low-ranking interaction energy.

The molecular modeling, particularly molecular mechanics and dynamics, are highly complementary to macromolecular NMR and X-ray crystallography. Molecular dynamics simulation can, in principle, provide a complete theoretical description of DNA structure and motions, and are thus a valuable independent means of developing models and interpreting experimental data. A combined approach is desirable and, where the parent experimental structure is available, the simulation can be partially validated by reproducing the structure, thus paving the way for 'rational drug-designing'. For "rational" drug design, choice of a target, the evaluation of a

structure of that target, the pivotal questions to consider in choosing a method for drug lead discovery, and evaluation of the drug leads.

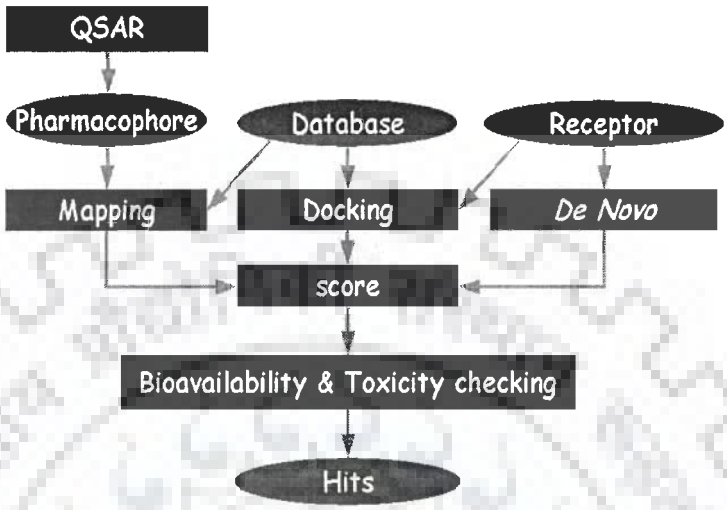

1.8 LITERATURE REVIEW

The role of natural products as a source for remedies has been recognized since ancient times [Cragg et al., 1999; Farnsworth et al., 1985]. Several plant-derived compounds are currently successfully employed in cancer treatment. One of the most significant examples is the vinca alkaloid family isolated from the periwinkle *Catharanthus roseus*, which is found in the rain forests of Madagascar [Noble, 1990]. Vincristine inhibits microtubule assembly, inducing tubulin self-association into coiled spiral aggregates. Another example of a highly active agent derived from a natural product is etoposide, which has produced high cure rates in testicular cancer when used in combination with bleomycin (also derived from a natural product) and cisplatin [Williams et al., 1987]. In addition, the camptothecin derivatives irinotecan and topotecan, have shown significant antitumor activity against colorectal and ovarian cancer respectively [Creemers et al., 1996]. These compounds were initially

obtained from the bark and wood of Nyssacea *Camptotheca accuminata* and act by inhibiting topoisomerase I [Liu et al., 2000]. The taxanes and the camptothecins are presently approved for human use in various countries. Flavopiridol is one of the most exciting plant-based agents currently under development, representing the first cyclindependent kinase inhibitor to enter the clinic [Kelland, 2000]. Flavopiridol is a synthetic flavone derived from the plant alkaloid rohitukine, which was isolated from the leaves and stems of *Amoora rohituka* and later from *Dysoxylum binectariferum* (Maliaceae) [Cragg and Suffness, 1988; Kelland, 2000]. However, an increasing reliance on the use of medicinal plants in the industrialized societies has been traced to the extraction and development of several drugs and chemotherapeutics from these plants Medicinal values of these plants are due to the presence of small doses of active compounds which produces physiological actions in human and animal bodies. Some of the important bioactive compounds in these plants are alkaloids, glycosides, resins, gums, & mucilage's. Protoberberines constitute an important class of isoquinoline alkaloids widely present as active constituents of folk medicines having potential medicinal and pharmacological properties. They are found in many plant families like Papaveraceae, Berberidaceae, Fumariaceae, Menispermaceae, Ranunculaceae, Rutaceae, Annonaceae, as well as a few examples in Magnoliaceae and Convolvulaceae (Bentley, 1997, 1998a, b, 1999, 2000, 2001, 2002, 2003, 2004, 2005, 2006). Most of these alkaloids exist in plants either as tetrahydroprotoberberines or as quaternary protoberberine salts. The basic skeleton of the quaternary protoberberine alkaloids is 5, 6-Dihydrodibenzo [a,g] quinolizinium (C17H14N+). The substituents are usually present at positions 2, 3, 9, 10 or 2, 3, 10, 11 and the prefix pseudo is often used for the latter substitution pattern. The protoberberine alkaloid palmatine is among the most widely distributed alkaloid of

the isoquinoline series. It bears the 5, 6 dihydrodibenzo[a,g]quinolizinium (C17H14N+) basic skeleton of protoberberines and has four methoxy groups at 2, 3, 9 and 10 positions (Fig.1.9).

1.8.1 Spectroscopic Studies

1.8.1.1 NMR Spectroscopic Studies

There are very few detail NMR studies on the structure of palmatine. The ^{1}H NMR, ^{13}C NMR, (500MHz, DMSO-d_6) of palmatine along with other alkaloids extracted from the stems of plants *A. flava, C. blumeanum* and *F. tinctoria* plants has been done (Keawpradub et al., 2005). The unambiguous assignement of the alkaloids were done using 2D NMR particularly HMBC and HMQC. A novel protoberberine alkaloid 7, 8-dihydro-8-hydroxypalmatine, along with palmatine was isolated from the plant *Enantia chlorantha* [Wafo et al., 1999]. NMR (1D and 2D, using 100MHz spectrometer, DMSO-d6), IR, and EI-MS spectroscopy data were used to elucidate the structures of the compounds.

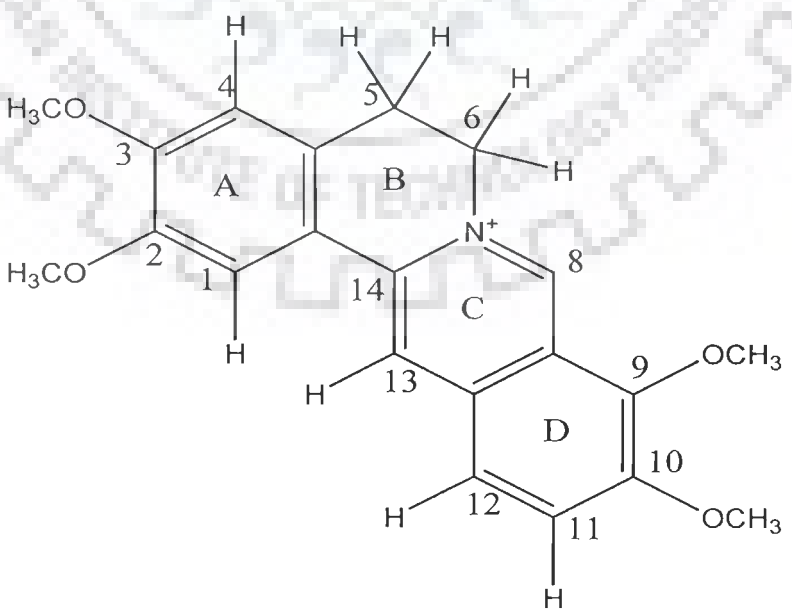

Fig. 1.9: Chemical Structure of Palmatine

Haberlein et al has isolated protoberberines from the rhizome of *Corydalis cava* and also carried out their EI-MS and ^{1}H NMR studies [Haberlein et al., 2003]. They categorized the alkaloids as protoberberine Type 1 (palmatine is one among them) and protoberberine Type2. The protoberberine type 2 alkaloids showed positive cooperation in $GABA_A$ binding site whereas protoberberine type I alkaloids had no influence on $GABA_A$ receptors. A highly specific and sensitive method using ^{1}H NMR (400MHz spectrometer-methanol-d4) for the quantitative determination of protoberberine alkaloids in *Phellodendron* species and in Chinese medicines, Huangbai has been done [Li et al., 2006]. The first unambiguous assignment of the proton and carbon-13 spectra of the protoberberine alkaloid berberine along with the benzophenanthridine alkaloid sanguinarine has been reported by Blasko et al., 1988. Berberine differs from palmatine in the nature of substituent present at positions 2, 3 on the benzo ring with methylene dioxy for berberine and dimethoxy for palmatine. The assignment of the ^{1}H and ^{13}C NMR resonances of some isoquinoline alkaloids were discussed using two-dimensional shift correlated NMR and ^{1}H NOE difference experiments [Janssen et al., 1989]. NMR studies on berberine and berberrubin were carried out by Jeon et al, 2002. The carbon and proton resonances of the alkaloids were assigned from the combined use of HMBC and DQF-COSY. Berberrubin differs from berberine only at position 19. The different NMR resonances of these two drugs suggested their different chemical environment and explained the differences in their Topoisomerase II mediated DNA cleavage activity. The NMR chemical shift contains very detailed information about the electron distribution around the atomic nucleus.

There are marked changes in the chemical shifts on structural modifications of the compounds. ^{1}H and ^{13}C chemical shift values for berberine, palmatine and their isolation artifacts in different solvents have been determined [Marek et al., 2003] to show the direct effect of internal and external environment on the chemical shifts of these compounds. Further, attempt has been made to know the influence of interconversion between the salt and the base of the alkaloid berberine and coptisin. Dostal et al reported the structural study of berberine and coptisine free bases with the help of 1D, 2D NMR and X-ray Diffraction techniques [Dostal et al., 2004]. The fact that ^{15}N Nuclei are sensitive indicators of structural motifs in organic and bioorganic compounds has been elaborated [Marek et al., 1999]. They performed the direct measurement ^{15}N NMR chemical shift for several isoquinoline alkaloids using application of inverse detected NMR experiments. The ^{15}N NMR chemical shifts of the salts 8- hydroxydihydroberberine and 8-oxoberine were studied [Marek et al., 2002]. It was shown that the substitution patterns on rings A and D had no effect on the shielding of N-7 atom. The reduction of ring C (dihydroderivative) has a crucial effect on the aromatic isotropic shielding of the nitrogen nucleus as it disturbs the aromatic nature of the ring. Moreover, nitrogen shielding is influenced by the electronic properties of the substituent at position C-8. Till today there are no NMR studies on plamatine binding to DNA. However, few studies has been done on the other protoberberine, i.e. berberine. Berberine differ from palmatine by the nature of substituent at positions 2, 3 on the benzo ring being methylene dioxy for berberine and dimethoxy for palmatine. NMR studies on the binding of alkaloids berberine and sanguinarine to calf thymus DNA showed that berberine intercalate partially with calf thymus DNA while

sanguinarine binds more firmly with the mode of normal intercalation [Saran and Srivastava, 1995]. Mazzini et al elucidated the structural features of the complex of berberine with several oligonucleotides, by NMR spectroscopy in aqueous solution [Mazzini et al, 2003]. Their studies indicated that berberine binds to minor groove of the duplexes with AT rich sequences. The phosphorus studies did not show any new peaks for the bound and free species as the binding process was fast with respect to the NMR time scale. The addition of berberine did not induce significant chemical shift variation of the phosphate signals in the ^{31}P NMR spectra ($\Delta\delta < 0.2$ ppm). This result was the first evidence for excluding the intercalation of berberine into the double helix. The proton NOESY experiments enabled the detection of intermolecular peaks between protons of berberine and protons of the self–complementry oligomer $d(AAGAATTCTT)_2$. The berberine molecule was found to be located with the convex side on the minor groove of the double helix at the level of A4-T7 and A5-T6 base pairs. This presents the positive nitrogen atom of the alkaloid close to the negatively ionic surface of oligonucleotide. Ring A and the methylene dioxy group were external to the helix, while the aromatic protons H-11 and H-12 were close to the ribose of cytidine C8. These results suggested that external non-specific interaction between the positively charged drug and the negatively charged ionic surface of the DNA play an important role in the binding process. NMR studies on the interaction of berberine and berberrubin with HP14 showed the broadening and upfield shifts of DNA peaks on the addition of alkaloids (Park et al, 2004 a, b). The resonances of drug shift upfield in the drug-DNA complex with respect to the free drug. No separate signals were found for free and bound species as the binding process is of intermediate rate

w.r.t the NMR time scale. No significant interruption in the sequential base-sugar NOEs connectitivities were evident. Due to few intermolecular NOES between the oligonucleotide and berberine, model of the complex was not built. Their studies suggested that berberine binds to DNA non specifically then berberrubin and the rate of exchange process between the protoberberine analogs bound and free HP14 is altered by substitution at position 19.

1.8.1.2 UV–Visible, Fluorescence and Vibrational Spectroscopy, Circular Dichorism studies

Spectroscopic studies are used since ancient time to elucidate the drug DNA interaction for anticancer drugs [Shafer, 1977]. The pattern of the UV absorption spectra of the quaternary protoberberine alkaloid (QPA) bases is determined by the auxochromic groups bound to ring D [Pavelka and Smekal, 1976], the methoxy groups on carbons C-6 and C-7 or C6 and C-4. Quaternary salts of protoberberine alkaloids in polar media exhibit four well-defined absorption bands. The oxygenous electron-donating groups (methoxy and hydroxy) in the quaternary protoberberine alkaloids appreciably reduce the energy of electron transfers between the ground and the excited singlet state for these molecules and also influence their absorbances and fluorescence intensities. The interaction of berberine and burasine (palmatine) to DNA was studied by absorption, melting and ELD experiments [Kluza et al., 2003]. The group suggested the mode of binding by the mechanism of intercalation. The interaction studies of palmatine to four polynucleotides poly(dA).poly(dT), poly(dA–dT).poly(dA–dT), poly(dG–C).poly(dG–dC), poly(dG).poly(dC) has been done using competition dialysis, spectrophotometery, spectrofluorometric, thermal melting, circular dichorism, viscometric and isothermal titration calorimetric (ITC) techniques

[Bhadra et al., 2007]. The UV-visible spectra of palmatine has two absorption bands in the visible region with maxima centered at 344 nm and 425 nm. The titration studies of palmatine with polynucleotides showed hypochromic and bathochromic effects with three sharp isosbestic points at 354, 378 and 448 nms respectively indicating equilibrium between the free and bound alkaloid molecule. The binding affinity values obtained from absorbance measurments for the polymers varied in the order poly(dA).poly(dT)> poly(dA–dT).poly(dA–dT)> poly(dG–dC).poly(dG–dC)> poly(dG).poly(dC). The fluorescence experiment showed enhancement of the fluorescence quantum yield of palmatine on binding to both the AT polymers and being highest with the AT homopolymer. The fluorescence quantum yield was significantly lower with both the GC polymers. This affinity was also revealed by circular dichoric spectrum. The CD spectra of all the polymers were remarkably perturbed in presence of the palmatine resulting in a rapid increase of the positive band. The extent of change was more pronounced in the two AT polymers compared to the GC polymers. Palmatine has shown the stabilization of the polynucleotides against thermal denaturation. Increase in the melting temperature was of the order of about 15° in case of the AT homo polymers and 12° for the AT hetero polymer at identical D/P ratio, while it was smaller i.e. about 4 °C with the homo GC polymer. Isothermal titration calorimetric showed a single entropy driven binding event in the AT homopolymer while the heteropolymer involved two binding modes i.e. entropy driven strong binding followed by an enthalpy driven weak binding. These data suggested that palmatine binds strongly to AT homopolymers and heteropolymers by mechanism of intercalation. Further studies by Bhadra et al, on berberine binding to various DNA reported its positive cooperativity to polypurine–polypyrimidine sequences and non-cooperativity to alternating purine–pyrimidine sequences [Bhadra

et al., 2008]. The binding suggested that cooperativity depends on the salt concentration and the non polyelectrolytic part contributes predominantly to the free energy of the binding. Isothermal titration calorimetric (ITC) studies revealed that the binding with the two AT polymers was entropically driven and the temperature dependence of binding enthalpy yields negative heat capacity indicating the predominant role of hydrophobic interactions in the AT specific binding of berberine. Interaction studies of berberine and sanguinarine with DNA and RNA triplexes and duplexes has been carried out by Das et al, 2003. It was determined that both the alkaloids binds to triplex and duplex in a non cooperative manner and the binding was more to triplex then to duplex structures. Thermodynamic data showed the binding of berberine to duplexes and triplexes as negative enthalpy and positive entropy changes. These results suggested that berberine binds to DNA and RNA triplexes more strongly then to to their respective parent duplexes. The interaction of berberine with the homo and hetero-polymers of guanosine–citydine (G.C) sequences were investigated using spectrophotometric and circular dichroic techniques [kumar et al., 2003]. The binding data indicated non-cooperative binding to both the protonated forms similar to that of their respective B-form structures. Fluorescence spectral studies showed remarkable increase in the intrinsic fluorescence of the alkaloids in the presence of the protonated forms compared to their respective B-form structures. These results suggested the use of berberine as a probe to detect the alteration of structural handedness due to protonation and may potentiate its use in regulatory roles for biological functions. The spectroscopic, viscometric and thermodynamic studies [Yadav et al., 2005] has shown the strong binding of berberine to single stranded polyriboadenylic acid by the mechanism of partial intercalation leading to its use in gene regulation in eukaryotic cells. Interaction studies of palmatine with poly(A),

double stranded DNA, t-RNA, poly(C)·poly(G), poly(U) and poly(C) were done using competition dialysis, fluorescence, and absorption spectral studies [Girri et al, 2006a,b]. The binding affinity of palmatine to natural DNA, t-RNA and double stranded poly(A) was found to be weaker while no binding was apparent with single stranded poly(U), poly(C) and double stranded poly(C)·poly(G). It was found that palmatine bind strongly to single stranded Poly (A) by partial intercalation mechanism suggesting it as a potential target for RNA based targeting drugs. ITC data has shown the binding of palmatine to Poly (A) as exothermic and enthalpy driven. The binding of palmatine and berberine with Poly (A) has shown hypochromic and bathochromic effects. The binding was found to be non cooperative binding but was not able to induce self structure in single stranded poly (A) molecules [Giri et al., 2008]. The interaction studies of palmatine and berberine to tRNA has also shown partial intercalation as the mechanism of binding [Islam et al., 2007, 2008]. Non-electrostatic interactions play an important role in the binding of these positively charged drugs to tRNA. It was found that berberine binds to the protonated form of poly(rC).poly(rG) by partial intercalation process, while its binding to the A-form was very weak [Sinha et al., 2006]. The binding affinity energetics and conformational aspects of the drugs palmatine and berberine to four single stranded polyribonucleotides: polyguanylic acid [poly(G)], polyinosinic acid [poly(I)], polycytidylic acid [poly(C)] and polyuridylic acid [poly(U)] were investigated [Islam et al., 2008]. Berberine and palmatine binds strongly to poly(G) and poly(I) while their binding to poly(C) and poly(U) was found to be very weak. The binding of these compounds to poly(G) and poly (I) was exothermic and favoured by negative enthalpy and positive entropy change. The DNA binding affinities of berberrubine, jatrorubine and palmatrubine the demethylated derivative of berberine, jattrohizine

and palmatine respectively has been investigated [Qin et al., 2007]. Competitive ethidium bromide (EB) displacement experiment results showed that demethylation has improved the DNA- binding affinities of these drugs and all of these have preferable binding affinities towards AT- rich DNA. Intercalation was shown to be the most probable way of binding of these demethylated derivatives to double stranded DNA. Recently, the interaction between calf thymus DNA and palmatine has been investigated by using UV, SS-RTP and cyclic voltammogram spectroscopy [Junfen et al., 2009]. Absorption and fluorescence studies revealed strong binding affinity of palmatine to DNA and indicated intercalation as the binding mode. Whereas, fluorescence polarization, phosphorescence lifetime anion quenching and denatured DNA measurements, indicated groove binding as the main binding mode.

1.8.1.3 Mass spectrometry

Mass spectrometry has been used as a powerful tool for investigating the structures of complex molecules and natural products since long time. The base peaks produced by ESI-MS without CID (collision induced dissociation) of the abundantly occuring quaternary protoberberine alkaloids are: berberine 336, palmatine 352, jatrorrhizine 338, columbamine 338, coptisine 320, epiberberine 336, and berberastine 322. The ESI-MS spectra with CID (30 V) contain 4–5 fragments [Chuang et al., 1996]. The fragmentation pathway of the quaternary alkaloids berberine, jatrorrhizine, coptisine, palmatine, and 13-methylberberine were studied using multi-stage tandem mass spectrometry (MS^n) [Wang et al., 2004]. The identification and quantification of five protoberberine alkaloids (berberine, palmatine, coptisine, epiberberine and jatrorrhizine) in rat plasma has been carried out by using liquid chromatography-electrospray ionization-mass spectrometry (LC-ESI-MS) [Yu et al., 2007]. The

analytes were separated by linear gradient elution method and analysed by positive ESI-MS using the respective [M+] and [M + H] + ions with [M+] = 352 for palmatine. The noncovalent complexes of the four protoberberine alkaloids i.e palmatine, berberine, jatrorrhizine and coptisine with $d(AAGAATTCTT)_2$ have been investigated using ESI-MS [Chen et al., 2004]. The results have shown a 1:1 and 1:2 binding stoichiometries. These results indicated that palmatine exhibited the greatest binding affinity with the double-stranded DNA, while berberine had the lowest affinity. Chen et al. studied these above four cytotoxic protoberberine alkaloids including berberrubine with several double stranded oligodeoxynucleotides using ESI-MS and fluorescence spectrometric methods [Chen et al., 2005]. ESI-MS spectrometric reports indicated that these five alkaloids showed both 1:1 and 1:2 binding stoichiometries with $d(AAGAATTCTT)_2$, $d(AAGGATCCTT)_2$, and $d(AAGCATGCTT)_2$. The results from ESI-MS and fluorescence titration experiments indicated that the sequence selectivity of these five alkaloids was not significant and remarkable, AT- or GC-rich DNA binding preference was not obtained. This is in clear contrast to the earlier reports [Mazzini et al., 2003; Bhadra et al., 2007] which described the preferential binding of berberine to AT – rich DNA.

1.8.2. X-ray studies

Single –crystal X-ray diffraction is a precise method suitable for studying the bond length, bond and torsion angles, intermolecular interactions, and complete topology of crystal systems. Few attempts have been made to elucidate the crystal structure of protoberberines and their salts [Dostal et al., 2004; Man et al., 2001a, b; Marek et al., 2003a, Kariuki, 1995]. Quaternary protoberberine cations are relatively planar species. Their planarity is disturbed only in the partially saturated ring B, which adopts a twisted half-chair conformation with the atoms C5 and C6, deviating

from the plane of rings A, C and D. The methoxy group at C-10 is positioned in-plane while the neighboring 9-OMe is almost perpendicular to the plane of the D-ring. This is a common feature of the tertiary 8-adducts, 8-oxoderivatives, and quaternary protoberberine salts. Crystallographic studies [Abadi et al., 1984; Kariuki & Jones, 1995] on berberine, which like palmatine contains a 9, 10-dimethoxy substitution on its D-ring, indicate that the two methoxy groups are twisted above and below the plane formed by rings C and D, with the methoxy group at the 9 position being displaced by 0.1 Å below the C-D plane and the methoxy group at the 10 position being displaced by 0.3 Å above the C-D plane. These displacements of the bulky methoxy groups from the C-D plane may sterically interfere with the proper insertion of the C and D-rings between base pairs, thereby diminishing the extent of ligand base stacking and, ultimately, reducing the duplex binding affinity.

1.8.3 Theoretical Studies

Molecular mechanics studies were done on two protoberberine analogues i.e. 8-desmethylcoralyne (DMC) and 5, 6-dihydro-8-desmethylcoralyne (DHDMC) along with palmatine, which differ in the chemical structures of their B- and/or D-rings [Pilch et al., 1997]. On the basis of their drug modeling and DNA binding studies, the group proposed a mixed-mode DNA binding model for protoberberine analogs in which rings C and D are intercalated into the helical stack, while ring A protrudes into the minor groove of the host duplex, where it is thereby available for interactions with atoms lining the floor and/or walls of the minor groove. Molecular modeling studies using Macro- Model version 5.0 and the AMBER* force field [Mohamadi et al., 1990] revealed that DMC is an essentially planar molecule. Whereas, DHDMC deviated from planarity, with the plane of the A-ring being tilted by approximately

25° relative to the plane formed by rings C and D. Saturation of the 5-6 double bonds in the B-ring induced a tilt in the ligand molecule that does not existed when the 5, 6 positions were unsaturated. This tilting at the B-ring facilitated the interactions (e.g., van der Waals contacts) between the nonintercalated portion of the protoberberine molecule and atoms lining the floor and/or walls of the DNA minor groove. Molecular modeling studies on DHDMC [Mohamadi et al., 1990] revealed that the two methoxy groups on ring A are twisted above and below the plane to minimize the sterically unfavorable interactions that arise from their *ortho* positioning on the ring, an observation in agreement with previous crystallographic studies on berberine [Abdol Abadi et al., 1984; Kariuki & Jones, 1995], which, like DHDMC, contains two *ortho*-substituted methoxy moieties. The tilting of the A-ring allows the minor groove of host duplex to accommodate the twisted structure adopted by the two *ortho*-substituted methoxy groups, while also positioning the 2-methoxy group for favorable Van der Waals contacts with backbone sugar atoms lining the minor groove. The ability of a protoberberine analog to poison TOP1 is correlated with its preferential binding to duplexes with accessible minor grooves. The transfer of a methoxy group from the 11^{th} to the 9^{th} position of the D-ring in a protoberberine molecule whose 5, 6 positions are saturated is associated with a reduction in DNA binding affinity and reduced top1 poisoning. The reduction in the DNA binding affinity of DHDMC as a result of the methoxy group transfer suggests that a 10, 11- dimethoxy substitution of the D-ring may be sterically more compatible with the structural geometry of the duplex intercalation site than a 9, 10-dimethoxy substitution. Similar studies [Li et al., 2000] on four protoberberines were consistent with the results shown by Pilch et al., 1997. The stable structures and electronic properties for the berberine cation as well as possible ammonium, carbinol and amino-aldehyde forms of protoberberine salts in

the presence of hydroxyl ions was investigated by the B3LYP/6-31G(d,p) and MP2/6-31++G(d,p) methods (Danilov et al., 2006). The tautomeric forms of berberine alkaloid as well as its cationic form gave comparable structural parameters to the experimentally observed ones. The comparison of total energies elucidates that the amino-aldehyde form is the most preferable tautomer in gas phase, while the carbinol form is least stable. In spite of the nonplanar propeller-twisted and buckled structures for all berberine alkaloid forms, two rings i.e. C and D in the cation remain coplanar structure that is favored for the intercalation into DNA helix.

1.8.4 Anti-microbial, Anti-inflammatory, Anti-malarial activity and other effects

Protoberberines exhibit a wide range of biological and pharmacological activities. The biochemical properties of the alkaloid berberine, palmatine and sanguinarine has been explored to analyse their allelochemical activities [Schmeller et al., 1997]. Palmatine and berberine were found to be most active at the α_2 - receptor. Berberine has demonstrated a significant anti-microbial activity towards a variety of organisms including bacteria, fungi, protozoans, viruses, chlamydia and helminths [Creasy et al, 1979, Amin et al., 1969, Hwang et al., 2003, Okundae et al., 1994, Mahajan et al., 1982, Basha et al., 2002 & Nakamoto et al., 1990]. It can also be used as an antidiarrhea, antihypertension, antiarrhythmias and the antiiflamantory agent [Yamamoto et al., 1993, Takase et al., 1993; Ivanovska and Philipov, 1996; Tai et al., 1981, Shen et al., 1997, Lau et al., 2001, Huang et al., 1989, Fukuda et al., 1999a & Fukuda et al., 1999b]. Berberine, jatrorrhizine, and the crude extract of Mahonia aquifolium have shown strong activity against twenty clinical isolates of *Propionibacterium acnes* [Slobodnı´kova´ et al., 2004]. Berberine seems to be more active than jatrorrhizine against coagulase-negative staphylococci. The antifungal

activity tested against candida showed that only *C. tropicalis* was strongly inhibited by all of the agents tested. Experiments with the 8-alkyl and 8-phenyl-substituted berberines and their bromo derivatives showed that the introduction of hydrocarbon groups at position C-8 increased the antimicrobial activity [Iwasa et al., 1998]. The 12-bromo derivatives of the 8-alkyl- and 8-phenyl-protoberberines showed higher activity against the microorganisms tested than did their non–brominated analogs. The side carbon chain at position C-13 of quaternary protoberberines was investigated for its potential to increase the fungicidal and herbicidal activities [Iwasa et al., 2000]. While the tertiary forms of alkaloids did not exhibit significant activity, a few of the quaternary forms showed some activity against *Leptosphaeria nodrum* and *Puccinia recongita*. 13-Hexylberberine and 13-hexylpalmatine showed strong activity against *Staphylococcus aureus*, being more active than berberine and kanamycin sulfate. Both hexylderivatives possessed antifungal activity [Iwasa et al., 1997]. Berberrubine, the isolation artifact, was found to be active against *Mycobacterium smegmatis* [Gharbo et al., 1973]. The inhibitory activity of berberine against telomerase of human malaria P. falciparum has been studied by Sriwilaijareon et al., 2002. It was found to be a potent *in vitro* inhibitor of both nucleic acid and protein synthesis in human malaria *P. falciparum* FCR-3 [Elford, 1986; Vennerstrom and Klayman, 1988]. In vitro structure–activity relationship studies for antimalarial activity against P. falciparum showed that the oxygen substituent on rings A, C, and D and the position of the oxygen functions on ring D influenced the activity of the protoberberine alkaloids [Iwasa et al., 1998, 1999]. Shifting the oxygen function from C-5 and C-6 to C-6 and C-4 resulted in a significant increase of the activity. The activities of twenty alkaloids against *Plasmodium falciparum* (multidrug- resistant strain K1) has been studied *in vitro* [Wright et al., 2000]. The protoberberine alkaloids, dehydrodiscretine and

berberine, were found to have antiplasmodial IC (50) values less than 1M, while other alkaloids had values between 1 and 10M. Compounds were also assessed for antiamoebic and cytotoxic activities, but none was significantly active except for berberine, which was moderately cytotoxic. The anti-human cytomegalovirus (anti-HCMV) activity of berberine chloride was found to be equivalent to that of ganciclovir (GCV) which is a DNA polymerase inhibitor [Hayshi et al., 2007]. Palmatine inhibited carbachol-induced Ca^{2+}-activated Cl^- secretion and the carbachol-induced increase of intracellular Ca^{2+} concentration. Palmatine also inhibited cAMP-activated Cl^- secretion induced by prostaglandin E_2 (PGE_2) or forskolin [Wu et al., 2008]. The sedative effect of palmatine on locomotor activity and the concentration of monoamine in rats using behavioral and biochemical methods was investigated [Hsieh et al., 1993]. The sedative mechanism of palmatine may be related to a decrease in the concentration of catecholamine in the cortex and serotonin in brain stem and an increase in the concentration of 5-HT in the cortex. The effect of palmatine on isometric force and intracellular free calcium levels in isolated rat arterial strips has been studied [Chang et al., 1999]. These results suggested that vasodilatory effect of palmatine was mediated by reducing [Ca2']i as well as affecting [Ca"]i sensitivity of the contractile apparatus. Palmatine-induced [Ca"]i decreases appeared to involve decreases in both Ca'+ release from intracellular stores and Ca2+ influx through calcium channels. Shigeta, et al [Shigeta, et al., 2002] demonstrated the effect of berberine, palmatine and coptisine in enhancing the NGF- induced differentiation in rat PC12 cells and suggested their use in developing pharmacological agents which help to restore and maintain neural cells in the central nervous system. It has been found that palmatine improve the bladder outlet obstruction associated with benign prostatic hyperplasia by lowering the urethral

pressure through its 1-adrenoceptor antagonistic action. The antihyperglycemic and antioxidant activity of the root extract of *Berberis aristrata* (DA) was shown in alloxan induced diabetic rats [Singh & Kakkar, 2009]. The main constituents of the extract were found to be berberine, berbamine and palmatine. The EPR studies of the protoberberinium salts of berberine, palmatine and jatrorrhizine provided evidence of the formation of super-oxide anion radicals and singlet oxygen after UVA excitation which would be integrated in biological activity investigations [Brezova et al., 2004]. Inbaraj et al., 2001 studied berberine in the herb Goldenseal, which is widely used in many medical applications such as in eyewashes and skin lotions. They detected oxygen-centered radicals photogenerated by berberine in water and acetonitrile, by using electron paramagnetic resonance (EPR) spin trapping technique and (DMPO). UVA irradiation of HaCaT keratinocytes in the presence of berberine resulted in a decrease in cell viability and a 3-fold increase in DNA damage as measured by the comet assay. These findings suggested that exposure to sunlight or artificial light sources emitting UVA should be avoided when topical preparations derived from *Goldenseal* or containing berberine are used. Berberine and palmatine effect of the interaction between DNA and the photosensitizer singlet oxygen ($^1O_2$) were also investigated [Hirakawa et al., 2008]. The study showed that both the alkaloids bind to DNA, and their photosensitizer activity was markedly enhanced on binding to DNA .

1.8.5 Antitumour activity

Several protoberberine alkaloids and their derivatives have been investigated as potential antitumor agents. Sanders et al reported that palmatine along with other protoberberines exhibited greater in vitro cytotoxicity against cell lines derived from solid tumors (SF268) than leukemias (RPMI 8402) [Sanders et al., 1998]. Their studies revealed that the most important structure for determining selective

cytotoxicity is the imminium nitrogen at the ring junction. It has also been found that substituent on the A ring mainly 3, 4 methylenedioxy substituent affect consistency of selective cytotoxicity. Palmatine inhibited coralyne accumulation and also reduced cytotoxicity against SF268 cells, but not against RPMI 8402 cells. While berberine induced apoptosis in HL-60 cells, palmatine decreased only their viability with no sign of apoptosis [Kuo et al., 1995]. The ability of the protoberberines to act as a poison against Topoisomerase-I and Topoisomerase –II has been related to their antitumour activity. Replacement of OCH_3 group at position 7 in berberine with OH group, resulting in a derivative called berberrubine, induces a large change in the antitumor activity (Kim et al., 1998). The mechanism by which protoberberines kill the cancer cells is not fully understood, but the main mechanism is thought to be topoisomerase mediated strand breakage. The binding of the protoberberines to DNA is thought to stabilize the cleaved state of DNA so that it is not resealed, resulting in a permanent double strand break, leading to cell death. Topoisomerases are most active during cell cycle periods of high DNA synthesis. Generally speaking, the topoisomerase concentration of proliferating tumor cells is elevated substantially as compared to that in the normal somatic cells. This makes topoisomerases a semi-selective target for cancer chemotherapy. The DNA binding and topoisomerase poisoning properties of palmatine along with the other two protoberberine analogs i.e. DMC and DHDMC was investigated [Pilch et al., 1997]. They have employed spectroscopic, calorimetric, DNA cleavage, electrophoretic, and computer modeling techniques for these studies. It was found that the topoisomerase I poisoning by these protoberberine followed DHDMC> DMC > Palmatine. The binding studies revealed that the protoberberine analogs do not behave like classical intercalators. A "mixed mode" DNA binding model for protoberberines was presented in which a portion of

drug intercalates into the double helix, and the non intercalated portion of the ligand protrudes into the minor groove of the duplex. The comparison between DHDMC and palmatine showed that transferring methoxy group from the 11^{th} to 9^{th} position of the D ring in a protoberberine molecule whose 5, 6 positions were saturated was associated with a reduction in DNA binding affinity and TOPI poisoning activity. Li et al., 2000 further cross correlated the TOPI poisoning and DNA binding properties of the four protoberberine analogues and palmatine. These analogues differed with respect to the chemical substituents on their A- and/or D-rings. The results also suggested that modification of D ring influenced both the DNA binding and Topoisomerase I poisoning properties whereas, modifications of the A ring has a negligible impact on DNA binding but has profound impact on Topoisomerase I poisoning. They proposed a mechanistic model in which both ligand-DNA and ligand-enzyme interactions were important for the poisoning of topoisomerase I by protoberberines, with the DNA-directed interactions involving ring D and the enzyme-directed interactions involving ring A. Characterization of the quaternary berberines modified at the position C-9 showed that the berberine derivatives, especially those with a primary amino group, strongly bind with calf- thymus DNA, presumably via an intercalation mechanism [Pang et al., 2005]. Structure- activity relationships of the protoberberines analogs demonstrated that substituition at the C-9 position is an important determinant of the biological activity [Park et al., 2004]. Kluza et al., 2003 reported that Burasine (palmatine) does not promote DNA cleavage by topoisomerase I and topoisomerase II. Their studies have shown that the drug burasine has limited cytotoxicity and has minimal effect on the viability of Human leukemia cell line HL-60 as compared to pro-apoptotic drug camptothecin. The bridged berberine derivatives compounds with a propyl chain exhibited highest

binding affinity to DNA [Chen et al., 2005a, Qin et al., 2006]. The cytotoxicity of two protoberberine alkaloids: berberine and lincangenine, their 8-hydroxy-7, 8-dihydro-derivative and tetrahydroprotoberberine:thaicanine, was evaluated [Orifolia et al., 2000]. Berberine showed the highest cytotoxicity among all the compounds tested. The structural requirements concerning antitumor activity are in connection with the planarity and rigidity of molecules, alkyl substituting on C-8, as well as the presence of methoxy or methylenedioxy groups on A and D rings. Berberine also showed antiproliferating and cytotoxic effects on the human cancer HeLa and murine leukemia L1210 cells [Jantova et al., 2003]. Berberine induces apoptosis in hepatoma and human promonocytic U937 cells through a mitochondrial /caspases dependent pathway (Hwang et al., 2006; Jantova et al., 2007). It has been found that toxic concentrations of berberine induced dual necrotic/apoptotic cell death in B16 cells, while nanomolar concentrations of berberine demonstrated the reorganization of the actin cytoskeleton [Letasiova et al., 2005]. *In vivo* studies of berberine activity revealed that it significantly reduces tumor weight in mice implanted with B16 melanoma cell [Letasiova et al., 2006]. The cytotoxic activity of twenty four quaternary protoberberine alkaloids was evaluated on thirty eight human cancer cell lines [Iwasa et al., 2001]. Six compounds were found to be cytotoxic and some others exhibited lower levels of cytotoxicity. From a structure–activity point of view, some trends were observed. For berberine and palmatine derivatives bearing a 13-alkyl side chain, the cytotoxicity increased parallel to the number of CH_2 units in the side chain. 12-Bromo-8-hexylberberine was more cytotoxic than the corresponding 8-phenyl and 8-butylderivatives, suggesting that the length of the carbon unit at C-8 also influences the cytotoxicity. Bromination at C-12 increased the cytotoxicity. These studies showed a clear relationship between structure and activity of the alkaloid. Slaninova´

et al., 2001 investigated the effects of berberine, coptisine, and some benzo[c]phenanthridine alkaloids on the yeasts Saccharomyces cerevisiae and Schizosaccharomyces japonicus. The protoberberine alkaloids exhibited some effects; however, these effects were significantly smaller than those of the benzophenanthridines. Berberine treatment on nasopharyngeal carcinoma cells (NPC/HK1) demonstrated a high killing efficacy [Szeto et al., 2002]. The DNA damaging effect and the inhibition of DNA repair contributing to the cytotoxic activity in the cancer cells was considered to be the mechanisms of action of berberine on cancer cell. The introduction of a side chain with proper length of methylene and terminal amino group at position 9 of berberine significantly strengthen the binding affinity with G-quadruplex, resulting in increasing inhibitory effects on the amplification of telo21 DNA and on the telomerase activity [Zhang et al., 2007]. The enhancement in the apoptosis rate of human hepatocellular carcinoma SMMC – 7721 through synergy of berberine and evodiamine has been reported [Wang et al., 2008]. Recent findings has shown that berberine induced apoptosis in human tongue cancer SCC-4 cells in vitro and also inhibited tumour growth in xenograft animal model [Ho et al., 2009]. Coralyne a synthetic protoberberine alkaloid has shown more pronounced antitumor activity relative to berberine and palmatine. It has shown significant antitumor activity *in vivo* in mice against L1210 and P388 leukemias [Cheng et al., 1974: Chang, et al., 1976]. It has been shown that the presence of methyl substituent at the 8^{th} position and unsaturation at the 5, 6 position of coralyne are strongly associated with their antitumor activity against L1210 and P388 leukemia in mice. It has been proposed that the ability of coralyne binding to duplex and triplex DNA has contributed to its observed anti-leukemic activity [Wilson, et al., 1976 and Lee et al., 1999]. The antitumor activity of coralyne relative to its low cytotoxicity,

prompted studies on the synthesis of a number of derivative, as well as a practical large scale synthesis of coralyne itself.

1.9 SCOPE OF THESIS

Interactions of small molecules with DNA have been studied extensively in the hope of learning design principles for targeting of specific DNA sequences in order to control gene expression. Many small molecules that bind to DNA are clinically proven as therapeutic agents although their exact mode of action remains incompletely defined. There is a renewed focus on the use of small molecules as therapeutic agents in the biotechnology industry. Several physico-chemical techniques like absorbance, fluorescence, circular dichroism, etc., were used for the drug-DNA interaction studies of palmatine with DNA. These studies are aimed in particular at the development of new anticancer drugs whose anti-tumor efficacy is associated with their interactions with DNA, i.e. for which DNA is the main target inside tumor cells. Understanding the structure-function directed macromolecule-target interactions of anticancer drugs, and rationally design the improved anticancer agents are the long-term research goals of our laboratory. The facilities of this laboratory make it possible to understand drug-DNA interactions, which are needed for design and synthesis of new cytostatics and suggestions for structure-pharmacological activity. This thesis deals with (i) obtaining the structure of the drug using Nuclear Magnetic Resonance (NMR), Restrained Molecular Dynamics approach along with the quantum mechanical calculations (ii) structure elucidation of the anticancer drug complexed with oligodeoxynucleotides (iii) the investigation of the relationship between the structure and biological activity of the drug (iv) suggesting the functional groups of drug which may be modified to get the drug with better anticancer activity and lesser

side effects. The Ph.D thesis work has been reported in the form of six chapters. Chapter 1 contains introduction of the subject as well as highlights the earlier work carried out in literature. Chapter 2 deals with the materials and methods used. Chapters 3 deal with NMR, restrained Molecular Dynamics and quantum mechanical calculations studies of the drug palmatine. Chapter 4 deals with the studies of the Drug-DNA interaction by using absorption and fluorescence spectroscopy. In chapter 5 the results of ^{31}P and ^{1}H NMR studies of Palmatine- d-$(CGATCG)_2$ complex along with the Restrained Molecular Dynamics have been discussed. The helical parameters and backbone torsional angles etc. have been analyzed using CURVES software version 5.1. Sequence dependent variations have been observed. Besides this, fluorescence life-time measurement studies and Diffusion Ordered Spectroscopy (DOSY) studies were performed to study the formation of the complex. All these studies can be used as a part of strategy of regulation of the medico-biological activity of aromatic drugs in clinical practice, e.g., in reduction of the consequences of drugs overdosing during chemotherapy or in production of anti-mutagenic effects in vivo. Chapters 6 summarize and conclude the highlights of the present work.

Chapter 2

Materials and Methods

2.1 MATERIALS

The deoxyribonucleic acid sequences d-$(CGATCG)_2$, d-$(CGTACG)_2$, $(CGATCGCGATCG)_2$, $(CGTACGCGTACG)_2$, $(CGCGCGCGCG)_2$, $(ATATATATAT)_2$, $(CCAATTGG)_2$, Calf thymus DNA, Poly (dA-dT), poly (dG-dC), palmatine, Deuterium Oxide (D_2O) with isotopic purity 99.96% and (Trimethylsilyl) propionic-2, 2, 3, 3-d_4 acid sodium salt (TSP) were purchased from Sigma Chemical Co., USA. HPLC grade reagents like sodium dihydrogen phosphate (NaH_2PO_4), disodium hydrogen phosphate (Na_2HPO_4), sodium chloride (NaCl), etc. used for phosphate buffer preparation were purchased from Qualigens Fine Chemicals India, Ltd.

2.2 UV-VISIBLE AND FLUORESCENCE SPECTROSCOPY

2.2.1 Preparation of Buffer Solution

The stock buffer BPES was prepared by mixing 1.5 mM of $Na_2HPO_4.2H_2O$ and 0.5 M of $NaH_2PO_4.H_2O$ to get 10 mM Phosphate buffer (pH=6.8 ± 0.2) at room temperature with 10 mM NaCl and 0.25 mM EDTA. The buffer was filtered through 0.2 μM pore Millex Millipore filters.

2.2.2 Preparation of palmatine solution

Palmatine solution was prepared freshly by dissolving it in to the BPES buffer (pH 7.0). The concentration of palmatine in the buffer solution was determined spectrophotometrically by using the extinction coefficient ε = 25,000 $m^{-1}cm^{-1}$ at 343 nm. Palmatine concentration of 7-10 μM was used for all the experiments.

2.2.3 Preparation of DNA Samples

The DNA samples were prepared in 10 mM BPES buffer containing 10 mM NaCl. The concentration of all DNA samples were determined by absorbance measurement using their standard values of the molar extinction coefficients as given in Table 2.1.

Table 2.1 Extinction coefficient (ε) of various DNA and oligonucleotides

DNA	Extinction coefficient (ε) ($M^{-1}cm^{-1}$ at 260 nm)
CT DNA	6600
Poly d(A-T)	8600
Poly d(G-C)	7750
d-$(CGATCG)_2$	57200
d-$(CGTACG)_2$	57600
d-$(CGTACGCGTACG)_2$	97200
d-$(CGATCGCGATCG)_2$	97200
d-$(ATATATAT)_2$	111200
d-$(CGCGCGCG)_2$	84800
d-$(CCAATTGG)_2$	76300

The amount of the samples required in the absorbance and fluorescence spectroscopy is very small, so it is not advisable to weigh the substance. There are chances of losing the sample, while transferring it. So, to prepare the solutions, a small amount of the sample was dissolved in a known volume of the solvent and the

absorbance was recorded on a CARY-100 Bio, UV-Visible spectrophotometer over a suitable range. The concentration of the stock solution was calculated by using the Beer Lambert's law-

$$A = \varepsilon.c.l$$

Where,

A= Absorbance

c = Concentration of solution (in moles/ liter)

ε = Molar extinction coefficient (in $M^{-1}cm^{-1}$)

l = Path length of quartz cuvette (in cm)

From the stock solution of the known concentration, the solution of desired concentration was prepared by diluting the sample suitably, in BPES buffer and scanning the sample within the range of 200-800 nm for palmatine and 200-400 nm for DNA samples. The absorbance at the λ_{max} is noted for each scan and the concentration is calculated with the Lambert-Beer's equation considering the known molar extinction coefficient of palmatine and DNA. The path length of the cuvette is fixed in each case i.e., 1 cm. The concentration of samples was taken in the range of 100-200 μM for CT DNA, poly dG-dC and poly dA-dT, 20-50 μM for oligonucleotides and 7-10 μM for palmatine.

2.2.4 Spectrophotometric Titration

Absorbance measurements were performed in Carry l00 Bio (Varian) UV-Visible spectrophotometer equipped with the Peltier thermostat cell holder and quartz cuvette (optical path length 1 cm). Absorbance titration experiments of the palmatine-DNA complexes were performed by keeping the drug concentration fixed and

increasing the concentration of DNA with continuous stirring throughout the course of titration. The spectrum was recorded in the wavelength range 220-700 nm after each addition. The absorbance maxima at 344 nm for alone drug was denoted by A_o. During the course of titration absorption maxima (A) was recorded at each step. The change in the absorbance of the drug (Δ A) on addition of nucleic acid sequences is calculated by

$$\Delta A = A_o - A$$

2.2.5 Fluorimetric Titration

Fluorescence spectra were measured on Fluorolog-3 spectrofluorimeter LS55 (HORIBA Jobin Yvon Spex®). The same sample which was used for UV –visible studies was used to record the fluorescence spectrum at each titration step. This action reduces any error or differences in results through both the techniques due to changes of sample conditions. The emission spectra were recorded in the range of 400-800 nm. All the titrations experiments were carried out at 25 ^{0}C and change in fluorescence intensity was recorded. At each step, the fluorescence intensity maxima (I) were recorded at 530 nm. The excitation wavelength was kept as 350 nm for all the experiments. The fluorescence intensity for pure drug was denoted by I_0. At each step of titration the enhancement in fluorescence (I) was recorded. The change in fluorescence intensity (ΔI) in each case was calculated by:

$$\Delta I = I - Io$$

2.2.6 Life Time Measurement using Fluorescence Spectroscopy

Model FluoroLog®-TCSPC, make HORIBA Jobin Yvon Spex® was used for the life time measurement study. This is an ultra compact fluorescence lifetime

spectrometer based on time correlated single photon counting (TCSPC) and ready to perform time-domain lifetime spectroscopy building up a histogram of the sample's fluorescence decay. This instrument has sub-ns pulsed LED. For our study, we used fixed-wavelength Nano LED of 470 nm. Standard optical pulse durations are <1.5 ns for LEDs. Resolution 0.2 nm, accuracy ± 0.5 nm, speed 150 nm/s, range 0-1300 nm, TAC range given is 50 nm, excitation wavelength is 350 nm for the experiment. 2:1 complex of palmatine-d-$(CCAATTGG)_2$ was used for this study.

2.3 NUCLEAR MAGNETIC RESONANCE STUDIES

2.3.1 Preparation of drug solution

Solution of Palmatine (30.0 mM) was prepared by dissolving the known quantity of sample in D_2O. It was lyophilized and redissolved in D_2O and the process was repeated twice. The final concentration was checked by absorbance measurements at wavelength of 344 nm using Cary 100 UV-visible spectrophotometer. The extinction coefficient (ε) value used for palmatine was ε = 25 000 M^{-1} cm^{-1}. TMS signal was used as internal NMR reference for recording spectra in the solvent.

2.3.2 Preparation of DNA solution

Solution of purified deoxynucleotide, d–$(CGATCG)_2$ (3.14 mM duplex concentration) was prepared by dissolving known quantity of sample in 0.6 ml of BPES buffer (10 mM, pH 6.8 ±2) having 10 mM Na^+ salt. The sample was lyophilized and redissolved in D_2O and the process was repeated twice. Finally, d-$(CGATCG)_2$ was dissolved in 0.6 ml of D_2O and its concentration was determined by absorbance measurements at 260 nm using the extinction coefficient (ε) value =57,200 M^{-1} cm^{-1}. Ethylene diamine tetra acetic acid (EDTA), 0.1 mM, was added to

suppress paramagnetic impurity, which may cause line broadening during NMR measurements. Typically 1µl of 0.1 M solution of TSP was added to the complex of d-$(CGATCG)_2$ as an internal reference.

2.3.3 Preparation of complex

3.14 mM d-$(CGATCG)_2$ and 30.0 mM Palmatine samples were taken as a stock solution for preparation of the complex. The complex of d-$(CGATCG)_2$ and palmatine was prepared by titration. 120 µl of 30.0 mM palmatine was added in steps of 6 µl to 0.6 ml of 3.14 mM d-$(CGATCG)_2$ sample during titration in order to make 2:1 complex of palmatine: d-$(CGATCG)_2$. The concentration of d-$(CGATCG)_2$ (N_1) in total volume of 0.55 ml is determined as follows:

$$N_1V_1 = N_2V_2$$

$$N_1 \times 556 = 3.14 \times 550$$

$$N_1 = 3.11 \text{ mM}$$

The concentration of palmatine in this solution is determined as follows:

$$N_3V_3 = N_4V_4$$

$$N_3 \times 556 = 30 \text{ mM} \times 6$$

$$N_3 = 0.32 \text{ mM}$$

The concentration of Palmatine (D), d-$(CGATCG)_2$ (N) and drug/ nucleotide (D/N) ratio are shown in Table 2.2.

Table 2.2: Various concentration ratios (D/N) for the complex formed between palmatine and d-$(CGATCG)_2$

Nucleotide Concentration (mM) = N	Drug Concentration (mM) = D	D/N
3.14	0.00	-
3.11	0.32	0.10
3.08	0.64	0.21
3.05	0.95	0.31
3.02	1.25	0.41
2.99	1.55	0.52
2.96	1.84	0.62
2.93	2.13	0.73
2.90	2.41	0.83
2.87	2.68	0.93
2.84	2.95	1.03
2.81	3.21	1.14
2.78	3.47	1.25
2.75	3.72	1.35
2.73	3.97	1.46
2.70	4.22	1.56
2.67	4.46	1.67
2.64	4.69	1.77
2.62	4.92	1.87
2.59	5.15	2.00

2.4 METHODOLOGY

2.4.1 NMR Spectroscopy- Technique for biological structure determination

Nuclear Magnetic Resonance (NMR) spectroscopy stand today as one of the most powerful physical methods to probe the biological systems and processes. It has proved to be a valuable tool in the determination of structure and dynamics of biological macromolecules in aqueous solution, under conditions similar to those in the real systems.

2.4.1.1 The phenomenon

The subatomic particles (electrons, protons and neutrons) spin on their axis. A nucleus (of spin 1/2) when placed in a static magnetic field behaves like a small magnet. This nucleus is in the lower energy level (i.e. its magnetic moment does not oppose the applied field). In the absence of an external magnetic field, these orientations are of equal energy. Each level is given a magnetic quantum number, m, characterizing Z component of spin, I. On interaction with magnetic field, nuclei with spin I >1/2 distributes themselves among 2I + 1 energy level with the separation by:

$$\Delta E = h \gamma B_0$$

The overall spin, I, is important. A nucleus with spin 1/2 will have 2 possible orientations (Fig. 2.1a). These spins are capable of interacting with a beam of electromagnetic radiations. These energy levels correspond to the spins aligned along and against the applied magnetic field, B_0. The spin oriented to oppose B_0 has higher energy. These spin do not align perfectly along B_0 and this give rise to a permanent torque. The nucleus also has the property of angular momentum because of its spin

and thus as a result the nuclei precess (Fig. 2.1b), with frequency of precession given by:

$$\omega_0 = \gamma B_0$$

where, γ is proportionately constant, ω_0 is the resonant or Larmor frequency in radians/second and B_0 is the magnitude of the applied magnetic field. When the frequency of the beam is same as that of precessing spin then absorption of energy takes place, which causes the nuclei to flip from a lower energy state to a higher energy state by a process termed resonance (Fig 2.1c). In an NMR sample there are many molecules, each with its spin precessing about B_0 at same frequency and result in a net magnetization of M_z oriented along the Z-axis. On application of a rotation radio frequency field with frequency at or near $\omega_0 = \gamma B_0$, the spin resonate giving rise to net M_{xy} component which is phase coherent. The following are the spectral parameters in NMR:

2.4.1.2 Chemical Shift

When an atom is placed in a magnetic field, its electrons circulate about the direction of the applied magnetic field. This circulation causes a small magnetic field at the nucleus which opposes the externally applied field, B_0. The difference between the applied magnetic field and the field at the nucleus is termed as nuclear shielding. The induced field is directly proportional to B_0. This is represented by the equation:

$$Beff = B_0 (1-\sigma)$$

where, σ is the shielding constant which depends on the nature of electrons around the nucleus. The chemical shift of a nucleus is the difference between the resonance frequency of the nucleus and a standard, relative to the standard. Chemical shift is a function of the nucleus and its environment.

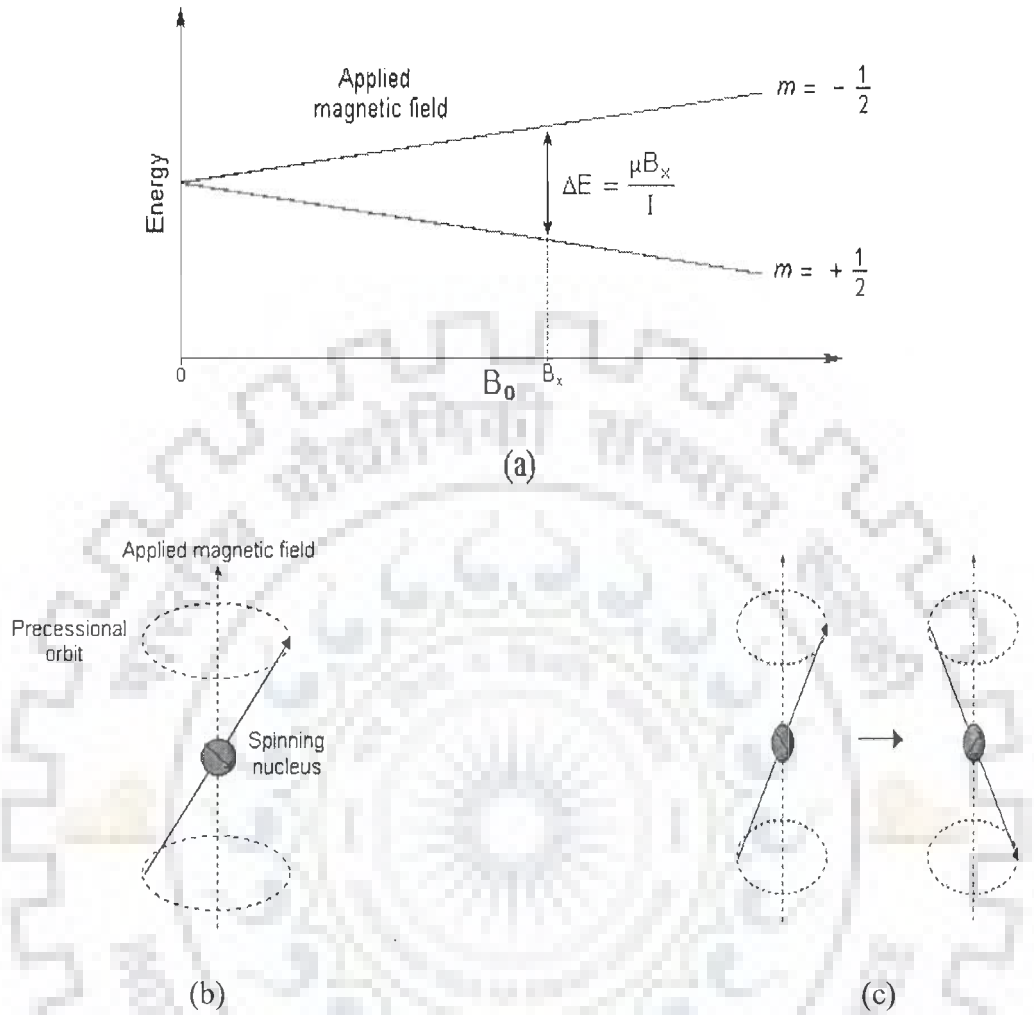

Fig. 2.1: (a) Energy levels for a nucleus with spin quantum number ½ (b) Precessional motion by the nucleus spinning on its axis in presence of the external magnetic field (c) Flipping of the magnetic moment on absorption of the radiations

It is reported in ppm and given the symbol delta, δ. It is measured relative to a reference compound. For ^1H NMR, the reference is usually tetramethylsilane, $Si(CH_3)_4$, abbreviated TMS.

$$\delta = 10^6 \times \frac{\delta_{ref} - \delta_{obs}}{\delta_{ref}}$$

where, δ_{ref} is the position observed for a reference compound and δ_{obs} is the position of the signal of interest. There are useful general conclusions that can be drawn from specific chemical shift value, or changes due to the binding of the ligand.

2.4.1.3 Spin-spin coupling constant (J)

Nuclei experiencing the same chemical environment or chemical shift are called equivalent. Those nuclei experiencing different environment or having different shifts are non-equivalent. Nuclei, which are close to one another, exert an influence on each other's effective magnetic field. This effect shows up in the NMR spectrum when the nuclei are non-equivalent. If the distance between non-equivalent nuclei is less than or equal to three bond lengths, this effect is observable. This effect is called spin-spin coupling or J coupling and is expressed in Hertz. This coupling causes splitting of lines. The appearance of multiplet patterns depends on relative magnitude of δ and J for coupled nuclei. Vicinal couplings (^3J) display a characteristic dependence upon the involved dihedral angle (Fig. 2.2 a) according to the relation dihedral couplings;

$$^3J = 8.5 \cos^2\theta - 2.8$$

$$^3J = 9.5 \cos^2\theta - 2.8$$

This relationship is known as the Karplus relation. Fig. 2.2a and 2.2b shows the definition of dihedral angle and relationship between J couplings and dihedrals.

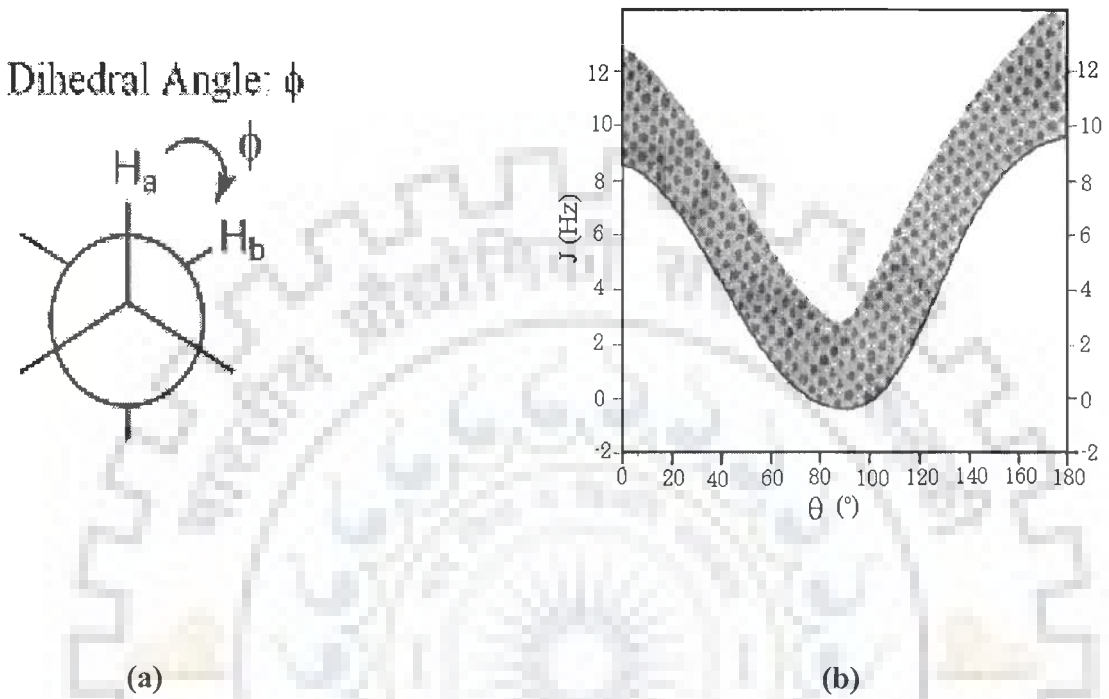

Fig. 2.2: (a) Definition of the dihedral angle (b) Karplus Curve showing relationship between J couplings and dihedral angle

2.4.1.4 Relaxation process

The magnetization does not precess infinitely in the transverse plane but turns back to the equilibrium state. This process is called relaxation. Two different time-constants describe this behaviour. The importance of these phenomena is in the nuclear Overhauser effect (NOE), which can be used to probe internuclear distances in a molecule. There are two major relaxation processes namely, Spin-lattice (longitudinal) relaxation (T_1) and spin-spin (transverse) relaxation (T_2). The relaxation time T_1 represents the "lifetime" of the first order rate process that returns the magnetization to the Boltzman equilibrium along the +Z axis. The components of the

lattice field can interact with nuclei in the higher energy state, and cause them to lose energy (returning to the lower state). The energy that a nucleus loses increases the amount of vibration and rotation within the lattice. The relaxation time, T_1 depends on the motion of the molecule. As mobility increases, the vibrational and rotational frequencies increase, making it more likely for a component of the lattice field to be able to interact with excited nuclei. T_1 spin-lattice relaxation rate is then measured by plotting M as a function of τ:

$$M(\tau) = Mo\ (1 - 2\exp^{-(\tau / T1)})$$

T_2 represents the lifetime of the signal in the transverse plane (XY plane) and it is this relaxation time that is responsible for the line width. In Solution NMR, very often T_2 and T_1 are equal. The very fast spin-spin relaxation time provides very broad signals. The transverse relaxation constant T2 is related to the linewidth of the signals. The width of the signal at half height is given by:

$$(\Delta\omega)_{1/2} = 1 / \pi\, T_2$$

Fast decay leads to broad signals, slow decay to sharper lines. The transverse relaxation constant T2 of spin I=1/2 nuclei is mainly governed by the homogeneity of the magnetic field and the strength of the dipolar interaction with other I=1/2 nuclei depending on the number and the distance of neighbouring nuclei the overall tumbling time of the molecule which is related to its size. Transverse relaxation (T_2) is faster than longitudinal relaxation. T_2 spin-spin relaxation rate is measured by plotting M as a function of τ:

$$M\ (\tau) = M_0\ [\exp\ (-\tau/T2)]$$

2.5 2D NMR SPECTROSCOPY

In one-dimensional pulsed Fourier transform NMR the signal is recorded as a function of one time variable and then Fourier transformed to give a spectrum, which is a function of one frequency variable. In two-dimensional NMR the signal is recorded as a function of two time variables, t_1 and t_2, and the resulting data Fourier transformed twice to yield a spectrum, which is a function of two frequency variables. The two-dimensional signal is recorded in the following way. First, t_1 is set to zero, the pulse sequence is executed and the resulting free induction decay recorded. Then the nuclear spins are allowed to return to equilibrium, t_1 is then set to $\Delta 1$, the sampling interval in t_1, the sequence is repeated and free induction decay is recorded and stored separately from the first. Again the spins are allowed to equilibrate, t_1 is set to $2\Delta 1$, the pulse sequence repeated and a free induction decay recorded and stored. The whole process is repeated again for $t_1 = 3\Delta 1$, $4\Delta 1$ and so on until sufficient data is recorded, typically 50 to 500 increments of t_1. Thus recording a two-dimensional data set involves repeating a pulse sequence for increasing values of t_1 and recording a free induction decay as a function of t_2 for each value of t_1. The general scheme for two-dimensional spectroscopy is (Fig. 2.3):

Preparation time: The sample is excited by one or more pulse. This consists of a delay time or a sequence of pulses separated by fixed time intervals saturation sequences. Thermal equilibrium is attained during this period.

Evolution Period (t_1): The resulting magnetization is allowed to evolve for the first time period, t_1. The evolution period is the pulse sequence element that enables frequency labelling in the indirect dimension. Further, one or several radiofrequency pulses may be applied to create coherence.

Mixing time (τ_m): During this period coherence is transferred between spins. Mixing sequences utilize two mechanisms for magnetization transfer: scalar coupling or dipolar interaction (NOE). After the mixing period the signal is recorded as a function of the second time variable, t_2. This sequence of events is called a pulse sequence.

Detection Period: The signal is recorded during the time t_2 at the end of the sequence, detection, often called direct evolution time; during this time the magnetization is labelled with the chemical shift of the second nucleus. The data is recorded at regularly spaced intervals in both t_1 and t_2.

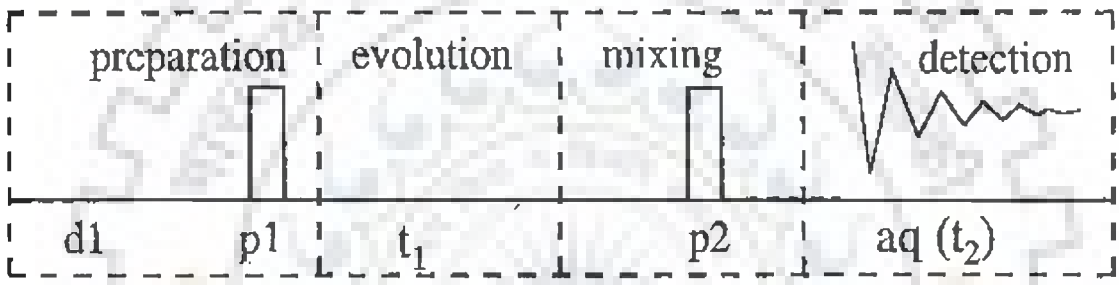

Fig. 2.3: Four different time segments of a 2D NMR experiment namely (i) preparation period (ii) evolution period (t_1) (iii) mixing period (τ_m) (iv) detection period (t_2)

2.5.1 Two-dimensional correlation spectroscopy (2D-COSY)

The COSY experiment is used in determining which atoms are connected through bonds. The basis of COSY experiment whose pulse sequence is the classical Jeener sequence (Jeener, 1971). After the preparation period of 90° pulse constitutes brief mixing period whose effect is to mix single quantum coherence into a whole range of orders of coherence. However, only the single quantum coherence will give rise to any measurable signal during the detection period. The mixing process interchanges orders of coherence, mixes coherence among the transitions associated with a given spin and exchanges coherence between spins having a mutual scalar coupling. Thus a magnetization, initially associated with the A spin of an A-X spin system, may be

transferred to spin X through the scalar coupling, J_{ax}. Therefore the A magnetization in the X-Y plane will also depend upon the Larmor frequency ωx and the 2D COSY will show signals with frequency coordinates (ωA, ωX) and (ωX, ωA) as well as (ωA, ωA). The former are the characteristic cross peaks of COSY spectrum and the latter, the diagonal peaks, which corresponds to 1D spectrum. COSY experiment can be carried out with special phase cycling and data processing to change the 2D line shape into pure 2D absorption mode, allowing the use of phase-sensitive display. There are two different methods in use, the first requires the results of two complete COSY experiments with different phase cycling to be added (States et al, 1982) and the second known as TPPI (Time proportional phase incrementation) method uses a single experiment with phase cycling which changes with t1 increment (Bodhenhausen et al, 1977; Keeler and Neuhaus, 1985; Marion and Wuthrich, 1983; Redfield et al, 1975). The phase sensitive COSY spectra have cross peaks in anti phase. The antiphase multiplet structure of a cross peak only occurs in the active coupling giving rise to cross peak. Extra splittings present in multiplet but which do not give rise to cross peaks are called passive couplings and appear in phase. Thus, the advantage of phase sensitive COSY is that the phase relation between peaks can be used for accurate assignment and calculation of coupling constants.

2.5.2 Phase sensitive COSY: Double quantum filtered COSY (DQF-COSY)

The experiment uses a pulse sequence 90_{ϕ}-t_1-90_{φ}-90_{ζ}-t_2 where ϕ, φ and ζ are the appropriate phase cycles [Piantini et al, 1982]. In double quantum filter COSY experiment the resonance from a COSY experiment is passed through a double quantum filter, thereby removing methyl and other singlets from the final spectrum. The short delays, Δ, immediately before and after the final pulse, are of order of

microseconds. Twice as many transients are needed in these experiments to achieve the same signal to noise ratio than in conventional COSY. Another advantage of DQF COSY is that it converts the phase of COSY diagonal signals from dispersive antiphase to absorptive antiphase. These signals then do not interfere with the cross peaks. So, the cross peaks lying close to diagonal can be observed in double quantum filtered phase-sensitive COSY. Double filter COSY can be used to determine the coupling constants [Celda et al, 1989; Gochin et al, 1990].

2.5.3 Nuclear Overhauser Enhancement Spectroscopy (NOESY)

Nuclear Overhauser Enhancement Spectroscopy is one of the most useful techniques as it allows correlating nuclei through space (distance smaller than 5Å). By measuring cross peak intensity, distance information can be extracted. The exact three–dimensional conformation of the molecule can be deduced by 2D Nuclear Overhauser Enhancement Spectroscopy. It gives us information about cross relaxation occurring between a pair of protons through dipole–dipole interaction and it gives us an idea about pairs of protons present in close proximity to each other in space. The pulse sequence starts as usual with a 90° pulse followed by an evolution time t_1. This delay is varied systematically as usual to provide chemical shift information in the F1 domain. Then a 90° pulse transmit some of the magnetization to the Z–axis and during the following mixing period, the non–equilibria Z–component will exchange magnetization through relaxation (dipole–dipole mechanism). This exchange of magnetization is known as NOE (Nuclear Overhauser Effect). After some time (shorter than the relaxation time T1), the transverse magnetization is restored and detected. If relaxation exchange (or chemical exchange) has taken place during the mixing time, τ_m, cross peaks will be observed in the spectra during t_2 which has

modulation frequencies different from their precessing frequencies during t_1. The complete set of data S (t_1, t_2) after Fourier transformation with respect to both t_1 and t_2 yields a 2D spectrum. The magnetization components which have the same frequency in time domains t_1 and t_2 lie along the diagonal of the NOESY spectrum, while those along magnetization components which have crossed over during the mixing time, τ_m, owing to NOE, lie on both sides of the diagonal and are called cross peaks. The phase cycling ensures proper detection of NOESY signal. In small / medium size molecules, the mixing time can be selected to be about 80% of the relaxation time. For larger molecules, shorter mixing time should be used to avoid "spin–diffusion" problems. In NOESY experiment, the distinction between cross peaks originating from NOE effect and those originating from chemical or conformational exchange is not easy. In small molecules, having long correlation time, $\omega\tau_c >> 1$, (where ω is the angular frequency $\omega = \gamma B$ and τ_c is the effective correlation time) and the phase of the peak can be used as evidence i.e., Diagonal signal phased "up"; NOE cross peak is phased "down"; Chemical Exchange cross peak is phased "up" for large molecule, having short correlation time, the phase of the diagonal, the NOE cross peak and the exchange cross peak is the same. A large number of cross peaks are observed, each indicating a NOE or exchange between nuclei of interest of the corresponding diagonal. Exchange also gives rise to cross peaks identical to negative NOE (same sign of the diagonal) and can only be distinguished from NOE by the use of the rotating frame NOE method (ROESY). The data in the NOE experiment is analyzed by measuring the peak volume of a cross peak in a series of 2D experiment with different mixing times,τ_m. The initial rate of growth of the NOE is directly proportional to $1 / r^6$ to calculate the proportionality constant; the rate is compared with some known distance.

2.5.4 Rotating–frame Overhauser Effect Spectroscopy (ROESY)

ROESY is an experiment in which homonuclear NOE effects are measured under spin–locked conditions. ROESY is especially suited for molecules with motional correlation times (ι_c) such that $\omega\iota_c \approx 1$, where ω is the angular frequency $\omega = \gamma B$. In such cases the laboratory–frame NOE is nearly zero, but the rotating–frame NOE (or ROE) is always positive and increases monotonically for increasing values of ι_c. In ROESY the mixing time is the spin–lock period. During this time spin exchange occurs among spin–locked magnetization components of different nuclei (recall that spin exchange in NOESY occurs while magnetization is aligned along the z axis). Contrary to NOE that can be positive (for small molecule), negative (for large molecule) or null (if the correlation time happen to cancel the NOE), the ROE (NOE in the rotating frame) is always positive. Alternation in sign of the ROE effect allows distinguishing the "three–spin effect" from true small ROE). Different spectral density functions are relevant for ROESY than for NOESY and these causes the ROE's to be positive for all values of τ_c. ROESY spectra can be obtained in 2D absorption mode. This is also useful for the identification of certain artifacts. Spurious cross peaks, both COSY–type and TOCSY–type, can be observed due to coherence transfer between scalar coupled spins. COSY–type artifacts (anti–phase) arise when the mixing pulse transfers antiphase magnetization from one spin to another (the long spin–lock pulse acts like the mixing pulse in COSY). TOCSY–type artifacts (which have the same phase as the diagonal peaks, while ROESY cross peaks have the opposite phase) arise when the Hartmann–Hahn condition is met (e.g., when spins A and B have opposite but equal offsets from the transmitter frequency or when they have nearly identical chemical shifts). In general, to minimize these artifacts, it is suggested to limit the strength of the spin–locking field. The peak phase behavior from the ROESY

experiment is as follows: If diagonal peaks are phased "up" or positive; ROE cross peaks will be phased "down" or negative; HOHAHA peaks will be phased "up" or positive; Exchange peaks will be phased "up" or positive.

2.5.5 Heteronuclear Single Quantum Correlation (HSQC)

The HSQC experiment is in fact a double INEPT experiment. This experiment correlates protons with their directly attached heteronuclei. Proton magnetization is detected (during t_2–detection time) while the low–gamma nuclei evolve during the evolution time (t_1). Because of the detection of the high frequency nuclei, this sequence is very sensitive. The enhancement in sensitivity this experiment permits is much greater than the enhancement obtained by simple NOE (Nuclear Overhauser Effect). This is why this experiment has been referred to as the "OverBodenhausen" experiment. The HSQC experiment starts with proton magnetization.

Therefore the recycle time is based on proton relaxation time ($1.26 * T_1$). The first INEPT step is used to create proton antiphase magnetization ($2\ \tau$ delay) which is then transferred to the directly attached heteronuclei (Carbon, Nitrogen). This X nuclei magnetization is left to evolve with its chemical shift (during t1–evolution time). The effect of proton coupling and chemical shift is removed by the use of a 180° proton pulse applied at mid evolution time. The double 90° pulse applied to both nuclei (in the beginning of the last INEPT step) transfers the magnetization back to proton as an anti–phased magnetization, which will then refocus during the last ($2\ \tau$ delay). The proton in–phase magnetization can then be detected in the presence of the X–nuclei decoupler.

2.5.6. Heteronuclear Multiple Bond Correlation (HMBC)

The HMBC experiment detects long range coupling between proton and carbon (two or three bonds away) with great sensitivity. The length of the τ (tau) delay can be adjusted to detect relatively large coupling constants (4–10 Hz) τ (tau) = 0.06 s or smaller couplings (2–7 Hz) τ = 0.1 s. In this sequence, the first 90° pulse on Carbon–13 serves as a low–pass filter that suppresses one–bond correlation and passes the smaller coupling. This pulse creates multiple quantum coherence for the one–bond coupling, which is removed from the spectra by alternating the phase of the Carbon–13 pulse. The second 90° pulse on C–13 creates multiple quantum coherence for the long–range couplings. After the evolution time t1, the magnetization is converted back into detectable single quantum proton magnetization. The carbon decoupler is never used in this sequence: therefore the protons displays homonuclear as well as heteronuclear couplings. This technique is very valuable to detect indirectly quaternary carbons coupled to protons– especially useful if direct Carbon–13 is impossible to obtain due to low amount of material available. This very useful sequence provides information about the skeleton of a molecule. It could be an alternative to the 2D–INADEQUATE experiment (which is so insensitive). It is also very useful in carbohydrate area as a sequence analysis tool that provides unique information concerning connectivities across glycosidic linkages

2.5.7 Diffusion Ordered Spectroscopy (DOSY)

The DOSY experiment is the measure of diffusion coefficients by NMR. In DOSY spectra, chemical shift is detected along the F2 axis and diffusion coefficient is along the F1 axis. We have used the method developed by Stejskal and Tanner (1965) which relies on two gradient pulses surrounding the 180° pulse in the spin echo. The

first gradient dephases the transverse magnetization in a spatially dependent manner along the z-axis and the second gradient then rephases the magnetization. The relation between translational self-diffusion and the measurable NMR parameters [Stejskal and Tanner, 1965] is:

$$A/A_0 = -\exp [D_t\gamma_H^2\delta^2G_z^2(\Delta - \delta/3)]$$

where A is the measured peak intensity (or volume), A_0 is the maximum peak intensity, D_t is the translational diffusion constant (in cm^2/s), γ_H is the gyromagnetic ratio of a proton (2.675197×10^4 G^{-1} s^{-1}), δ is the duration of the gradient, Δ is the time between gradients and G_z is the strength of the gradient (in G/cm). Data can be plotted as $-\ln (A/A_0)$ versus $\gamma_H^2\delta^2G_z^2$ $(\Delta-\delta/3)$. The slope of the line gives the value of D_t. The pulse program used is Pulsed gradient spin echo (stimulated echo sequence incorporating bipolar gradients) sequence modified with binomial water suppression. The gradient strengths were incremented as a square dependence in the range from 1 to 32 G cm^{-1}. The diffusion time (Δ) and the duration of the magnetic field gradients (δ) were 100 ms and 6 ms, respectively. Other parameters include a sweep width of 6000 Hz, 32 K data points, 1024 transients and an acquisition time of 2.7 s and relaxation delay of 2.0 s. It has been developed in order to facilitate the complex mixture analysis without physical separation. This experiment will monitor any modification of the solvent or of the solutes, and molecular events such as molecular interactions or associations.

2.6 EXPERIMENTAL PARAMETERS

All NMR experiments were recorded on Bruker Avance 500 MHz FT-NMR spectrometer at Central NMR Facility located at Indian Institute of Technology Roorkee.

Typical parameters for one-dimensional NMR experiments are pulse width = 10-12.5 μs (60° pulse); number of data points = 32-64 K; spectral width = 10 000 Hz; number of scans = 64-128 and digital resolution = 0.25-0.5 Hz/point. Receiver gain was optimized in each instance to obtain the best signal to noise ratio. Homonuclear ^1H 2D phase- sensitive DQF-COSY and NOESY experiments on d-$(CGATCG)_2$ and its complex with palmatine were carried out at 278 K in H_2O. Also, HMBC, HSQC and ROESY of Palmatine is recorded at 298 K. However 2D NOESY experiments were recorded with variable mixing times (τ_m) 100, 200 and 300 ms at 500 MHz for palmatine-d-$(CGATCG)_2$ complex. Typical parameters for 2D experiments at 500 MHz were: 1024-2048 data points along t_2 dimension; 512 free induction decays in t_1 dimension; pulse width ≈ 9.5-12 μs; spectral width ≈ 10 000 Hz; no. of scans = 64-128; digital resolution 2.30 – 4.60 Hz/point and relaxation delay ≈ 1.0 sec and ssb 2, 2. Since the solvent used is water, so the water suppression using excitation sculpting with gradients is done.

2.7 DETERMINATION OF THREE-DIMENSIONAL STRUCTURE

2.7.1 Resonance assignments in nucleic acids

Resonance assignment is the first endeavour in the structural determination of DNA. From the NMR point of view, the protons can be grouped into four categories; (i) exchangeable OH, NH and NH_2 protons of the bases and nonexchageable base protons between 7-15 ppm (ii) nonexchageable sugar protons between 2-6.5 ppm (iii) methyl protons of thymine between 0.5-2 ppm. In order to observe OH, NH and NH_2, protons, experiments have been carried out in water whereas the other protons were observed in D_2O solution. The strategy for resonance assignment consists of two steps. In the first stage, the J correlated spectra are used to identify network of

coupled spins. In the second stage, the spin systems so identified are assigned to particular nucleotides along the sequence of the molecule by making use of the NOESY spectrum as described below. The sugar protons H1', H2', H2", H3', H4', H5' and H5" form a complex J correlated network (Fig. 2.4). The various cross peaks observed in the 2D J-correlated between these protons was used in identification of spin system within individual nucleotide units. The H1' proton shows a cross peak with H2', H2" sugar protons. The H2' and H2" protons are further coupled to H3' proton. We have used phase sensitive DQF-COSY spectra to identify the various J-coupled cross peaks. In the second phase sequential assignment is carried out using NOESY spectrum. Short internucleotide distances between adjacent nucleotide units are used as shown in Fig. 2.4. In right handed DNA with sugars in C3'-endo/C2'-endo/O1'-endo pucker and glycosidic angle in anti domain, a convenient strategy for sequential assignment is

$$(H6/H8)_n \longrightarrow (H2', H2")_{n-1}$$

$$(H6/H8)_n \longrightarrow (H1')_{n-1}$$

$$(H6/H8)_n \longrightarrow (H6/H8)_{n-1}$$

where, n stands for nth residue in 5'-3' oligonucleotide sequence.

In case of Z-DNA, where the repeating unit is a dinucleotide. The internucleotide pathway is Base (2n–1) .... H5' (2n–1) .... Base (2n) .... H1' (2n) .... H2' (2n) and H2" (2n) .... Base (2n+1).

2.7.2 Pseudorotation

Because of the r^{-6} dependence of the pre-steady state NOE, the relative magnitude of the NOEs provide a sensitive probe which can be used to obtain a qualitative view of the solution structures of short oligonucleotides. The glycosidic and sugar pucker

conformations can be assessed qualitatively on the basis of the relative magnitudes of the intranucleotide sugar-base NOEs. The flexible five-membered sugar ring plays a pivotal role in nucleic acid structure and dynamic behaviour. In B-DNA family sugar responds to its surroundings (e.g. base stacking pattern) by an appropriate adaptation of its geometry. X-ray studies have now shown that P values usually occur in two distinct ranges. In a conformational wheel (Fig. 1.7a of Chapter 1) one range of form occupies the "Northern" half of the circle (N-type, P_N 0° ± 90°); the second range occupies the "Southern" hemisphere (S-type, P_S 180 ± 90°). To a good approximation (0.4-0.7°) the torsion angles can be reproduced by a two-parameter pseudorotation equation:

$$\nu_j = \phi_m \cos [P + 0.8\pi (j-2)]$$

For j equals 0-4 and ϕ_m is amplitude of pucker. In crystal structures nucleotides usually a single pure N- or S-type conformer is found, but not necessarily the one that is predominant in aqueous solution. In some cases both N and S forms reside side by side in the same unit cell. Statistical analyses of X-ray data make it clear that details of sugar geometry of monomers are influenced by anisotropic crystal packing forces. The situation appears to be different in the helical oligomers, where stacking forces may play a more predominant role. NMR investigations in solution have demonstrated that N (C3'-endo) and S (C2'-endo) type conformations are in rapid equilibrium.

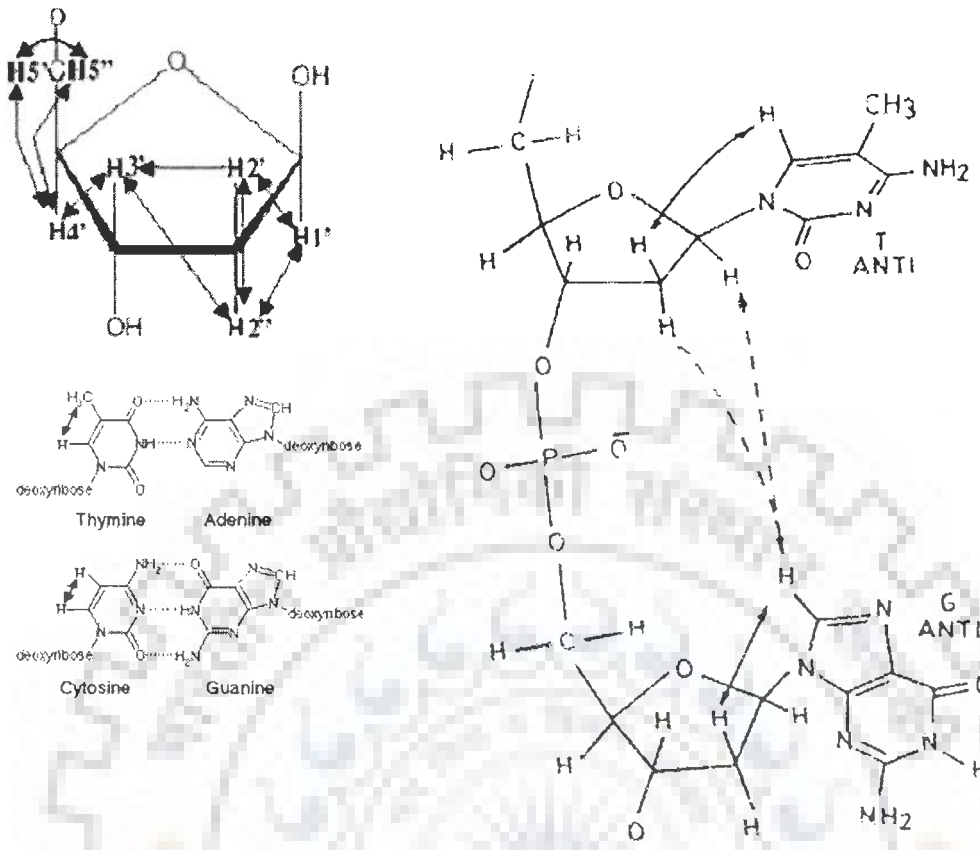

Fig. 2.4: Schematic representation of through bond J connectivities (⟷)and short interproton distances between adjacent nucleotides units in right handed DNA bases

If the interconversion rate between conformers is sufficiently rapid then observed couplings represent weighted average of couplings in individual conformers. Generally, in deoxyribose sugar, a trend to a larger proportions of C2'-endo pucker sugar is observed. A phase sensitive DQF-COSY spectrum allows J-coupling patterns to be delineated from the well-resolved crosspeaks. In general, the relation between ^3J and φ takes the form of the semiemprical Karplus equation:

$$^3J = A\cos^2(\varphi) + B\cos(\varphi) + C$$

The constants A, B and C have to be determined from ^3J values measured for compounds for which the value of φ, in solution, is known. There are five ^3J values in

deoxyribose sugar, H1'-H2', H1'-H2", H2'-H3', H2"-H3' and H3'-H4', which are related to the relevant H-C-C-H dihedral angle, φ, according to the relation:

$$J = 10.2 \cos^2\varphi - 0.8 \cos \varphi$$

The above dihedral angles are inter-dependent and their values can be calculated in terms of the two pesudorotation parameters, P and φ_m. φ_m is a constant for deoxyribose and thus various geometries can be expressed in terms of P. Fig. 2.5 [Hosur et al, 1986] shows the plots of five coupling constants in a deoxyribose ring as a function of P, (T_m = 38°). It is clear from the curves that the value of coupling constants ^{3}J(H1'-H2") and ^{3}J(H2'-H3') vary within a narrow range of 6-10 Hz and are

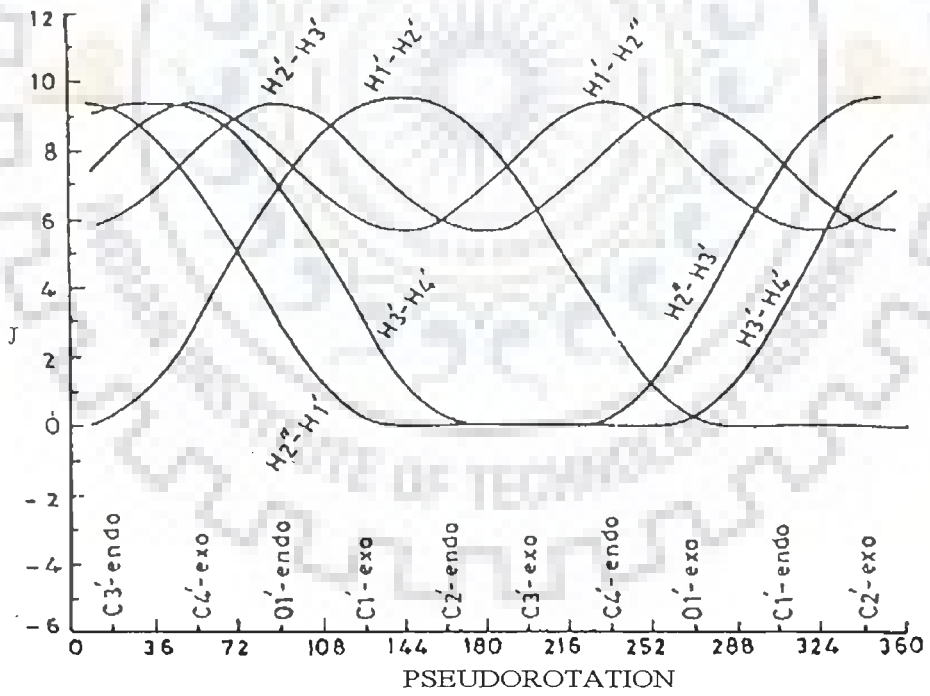

Fig. 2.5: Variation of the vicinal coupling constants in the deoxyribose ring as a function of the ring geometry

comparatively insensitive to the sugar geometry. On the other hand, values of ^{3}J (H2"-H3'), ^{3}J(H3'-H4') and ^{3}J(H1'-H2') coupling constants vary in the range 0-10 Hz and

can be utilized with greater advantage in fixing the domains of sugar geometry. ^{2}J (H2'-H2") is a geminal coupling which does not show significant conformational dependent variation. Rest five i.e. ^{3}J(H1'-H2'), ^{3}J(H1'-H2"), ^{3}J(H2'-H3'), ^{3}J(H2"-H3') and ^{3}J(H3'-H4') are vicinal coupling which show a strong dependence on the conformation of the deoxyribose ring [Hosur et al, 1986]. The approach used for determination of sugar geometry is based on interpretation of intrasugar proton-proton distances.

2.7.3 Conformation about the glycosidic bond

A large body of crystallographic data for nucleotides and nucleotides clearly establishes that the torsional angle, χ_{CN}, defining the orientation of base ring falls into two relatively narrow ranges designated as syn and anti conformation [Sundaralignam, 1969].

$$\chi \begin{cases} \text{O4'-C1'-N9-C4 (Purines)} \\ \text{O4'-C1'-N1-C2 (Pyrimidines)} \end{cases}$$

The relative magnitudes of the intranucleotide and internucleotide (H8/H6)-H1' and (H8/H6)-(H2', H2") cross peaks in NOESY spectra at different mixing times can be used to establish the domains of glycosidic dihedral angles of individual nucleotide unit [Hosur et al, 1985; Roche et al, 1994]. Below the spin diffusion limit, the intensity patterns of the cross peak look similar at all mixing times although the absolute intensity may vary with the mixing time. The expected intensity patterns for the above mentioned cross peaks for different glycosidic dihedral angles are given below:

1. For the syn conformation, a strong NOE between base H8/H6 and H1' protons should be observed. At the same time, the NOEs from base to H2' and H2" protons will be relatively weak and will have different intensities.
2. In the anti conformation, the NOE from base H8/H6 to H2' is stronger than the NOE from base H8/H6 to H2". Also, for right handed structures the H2" proton shows a stronger NOE to the base proton of the next nucleotide.
3. In the high anti conformation, the (H8/H6)-H2' and (H8/H6)-H2" NOEs will have similar intensities for C2'-endo geometry.

The (H8/H6)-H1' distance depends only on χ while, other distances depend on both P and χ. Iso-distance contours have been calculated by Wuthrich (Wuthrich, 1986) in (P, χ) space for H8/H6-H2', H2", H3', H4' and H5' distances.

2.8 ESTIMATION OF INTERPROTON DISTANCES

If one resonance A is irradiated, an increase (positive NOE) or decrease (negative NOE) of signal intensity of other resonances such as resonance C is observed when spin C is close in space to spin A. This phenomenon is called Nuclear Overhauser Effect or NOE. The NOE effect is the method for elucidation of 3D structural features and stereochemistry using NMR together with information from scalar spin-spin couplings. The most important quantity derived from NOE cross peaks is the cross-relaxation rate between protons i and j. The cross relaxation rate σ_{ij} between two protons spins i and j is related to the distance between protons i and j in the following way:

$$\sigma_{ij} = \langle d_{ij}^{-6} \rangle f(\tau_{ij}) \quad (1)$$

$\langle d_{ij}^{-6} \rangle$ denotes an ensemble average of molecular structures interconverting in thermal equilibrium where $f(\tau_{ij})$ is a function of correlation time τ_{ij} for the vector connecting

the two spins. This function accounts for the influence of motional averaging processes on the NOE. The cross relaxation rates can be measured from buildup rates of cross peaks in 2D NOE spectra at several mixing times. According to equation (1), the measured cross relaxation rates are a function of the ensemble average properties, which are dependent on the configurational space accessible to the molecular system at the temperature and time scale. If the interconversion between conformational equilibria in the oligonucleotide is fast on NMR time scale, NOEs from several equilibrium conformations will be observed simultaneously. This means the derived set of distance constraints does not necessarily represent the average structure, and there may be no single conformation that is consistent with the data set. Initially the intensity of the cross peak in equation (1) varies linearly with mixing time, and therefore this condition is referred to as "linear regime", but on higher mixing times, this condition does not exist due to multispin relaxation. Interproton distances can be estimated by measuring the intensities of cross peaks in the "linear regime". Two-spin approximation is used in NOE distance measurements in which only the rate of dipolar magnetization transfer between proximal spins i and j is monitored and all other spins are ignored. For two spin approximation, the intensity I_{ij} can be written as:

$$I_{ij} = \frac{\gamma^4 \hbar^2 \tau_c \tau_m}{10 r_{ij}^{-6}} \qquad \text{when } \omega \tau_c >> 1$$

where γ is gyromagnetic ratio and $\hbar$, is planck's constant divided by 2π. In order to determine the accurate value of τ_m for estimation of interproton distances, NOE build up curves should be obtained as a function of τ_m for several cross peaks, since spin diffusion can be different for different protons. Correlation times, τ_c, can be obtained from T_2 and T_1 measurements, according to the equation:

$$\tau_c = \quad 2\omega^{-1}(3T_2/T_1)^{-1/2}$$

which holds good for $\omega\tau_c >> 1$

If protons i, j, k, l have similar τ_c values and if r_{ij} is a known distance, then the unknown distance r_{kl} can be calculated by comparing the intensities I_{ij} and I_{kl} in a single spectrum.

$$\frac{I_{ij}}{I_{kl}} = \frac{r_{kl}^{6}}{r_{ij}^{6}}$$

The choice of known distance is important in the light of the mobility associated with different atoms in the nucleic acid. Gronenborn et al [Gronenborn and Clore, 1985] have expressed the opinion of using different yardsticks for NOEs involving different group of protons. The r(CH5-CH6) and r(H2'-H2") have different effective correlation times and can be used as reference depending on the cross peak being compared. The thymidine (H6-CH_3) distance of 3.0 Å can be used as reference for all NOEs involving CH_3 protons, the sugar H2'-H2" protons and for the rest, cytidine H5-H6 distance of 2.45 Å can be used. Reid et al [Reid et al, 1989] examined H2'-H2" and H5-H6 cross relaxation at 15, 30, 60, 90 and 100 ms in dodecamer DNA duplexes. Results indicate that sugars and bases have the same correlation times, therefore all proton-proton distances in short DNA duplexes can be determined by scaling the initial NOE build up rate to the slope of cytosine H5-H6 cross peak, as H2'-H2" NOE cross peak are close to diagonal and are usually unresolved.

The characteristics of NMR data can be summarized as below:

1. NOEs cannot be translated into the precise distances. In practice this means that NOEs give only a number of approximate upper limits (e.g., 3 Å, 4 Å and 5 Å for strong, medium and weak NOEs). Sometimes it is not possible to make this division and only one single upper limit is used. For some proton

pairs, corrections have to be applied to the upper limit value. This may arise due to stereo specific assignments (e.g., methyl group of thymine) or because of dynamic effects such as rotation of hydrogens in a methyl group and flipping of the aromatic rings.

2. Translating NOEs into reliable lower limit constraints is difficult, and it is preferable to take the sum of vander waals radii as a lower limit to the distance. The absence of NOEs between two assigned protons may be translated into a minimum distance of proton pair.
3. NMR data contain contributions from different molecular conformations. Not all distance constraints need to be consistent with the single conformation.
4. NOE information is limited to short distance relative to the size of the drug-DNA complex. For some part of the molecule none or only a few NOEs are observed.

2.9 RESTRAINED MOLECULAR DYNAMICS AND SIMULATED ANNEALING

When restrained energy minimization methods are used, inevitable local energy minima are encountered which can lead to inaccurate structures. To circumvent this, restrained molecular dynamics (rMD) are usually employed. This involves including NMR restraints in one of the many molecular dynamics simulation programs. Molecular dynamics solve Newton's equation of motion,

$$F_i = m_i a_i \qquad (1)$$

Where F_i is the force, m_i is the mass and a_i is the acceleration of atom i. The force on atom i can be computed directly from the derivative of the potential energy V with

respect to the coordinates r_i. The energy can be expressed in an explicitly differentiable form:

$$dV/dr_i = m_i d^2 r_i/d t^2 \quad (2)$$

Therefore, with an adequate expression for the potential energy and the known masses, this differential equation can be solved for future positions in time t_i. In general, this can be solved only approximately, since V is usually a complex function of the coordinates of all (or many) of the atoms (i.e. $V = V(r_1, r_2, r_3, \ldots\ldots, r_N)$). The temperature can be calculated from the atomic velocities

$$3N/2\ k_B T = \sum_{i=1}^{N} 1/2 m_i v_i^2 \quad (3)$$

where, k_B is Boltzmann's constant, m_i and v_i are the mass and velocity of atom i, and N is the number of atoms (and 3N is the number of degrees of freedom). For a simulation at constant energy, the temperature fluctuates due to the interconversion of kinetic and potential energy. If the temperature is held constant then the atomic velocities can be adjusted accordingly. If the pressure is held constant, the volume is allowed to fluctuate by rescaling the interatomic distances.

The total potential energy V_{total} is usually defined as the sum of a number of terms:

$$V_{total} = V_{bond} + V_{angle} + V_{dihedr} + V_{vdw} + V_{coulomb} + V_{NMR} \quad (4)$$

where, V_{bond}, V_{angle} and V_{dihedr} keep bond lengths, angles, and dihedral angles at their equilibrium values. The first five terms are empirical energy terms describing the physical interactions between the atoms, whereas the last term is a means of including the NMR information, but does not correspond to any real physical force. They can be summarized as follows:

$$V_{bond} = \sum_{bond} 1/2\ K_b(b - b_0)^2 \quad (5)$$

$$V_{angle} = \sum_{angles} 1/2\ K_\theta(\theta - \theta o)^2 \quad (6)$$

$$V_{dihedr} = \sum_{dihedr} K\phi\ (1+\cos\ (n\phi - \delta) \quad (7)$$

These are pseudo-harmonic potentials that constrain bond lengths (b), bond angles (θ), and the rotamer angles (ϕ, δ) for staggered and eclipsed conformations, and K is a constant. The van der Waals and electrostatic interactions are described by V_{vdw} and $V_{coulomb}$

$$V_{vdw} = \sum_{pairs\ (ij)} [C_{12}/ r_{ij}^{12} - C_6/r_{ij}^6] \quad (8)$$

$$V_{coulomb} = \sum_{pairs\ (ij)} q_i q_j / 4\pi \varepsilon_o \varepsilon_r r_{ij} \quad (9)$$

where equation (8) is the Lennard-Jones potential, containing repulsive and attractive terms (C is a constant), and equation (9) describes the coulombic interactions between two charged particles (i, j) with partial charges q that are a distance r_{ij} apart in a dielectric medium described by $\varepsilon_o\varepsilon_r$ term. The potential V_{NMR} contains the NMR restraints, and has the effect of pulling the protons that show an NOE interaction closer to the measured distance r_{ij}. Similarly, these potentials are also pesudoharmonic functions of similar forms to equations (5)-(7). Distance constraints which can be reasonably accurately determined may therefore be defined as follows:

$$V_{NOE} = \begin{cases} K_1 (r_{ij} - r_{ij}^0)^2 & \text{if } r_{ij} > r_{ij}^0 \\ K_2 (r_{ij} - r_{ij}^0)^2 & \text{if } r_{ij} < r_{ij}^0 \end{cases} \quad (10)$$

where, r_{ij} and r^0_{ij} are the calculated and experimental interproton distances, respectively, and K_1 and K_2 are force constants given by:

$$K_1 = k_B TS / [2(\Delta_{ij}^{+})^2] \quad \text{and} \quad K_2 = k_B TS / [2(\Delta_{ij}^{-})^2 \tag{11}$$

Where k_B is Boltzmann's constant, T, absolute temperature of the simulation, S a scale factor, and Δ^{+}_{ij} and Δ^{-}_{ij} are the positive and negative error estimates, respectively, of r_{ij}. If, however, only ranges of distances can be specified, then the distance restraints are incorporated into a pseudo-square-well potential of the form:

$$V_{NOE} = \begin{cases} K_{NOE}(r_{ij}-r_{ij}^{u})^2 & \text{if } r_{ij} > r_{ij}^{u} \\ 0 & \text{if } r_{ij}^{l} \le r_{ij} \le r_{ij}^{u} \\ K_{NOE}(r_{ij}-r_{ij}^{l})^2 & \text{if } r_{ij} < r_{ij}^{l} \end{cases} \tag{12}$$

where $r^{u}_{ij\ and}\ r^{l}_{ij}$ are the upper and lower limits, respectively, of the target distances obtained from the experimental, and K_{NOE} is the force constant, which is typically chosen to be the order of 1000 kJ mol^{-1} nm^{-1}.

To ensure that the experimental restraints are the dominating factor in determining the conformation of the molecule, it is very important that the force constants for the restraints are set sufficiently high that the experimental data are satisfied within the precision of the measurements. At the same time, the contribution from the empirical energy function should be such that any individual rMD structure, the deviations from ideal geometry are small, and the non-bonded interactions are good (i.e. the Lennard-Jones potential is negative). Thus convergence on the structure is guided by the requirement to minimize NOE or other restraint violations. The number of distance restraint violations N_{viol} is counted when, for example, $r_{ij} \ge r_{ij}^{0} + 1$, which would for 1 Å fluctuations. Another parameters which can be minimized in addition to N_{viol} is the sum of the distances in excess of the constraints $\sum \Delta r_{viol}$, which is defined as:

$$\sum \Delta r_{viol} = \sum_{K=1}^{N_{viol}} (r_{ij})_k - [(r_{ij}^{0})_k + 1] \tag{13}$$

where the sum runs over all those interproton (or pseudoatom) distances for which N_{viol} is defined. Although an arbitrary structure may be used for restrained molecular dynamics calculation, in practice a starting structure obtained from distance geometry and energy minimization is often used. The rMD approach requires a relatively large amount of computation time compared to distance geometry methods. This problem can be overcome by using a simplified potential energy function, where all non-bonded contact interactions are described by a single van der waals repulsion term. Also by using a cut off distance, in which non-bonded interactions for pairs of atoms that are separated by a distance greater than some reasonable value (e.g. 5-10 Å) are excluded, the number of non-bonded interactions is decreased considerably. Simulated annealing involves raising temperature of the system followed by slow cooling in order to overcome local minima and locate the global minimum region of the target function. It is computationally more efficient than rMD and yield structures of similar quality. The potentials are very similar to rMD and again Newton's laws of motion are solved as a function of time. However, in implementations found in commercial programs, the non-bonded interaction potential is modified so that there is a simple van der waals repulsion term with a variable force constant K_{rep}:

$$V_{repel} = \begin{cases} 0 & \text{if } r \geq s.r_{min} \\ K_{rep}\,(s^2 r^2_{min} - r^2)^2 & \text{if } r < s.r_{min} \end{cases} \qquad (14)$$

The values of r_{min} are given by the sum of the standard values of the van der Waals radii between two atoms as represented by the Lennard-Jones potential.

2.10 DEFINING DNA STRUCTURE

The structure of DNA can be described by a number of parameters that define the helix (Dickerson et al, 1989) termed as Helical Parameters. The output from helix analysis program CURVES 5.1 version of Richard Lavery [Lavery and Sklenar, 1988], includes "global helical parameters" defined relative to a global helix axis, that is, it depends on all the atoms in the structure and "local helical parameters" defined relative to local helix axis at each base pair, that is, arises if only a subset of neighboring atoms is used to determine that quantity. The helicoidal parameters are classified into three categories: 1.Global base pair-axis parameters 2. Intra-base pair or global base-base parameters 3. Inter-base pair or base pair-step parameters.

The global as well as the local inter-base pair parameters are related to particular base pair steps. These parameters are vector quantities, which have a defined location in 3-dimensional space and with respect to the nucleic acid sequence. In contrast, the average inter-base pair parameters are scalar values that are not related to any part of the structure. They characterize properties of the whole structure. Intra–base pair or global base–base parameters comprises of the translational components as stagger, stretch and shear, and the rotational components are propeller twist, buckle, opening. Propeller twist refers to the angle between the planes of two paired bases. A base pair is rarely a perfect flat plane with each aromatic base in the same plane. Rather, each base has a slightly different roll angle with respect to the other base. This makes two bases look like an aeroplane propeller. Twist or rotation per residue refers to the angle between two adjacent base pairs. Each step from one plate to the next can be described as a combination of a translational and a rotational movement.

The translational and the rotational displacements are three-dimensional vectors, which can be split into three orthogonal components. In inter-base pair or base pair-step parameters the three translational components are rise, shift and slide. Twist, roll and tilt are the three rotational components. Rise is the distance between adjacent planar bases in the DNA double helix i.e. it is a translation in the direction of the helical axis (z-axis), and shift is orthogonal to the helical axis and directs to the major groove side. Twist is a rotation about the helical axis (z-axis). Base pair roll refers to the angle of deflection of the base pair with respect to the helix axis along a line drawn between two adjacent base pairs relative to a line drawn perpendicular to the helix axis. A positive roll indicates that there is a cleft between two stacked base pairs, which opens towards the minor groove. A negative roll is related to an opening towards the major groove. Base pair tilt refers to the angle of the planer bases with respect to the helical axis. In the B-form DNA the bases are tilted by only –6°. In the A-form DNA the base pairs are significantly tilted at an angle of 20°. The sense of the base-pair tilt is associated with sugar puckering. In double helical polynucleotide, the normal to the base pair are not exactly parallel to the helix axis but inclined to it by up to 20°. The sense of tilt is positive in A-type and negative in B-type of helices, and hence is correlated with sugar puckering. Base tilt angle is correlated with rise per residue. If the bases in base pairs were coplanar and the base pairs exactly perpendicular to the helix axis, the axial rise per nucleotide should correspond to the van der Waal's distance, 3.4 Å.

Global base pair–axis parameters: x- and y- displacement refers to the shift of bases in positive or negative x and y direction with respect to each other, besides this tip and inclination are also there (Fig.2.6a).

Inter-base parameters (Base pair step parameters): The helical parameters are derived from the spatial location of the bases, while the sugar phosphate backbone is not taken into account.

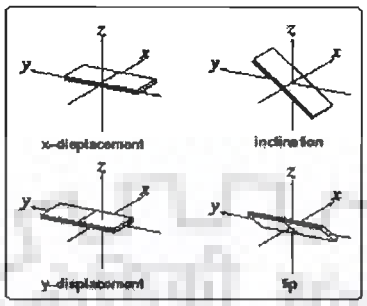

Fig. 2.6(a): Pictorial representation of global base pair–axis parameters

The six inter base pairs parameters (***rise***, ***twist***, ***shift***, ***roll***, ***tilt***, ***slide***) describe the local conformation of a double helix at every base pair step (Fig. 2.6b). In the below figure the base pairs are shown as planar plates. In a regular helix such planar elements are stacked on each other. Each step from one plate to the next can be described as a combination of a translational and a rotational movement. The translational and the rotational displacements are 3-dimensional vectors, which can be split into three orthogonal components. The three translational components are **rise, shift and slide**. **Rise** is a translation component in the direction of the helical axis (z-axis) and **shift** is orthogonal to the helical axis and directs to the major groove side. **Twist, roll and tilt** are the three rotational components. **Twist** is a rotation about the helical axis (z-axis). A **positive roll** indicates that there is a cleft between two stacked base pairs which opens towards the minor groove. A **negative roll** is related to an opening towards the major groove. The definitions of the six inter base pair parameters are rigorous but the Cambridge convention does not define how to establish the reference coordinate system.

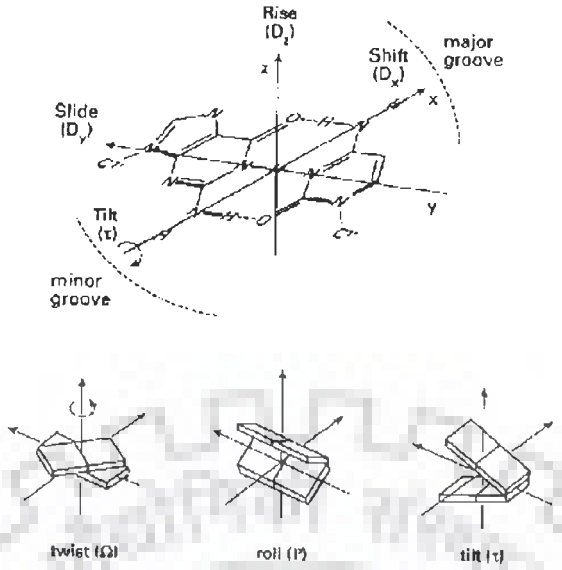

Fig. 2.6(b): Six inter-base pair parameters of DNA

The decomposition of the total translational and rotational movement into orthogonal components depends crucially on the reference system used. Several different algorithms and programs exist for calculating the helical parameters. The algorithms differ mainly in the methods used to derive the reference coordinate systems.

Intra-base pair step parameters (Base pair parameters): The base pairs in nucleic acid structures are not really planar. For example, the propeller twist of AT base pairs in B-DNA is usually in the range of -15° to -20°. If the base pairs are not planar, the six inter base pair parameters will give only a rough model of the helix. A more detailed picture is obtained if also the intra base pair parameters are taken into account. The Cambridge convention defines six base pair parameters which describe the deviation from planarity within a base pair. These six parameters describe the translational and rotational displacement between the two bases of a base pair. Again, the translational and rotational displacement is divided into orthogonal components. The translational components are ***stagger***, ***stretch*** and ***shear***, and the rotational components are ***propeller twist***, ***buckle***, ***opening*** (Fig. 2.6c). Instead of determining

the (intra) base pair parameters, it is also possible to calculate the inter base pair separately for each strand.

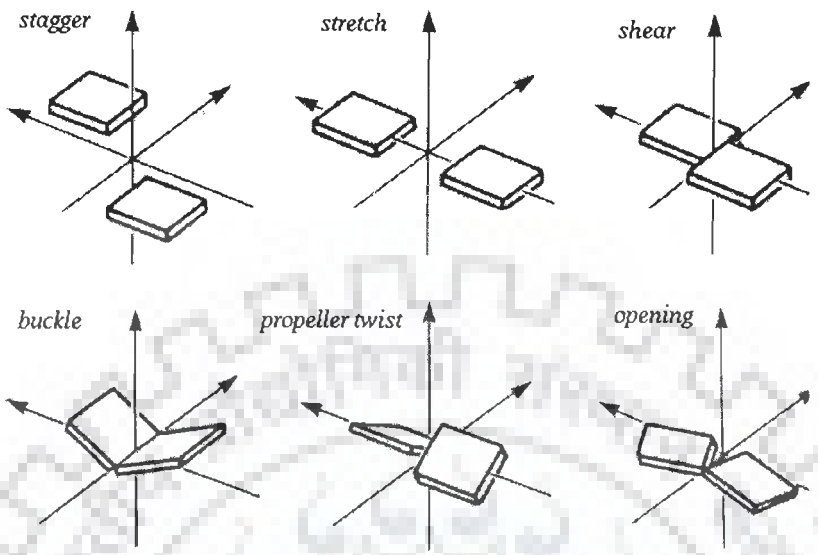

Fig. 2.6(c): Six Intra-base pair step parameters of DNA

2.11 QUANTUM MECHANICAL CALCULATIONS

The popularity of density functional methods and their applications to a broad range of problems and biochemical interest has been growing rapidly each year [Parr et al, 1989, Labauowski et al, 1991, Kohn et al, 1996]. Therefore the calculations are carried out using a Density Functional Theory (DFT). Along with it, Hartree-Fock wave function (HF) with self -consistent field (SCF) calculation is used for the comparison. The DFT method used is as follows: Hybrid B3LYP based on Becke's three parameters functional [Lee et al, 1988] and the correlation functional provided by LYP [Becke et al, 1993]. In all of these calculations, Cartesian Gaussian type orbitals (GTO's) are used as basis function for the molecular orbital. Although the capability of the basis functions to describe bonding deformations of the electronic density can be enhanced by increasing the number of basis functions for each orbital or including higher angular functions, yet as a thumb rule it should be able to yield

results which are comparable with larger basis set while remaining computationally manageable, and thus at least a basis set of the split- valence type with polarization function should be employed.

All calculations presented are done using the Gaussian 98 program package [Marek et al, 2003]. Full unconstrained geometry optimizations were performed using the density function as well as Hartree-Fock wave function as outlined above. For each of these density functional methods several basis sets like STO-3G, 6-31G, 6-31G**, 6-311G, 6-311G** are used for optimizing the geometry. All the molecular properties and chemical shifts are computed using the optimized structure of the molecule. The chemical shifts were also calculated using the same Gaussian package with the Gauge Independent Atomic Orbital (GIAO) approach. This approach allows the computation of the absolute chemical shielding due to the electronic environment of the individual nuclei. On the ground of variational theory, the quality of wave functions has been traditionally determined by the total energy which is the average of the Hamiltonian over the wave function. The lower the energy, the better the quality and we retain this concept despite the fact that for properties other than the total energy it may not be acceptable. In view of this, the calculations for structural properties and chemical shifts only using B3LYP method are reported.

Chapter 3

Structure Elucidation of Palmatine by Nuclear Magnetic Resonance Spectroscopy and Comparison using Quantum Mechanical and Restrained Molecular Dynamics Approach

For the structure based design of new ligands the knowledge of exact conformational behaviour is necessary. The aim of this study is to understand conformational behaviour of the drug palmatine (Fig. 3.1). The following is presented in this chapter:

- The structure elucidation of 25.78 mM palmatine by One- and two-dimensional NMR techniques; NOESY, HSQC (^{1}H - ^{13}C) and HMBC (^{1}H - ^{13}C) in D_2O at 298 K.
- Restrained Molecular Dynamics (rMD) simulations of palmatine using NOE interproton distance constraints from 2D NOESY spectra.
- Structural and electronic properties of the drug using Density Functional Theory (DFT) employing B3LYP exchange correlation at different levels of basis sets and calculation of chemical shift of ^{1}H and ^{13}C resonances in Nuclear Magnetic Resonance (NMR) spectra of these molecules using the Gauge–Invariant Atomic Orbital (GIAO) method as implemented in Gaussian 98.
- B3LYP and HF method with 6-31G** basis set has been employed to compute the bond length, bond angle and dihedral angles. Tomasi's Polarizable Continuum Model (PCM) was used to evaluate the influence of solvent on the structural parameters and chemical shift values. In addition to DFT we have also examined these properties at different levels of correlation such as MP2/6-31G* only in the gas phase

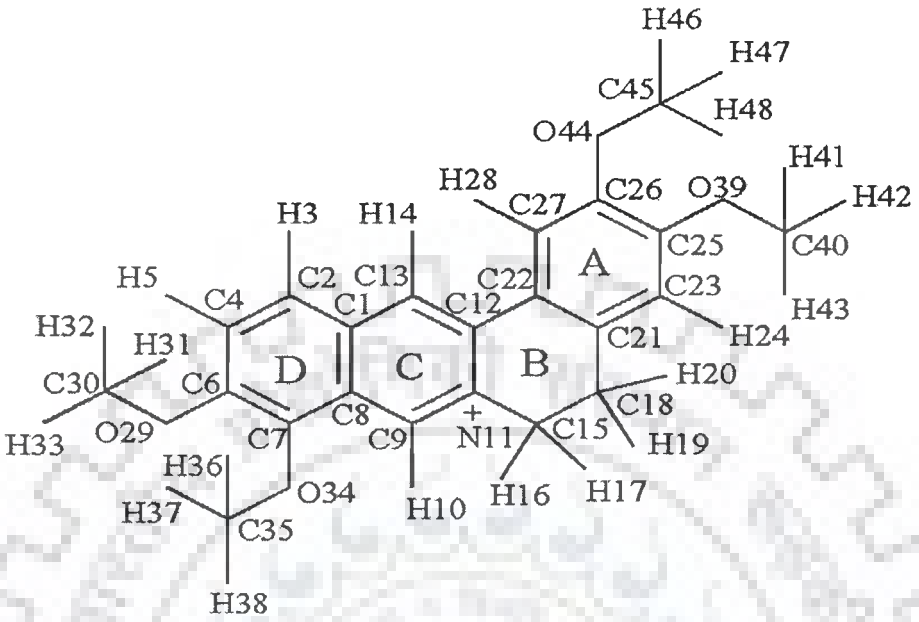

Fig. 3.1: Chemical Structure of Palmatine

In recent years the NMR chemical shift has become an important tool in the spectral assignment and rationalizing the experimental chemical shift data. The chemical shift is widely calculated using Gauge Invariant Atomic Orbital (GIAO) method as implemented in Gaussian 98 and Gaussian 03 package [Frisch et al., 1998]. We have followed the same approach to obtain these chemical shift positions along with other structural parameters. Several authors [Abraham et al., 2004; Casanovas et al., 2001; Colombo et al., 2002; Kupka et al., 2000; Lampert et al., 1997; Pulay and Hinton, 1995] have used this method successfully for calculating the chemical shifts of heavy atoms, organic compounds and complexes used in pharmaceutical systems. The popularity of density functional methods and their applications to a broad range of problems of biochemical interest has been growing rapidly each year [Kohn and Sham, 1965; Labanowski and Andzelm, 1991; Parr and Yang, 1989]. The most

important contributing factor is simply the reliability and cost effectiveness of the calculations. The results of our rMD simulations in combination with DFT calculations provide a better insight of the observed features of the measured NMR spectra.

3.1 RESULTS AND DISCUSSION

3.1.1 Nuclear Magnetic Resonance Studies of Palmatine

The ^{1}H NMR spectra of 25.78 mM palmatine in D_2O is shown in Fig. 3.2. Typical parameters for one–dimensional NMR experiments were: pulse width ~ 7.7 µs, no. of data points = 32 to 64 K, spectral width 5000 Hz, number of scans = 32–64, relaxation delay 1.0 s and digital resolution 0.08 Hz/point. The typical parameters for the 2D Rotating frame nuclear Overhauser Enhancement Spectroscopy (ROESY), Hetero-nuclear Single Quantum Correlation (HSQC), and Hetero-nuclear Multiple Bond Correlation (HMBC) experiments were: 1024-2048 data points along t2 dimension, 512 free induction decays in t1 dimension, pulse width ~7.7 µs, spectral width 6000 Hz (^{1}H) / 24000 Hz (^{13}C), number of scans 64, digital resolution 3.0 Hz/point and relaxation delay 1.0 s. A mixing time of 300 ms was used for ROESY experiments. A constant temperature of 298 K was maintained all through by using temperature controller.

3.1.1.1 Resonance Assignment of Palmatine

The ^{1}H NMR spectrum of palmatine in D_2O has been analyzed to do assignment for all the protons (Fig. 3.2). The area under peaks shows that the resonances at δ 3.79, 3.84, 3.97 and 4.07 ppm correspond to three ($-CH_3$) protons, while those at δ 3.06 and 4.69 ppm correspond to two protons ($-CH_2$) and all other

resonances correspond to one proton (–CH). Since OCH_3 protons attached to C7 atom are closer to electronegative atom N11, it is expected to be shifted downfield than those attached to C6, C25 and C26 atoms.

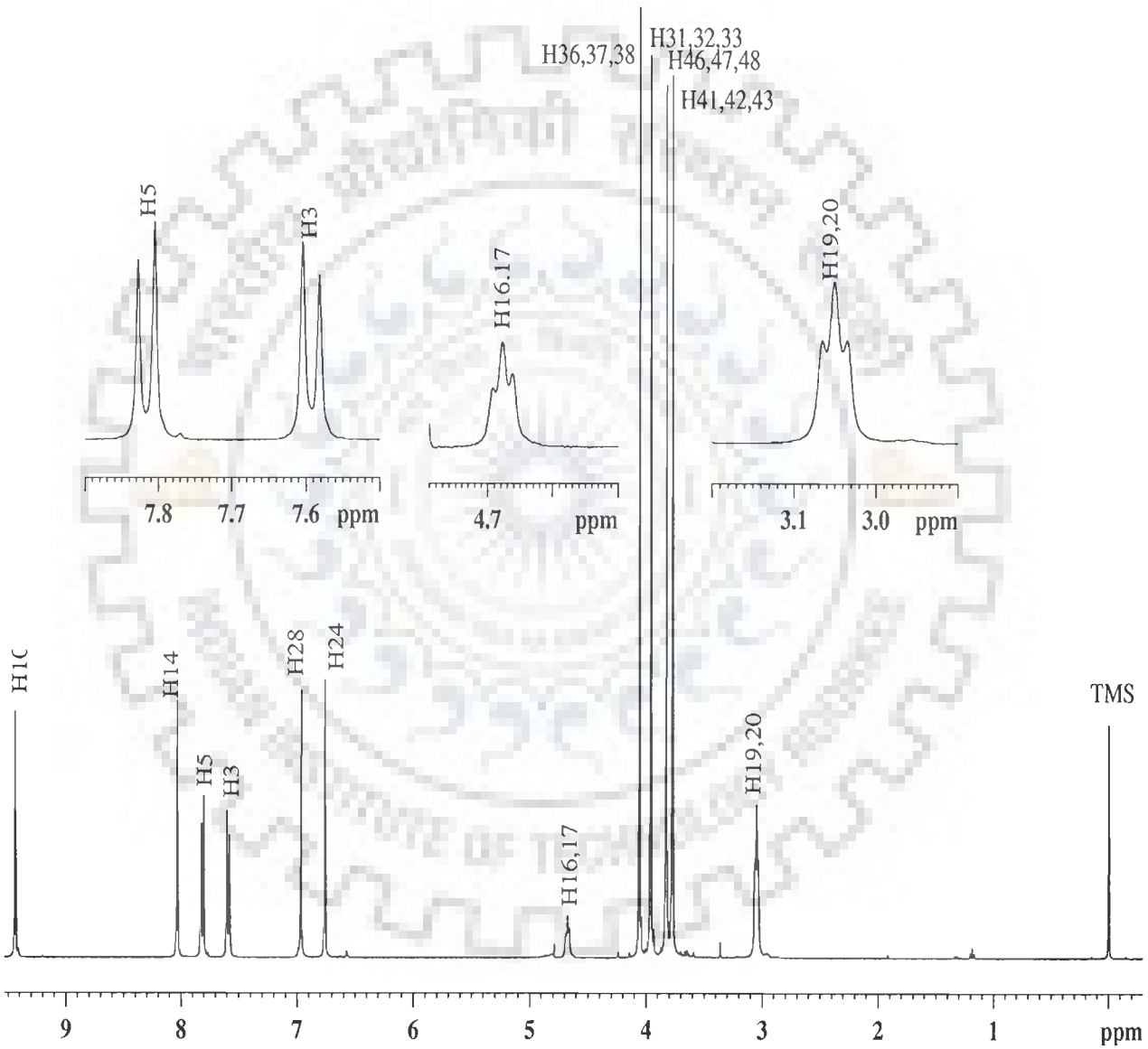

Fig. 3.2: 1D-^{1}H Spectra of Palmatine in D_2O

Accordingly H^a (36, 37, 38) (H^a denotes pseudoatoms), H^a (31, 32, 33), H^a (41, 42, 43) and H^a (46, 47, 48) are assigned to peaks at 4.07, 3.97, 3.79 and 3.84 ppm, respectively. In the same way the methylene protons at 4.69 and 3.06 ppm are triplets having a spin – spin coupling of 6.0 Hz and are assigned to CH_2 protons attached to C15 and C18, and designated as H^a (16, 17) and H^a (19, 20) atoms, respectively. The two doublets are assigned to H3 and H5 protons having ^3J = 9.1 Hz; H5 is shifted downfield with respect to H3 due to proximity to O29 atom. Among the ring C protons (H10, H14), H10 is expected to be more downfield being closer to N11 atom. Accordingly assignment has been made to H10, H14, H28 and H24 protons and is listed in Table 3.1. The ^1H–^{13}C Heteronuclear Single Quantum Coherence (HSQC) spectra (Fig. 3.3) shows the coupling of 12 carbon atoms to protons to which they are directly bonded through a single bond. The other eight carbon atoms are easily assigned with the help of Heteronuclear Multiple Bond Correlation (HMBC) spectra (Fig. 3.4). The observed carbon chemical shifts and carbon–proton bond correlations are listed in Tables 3.2 and 3.3, respectively. It may be noted that the chemical shifts of H14 and H28 protons are somewhat different (0.7–1.0 ppm) from those observed in the literature [Li et al, 2006; keawpradub et al, 2005; Halbsguth et al, 2003; Wafo et al, 1999]. All other proton and carbon chemical shifts show no significant difference from the corresponding values observed in the literature. The observed difference in resonance positions are attributed to the effect of solvents on the conformation of the molecule.

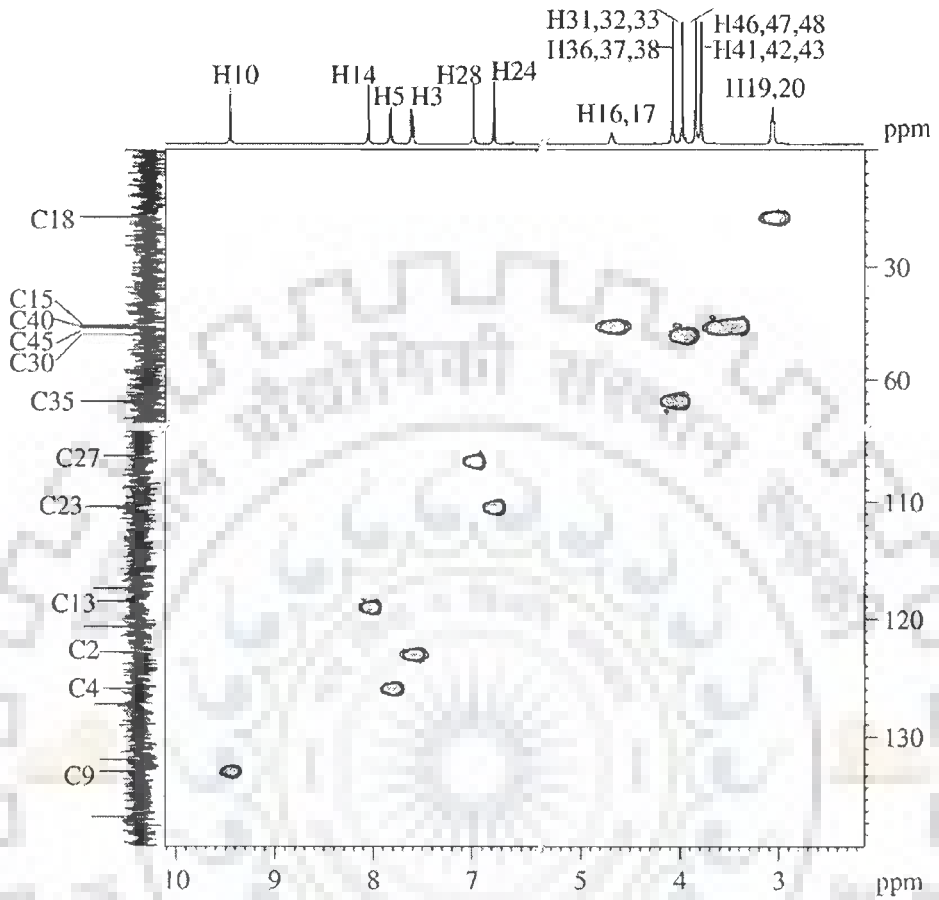

Fig. 3.3: HSQC spectra of palmatine in D_2O showing ^{1}H–^{13}C single bond Correlations

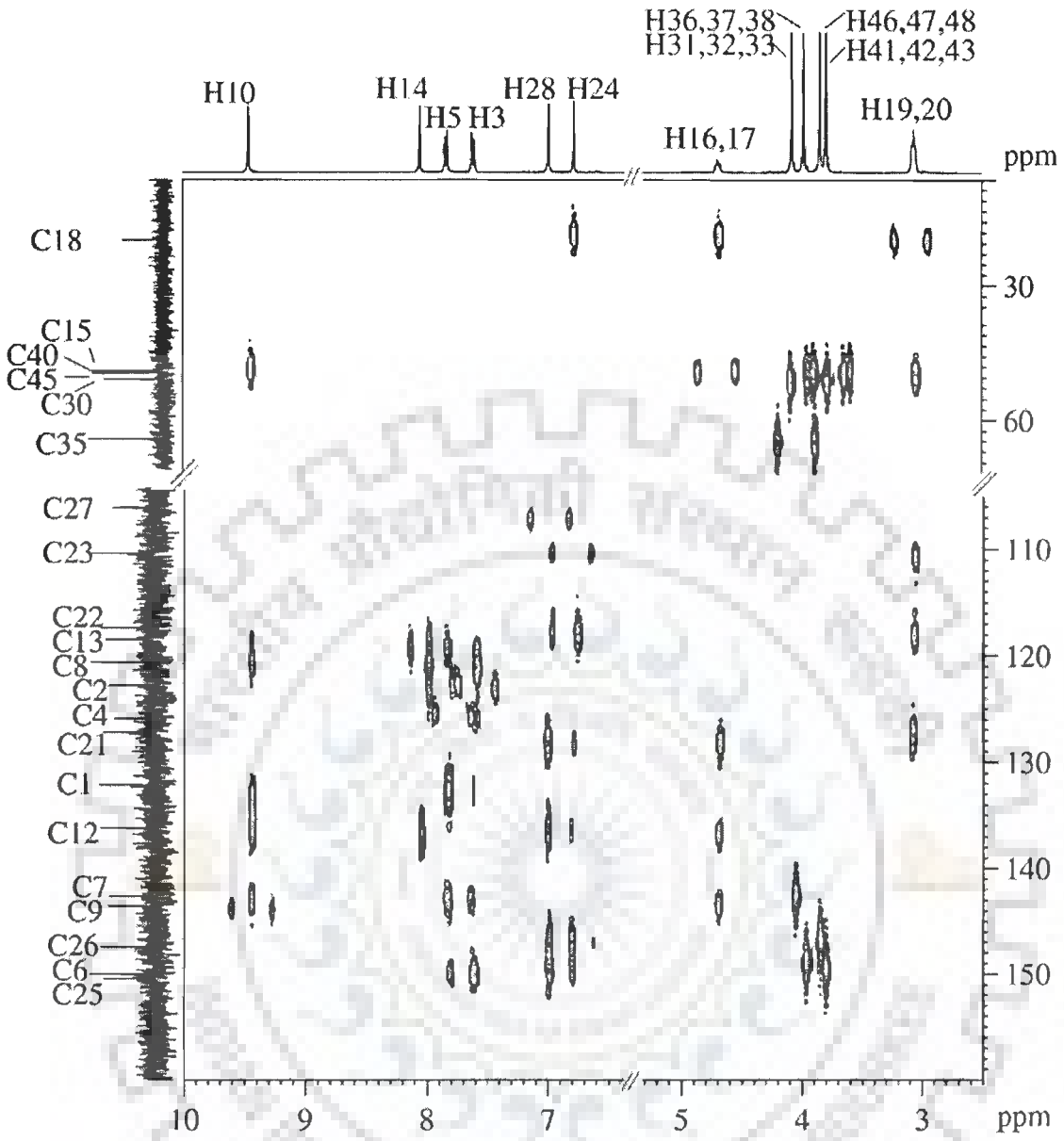

Fig. 3.4: HMBC spectra of palmatine in D2O showing ^{1}H–^{13}C multiple bond Correlations

Table 3.1: Comparison of NMR Proton chemical shifts (ppm) with calculated chemical shift by GIAO method using B3LYP and HF methods 6-31G wavefunction for palmatine.**

	Experimental				Theoretical					
Protons	Present Experiment (D_2O)	Niwat *et al* (DMSO)	Christiane *et al* & Chia et *al* (CD_3OD)	Wafo *et al* (DMSO)	B3LYP STO-3G	B3LYP 6-31G	B3LYP 6-31G*	B3LYP 6-31G**	B3LYP 6-311G**	HF 6-31G*
H3	7.60	8.03	8.02	8.10	7.86	7.84	7.62	7.89	7.94	8.09
H5	7.83	8.20	8.11	8.15	7.72	8.17	7.90	8.17	8.23	8.34
H10	9.45	9.88	9.77	9.95	9.38	9.20	8.78	9.08	9.15	9.18
H14	8.04	9.07	8.81	9.15	8.42	8.20	7.87	8.17	8.30	8.30
H^a(16, 17)	4.69	4.95	4.95	4.95	4.59	4.66	4.41	4.51	4.51	4.79
H^a(19, 20)	3.06	3.22	3.28	3.25	3.21	3.26	3.06	3.16	3.18	3.42
H24	6.78	7.08	7.04	7.15	6.70	6.60	6.46	6.76	6.73	6.85
H28	6.98	7.72	7.66	7.75	6.95	7.64	7.37	7.71	7.80	7.76
H^a(31, 32, 33)	3.97	4.06	4.10	4.00	3.75	4.47	4.04	4.16	4.12	4.38
H^a(36, 37, 38)	4.07	4.09	4.20	4.15	4.6	4.84	4.22	4.36	4.36	4.61
H^a(41, 42, 43)	3.79	3.93	3.94	3.88	3.71	4.34	3.95	4.06	4.03	4.30
H^a(46, 47, 48)	3.84	3.86	3.99	3.90	3.59	4.65	4.01	4.14	4.17	4.26

Table 3.2. Comparison of observed carbon (^{13}C) chemical shifts (ppm) from spectra of palmatine in different solvents with the experimental results reported in literature and with present calculated chemical shifts (ppm) with different wave function by GIAO method using B3LYP and HF methods.

Experimental				Theoretical					
Carbon	Present experiment (D_2O)	Niwat *et al* (DMSO)	Wafo *et al* (DMSO)	B3LYP STO-3G	B3LYP 6-31G	B3LYP 6-31G*	B3LYP 6-31G**	B3LYP 6-311G*	HF 6-31G*
C1	132.46	132.3	135.4	116.27	133.66	129.91	132.48	142.36	141.16
C2	123.65	123.6		109.17	121.36	117.73	119.49	128.71	127.58
C4	126.41	127.0	128.0	113.52	137.84	134.47	136.18	147.15	145.41
C6	150.30	150.4	56.5	134.60	153.49	147.51	149.98	160.99	156.13
C7	142.65	143.8	145.6	132.73	151.20	144.84	147.26	157.97	153.48
C8	121.01	121.5	124.3	109.79	121.65	116.86	119.54	127.64	126.83
C9	143.81	145.6	151.5	127.55	140.85	136.47	138.10	147.07	145.92
C12	137.14	137.9	139.9	125.67	139.86	135.15	137.78	147.86	144.11
C13	119.40	120.1	121.1	109.76	119.02	115.46	117.12	125.54	125.04
C15	55.43	55.5	56.5	61.90	59.62	56.73	57.89	61.41	66.76
C18	25.91	26.1	27.8	35.00	30.54	28.66	29.76	31.96	36.865
C21	127.27	128.8	129.8	110.91	125.53	123.68	126.11	135.68	133.85
C22	125.92	119.1	120.4	106.86	117.35	112.21	114.81	123.03	121.92
C23	110.41	128.8	112.0	104.36	111.24	106.61	108.22	114.84	115.51
C25	150.52	151.7	153.7	137.95	156.60	152.39	154.99	166.97	160.60
C26	147.50	148.9	150.8	133.91	150.23	144.94	147.48	159.75	154.00
C27	106.83	109.2	145.6	102.22	118.36	116.19	117.79	126.68	125.83
C30	56.21	57.2	57.4	56.72	63.57	57.41	58.00	62.24	68.61
C35	61.91	62.1	62.4	59.18	62.74	56.93	57.61	61.74	66.85
C40	55.51	56.0	56.8	57.04	57.36	53.61	54.17	57.68	61.91
C45	55.66	56.4	57.3	56.02	64.40	57.19	57.78	62.41	66.85

Table 3.3 Observed correlation of carbon atoms with specific protons in HSQC and HMBC spectra of palmatine

Carbons	HSQC		HMBC	
		ss	mm	ww
C1	-	H10, H5	-	-
C2	H3	H14	-	-
C4	H5	-	H3	-
C6	-	H3, H^a(31,32,33)	H5	-
C7	-	H5, H10, H^a(36,37,38)	-	H3, H^a(16,17)
C8	-	H10	H14	-
C9	H10	H^a(16, 17), H5	H3	-
C12	-	H14, H28, H10	H^a(16,17)	-
C13	H14	-	-	-
C15	H^a(16, 17)	H10, H^a (19,20)	-	-
C18	H^a(19, 20)	H24, H^a (16,17)	-	-
C21	-	H28, H^a(16,17), H^a(19,20)	-	-
C22	-	H28, H^a(19,20)	-	-
C23	H24	H^a (19,20)	-	-
C25	-	H^a(41,42,43), H28	H5	-
C26	-	H24, H^a(46,47,48), H28	-	-
C27	H28	-	-	-
C30	H^a(31,32, 33)	-	-	-
C35	H^a(36, 37, 38)	-	-	-
C40	H^a(41, 42, 43)	-	-	-
C45	H^a(46, 47, 48)	-	-	-

3.1.1.2 Temperature dependent study of palmatine

We have also studied the temperature dependence of palmatine (25.78 mM) protons, by monitoring the change in chemical shift with increase in temperature (Fig. 3.5). No significant variation was observed for any of the proton chemical shift. It may be attributed to the presence of monomeric palmatine at all the temperature as there is no change in the chemical environment of any of the protons and palmatine remains in the same conformational and configurational state even at high concentration of 25.78 mM.

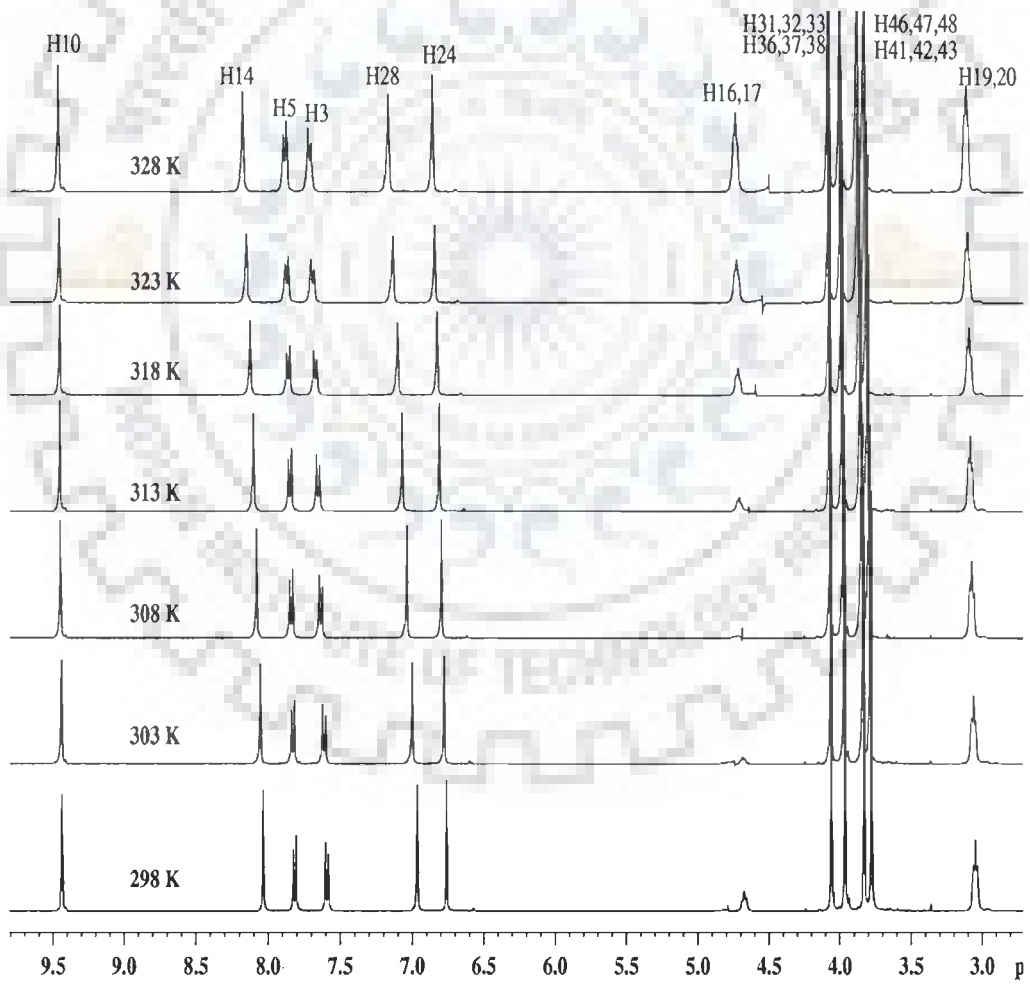

Fig. 3.5: ^{1}H Proton spectrum of palmatine with varying temperature in the range 298-328 K

3.1.2 Restrained Molecular Dynamics and solution structure of palmatine

Figure 3.6 shows the ROESY spectra of palmatine in D_2O solvent. We observed 10 cross-peaks and calculated interproton distances from the integrals (Table 3.4). The interproton distance H3–H5 = 2.45 A° is taken as reference distance. A range of ±0.2 A° was provided to account for any error in integrals. Using these 10 distance constraints restrained Molecular Dynamics simulations were carried out to search for optimum conformation. The initial structure of palmatine is built by using builder module in MOE (Molecular Operating Environment, Chemical Computing Group, Canada) software. Pseudo atom correction was used for methyl and other equivalent protons. Conformational search was performed by following simulated annealing restrained Molecular Dynamics protocol. The molecule was heated to a temperature of 800 K in steps of 100 K and equilibrated at this temperature. Molecular Dynamics simulations were carried out for 250 ps at 800 K during which 100 structures were saved at regular intervals. Each of them was then slowly cooled at 300 K in steps of 100 K. At the end of simulated annealing all the structures were minimized. Out of 100 structures 10 minimum energy structures were selected for further analysis. During the final equilibrium stage, there was no significant change in either in the potential energy or restraint deviation energy. The various structures at these time intervals differed only marginally from each other and hence indicate that the structure obtained is a minimum energy conformer. The minimum energy conformer is shown in Fig. 3.7a. The bond length, bond angle, torsional angles, etc. for all these are shown in Table 3.6

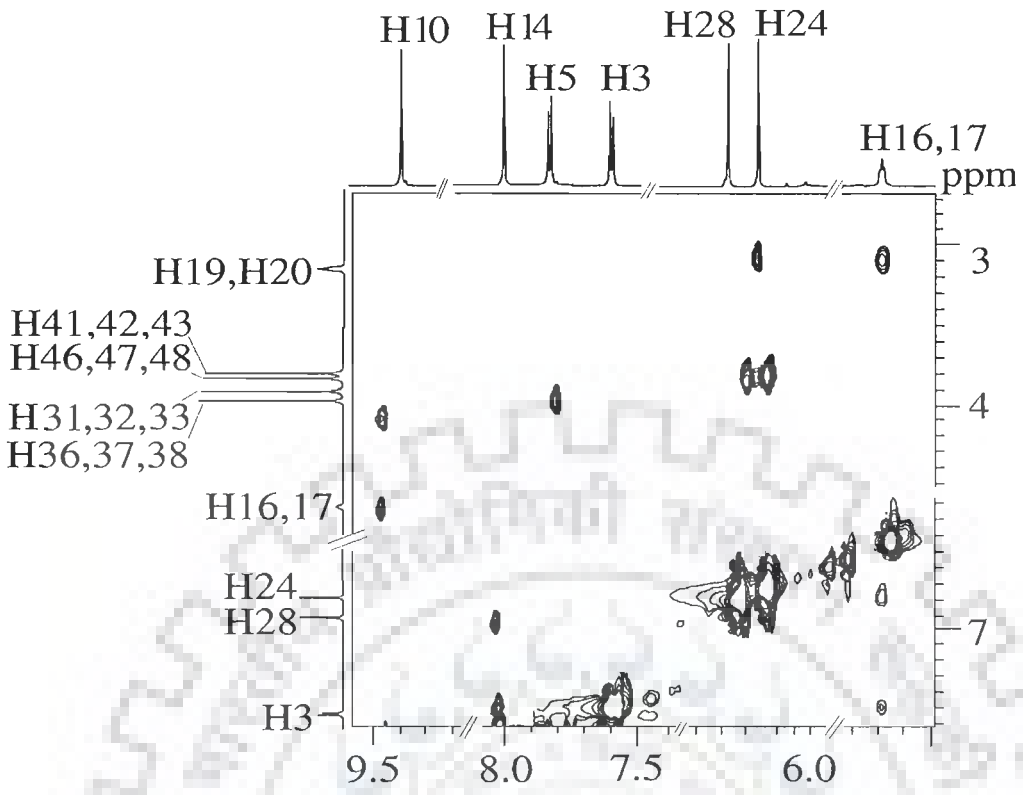

Fig. 3.6: ROESY spectra of palmatine in D_2O showing interproton contacts.

Table 3.4 Connectivities and inter proton distances (Å) from ROESY spectra of palmatine.

S. No.	Connectivities	Inter proton distances (Å)	Distances in rMD structure (Å)
1.	H3 - H14	2.51	2.48
2.	H3 - H5#	2.45	2.42
3.	H28 - H14	1.98	2.23
4.	H5 – H^a(31, 32, 33)	2.16	2.27
5.	H^a(16, 17)-H10	2.39	2.42
6.	H10 – H^a(36, 37, 38)	3.38	3.73
7.	H^a(19, 20)-H24	2.48	2.38
8.	H28 – H^a(46,47,48)	2.06	2.46
9.	H24 – H^a(41, 42, 43)	2.03	2.31
10.	H^a(16, 17) – H^a(19, 20)	2.46	2.66

[a] **Pseudoatoms**

 # Reference peak

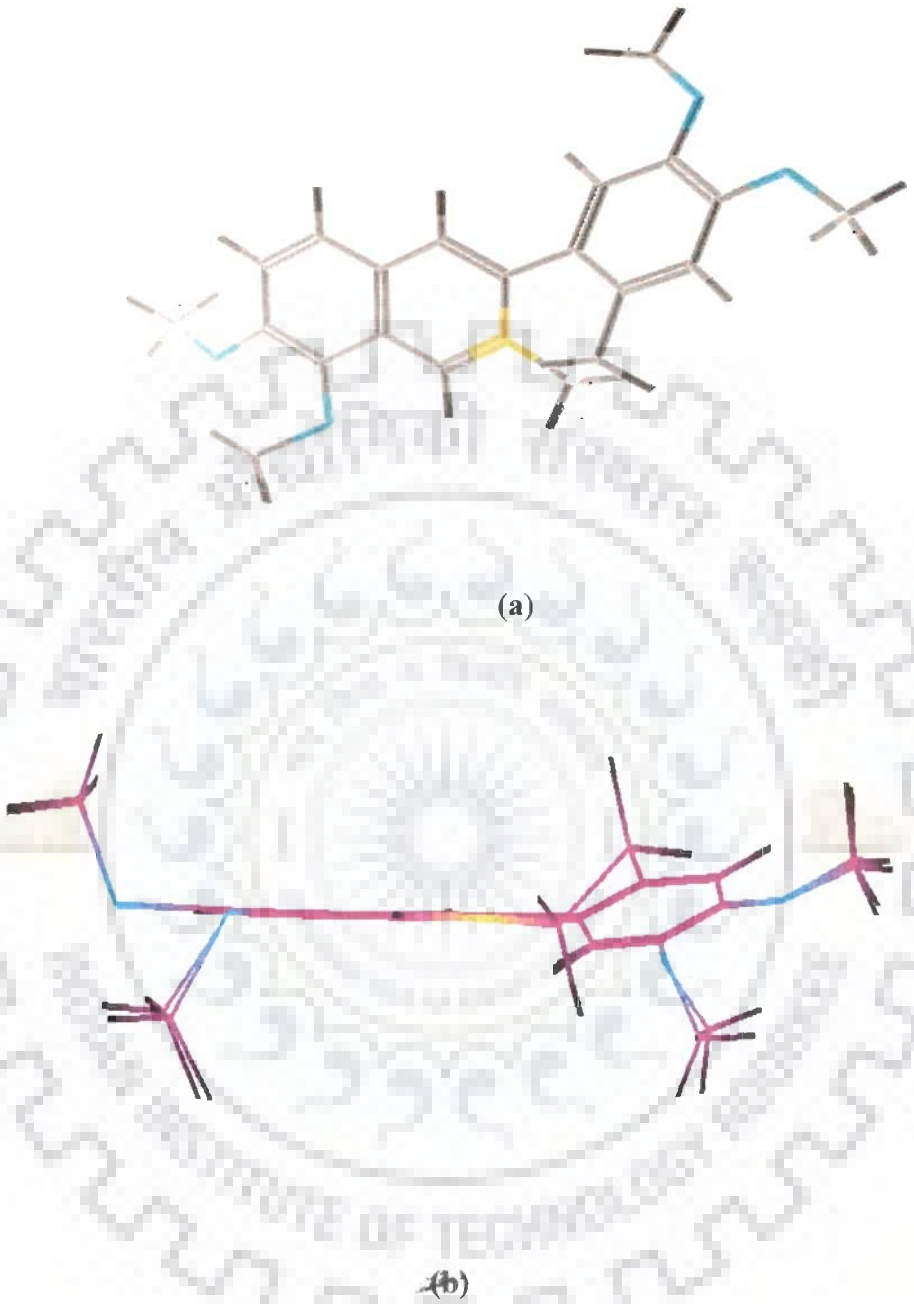

Fig. 3.7: (a) Minimized solution structure of palmatine. (b) Superimposed optimized structure of palmatine from solvent and gas phase with the help of B3LYP/6-311G.**

3.1.3 Quantum Chemical calculations

In the present study, we choose the hybrid B3LYP method based on Becke's three parameter functional [Becke, 1993] with correlation provided by LYP [Lee, et al., 1988] of Density Functional Theory (DFT) and the second-order Moller–Plesset (MP2) method of *ab initio* calculations. Both methods include the electron correlation but the latter one has become a standard method to explore the bio-molecular interaction as electron correlation plays an important role. In many of the earlier work B3LYP functional had been shown to yield best results for the systems. It provides computationally efficient quantum-mechanical approach for the study of large systems. On the other hand *ab initio* MP2 method is time consuming with extended basis sets.

In all of these calculations, Cartesian Gaussian type orbitals (GTO's) were used as basis function for the molecular orbitals. Although the capability of the basis functions to describe bonding deformations of the electronic density can be enhanced by increasing the number of basis functions for each orbital or including higher angular functions. Yet as a thumb rule it should be able to yield results which are comparable with larger basis set while remaining computationally manageable, and thus at least a basis set of the split-valence type with polarization function should be employed.

All calculations presented here were done using the Gaussian 98 and Gaussian 03 program package [Frisch et al., 1998]. Full unconstrained geometry optimizations were performed using three different density functional methods as outlined above. Several basis sets like STO-3G, 6-31G, 6-31G*, 6-31G**, 6-311G** were used with B3LYP method. But at HF (SCF) and MP2 level only 6-31G* basis were employed. Since MP2 calculations were time consuming, we have used only 6-31G* basis set.

For solvent effects, we have used the PCM model at B3LYP/6-311G** and 6-31G** level as implemented in Gaussian 03. Full geometry optimization was performed using B3LYP, HF and MP2 methods. All the molecular properties and chemical shifts are computed using the optimized structure of the molecule. All the molecular properties and chemical shifts were computed using the optimized structure of the molecule. The chemical shifts were also calculated using the same Gaussian package with the gauge independent atomic orbital (GIAO) approach. This approach allows the computation of the absolute chemical shielding due to the electronic environment of the individual nuclei. On the ground of variational theory, the quality of wave functions has been traditionally determined by the total energy which is the average of the Hamiltonian over the wave function. The lower is the energy, the better is the quality; we retain this concept despite the fact that for properties other than the total energy, it may not be acceptable. In view of this we report our calculations for structural properties using B3LYP, HF and MP2 methods. The calculation of isotropic shielding constant with respect to even small basis set using GIAO-MP2 method requires large computational time and memory; consequently, it is not calculated. Thus, chemical shift is compared only with B3LYP and HF methods.

3.1.3.1 Chemical Shifts

All the ^{1}H and ^{13}C chemical shifts were referenced to those of Tetra Methyl Silane (TMS). The absolute ^{1}H and ^{13}C shielding of TMS based on the B3LYP were calculated at the level basis set which was same as that used in the calculation to which they refer. These values are listed in Table 3.5. In this way we compute chemical shifts to values in ppm, by subtracting the absolute shielding of each atom (^{1}H and ^{13}C) from the reference value for TMS.

Table 3.5 Calculated isotropic shielding of carbon and proton for Tetra Methyl Silane (TMS) with different wave functions by GIAO method using B3LYPand HF methods

Basis sets	Carbon chemical shielding	Proton chemical shielding
B3LYP/STO-3G	233.16	32.92
B3LYP/6-31G	195.86	32.93
B3LYP/6-31G*	189.72	32.18
B3LYP/6-31G**	192.17	31.81
B3LYP/6-311G**	184.51	32.01
HF/6-31G*	201.75	32.91

The calculated chemical shift from STO-3G to 6-311G** with GIAO method along with the present experimental results are listed in Tables 3.1 and 3.2. A quick look at the values in the tables shows that the calculated chemical shifts for ^{1}H are more sensitive to the variation of basis sets as compared to that of ^{13}C. This can be rationalized by the fact that ^{1}H atoms are the smallest of all atoms and are mostly localized on periphery of the molecules therefore their chemical shifts would be more susceptible to intermolecular interactions in the aqueous solutions as compared to that for other heavier atoms. The tabulated value show that the percentage variation of the difference between measured data and calculated results, is largest for proton than that for the carbon; it being 43 % and 10 % for proton and carbon, respectively. Further we also see in Table 3.2 that largest difference between the calculated carbon chemical shifts is at positions of C4, C27, C25, C7 and C26. The magnitude of

difference in ppm for carbon are 20.7, 19.8, 16.4, 15.3 and 12.0, respectively, while for the proton the difference lies at the position of H5 and H28 with magnitude of 0.40 and 0.82, respectively. Considering the fact that NMR chemical shifts are affected by the chemical environment of the atoms i.e. molecular conformation and interaction with the solvent molecules, it is seen that the overall agreement between the calculated and measured values both for ^{1}H and ^{13}C chemical shifts is satisfactory. It is of interest, however to see, how good is the correlation between experimental and calculated results? We therefore plot our experimental NMR results versus theoretical calculations obtained with different basis sets (Tables 3.1 and 3.2). A linear correlation between theoretical and experimental results both for proton and carbon chemical shifts is clearly seen in Fig. 3.8 a-b and Fig.3.9 a-b, respectively. Here the correlation coefficient for proton and carbon in gas phase are 0.9824 and 0.9821, and the corresponding values in solvent are 0.984 and 0.986, respectively, which are reasonably good and approaches to a value of 1. On the whole good correlation demonstrates that in general 6-311G** basis set predicts the best NMR parameters.

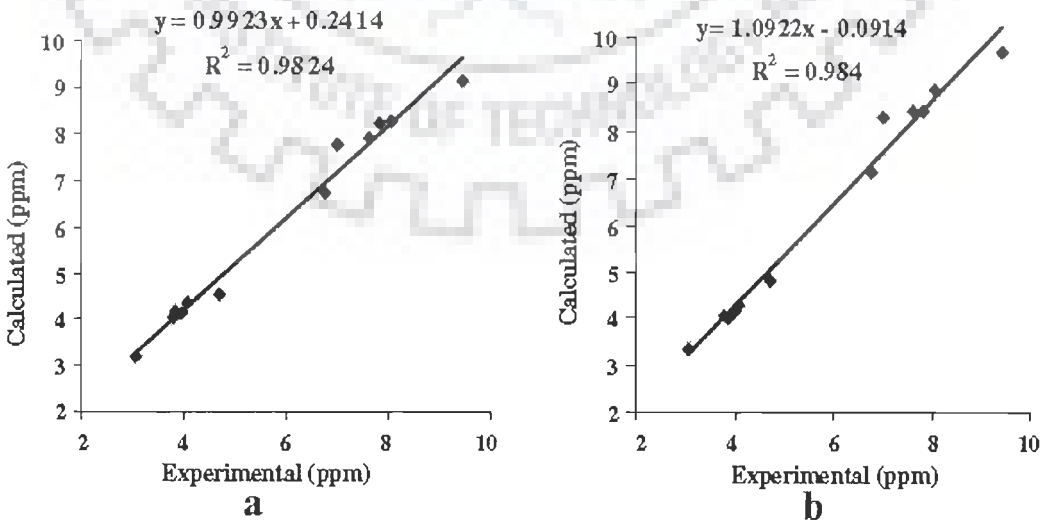

Fig. 3.8 Correlation of experimental and calculated proton chemical shifts of palmatine with B3LYP/6-311G/GIAO method in (a) gas phase and (b) solvent phase.**

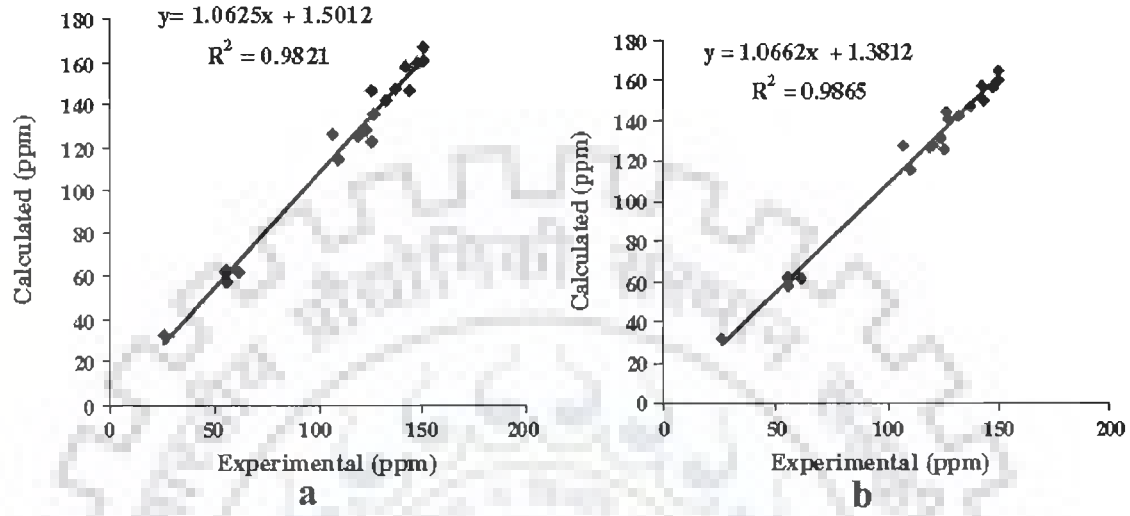

Fig. 3.9: Correlation of experimental and calculated carbon chemical shifts of palmatine with B3LYP/6-311G/GIAO method in (a) gas phase and (b) solvent phase**

3.1.3.2 Structural parameters

We have calculated values for bond lengths, bond angles and dihedral angles for five basis sets ranging from minimal parameters, PCM-B3LYP/6-311G** was employed. The comparison of these structural parameters with the X-ray data, present NMR based solution structure along with the calculated values using B3LYP, HF and MP2 methods and is shown in Table 3.6. It is noticed that the effect on the B3LYP model with increasing basis set narrows down the difference between the calculated and experimental results, indicating that the polarization functions do play important role. All calculated structural parameters at MP2/6-31G* ab initio level in general agree well with B3LYP/6-311G** results but resemble slightly with basis set HF/6-31G*. Further, the influence of the solvent on the geometrical parameters is found very negligible as can be seen from the tabulated values in Table 3.6. It is also noticed

that all the calculated bond lengths are very close to the present solution structure based on NMR experimental data and also compare reasonably well with the X-ray measurements reported in the literature; the difference lies within a few hundredth of an angstrom. But this trend is not seen in case of bond angles, the calculated bond angles are close to the present experimental results but differ with the X-ray measurements. On comparing our calculated structural parameters with solution parameters we found that the maximum variation in the calculated and measured values is less than 5 Å except that for angles which are related to OCH_3 group position. For example, these angles C7–O34–C35, C4–C6–O29, C27–C26–O44 and C23–C25–O39 have a difference of 7 Å approximately. From the analysis of bond lengths and bond angles, we notice that such differences between calculated and measured values arise due to the fact that the molecule is in dynamic state in solution phase (i.e. Ring B and OCH_3 groups) as compared to that in the gas phase. These changes in the optimized structures can be seen more clearly through the difference in the magnitude of the dihedral angles at OCH_3 group rather than at the ring B position. The difference between their dihedral angles (C25–O39–C40–H41, C27–C26–O44–C45, C25–C26–O44–C45 and C4–C6–O29–C30) is greater then 110°, implying that the molecule in solution phase has more freedom at the OCH_3 group. For the sake of clarity, a few words on its structure are in order. The structure of palmatine shows that the methoxy group at position C6 is displaced above the plane of CD ring and the methoxy group at C7 is below the C–D plane, whereas the other two methoxy groups in ring A are twisted above and below the plane of the ring.

Table 3.6 Comparison of experimental structure (in solution) and optimized structure of palmatine with B3LYP method using STO-3G, 6-31G, 6-31G*, 6-31G, 6-311G**basis sets along with HF and MP2 methods using basis set 6-31G*.**

Bond Length (Å)	B3LYP STO-3G	B3LYP 6-31G	B3LYP 6-31G*	B3LYP 6-31G**	B3LYP 6-311G**	HF 6-31G*	MP2 6-31G*	Present solution structure	X-ray palmatine
C6-O29	1.415	1.390	1.362	1.362	1.361	1.349	1.361	1.39	1.361
C7-O34	1.401	1.382	1.394	1.360	1.358	1.343	1.369	1.40	1.383
C9-N11	1.379	1.347	1.394	1.339	1.337	1.317	1.339	1.35	1.462
N11-C12	1.440	1.403	1.488	1.394	1.392	1.382	1.386	1.36	1.475
N11-C15	1.526	1.499	1.384	1.488	1.489	1.483	1.486	1.49	1.465
C26-O44	1.412	1.377	1.360	1.384	1.357	1.348	1.364	1.39	1.375
O29-c30	1.479	1.482	1.443	1.083	1.445	1.419	1.451	1.43	1.425
O34-C35	1.489	1.486	1.447	1.093	1.450	1.427	1.093	1.43	1.431
O39-C40	1.481	1.460	1.089	1.090	1.431	1.083	1.434	1.43	1.418
O44-C45	1.477	1.472	1.438	1.438	1.441	1.077	1.444	1.43	1.422
Bond Angle (deg.)									
N11-C9-C8	122.107	121.870	122.189	122.135	122.180	122.464	121.142	122.3	112.1
C9-N11-C15	119.131	119.136	119.154	119.133	119.096	119.184	119.271	117.9	109.7
C9-N11-C12	121.752	122.202	122.246	122.260	122.227	121.929	122.900	121.1	109.8
C12-N11-C15	119.072	118.616	118.551	118.558	118.628	118.857	119.271	121.0	111.1
C12-N11-C13	116.792	117.339	117.283	117.317	117.345	118.021	117.391	118.8	107.5
C12-N11-C22	117.914	118.279	118.241	118.234	118.20	117.831	118.065	116.8	112.2
N11-C15-C18	109.614	110.243	110.345	110.343	110.278	110.048	109.087	110.1	110.2
C6-029-C30	114.570	116.537	115.961	115.957	116.021	115.974	114.370	117.4	-
C4-C6-O29	123.874	117.851	117.514	115.514	117.659	118.557	117.271	124.5	-
C27-C26-O44	127.669	115.813	118.143	118.125	117.843	119.401	118.305	125.0	
C23-C25-O39	127.405	123.898	124.677	124.658	124.589	124.821	125.183	117.6	
C7-O34-C35	115.161	118.670	116.890	116.810	117.157	118.089	113.396	113.8	-
C25-O39-C40	113.327	119.885	119.270	119.258	119.519	120.660	117.496	117.5	-
C26-O44-C45	112.861	122.058	117.836	117.844	118.540	117.111	114.907	117.7	-
C13-C12-C22	125.280	124.363	124.458	124.430	124.431	124.268	124.46	124.6	-
Dihedral angle (deg.)									
C4-C6-O29-C30	-7.935	-108.262	113.891	-1.119	-112.785	-94.754	-113.891	2.3	-
C25-O39-C40-H41	-179.723	-178.696	-178.095	-178.195	-178.144	177. 311	-177.717	40.4	-
C27-C26-O44-C45	179.776	39.727	63.588	63.321	60.045	65.004	67.224	176.9	-
C6-C7-O34-C35	-24.587	53.436	58.280	58.399	58.013	61.688	64.284	-52.5	-
C23-C25-O39-C40	-0.444	-1.406	-2.1941	-2.054	-2.181	-2.489	-3.110	-0.3	-
C25-C26-O44-C45	179.776	39.727	63.5878	63.321	60.045	65.004	67.224	176.2	-
Total Energy (a.u)	-1154.243	-1168.571	-1168.897	-1168.928	-1169.179	-1161.724	-1165.267	-	-

This is to minimize sterically unfavorable interactions. Palmatine shows deviation from planarity due to the fact that saturated ring B adopts a twisted half chair conformation with atoms C15 and C18 deviating from the plane of aromatic rings A and C. Further, it is also noticed from the experimental data that the two aromatic rings A and fused ring C–D are tilted to each other approximately by an angle of 22°, both in solution structure and B3LYP/6-311G** optimized structure. These observations are in agreement with the recent studies done on berberine [Danilov, et al., 2006]. A superimposed optimized structure of palmatine in solvent and in gas phase with the help of B3LYP/6-311G** is shown in Fig. 3.7b.

3.2 CONCLUSIONS

One- and two-dimensional ^{1}H and ^{13}C NMR spectra for palmatine in D_2O solution were recorded. All proton and carbon resonances have been assigned. An optimized solution structure has been determined by using distance restraints from the 2D NMR data. The experimental findings were combined with a theoretical investigation using Density Functional Theory (DFT), MP2 and HF methods for palmatine molecule. All the geometries for the molecules studied were fully optimized without using constraints with all the three different methods. Among all the methods B3LYP functional shows reasonably good results for geometries, energies, and all other NMR parameters and the same are reported here. A variety of basis sets (STO-3G, 6-31G, 6-31G*, 6-31G**, 6-311G**) were used. The effect of increasing size of the basis set slows down the calculations but tends towards accurate results. Further, the geometrical parameters are relatively less influenced by the solvent effect but a noticeable change is seen in the values of chemical shifts due to inclusion of solvent. An overall analysis shows that B3LYP/6-311G** level of theory predicts results which are quantitatively good and compare well with the experiment.

Studies on the binding of palmatine to DNA by Absorption and Fluorescence spectroscopy

The interaction of small molecules with DNA plays an important role in many biological processes. DNA is the pharmacological target of many drugs that are currently in clinical use or in advanced clinical trials. It is more efficient to treat a disease by designing drugs that act at the DNA or messenger level rather than at the protein level. Therefore, intense interest exists in designing small molecules that might selectively binds to defined sites in DNA or RNA [Chaires, J.B. 1998]. Natural products in general due to their unmatched chemical diversity and biological relevance have been widely accepted as potential high quality pools in drug screening. The medicinal value of protoberberine alkaloids found in root, rhizome and stem bark of many plant species has been recognized since ancient times. The emerging diverse biological properties of protoberberines clearly emphasize the need to understand the molecular basis of their action. Palmatine (Fig. 3.1) belongs to this important class of alkaloids having promising lead structure for the development of functional DNA-binding drugs. It has shown antitumor activity against HL-60 leukemic cells and has antimicrobial properties [Kuo, et al., 1995; Schmeller, et al., 1997]. The Inhibition of reverse transcriptase has also been suggested to be one of the many reasons for the antitumor activity of palmatine [Sethi, M. L., 1983]. In most of the palmatine-DNA studies the ultimate aim is to develop understanding about designing improved derivatives for better sequence recognition and site specific binding in DNA because of its potential application in medicine.

So, in context of this we present the following studies on the protoberberine palmatine: The sequence specificity and mode of binding of palmatine and its interaction with different DNA sequences has been investigated by using UV-visible and fluorescence spectroscopic techniques. Calf thymus DNA, Poly dA-dT, Poly dG-dC and several oligonucleotides with different sequences and lengths were used to elucidate the binding affinity of palmatine. The studies done on the mode of interaction of palmatine with DNA has suggested partial intercalation as the mechanism of binding with adenine-thymine base pair specificity [Kluza et al., 2003; Bhadra, et al., 2007]. Whereas, ESI-MS studies on several protoberberines including palmatine indicated that the sequence selectivities of these alkaloids are not significant and remarkable [Chen et al., 2005]. Since, the mode of binding of palmatine is still indistinguishable, its interaction with oligonucleotides with different number of AT sites and different lengths (6to 12 bases) were studied.

4.1 Results and Discussion

4.1.1 Absorption studies

To know the sequence specificity, a fixed concentration of the drug (7-10 μM) was titrated against the increasing concentrations of various nucleic acids [Calf thymus DNA, Poly(dA-dT), Poly(dG-dC), d-$(CGATCG)_2$, d-$(CGTACG)_2$, $(CGATCGCGATCG)_2$, d-$(CGTACGCGTACG)_2$, d-$(CGCGCGCGCG)_2$, d-$(ATATATATAT)_2$ and d-$(CCAATTGG)_2$. Palmatine has two absorption bands in the visible region with maxima centered at 344 nm and 420 nm, respectively (Fig. 4.1). It is noted that the successive addition of DNA to palmatine can be easily monitored by calculating the absorbance at 344 nm. The band at 420 nm is less intense and band at 260 nm can not be used as it coincides with the DNA absorption maxima. So, in the present study of palmatine-DNA interaction, the change in the absorption intensity of

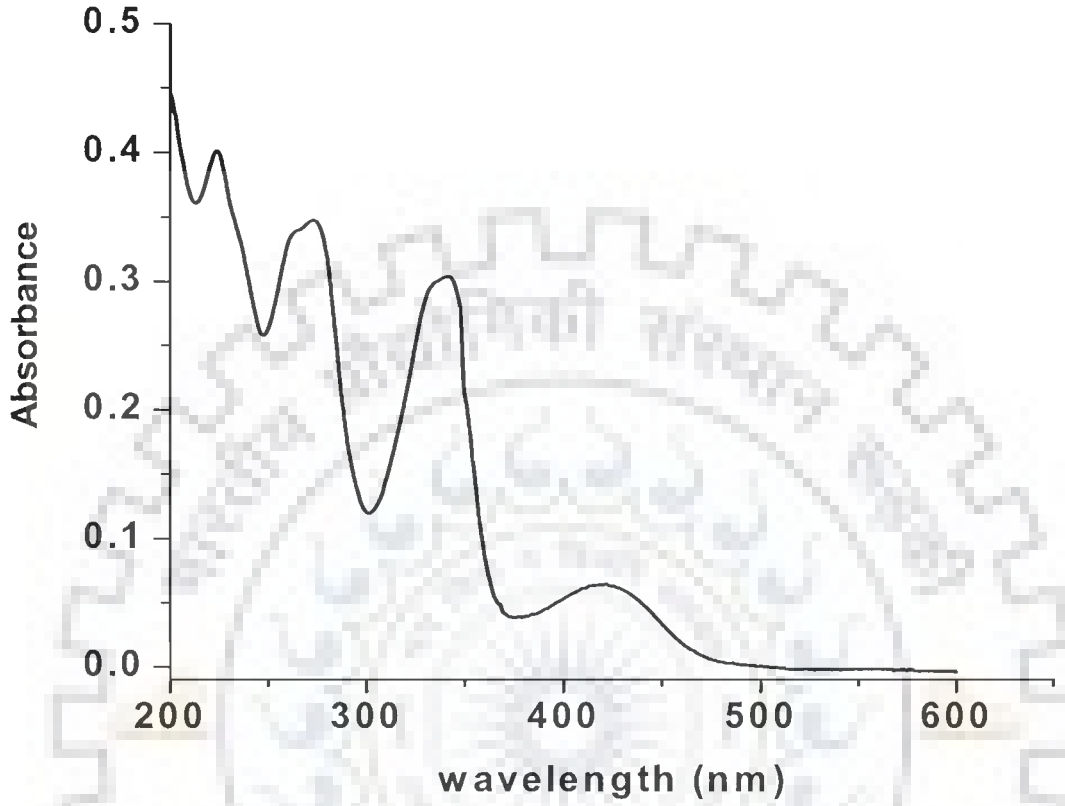

Fig 4.1: UV-visible absorption spectrum for palmatine

344 nm band is observed. All the experiments involving DNA interactions were carried out in BPES buffer (pH 7.0). The concentration of palmatine was determined by visible absorbance measurements using molar extinction coefficient ε_{344}=25, 000 M^{-1} cm^{-1}. The concentration of DNA samples per nucleotide were determined by absorption spectroscopy using their respective molar extinction coefficient as listed in Table 4.1. Absorption titration experiments were carried out as described earlier [Barve et al., 2005].

The intrinsic binding constant, K_b, of palmatine to these nucleic acids were determined according to Equation 1 [Kumbhar et al, 2005]

$$[DNA] / (\varepsilon_a-\varepsilon_f) = [DNA]/ (\varepsilon_b-\varepsilon_f) + 1/Kb\ (\varepsilon_b-\varepsilon_f) \quad (1)$$

Where, [DNA] and [Drug] is the total concentration of DNA and drug, respectively at each step of titration, ε_a is the extinction coefficient of palmatine-DNA complex at each step, ε_f is the extinction coefficient of free alkaloid, ε_b is the extinction coefficient of fully bound drug (it is assumed that when further addition of DNA does not change the absorbance, all the drug is bound and ε_b can be calculated from Beer's Law). The value of intrinsic binding constant (K_b) is obtained by the ratio of slope to the intercept in the plots of [DNA] / (ε_a-ε_f) versus [DNA]. The addition of calf thymus DNA, polydeoxynucleotides (Fig. 4.2a-c) and designed deoxyoligonucleotides d-$(CCAATTGG)_2$, d-$(CGATCG)_2$, d-$(CGTACG)_2$, d-$(ATATATATAT)_2$, d-$(CGCGCGCGCG)_2$, d-$(CGATCGCGATCG)_2$, d-$(CGTACGCGTACG)_2$, , (Fig. 4.2d-j) to the solution having fixed concentration of palmatine induces bathochoromic and hypochromic effects in its absorption spectra. The hypochromic effect in the electronic absorption spectra at 344 nm and 420 nm could be due to a strong interaction between the molecule and DNA double strands. The hypochromic and bathochromic effects essentially indicate strong intermolecular interactions involving effective overlap of the π electron cloud of palmatine with the polydexoynucleotides and oligodeoxynucleotides bases and are speculative of intercalative ligand-DNA complexation. The Absorption spectra of palmatine with Poly (dA- dT) shows three sharp isobestic points at ~ 354, 378, and 448 nms

respectively, indicating clearly an equilibirium between free and bound alkaloid molecule. A red-shift from 344 to 349 nm occurred, which indicates the binding of palmatine with Poly (dA- dT). Similar effects were also observed for Poly (dG - dC) and CT DNA but the extent of spectral changes were found to be comparatively lesser for Poly (dG- dC). From the titration studies, percentage of hypochromicity, epsilon for bound drug (ε_b) and binding constant were calculated and are tabulated in Table 4.1. Hypochromicity % observed for all the DNA sequences are shown in Fig. 4.3. It was observed that in case of Poly (dA-dT), percentage of hypochromicity and value of change in epsilon were higher; 64 % and 13924 $M^{-1}cm^{-1}$ as compared to 38 % and 9878 $M^{-1}cm^{-1}$ for Poly dG-dC. The evaluated binding constants for the complex of palmatine with Poly (dA- dT) and Poly (dG- dC) were found to be 2.25 x 10^5 and 8 x 10^4, respectively. These results indicated the preferential binding of palmatine with AT rich sequences as compared to the GC rich DNA, also previously reported by authors [Pilch et al., 1997; Bhadra et al., 2007]. The intrinsic binding constant for the other DNA sequences were also determined and the values were found to be in accordance to those obtained for protoberberine-oligonucleotide complexes in literature [Bhadra et al., 2007; Chen et al., 2005; Giri et al., 2006a; Giri et al., 2006b; Long et al., 2006; Mazzini et al., 2003]. Further, the small oligonuclotides having variable number and position for AT sites in base sequences were selected to investigate the sequence specificity of palmatine. Hypochromicity and epsilon bound value obtained on binding with palmatine were analyzed for these sequences. It can be noted from Table 4.1 that hypochromicity and change in epsilon bound value is 58 % and 6025 $M^{-1}cm^{-1}$ for d-$(CGATCG)_2$, 52 % and 5834 $M^{-1}cm^{-1}$ for d-$(CGTACG)_2$, whereas it is 69 % and 9058 for $CGATCGCGATCG\text{-}3')_2$ and 65 % and 5776 for $(5'\text{-}CGTACGCGTACG\text{-}3')_2$. It is found from the results that binding affinity of

palmatine is in the order of (5′-CGATCGCGATCG-3′)$_2$ >(5′-CGTACGCGTACG-3′)$_2$ and (5′-CGATCG-3′)$_2$ >(5′-CGTACG-3′)$_2$. These results show the base pair recognition of palmatine to ApT then to TpA, though it is not remarkable

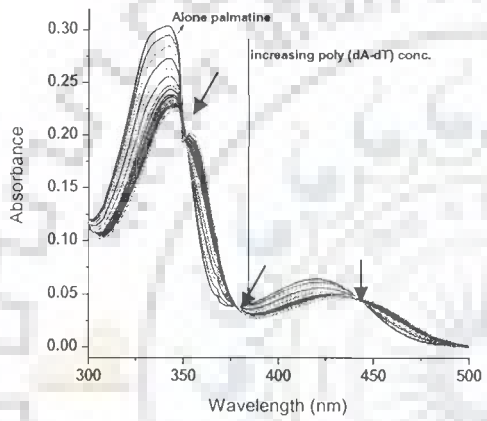

Fig 4.2 (a)

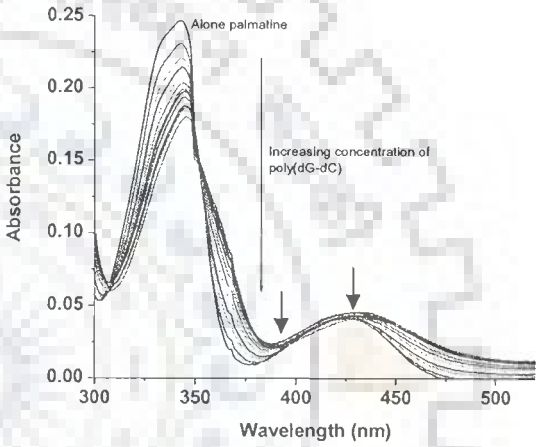

Fig 4.2 (b)

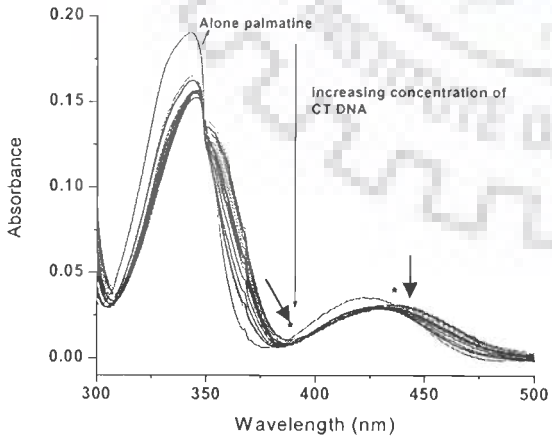

Fig 4.2 (c)

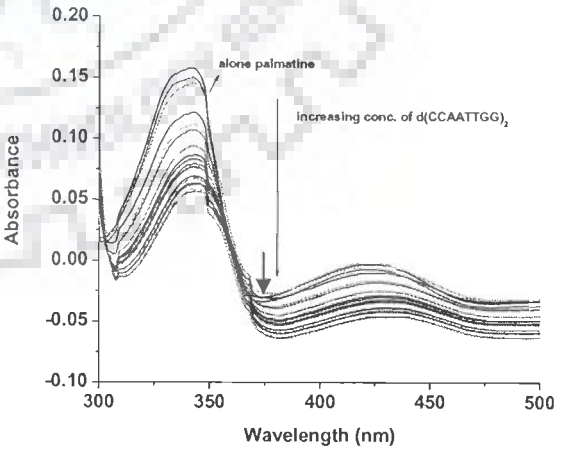

Fig 4.2 (d)

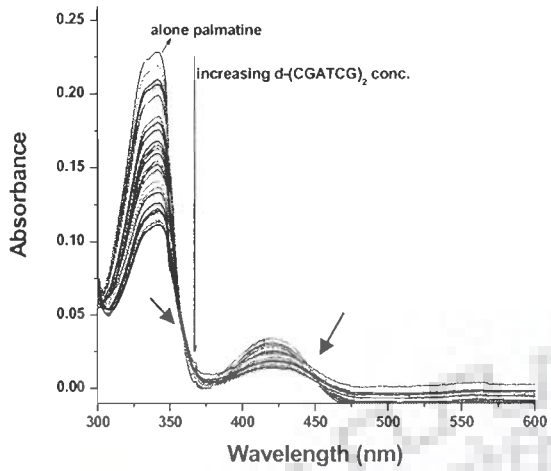

Fig 4.2 (e)

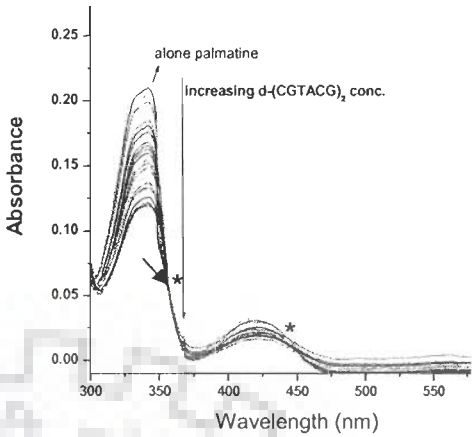

Fig 4.2e

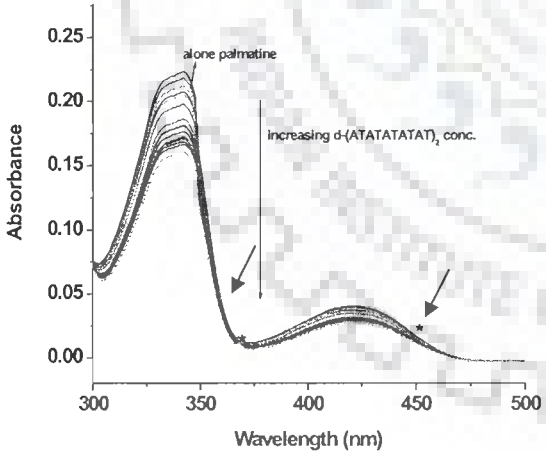

Fig 4.2 (g)

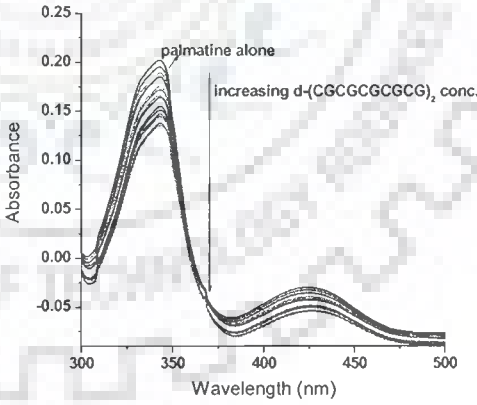

Fig 4.2 (h)

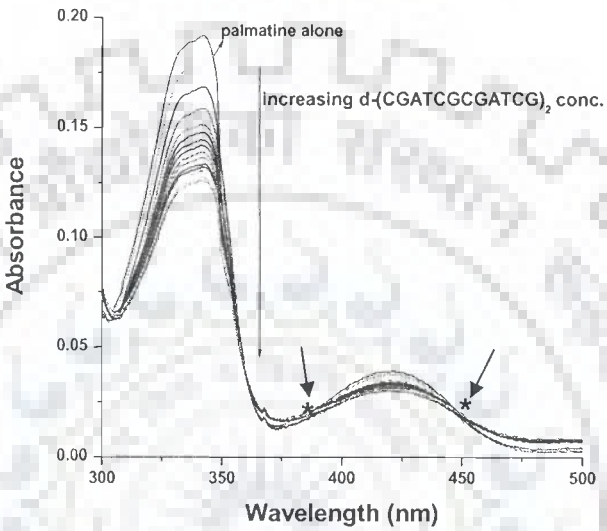

Fig 4.2 (i)

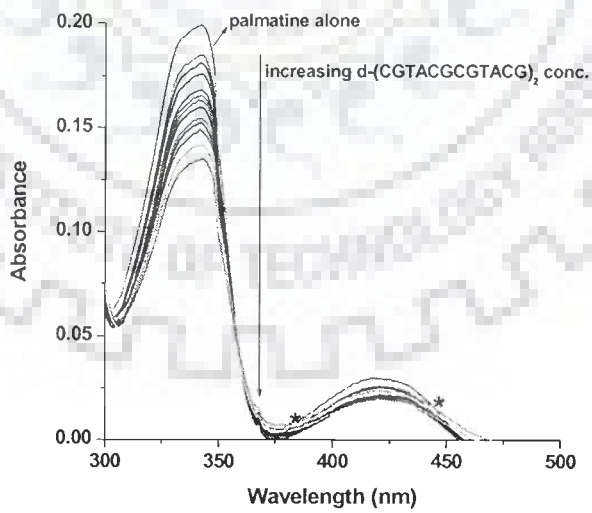

Fig 4.2 (j)

Fig. 4.2 Absorption spectra of palmatine in the presence of increasing concentration of (a) Poly (dA-dT) (b) Poly (dG-dC) (c) CT DNA (d) d-(5′-CCAATTGG-3′)$_2$ (e) d-(5′-CGATCG-3′)$_2$ (f) d-(5′-CGTACG-3′)$_2$ (g) d-(5'-ATATATATAT-3')$_2$ ((h) d-(5′-CGCGCGCGCG-3′)$_2$(i) d-(CGATCGCGATCG)$_2$ (j). d-(CGTACGCGTACG)$_2$. Small arrow represents the isobestic point

Table 4.1- Absorption spectral characteristics of palmatine interaction with various DNA and oligonucleotides.

DNA	ε_{free} DNA	ε_{bound} Drug	$\Delta\varepsilon$ (drug) ($\#\varepsilon_{free}$-ε_{bound})	λ_{Final}	$\Delta\lambda$*	Isobestic points	Hypochromicity	Binding constant
CT DNA	6600	14500	10500	348	5	378, 448	52%	1.25×10^5
Poly d(A-T)	8600	13924	11076	349	6	354, 378, 448	71%	2.25×10^5
Poly d(G-C)	7750	15122	9878	347	3	448, 354	32%	8×10^4
$(5'\text{-CGATCG-}3')_2$	57200	18975	6025	345	1	378, 448	58%	-
$(5'\text{-CGTACG-}3')_2$	57600	19166	5834	344	0	358	52%	-
$(CGTACGCGTACG)_2$	97200	19234	5776	345	1	448	69%	9.9×10^4
$(CGATCGCGATCG)_2$	97200	19942	9058	346	2	378, 448	65%	1.02×10^5
$(ATATATAT)_2$	111200	14579	10421	346	2	358, 378, 448	70%	1.98×10^5
$(CGCGCGCG)_2$	84800	20125	4875	344	0	-	28%	2×10^4
$(5'\text{-CCAATGG-}3')_2$	73000	8619	16381	348	5	354	75%	5.27×10^5

* ($\Delta\lambda = \lambda_{344} - \lambda_{Final}$)

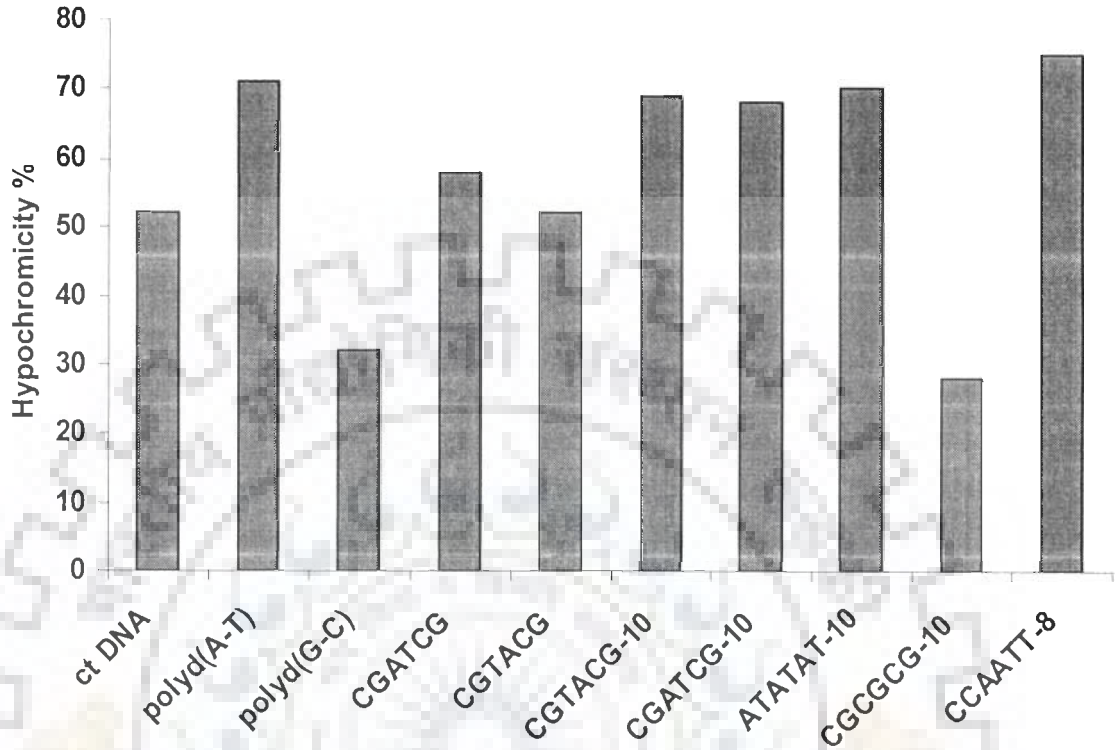

Figure 4.3: Observed hypochromicty of palmatine DNA complexes.

To see the effect of binding affinity of palmatine to DNA due to variation in length and number of sites present, oligonucleotides containing 8-12 bases for e.g. d-$(CGATCGCGATCG)_2$, d-$(CGTACGCGTACG)_2$, d-$(CGCGCGCGCG)_2$, d-$(ATATATATAT)_2$ and d-$(CCAATTGG)_2$ were used. It was observed that binding affinity observed for dodecanucleotides, used in this study was found to be in the order of d-$(ATATATATAT)_2$> d-$(CGATCGCGATCG)_2$> d-$(CGTACGCGTACG)_2$> d-$(CGCGCGCGCG)_2$, which again show the AT preference of palmatine. It was found that among all the oligodeoxycucleotides studied, d-$(CCAATTGG)_2$ has shown the most effective binding to palmatine. Our results are in accordance with the earlier

study done on the protoberberine, berberine. It was reported that berberine bound in the minor groove of d $(AAGAATTCTT)_2$, with a preference for AATT sites over ATCG sites [Mazzini et al., 2003]. Whereas, the ESI-MS experiments indicated that the sequence selectivity of the protoberberine akaloids was not significant and remarkable, AT or GC preference was not obtained. The replacement of AATT site with other bases on these studies of the protoberberines-DNA complexes has not shown prominent sequence selectivity [Chen et al., 2005].

4.2 Fluorescence spectral study

Various techniques have been developed which help to determine binding and provide information for understanding the nature of complexes between small molecules and biomacromolecules. Fluorescence spectrometry is one such technique. It has been widely used in the investigation of non covalent complexes of small organic molecules with DNA [Chaires and Waring, 2001; Fox, 1997] and the complex formation occurrence is reflected in terms of the change observed in the fluorescence intensities (either enhancement or quenching). The binding of palmatine to the above nucleic acid sequences was further examined by fluorescence spectroscopy measurements. In aqueous buffer, palmatine has a weak fluorescence spectrum in the range 450-650 nm with an emission maximum around 530 nm when excited at 350 nm. This weak intrinsic fluorescence of palmatine enhances on binding with DNA, indicating that the bound alkaloid is located in the regions of low polarity. Palmatine shows higher degree of fluorescence enhancement with Poly (dA-dT) and calf thymus DNA (Fig. 4.4a-b Table 4.2). Whereas, the fluorescence enhancement with poly (dG-dC) is significantly lower (Fig.4.4c). These data again clearly underscore the remarkably higher affinity of palmatine to AT polymers then to GC polynucleotides.

Addition of d-$(CGTACG)_2$ and d-$(CGATCG)_2$ sequences to palmatine did not increase the fluorescence but the sequences with at least 8 bp length showed enhancement in the fluorescence intensity. The order observed was d-$(CCAATTGG)_2$>d-$(ATATATATAT)_2$>d-$(CGATCGCGATCG)_2$>d $(CGTACGCGTACG)_2$ >d $(CGCGCGCGCG)_2$ (Fig. 4.4d-h). Relative fluorescence intensity of palmatine DNA complex with CT DNA, Poly (dA-dT), Poly (dG-dC) and d$(CCAATTGG)_2$ are shown in Fig. 4.5a-b. The results obtained shows that relative fluorescence enhancement was found to be maximum for Poly (dA-dT) among polydeoxynucleotides and for $(CCAATTGG)_2$ for small oligonucleotides, respectively. It is clear from Fig. 4.5a-b and Table 4.2 that at saturation level, the steady state fluorescence of palmatine is enhanced by more than 90 % by Poly (dA-dT) and CT DNA and by more than 75 % by $(CCAATGG)_2$ indicating a strong association of palmatine chromophore with AT rich DNA. This study shows the specific and higher affinity of binding of palmatine to AT rich DNA sequences and AATT containing sequence.

4.2.1 TCSPC Analysis: Time-Resolved Fluorescence Measurements of Palmatine d-$(CCAATTGG)_2$ Complex

Fluorescence excited state lifetimes are very sensitive to the structure and dynamics of a fluorescent molecule. Time resolved fluorescence decays were obtained by the Time-Correlated Single-Photon Counting method on the Spectrofluorimeter (model FluoroLog-TCSPC, make HORIBA Jobin Yvon Spex), used for the life time measurement study of palmatine and its complex with $(CCAATTGG)_2$. The excitation source, λ_{ex} = 344 nm was a fixed-wavelength NanoLED. The emission was detected at the emission wavelength, λ_{em} = 530 nm.

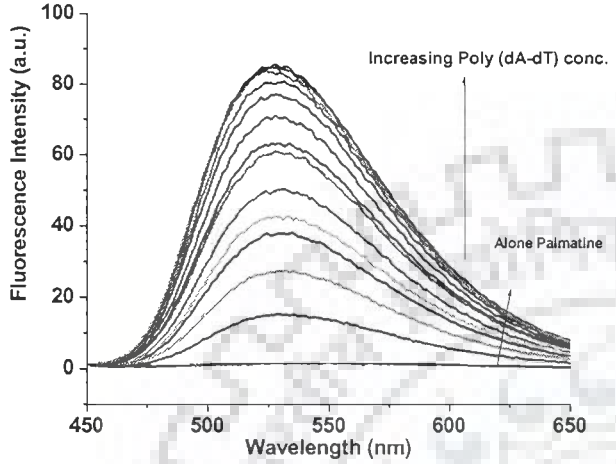

(Fig 4.4a)

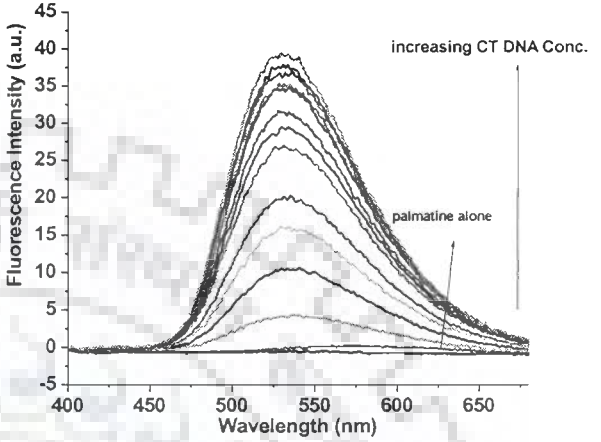

(Fig 4.4b)

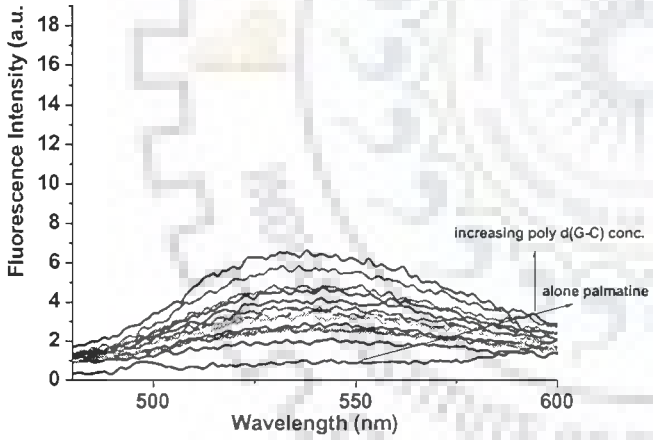

(Fig 4.4c)

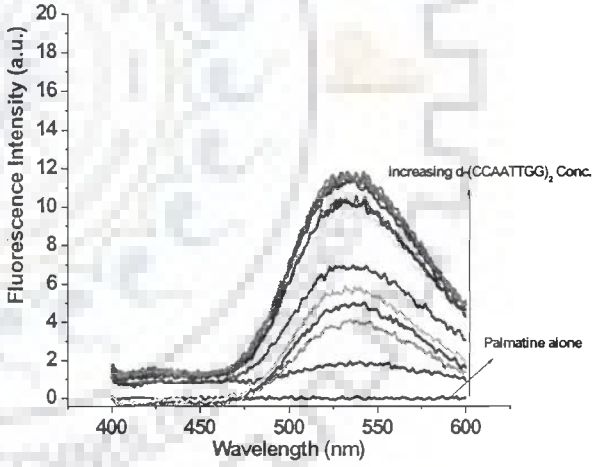

(Fig 4.4d)

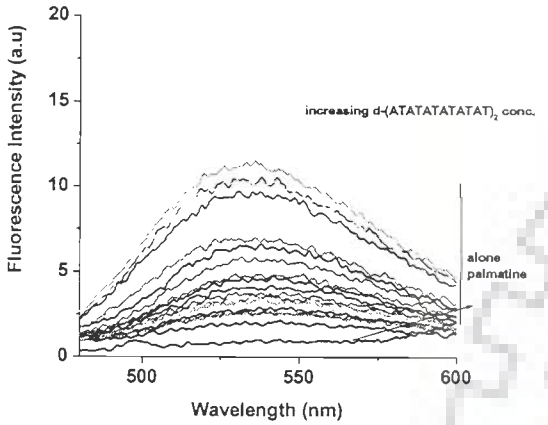

(Fig 4.4e)

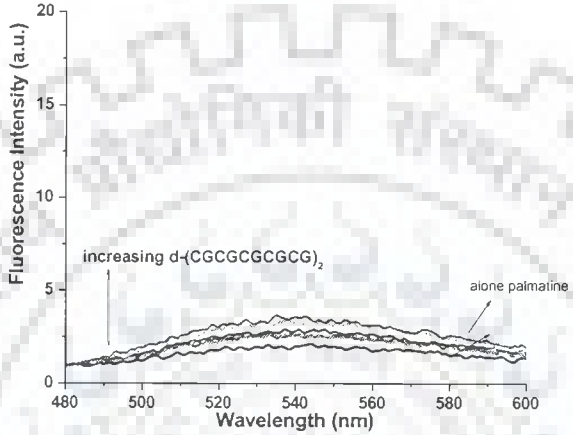

(Fig 4.4f)

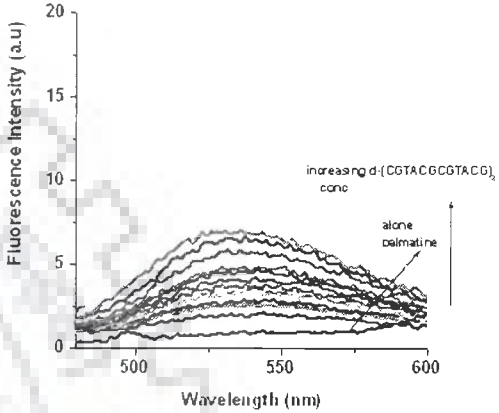

(Fig. 4.4g)

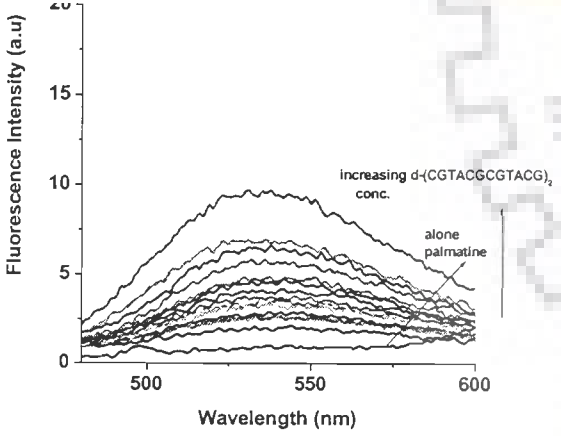

(Fig. 4.4h)

Fig. 4.4 Fluorescence spectra of palmatine in the presence of increasing concentration of (a) Poly A-T (b) CT DNA (c) Poly G-C (d) (5′-CCAATTGG-3′)$_2$ (f) (5'-ATATATATAT-3') (g) (5'-CGCGCGCGCG-3')(h)(5′-CGATCGCGATCG-3′)$_2$, (i) (5′-CGTACGCGTACG-3')

Table-4.2 Enhancement in the fluorescence intensity of palmatine by various nucleic acids.

DNA	Increase in Fluorescence
Poly d(A-T)	96%
Poly d(G-C)	51%
CT DNA	94%
(5'- CCAATTGG-3')$_2$	75%
d-(5′-CGTACGCGTACG-3′)$_2$	69%
d-(5′-CGATCGCGATCG-3′)$_2$	73%
d-(5′-ATATATAT-3′)$_2$	84%
d-(5′-CGCGCGCG-3′)$_2$	28%

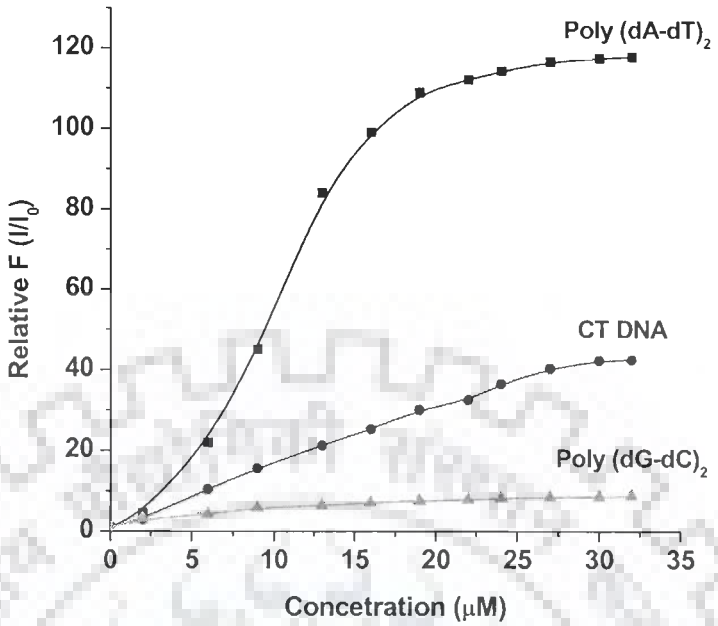

(Fig. 4.5a)

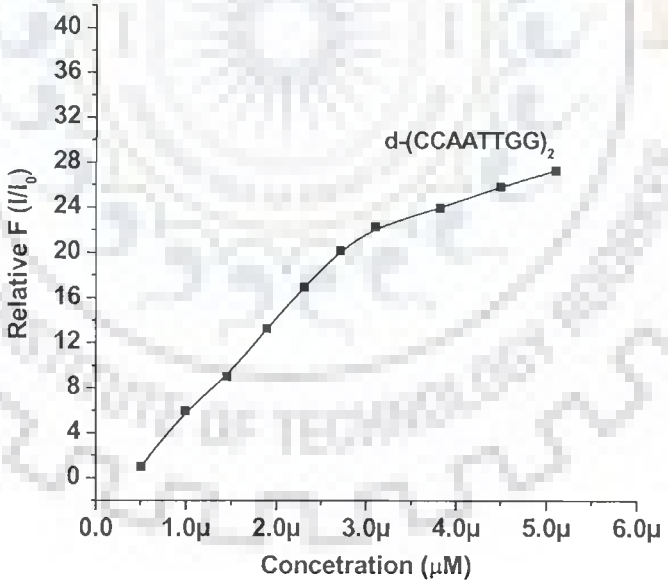

(Fig. 4.5b)

Fig. 4.5: Relative fluorescence intensity of palmatine DNA complex with (a) CT DNA, Poly d-(A-T) and Poly d(G-C) and (b) d-$(CCAATTGG)_2$

The fluorescence emission of the palmatine and its complex with d- $(CCAATTGG)_2$ was counted by a micro channel plate photo multiplier tube, after passing through the monochromator and processed through constant fraction discriminator (CFD), time-to-amplitude converter (TAC) and multi channel analyzer (MCA).

All measurements were performed at 298 K in 10 mM BPES buffer. The fluorescence decay was obtained and all the parameters were systematically analysed and processed by the software program DAS provided by FluoroLog-TCSPC instrument.

Global analysis was performed on each set of fluorescence decays and found that complexity of the model is well calculated with a tri exponential decay function which fits with an excellent statistical quality having global χ^2 value of 1.34 and 1.16 for palmatine and its complex with -d- $(CCAATTGG)_2$ respectively (Table 4.4). The low global values for χ^2 indicate that the tri exponential decay function is an excellent statistical description of both the systems [Byrne and de Mello, 1998]. The exponential function with three lifetimes ($\tau1$, $\tau2$ and $\tau3$) and three amplitudes (B1, B2 and B3) indicate the presence of three conformation of palmatine correspondingly. This is because palmatine is a heterocyclic compound containing one saturated ring, and four methoxy groups having rotation and can have more than one conformer in solution [Ojha et al., 2009]. For free palmatine, the values $\tau1$, $\tau2$ and $\tau3$ are 3.1 ns, 0.24 ns and 7.8 ns respectively. The relative contributions from these components were 38 %, 19 % and 36 % respectively. Most dyes of high quantum efficiency, such as laser dyes and fluorescence markers for biological samples have natural fluorescence decay times of the order of 1 to 10 ns due to their aromatic chromophore while less fluorescence chromphores have lesser lifetimes of 100 ns to 200 ns. Therefore $\tau1$ and $\tau2$ can be correlated to the planer structure of palmatine and $\tau3$ can

be correlated to non planer moiety of the palmatine. It can be noted from Table 4.3 that the numerical values of τ1, τ2 and τ3 and their relative distribution have varied in the presence of d-(CCAATTGG)$_2$. The values of τ1, τ2 and τ3 were decreased to 0.23, 0.18 and 2.6 respectively, showing that there is shortening of the decay time of palmatine due to binding (Table 4.3, Fig. 4.6). However, the relative contributions of τ1 increased to 47 % and the contribution from τ2 and τ3 has decreased to 15 % and 12 % (Table 4.3) which clearly elucidate the involvement of the planer moiety of palmatine in interaction with the d-(CCAATTGG)$_2$.

The analysis of fluorescence decay time of palmatine and palmatine d-(CCAATTGG)$_2$ complex clearly elucidate the binding of palmatine. Also the increase in the relative contribution of t1 and decrease in the relative contribution of t2 and t3 indicates that palmatine mostly interact with the planer conformation in complex [Ojha et al., 2009]. The significant change in the values of both the decay components and their relative contributions of palmatine upon binding with d-(CCAATTGG)$_2$ indicate the change in the microenvironment of palmatine in the presence of d-(CCAATTGG)$_2$.

Table 4.3: Lifetimes parameters of palmatine fluorescence and its 2:1 complex with d-(CCAATTGG)$_2$ in BPES buffer at 298 K.

Samples	Lifetime decay (ns)			Amplitude %			
	τ1	τ2	τ3	B1	B2	B3	χ^2
Palmatine	3.1	0.24	7.8	38	19	36	1.34
Palmatine d-(CCAATTGG)$_2$ 2:1 complex	0.23	0.18	2.6	47	15	12	1.16

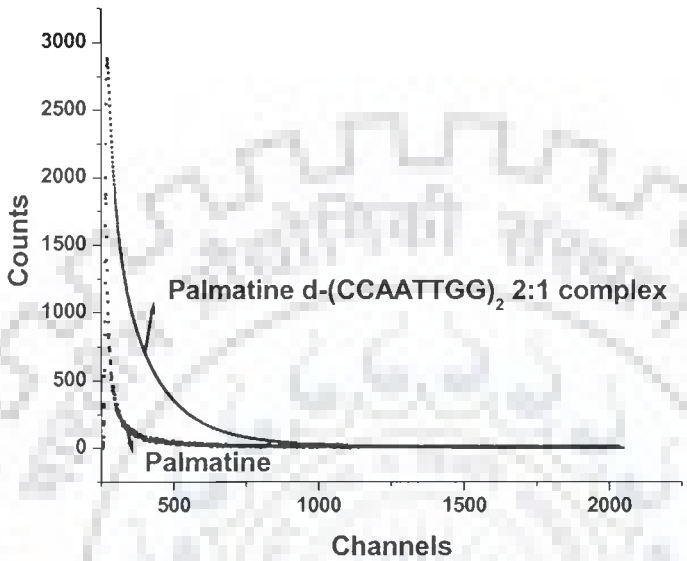

Figure 4.6: Fluorescence lifetime decay measurement profile of palmatine and 2:1 palmatine-d-(CCAATTGG)$_2$ complex

4.3 Summary and Conclusions

In conclusion, we have studied the interaction of palmatine with natural and synthetic double stranded DNA using spectrophotometric and spectrofluorometric techniques. The absorption spectrum of palmatine showed hypochromic and bathochromic effects with sharp isobestic points on binding to DNA. The intrinsic binding constant value and percentage of hypochromicity indicated the preference of palmatine for AT rich sequences. The fluorescence of palmatine was enhanced to varying extent on binding with the DNA sequences. The enhancement in fluorescence of palmatine on binding with Poly d(G-C) was found to be significantly lower then

the binding with Poly d(A-T). These results indicated that palmatine exhibited the greater binding affinity with AT rich sequences. These studies show that the binding of palmatine not only depends on the length of oligonucleotides, but also shows a preference for AATT containing sequences. The above study would potentiate the use of natural occurring palmatine and other protoberberines as lead compounds in the development of DNA based therapeutic agents.

Chapter 5

Studies on palmatine complexed with d-(CGATCG)$_2$ by using Phosphorous-31, Proton Nuclear Magnetic Resonance Spectroscopy and Restrained Molecular Dynamics

The distinguishing feature of drug-DNA interaction studies is to know about the structural and dynamic characterization of intermolecular interactions at the atomic resolution level. In this chapter, we highlight the specific intermolecular contacts between drug and DNA molecule and provide information on the conformational changes occurring in DNA and drug during complex formation. We report here for the first time the following studies on palmatine-d-(CGATCG)$_2$ complex by ^{1}H, ^{31}P NMR followed by restrained molecular dynamics simulations.

- The two dimensional ^{1}H - ^{31}P Heteronuclear Multiple Bond Correlation (HMBC) of 3.14 mM d-(CGATCG)$_2$ at 283 K for assignment of ^{31}P resonances.
- 1D ^{1}H , ^{31}P NMR titration studies of palmatine-d-(CGATCG)$_2$ complex at various drug (D)/DNA duplex (N) ratios of 0.10, 0.21, 0.31, 0.41, 0.52, 0.62, 0.73, 0.83, 0.93, 1.03, 1.14, 1.25, 1.35, 1.46, 1.56, 1.67, 1.77, 1.87, 1.97 and 2.00 at 278 and 298 K in 90% H_2O and 10% D_2O.
- ^{31}P and ^{1}H NMR study of 3.14 mM d-(CGATCG)$_2$ duplex as a function of temperature in the range 278-328 K.

• Temperature dependence of ^{31}P and ^{1}H NMR of the palmatine-d-$(CGATCG)_2$ complex having D/N = 1.0 and 2.0 in the range of 278 - 328 K.

• 2D ^{31}P - ^{31}P exchange spectra of palmatine-d-$(CGATCG)_2$ complex by phase-sensitive NOESY using mixing time of 200 ms at 278 K and 298 K for D/N = 0.5, 1.0, 1.5 and 2.0.

• 2D NOESY at D/N = 1.0, 1.5, 2.0 using mixing time τ_m =100, 200, 300 ms at 278 K in 90% H_2O and 10% D_2O.

• Diffusion Ordered Spectroscopy (DOSY) experiments of 2:1 complex of palmatine-d-$(CGATCG)_2$ and free palmatine at 298 K.

• Restrained molecular dynamics studies on the solution structure for the complex of palmatine with d-$(CGATCG)_2$ in drug to DNA duplex ratio of 2:1 using inter-proton distances obtained from 2D NOESY as restraints.

• Analysis of the converged structure in terms of time average of the various conformational and helical parameters as well as fluctuations and correlations among different structural parameters.

5.1 RESULTS AND DISCUSSION

5.1.1 Phosphorous-31 NMR Studies of Palmatine-d-$(CGATCG)_2$ Complex

^{31}P NMR is a useful probe for the geometric arrangement about the phosphate group since it provides direct information about DNA backbone. For the purpose of this discussion, the positions of the bases in the hexamer d-$(CGATCG)_2$ are designated as d–$(C1pG2pA3pT4pC5pG6p)_2$. The assignments of ^{31}P nuclei in d-$(CGATCG)_2$ is performed by using the 2D ^{1}H - ^{31}P HMBC (Fig. 5.1).

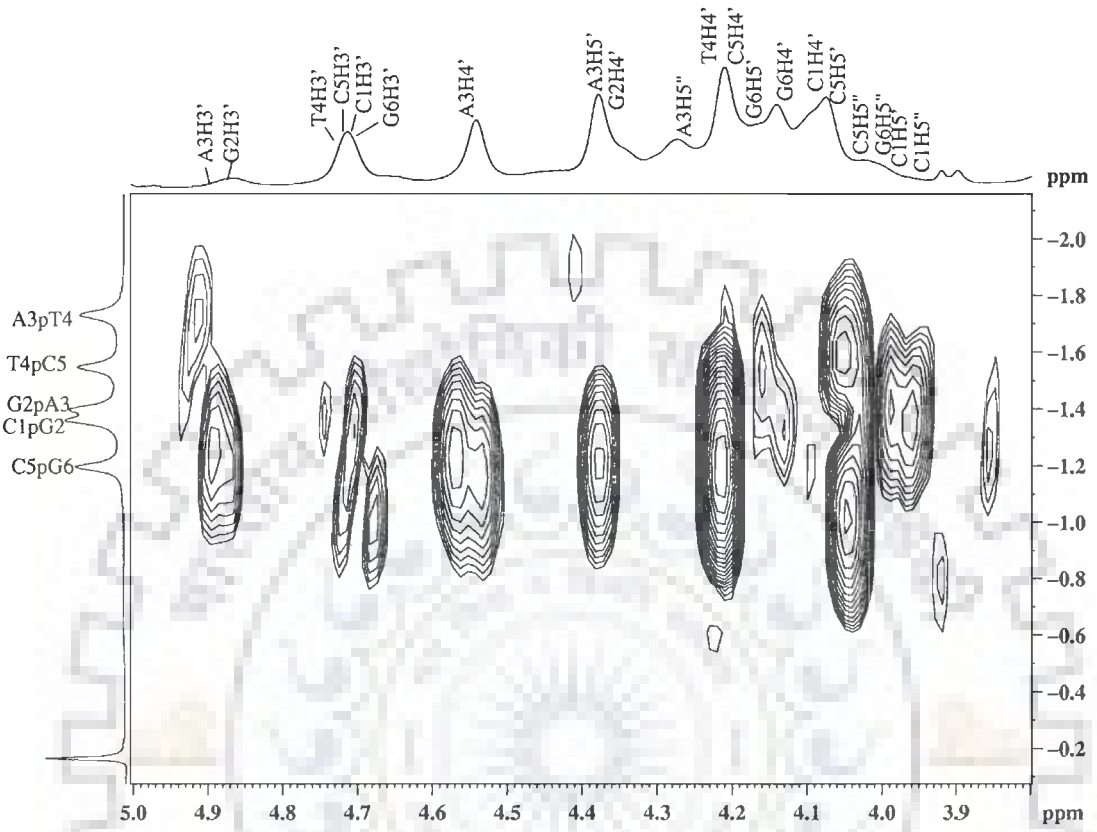

Fig 5.1: Two Dimensional ^{31}P –^{1}H Heteronuclear Multiple Bond Correlation (HMBC) spectra of d–$(CGATCG)_2$ at 283 K

The ^{31}P resonances resolve into five distinct signals corresponding to the five phosphate groups at the ambient temperature The cross peaks represent the scalar coupling between ^{31}P nuclei of the backbone and H3', H4'and H5' deoxyribose protons. The three-bond scalar couplings between $(^{31}P)_n$ nuclei in the phosphate backbone and the $(H3')_n$, $(H5'/H5'')_{n+1}$ protons and four-bond coupling with $(H4')_n$, $(H4')_{n+1}$ protons are observed The identification of the cross peaks are done on the basis of proton assignments, which have been done by using DQF COSY and 2D NOESY spectra (Barthwal et al., 2003). We are focusing mainly on H3' and H4' region for the assignment purpose as H5'/5" are overlapped highly. Accordingly the phosphate resonances at -1.36, -1.39, -1.73, -1.55 and -1.19 were assigned as C1pG2, G2pA3, A3pT4, T4pC5 and C5pG6 respectively in uncomplexed d-$(CGATCG)_2$ at 283 K (Table. 5.1)

5.1.1.1 Chemical Shift

The complex of d-$(CGATCG)_2$ with palmatine is made by the addition of palmatine from the stock solution (30 mM) to a fixed concentration of 3.14 mM d-$(CGATCG)_2$ solution till it reaches the ratio of 2:1. The sample is prepared in 90% water and 10% D_2O. To arrive at Drug to Nucleotide (D/N) stoichiometric ratios from 0 to 2.0 at 283 and 298 K a slow increment in D/N ratio of 0.1 is done. Fig. 5.2 show the change in ^{31}P chemical shift due to binding as a function of increased concentration of palmatine at 283 K. There are only five phosphate resonances observed on the formation of palmatine-DNA complex. These resonances showed a moderate shift as compared to the resonances from free hexamer but with increase in D/N ratio they broaden severely due to fast chemical exchange on the NMR time scale.

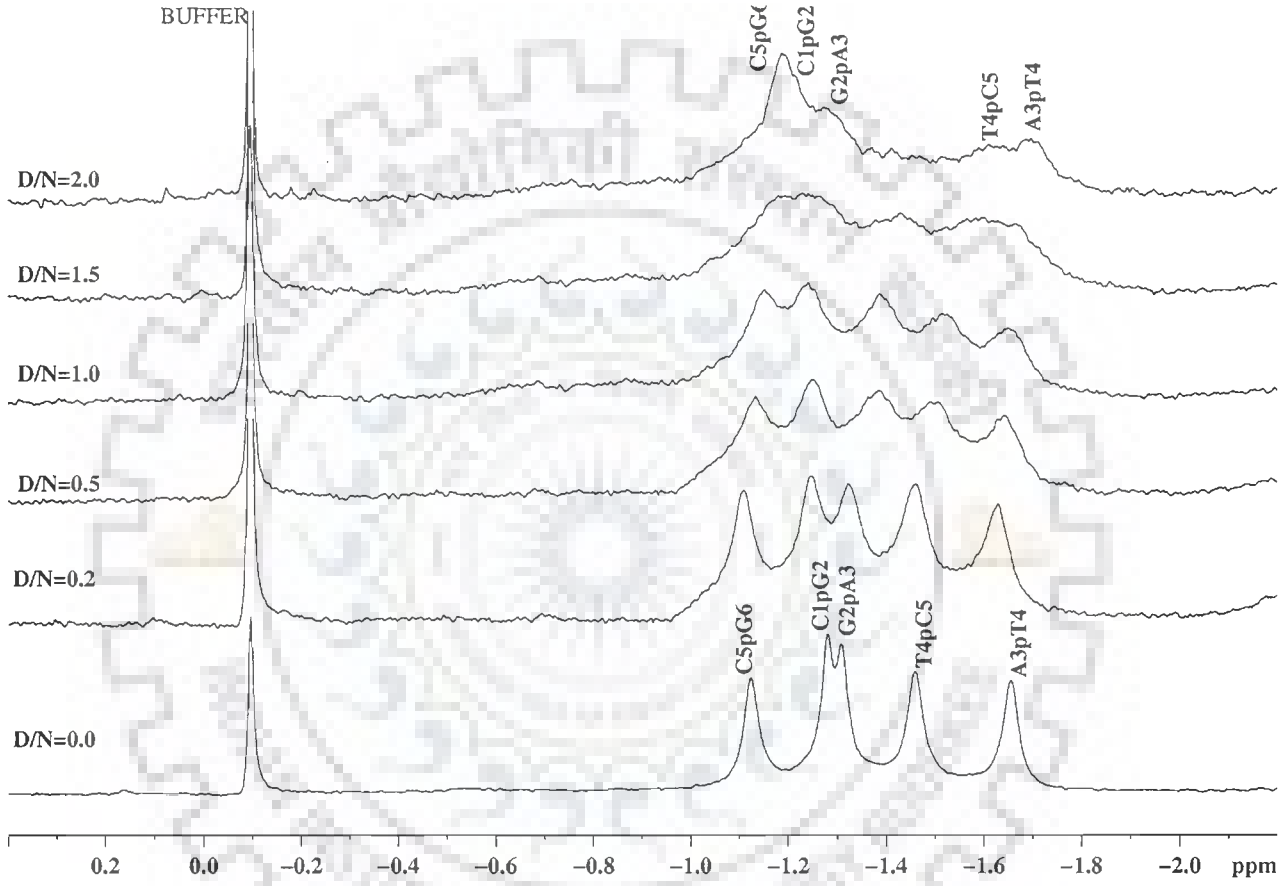

Fig. 5.2: Proton decoupled ^{31}P NMR spectra of 3.14 mM d-$(CGATCG)_2$ in uncomplexed state and complexed with palmatine with increasing drug (D) to nucleic acid duplex (N) ratio, D/N, at 283 K.

Table 5.1: Chemical shift of ^{31}P resonances of the phosphate groups of DNA in complex of palmatine with d-$(CGATCG)_2$ at 283 K with different drug (D) to nucleic acid duplex (N) ratios (D / N). $\Delta\delta = (\delta_{D/N=2.0} - \delta_{D/N=0})$.

D/N Ratios	C1pG2	G2pA3	A3pT4	T4pC5	C5pG6
0.00	-1.36	-1.39	-1.73	-1.55	-1.19
0.50	-1.28	-1.41	-1.71	-1.55	-1.22
1.00	-1.25	-1.42	-1.72	-1.60	-1.23
1.50	-1.27	-1.42	-1.73	-1.65	-1.25
2.00	-1.27	-1.42.	-1.74	-1.69	-1.27
$\Delta\delta$	+0.09	-0.03	-0.01	-0.14	-0.08

+ve $\Delta\delta$ indicates downfield shift
-ve $\Delta\delta$ indicates upfield shift

Chemical shift values for all the phosphorus signals at different D/N ratio are tabulated in Table 5.1. The addition of palmatine to the oligonucleotide induces upfield shift of all the phosphorus signals except C1pG2 which is shifted downfield. It was found that very less upfield shift was observed for all the phosphorus signals. T4pC5, resonance shifts upfield by 0.14 ppm, which was maximum among all the phosphorus signals observed. A3pT4, G2pA3 and C5pG6 showed upfield shift of 0.01, 0.03 and 0.08 ppm, respectively. Whereas a downfield shift of 0.09 ppm is found in C1pG2. Upfield shifts observed in phosphorus resonances shows that palmatine might be interacting with d-$(CGATCG)_2$ through electrostatic interaction [Patel, 1979; Wilson and Jones, 1982]. Fig. 5.3 shows the plot of chemical shift versus D/N ratio of phosphorus signal. It is known that ^{31}P chemical shifts vary in response to local, sequence specific and induced environmental distortions in the duplex geometry [Calladine, 1982; Dickerson, 1983; Ott and Eckstein, 1985; Schroeder et al., 1989].

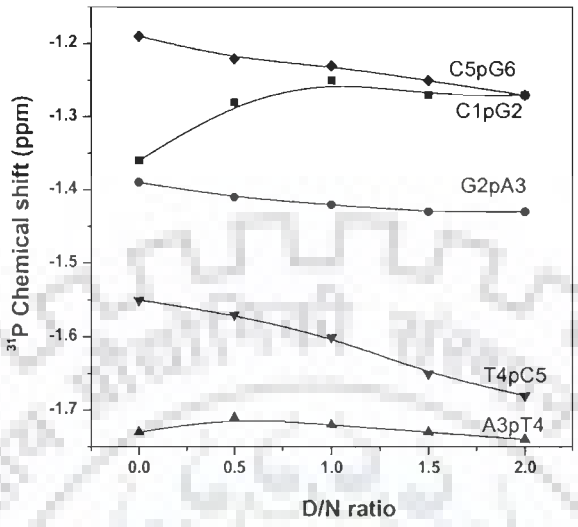

Fig. 5.3: ^{31}P Chemical shift variation of d-(CGATCG)$_2$ in complex with palmatine, as a function D/N ratio at 283 K.

Theoretical studies have shown that variation in the conformation of two (α: O3'-P-O5'-C5' and ζ: C3'-O3'-P-O5') out of six torsional angles can cause perturbations in ^{31}P shifts. Switching from energetically more favorable B_I conformation ($\zeta = g^-$, $\alpha = g^-$) to the more flexible B_{II} conformation ($\zeta = t$, $\alpha = g^-$) having 1 Kcal/mol higher energy than B_I, introduces a downfield shift of about 1.5 ppm [Gorenstein et al., 1977], which is the condition when intercalating drugs binds to B DNA. The dispersion in ^{31}P chemical shifts of oligonucleotides has also been attributed to different populations of B_I and B_{II} states [Gorenstein, 1992]. ^{31}P chemical shift has also been correlated with degree of duplex DNA unwinding resulting from increase in the length of sugar phosphate backbone to

accommodate intercalation of drug chromophore. Besides, the ester O-P-O bond angle distortions in drug-duplex DNA complexes also affect the chemical shift. Widening of ester O-P-O angle is expected to produce an upfield shift [Gorenstein and Kar, 1975; Gorenstein et al., 1984] while narrowing of this bond angle causes a downfield shift. Purely electrostatic associations between drug and nucleic acid on the other hand produce only small and generally upfield ^{31}P chemical shifts [Patel, 1979; Wilson and Jones, 1982].

The change in the chemical shifts obtained for ^{31}P resonances of palmatine-d-$(CGATCG)_2$ complex are compared with corresponding chemical shift values reported in literature (Table 5.2 and Table 5.3) for the binding of berberine with d-$(AAGAATTCTT)_2$ [Mazzini et al., 2003], binding of mitoxantrone with d-$(CGCG)_2$ [Lown and Hanstock, 1985] and d-$(CGATCG)_2$ [Kotovych et al., 1986], 2-pyrido[1, 2-e]purine-4-yl)amino-ethanol with d-$(CGATCG)_2$ [Favier et al., 2001], nogalamycin with d-$(GCATGC)_2$ [Searle et al., 1988], adriamycin and methoxy-morpholinodoxorubicin with d-$(CGATCG)_2$ and d-$(CGTACG)_2$ [Mazzini et al., 1998]. Drugs like adriamycin, morpholinoldoxorubicin, daunorubicin and nogalamycin [Mazzini et al., 1998; Ragg et al., 1988; Searle et al., 1988] which intercalate between two base pairs of DNA oligomer, lead to downfield shifts up to 1.57 ppm of phosphorus resonances at the intercalation site or at site adjacent to it. Earlier, shifts of ~2.6 ppm has been reported on intercalation of aromatic chromophores in DNA [Gorenstein, 1992; Patel, 1974; Patel and Canuel, 1976; Patel et al., 1982].

Table 5.2: Chemical shift of free (δ^f), bound (δ^b), and change in chemical shift due to binding, $\Delta\delta = \delta^b - \delta^f$ in phosphate groups of some of the drug-DNA complexes taken from literature.

Phosphate Group	[Mazzini et al., 1998], d-(CGATCG)$_2$ + Adriamycin			[Mazzini et al., 1998]., d-(CGTACG)$_2$ + Adriamycin			[Searle et al., 1988] d -(GCATGC)$_2$ + Nogalamycin		
	δ^f	δ^b	$\Delta\delta$	δ^f	δ^b	$\Delta\delta$	δ^f	δ^b*	$\Delta\delta$
C1pG2/ G1pC2	-0.91	-0.48	+0.43	-1.03	-0.58	+0.45	-3.30	-2.90	+0.20
G2pA3/ C2pA3	-0.86	0.67	+1.53	-1.40	-0.56	+0.84	-3.00	-2.50	+0.50
A3pT4/ T3pA4	-1.26	-1.28	≤-0.2	-1.12	-1.26	-0.14	-3.40	-3.20	+0.20
T4pC5/T4pG6	-1.06	-1.12	-0.06	-1.20	-1.34	-0.14	-3.10	-1.60	+1.50
C5pG6/G5pC6	-0.73	0.84	+1.57	-0.90	+0.63	+1.53	-3.00	-3.00	+0.00
	[Mazzini et al., 1998] d-(CGATCG)$_2$+ Morpholinodoxorubicin			**[Mazzini et al., 1998] d-(CGTACG)$_2$+ Morpholinodoxorubicin**			**[Ragg et al., 1988] d-(CGTACG)$_2$+ Daunorubicin**		
C1pG2	-0.91	-0.32	+0.59	-1.03	-0.56	+0.47	-1.02	-1.45	-0.43
G2pA3 / G2pT3	-0.86	0.19	+1.05	-1.40	-0.50	+0.90	-1.42	-1.95	-0.53
A3pT4/T3pA4	-1.26	-1.36	-0.10	-1.12	-1.45	-0.33	-1.08	-1.28	-0.20
T4pC5/A4pC5	-1.06	-1.11	-0.05	-1.20	-1.46	-0.26	-1.28	-1.48	-0.20
C5pG6	-0.73	0.52	+1.25	-0.90	+0.22	+1.12	-0.88	+0.44	+1.32

+ve $\Delta\delta$ indicates downfield shift.

-ve $\Delta\delta$ indicates upfield shift.

* Tentative assignment

Table 5.3: Chemical shift of free (δ^f), bound (δ^b), and the change in chemical shift due to binding, $\Delta\delta = \delta^b - \delta^f$ in phosphate resonances of some of the drug-DNA complexes taken from literature.

Phosphate Group	[Lown and Hanstock, et d-(CGCG)$_2$ + mitoxantrone			[Kotovych et al., 1986] d-(CGATCG)$_2$ + mitoxantrone				[Favier et al., 2001] d-(CGATCG)$_2$ + pyridopurine				[Mazzini et al., 2003] d-(AAGAATTCTT)$_2$ + berberine			
	δ^f	δ^b	$\Delta\delta$		δ^f	δ^b	$\Delta\delta$		δ^f	δ^b	$\Delta\delta$		δ^f	δ^b	$\Delta\delta$
C1pG2	-3.46	-3.31	+0.15	**C1pG2**	-1.71	-1.70	+ 0.01	**C1pG2**	1.2	1.1	-0.1	**A1pA2**	-1.31	-1.19	+0.12
G2pC3	-3.30	-3.40	-0.10	**G2pA3**	-1.71	-1.70	+ 0.01	**G2pA3**	1.1	1.1	0.0	**A2pG3**	-1.00	-0.98	+0.02
C3pG4	-3.46	-3.31	+0.15	**A3pT4**	-2.19	-2.21	-0.02	**A3pT4**	0.7	0.8	-0.1	**G3pA4**	-1.14	-1.12	+0.02
				T4pC5	-1.95	-1.97	-0.02	**T4pC5**	0.4	0.5	-0.1	**A4pA5**	-1.40	-1.23	+0.17
				C5pG6	-1.59	-1..25	+0.34	**C5pG6**	1.2	1.2	0.0	**A5pT6**	-1.37	-1.40	+0.03
[Mazzini et al., 2004] Topotecan+d(CGTACG)$_2$				**[Mazzini et al., 2004] Camptothecin+d(CGTACG)$_2$**				**[Mazzini et al., 2004] Camptothecin+d(CGTATACG)$_2$**				**T6pT7**	-1.18	-1.10	+0.08
C1pG2	-1.00	-1.00	0.00	**C1pG2**	-0.88	-0.95	+0.07	**C1pG2**	-0.94	-0.96	+0.02	**T7pC8**	-1.11	-1.07	+0.04
G2pT3	-1.29	-1.35	-0.06	**G2pT3**	-1.32	-1.33	+0.01	**G2pT3**	-1.33	-1.33	+0.00	**C8pT9**	-1.14	-1.10	+0.04
T3pA4	-1.08	-1.10	-0.02	**T3pA4**	-1.14	-1.17	-0.03	**T3pA4**	-1.03	-1.03	+0.00	**T9pT10**	-1.04	-1.07	+0.03
A4pC5	-1.12	-1.20	-0.08	**A4pC5**	-1.14	-1.17	-0.03	**A4pT5**	-1.33	-1.33	+0.00				
C5pG6	-0.90	-1.00	-0.10	**C5pG6**	-0.78	-0.85	+0.07	**T5pA6**	-1.10	-1.13	-0.03				
								A6pC7	-1.09	-1.11	+0.02				
								C7pG8	-0.82	-0.84	-0.02				

+ve $\Delta\delta$ indicates downfield shift
-ve $\Delta\delta$ indicates upfield shift

In case of external binding drugs like pyridopurine, [Favier et al., 2001] and mitoxantrone downfield shift up to 0.15-0.34 ppm were observed [Kotovych et al., 1986; Lown and Hanstock, 1985]. Mazzini et al has reported ^{31}P NMR studies of palmatine analog berberine with several oligonucleotides [Mazzini et al., 2003]. They have reported downfield shift in the range of 0.0-0.17 ppm, which indicated the external binding of berberine to the oligonucleotides studied .

^{31}P chemical shift variations in nucleotides reflect the conformation of the phosphodiester groups at the level of the P-O5' and O3'-P bonds i.e. the values of torsion angles α = O3'-P--O5'-C5'and ζ = C3'-O3'-P-O5'. B-DNA conformation have phosphate groups normally in gauche$^-$, gauche$^-$ (g^-, g^-) conformation with α and ζ angles of -60° and -90° respectively. When intercalating drugs bind to B-DNA, the backbone α and ζ angles change to g^-, t whereas the gauche$^-$, trans (g^-, t) conformation (α = -60°, ζ = 180°) is generally associated with deshielding of 1.5 ppm. Such transition from g^-, g^- to g^-, t on intercalation of drug chromophore by opening of adjacent base pairs at intercalation site from a distance of 3.4 to 6.8 Å have been reported in X-ray crystallographic structure of adriamycin and daunomycin binding to d-CGATCG, d-TGATCA, d-CGTACG sequences [Frederick et al., 1990] as well in similar NMR structures [Mazzini et al., 1998]. The pyridopurine [Favier et al., 2001] and berberine [Mazzini et al., 2003], which does not show such large shifts in the phosphorus resonances on binding to DNA, have been shown to bind externally in the restrained molecular dynamics structures obtained by using inter molecular inter proton distances from NOESY spectra.

We also found that change in the chemical shift values on binding of palmatine to d-$(CGATCG)_2$ is very less (0.01-0.14 ppm) as compared to other DNA binding drugs. It

may be inferred that binding of palmatine to d-$(CGATCG)_2$ does not lead to opening of base pairs, which is generally associated with large down field shifts of ^{31}P resonance of the order of 1.6-2.6 ppm [Gorenstein, 1992; Patel, 1974; Patel and Canuel, 1976; Patel et al., 1982]. Thus, intercalative mode of binding of palmatine can be excluded and the external mode of binding can be suggested. But still predicting the binding site of palmatine on the basis of alone ^{31}P chemical shift variation can be more imaginary.

5.1.1.2 2D ^{31}P - ^{31}P Exchange Spectra

Fig. 5.4a-b shows the ^{31}P-^{31}P 2D NOESY spectra of the palmatine-d-$(CGATCG)_2$ complex at drug to DNA (D/N) ratios of 1.0 and 2.0 at 298 K. The one dimensional ^{31}P spectra are shown along both axes. In 2D ^{31}P NMR exchange spectrum each of the five phosphorus signals seen in uncomplexed DNA are expected to give cross peak due to chemical exchange with its respective bound resonances. On binding of palmatine to d-$(CGATCG)_2$, as the drug is progressively added to the hexanucleotide considerable broadening is observed in the phosphorus resonances with no additional cross peaks due to exchange between the bound and free phosphate resonances. Since, only one set of resonances are observed for the complexes at different D/N ratios for free hexamer and hexamer bound to palmatine, it is expected that ^{31}P signals from the bound DNA are in fast exchange with the corresponding signals from free DNA to be followed individually at 298 K on NMR time scale. Even P-P NOESY recorded at 278 K shows no separate signals for free and bound species due to fast exchange on NMR time scale (data not shown).

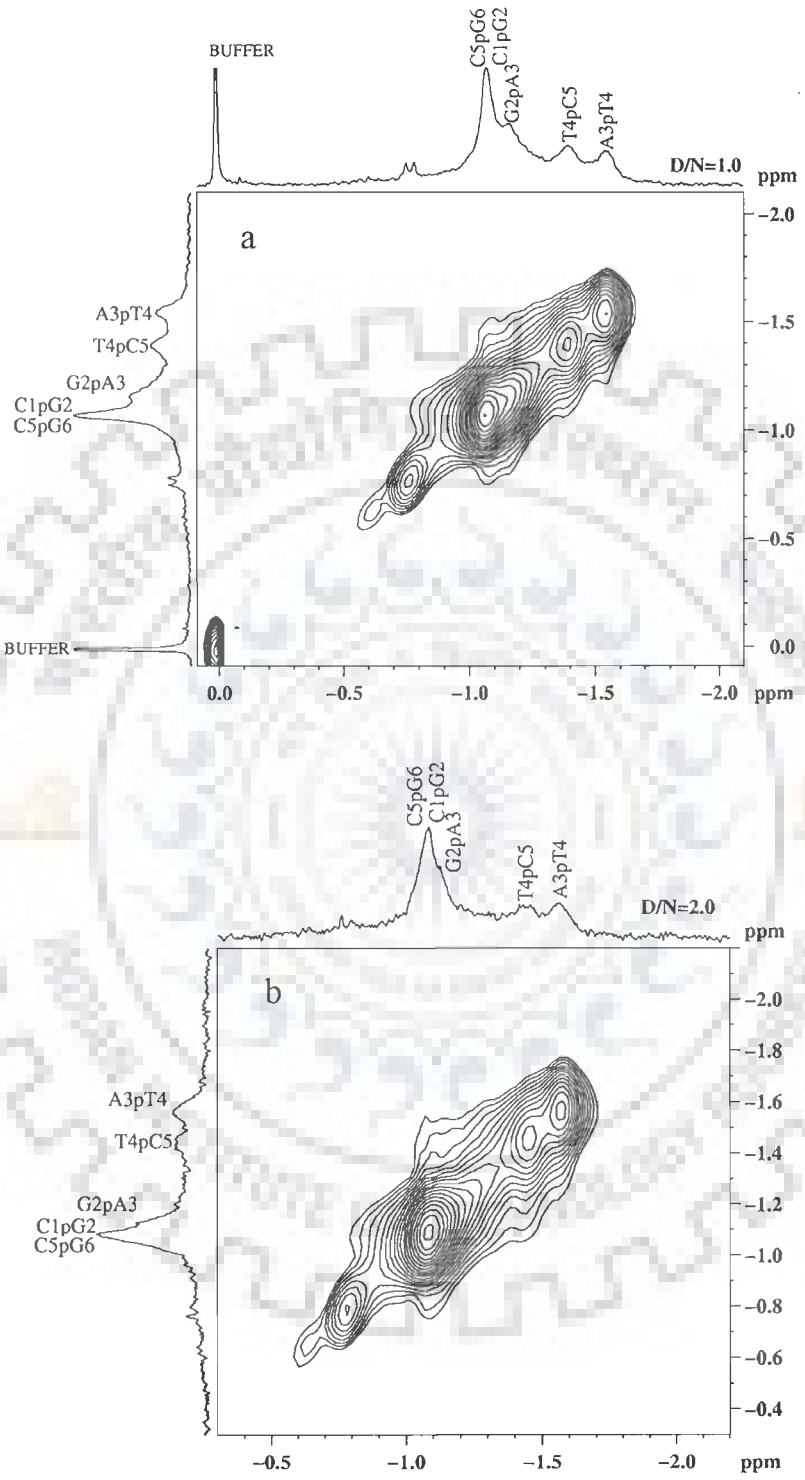

Fig. 5.4: ^{31}P - ^{31}P NOESY exchange spectrum at 200 ms of the complex of palmatine with d-$(CGATCG)_2$ at drug (D) to nucleic acid duplex (N) ratios, D/N of (a) 1.0 and (b) 2.0 at 298 K.

5.1.1.3 Temperature Dependence Studies

The variation of ^{31}P NMR spectrum of d-$(CGATCG)_2$ and its complex with palmatine at D/N ratios of 0.0, 1.0, and 2.0 in the range 283 K to 328 K is examined (Fig. 5.5a-c). Table 5.4 shows the variation of chemical shift as a function of temperature. The signals are found to be shifted with temperature, which may be due to shift in the following equilibrium:

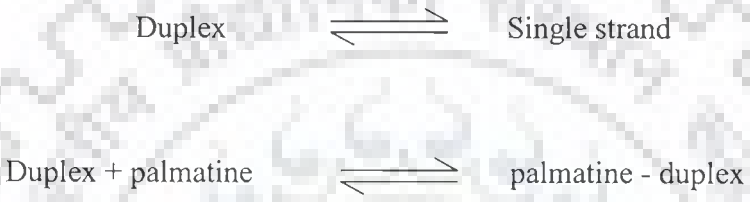

These reactions correspond to duplex to single strand transition and drug-DNA complexation respectively. There is a general downfield shift of ^{31}P resonances with increasing temperature which is consistent with the change in the backbone conformation, generally g^- for P-O ester bonds in the duplex, to a single stranded having random mix of g- and non-gauche conformation. It is observed that shifts in ^{31}P resonances in uncomplexed and complexed d-$(CGATCG)_2$ in the range 283-328 K are very gradual and not abrupt (Fig. 5.6). The observation is consistent with the earlier studies reported in literature on change in chemical shift with temperature due to helix to coil transition [Patel, 1977]. Table 5.4 shows the shift in ^{31}P resonances with temperature in the bound complex, which was found to be gradual and the total change i.e. $\Delta\delta = \delta_{328\ K} - \delta_{283\ K}$, is almost same in the complexes having different D/N ratios. A comparison of melting curve of uncomplexed d-$(CGATCG)_2$ with corresponding ^{31}P resonances in 1:1 and 2:1 palmatine-d$(CGATCG)_2$ complex (Fig.5.6) shows that there are no major

differences between the two curves, as expected. These data are indicative of the fact that the hexanucleotide remains intact over the temperature range 278 K to 328 K, or new signals would have become apparent. We can therefore conclude that palmatine is stabilizing the DNA.

The study on ^{31}P NMR of the drug-DNA complex provide an independent proof of the external binding of palmatine to d-$(CGATCG)_2$ and the rate of exchange which is faster on NMR time scale. Although ^{31}P NMR studies provide information on the conformation of the phosphate ester backbone and the mode of binding of palmatine but it is unable to provide detailed information on the overall conformation of the sugar rings and bases of oligonucleotides. ^{1}H NMR results discussed further in this chapter provide detailed conformational details of the interaction.

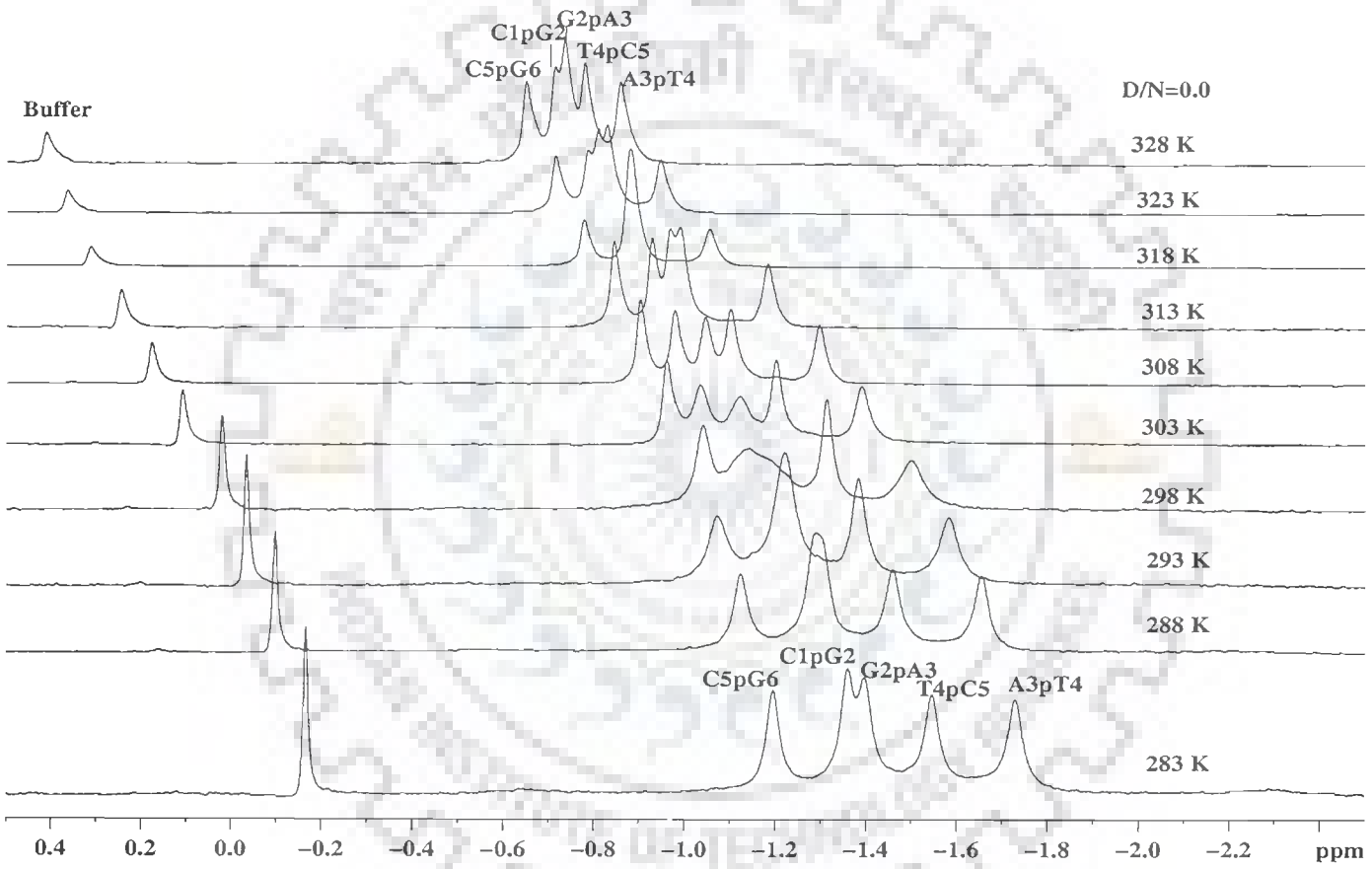

(Fig. 5.5a)

Fig. 5.5a-c: Proton decoupled ^{31}P NMR spectra of d-$(CGATCG)_2$ complexed with palmatine as a function of temperature in the range 283 – 328 K at (a) D/N 0.0 (b) D/N 1.0 (c) D/N 2.0.

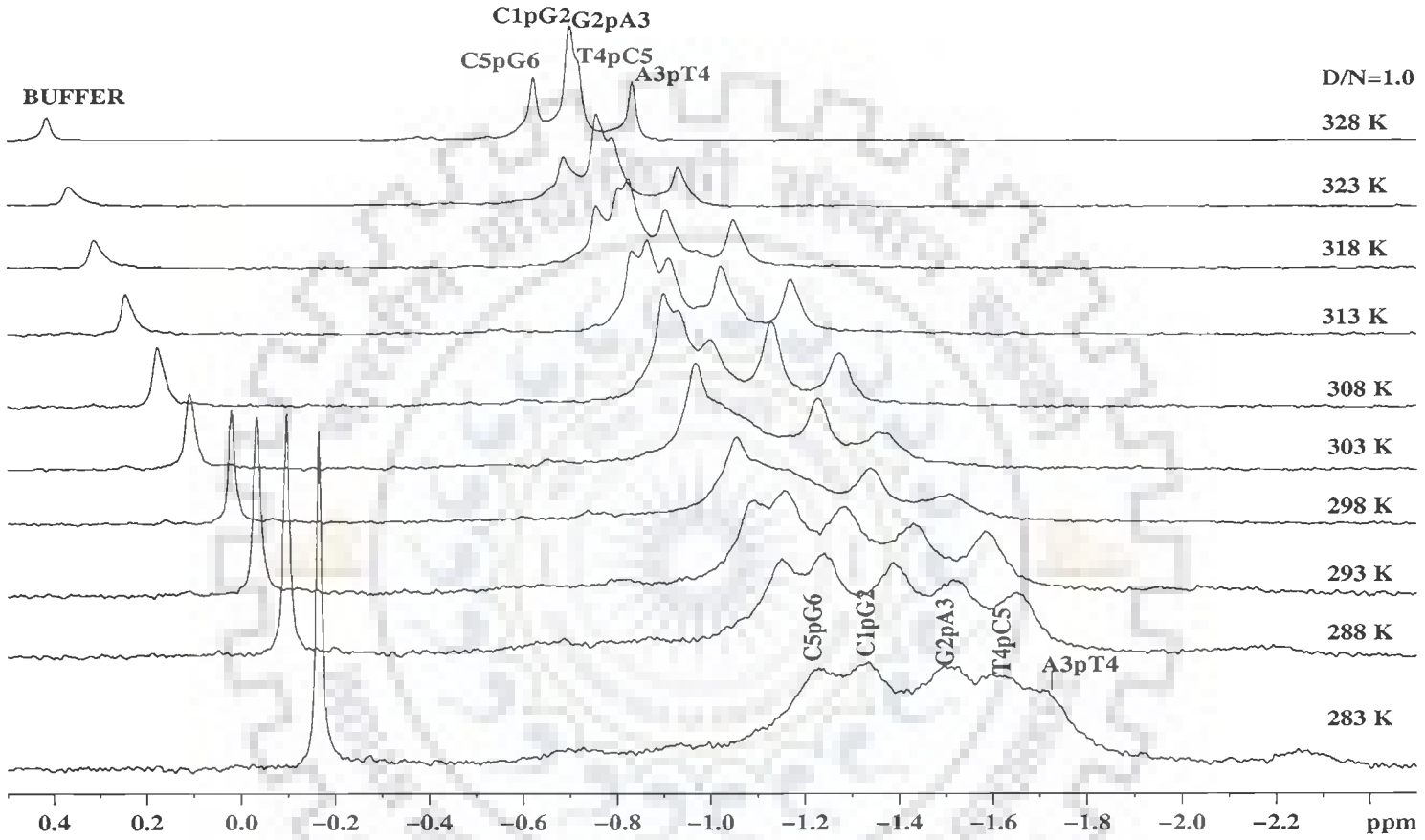
C1pG2
G2pA3
C5pG6
T4pC5
A3pT4
BUFFER
D/N=1.0
328 K
323 K
318 K
313 K
308 K
303 K
298 K
293 K
288 K
283 K
C5pG6
C1pG2
G2pA3
T4pC5
A3pT4
0.4
0.2
0.0
−0.2
−0.4
−0.6
−0.8
−1.0
−1.2
−1.4
−1.6
−1.8
−2.0
−2.2
ppm

Fig.5.5b

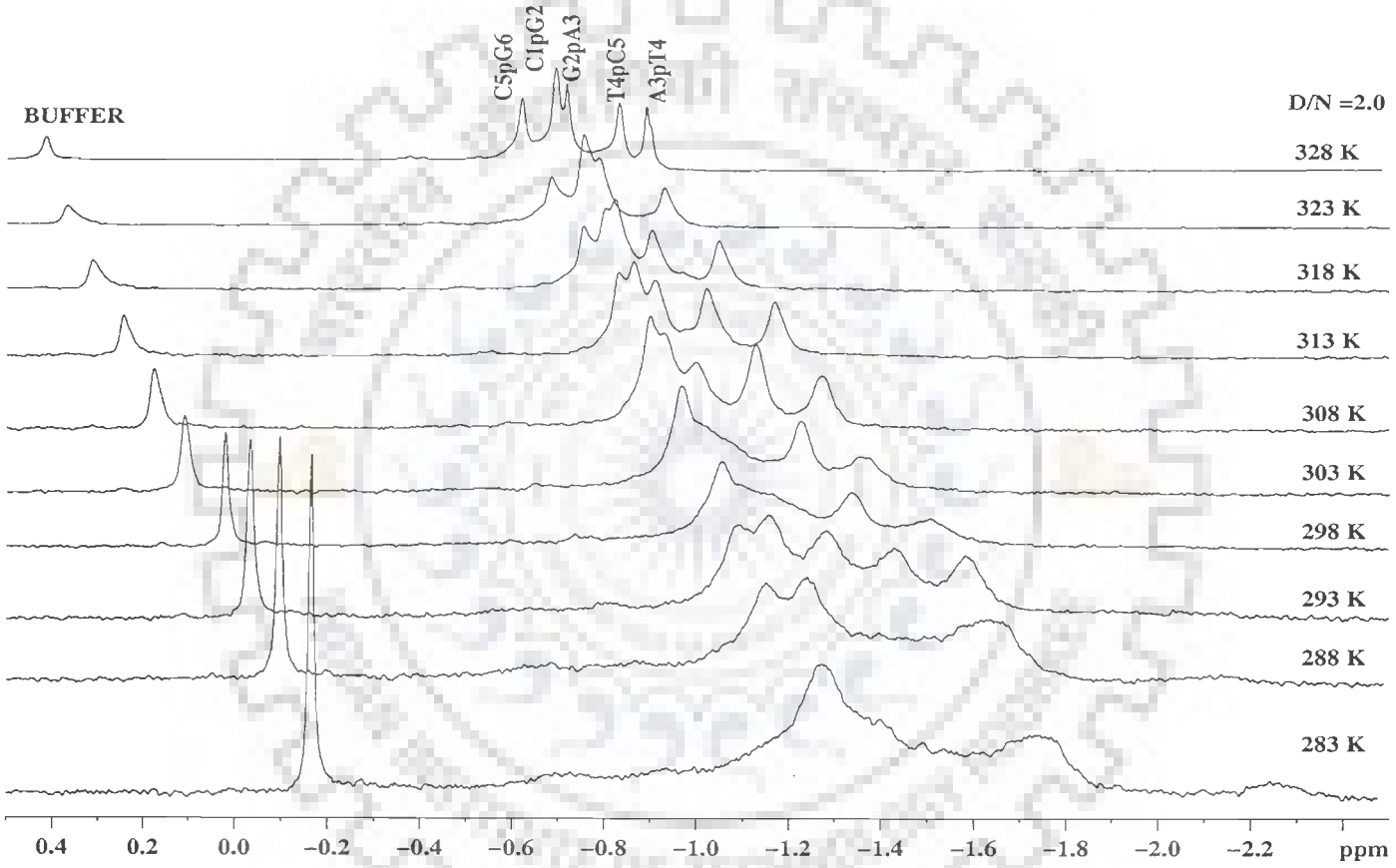
BUFFER
C5pG6
C1pG2
G2pA3
T4pC5
A3pT4
D/N =2.0
328 K
323 K
318 K
313 K
308 K
303 K
298 K
293 K
288 K
283 K
0.4
0.2
0.0
−0.2
−0.4
−0.6
−0.8
−1.0
−1.2
−1.4
−1.6
−1.8
−2.0
−2.2
ppm

Fig. 5.5c

Table 5.4: ^{31}P chemical shift d-$(CGATCG)_2$ -palmatine complex (D/N = 0, 1.0 and 2.0) as a function of temperature in the range 283-328 K where $\Delta\delta = \delta_{328K} - \delta_{283K}$.

	D/N=0.0					D/N=1.0				
Temp	**C1pG2**	**G2pA3**	**A3pT4**	**T4pC5**	**C5pG6**	**C1pG2**	**G2pA3**	**A3pT4**	**T4pC5**	**C5pG6**
283	-1.36	-1.39	-1.73	-1.55	-1.19	-1.25	-1.42	-1.72	-1.58	-1.23
288	-1.29	-1.30	-1.66	-1.46	-1.13	-1.24	-1.39	-1.65	-1.52	-1.15
293	-1.22	-1.22	-1.58	-1.38	-1.07	-1.16	-1.28	-1.59	-1.48	-1.09
298	-1.14	-1.14	-1.50	-1.31	-1.04	-1.11	-1.25	-1.48	-1.43	-1.06
303	-1.04	-1.12	-1.39	-1.20	-0.96	-1.02	-1.18	-1.37	-1.35	-0.97
308	-0.98	-1.05	-1.29	-1.10	-0.91	-0.93	-1.00	-1.27	-1.13	-0.90
313	-0.93	-0.97	-1.18	-0.99	-0.84	-0.86	-0.91	-1.17	-1.02	-0.83
318	-0.88	-0.88	-1.06	-0.88	-0.78	-0.80	-0.82	-1.05	-0.90	-0.76
323	-0.78	-0.81	-0.95	-0.83	-0.71	-0.75	-0.76	-0.93	-0.79	-0.69
328	-0.71	-0.73	-0.86	-0.78	-0.65	-0.70	-0.70	-0.83	-0.72	-0.62
δΔ	+0.65	+0.68	+0.87	+0.77	+0.54	+0.55	+0.72	+0.89	+0.76	+0.61
	D/N=2.0									
Temp	**C1pG2**	**G2pA3**	**A3pT4**	**T4pC5**	**C5pG6**					
283	-1.27	-1.42	-1.74	-1.69	-1.27					
288	-1.21	-1.28	-1.70	-1.62	-1.19					
293	-1.11	-1.18	-1.64	-1.53	-1.11					
298	-1.06	-1.10	-1.54	-1.42	-1.06					
303	-0.99	-1.00	-1.41	-1.35	-0.93					
308	-0.91	-0.94	-1.31	-1.28	-0.85					
313	-0.83	-0.85	-1.21	-1.15	-0.77					
318	-0.76	-0.77	-1.10	-0.95	-0.70					
323	-0.70	-0.71	-0.89	-0.84	-0.64					
328	-0.64	-0.66	-0.78	-0.75	-0.59					
δΔ	+0.63	+0.76	+0.86	+0.94	+0.68					

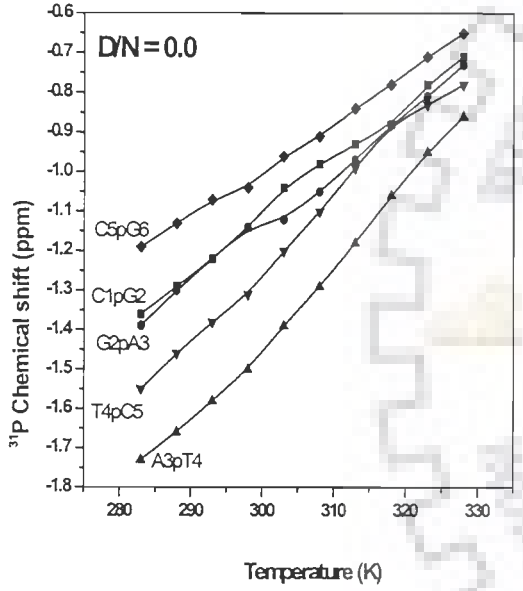

Fig.5.6a

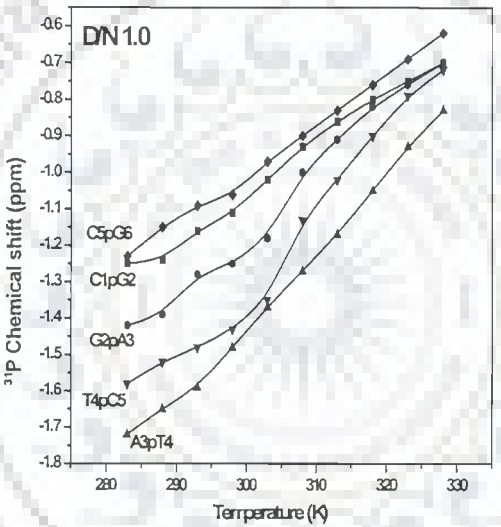

Fig.5.6b

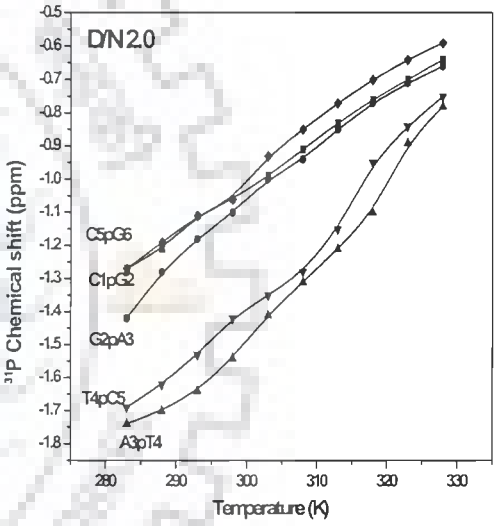

Fig.5.6c

Fig. 5.6: ^{31}P Chemical shift variation of d-$(CGATCG)_2$ in complex with palmatine, as a function temperature at different D/N ratio of (a)D/N=0.0 (b)D/N=1.0 (c) D/N=2.0

5.1.2 Proton NMR Studies of palmatine-d-$(CGATCG)_2$ Complex

Most of the NMR experiments are carried out at 278 K as imino protons are sharpened and intensified at this temperature. Besides, DNA is expected to be present completely in duplex state at 278 K. Fig. 5.7a–l show expansions of specific regions of 2D NOESY spectra of palmatine complexed to d–$(CGATCG)_2$. The assignments of nucleotide protons has been carried out by following strategies adopted for standard B–DNA structures that is, sequential NOEs (base H8/H6)$_n$–sugar (H1')$_{n-1}$ (Fig. 5.7a)., (base H8/H6)$_n$–sugar(H2")$_{n-1}$, (base H8/H6)$_n$–sugar(H2')$_{n-1}$ (Fig. 5.7b); expected NOEs due to several short intranucleotide distances (Wuthrich K., 1986) as well as our NMR data of uncomplexed d–$(CGATCG)_2$ published earlier [Barthwal et al, 2003]. The T4NH imino protons are assigned based on the basis of intense cross peak with A3H2 and NOEs with adenine amino protons of the corresponding base pair. G2NH shows connectivity with amino protons of the corresponding cytosine base pair (Fig. 5.7h). The position of each and every resonance is thus ascertained and unambiguous assignment is done. The chemical shift positions of uncomplexed d–$(CGATCG)_2$ and that bound to palmatine (D/N = 2.0) is given in Tables 5.5. The chemical shift positions of alone palmatine and that bound to the hexamer (D/N = 2.0) is given in Tables 5.6. The assignment of spectral lines to specific protons of drug have been made by following strategies used for assignments in NMR spectra of uncomplexed drug described in Chapter 3. The intramolecular peaks observed at different D/N ratios are shown by "# and "Ⓗ" in all the NOESY spectra (Fig. 5.7a-l). All the palmatine intramolecular cross peaks are listed in Table 5.7.

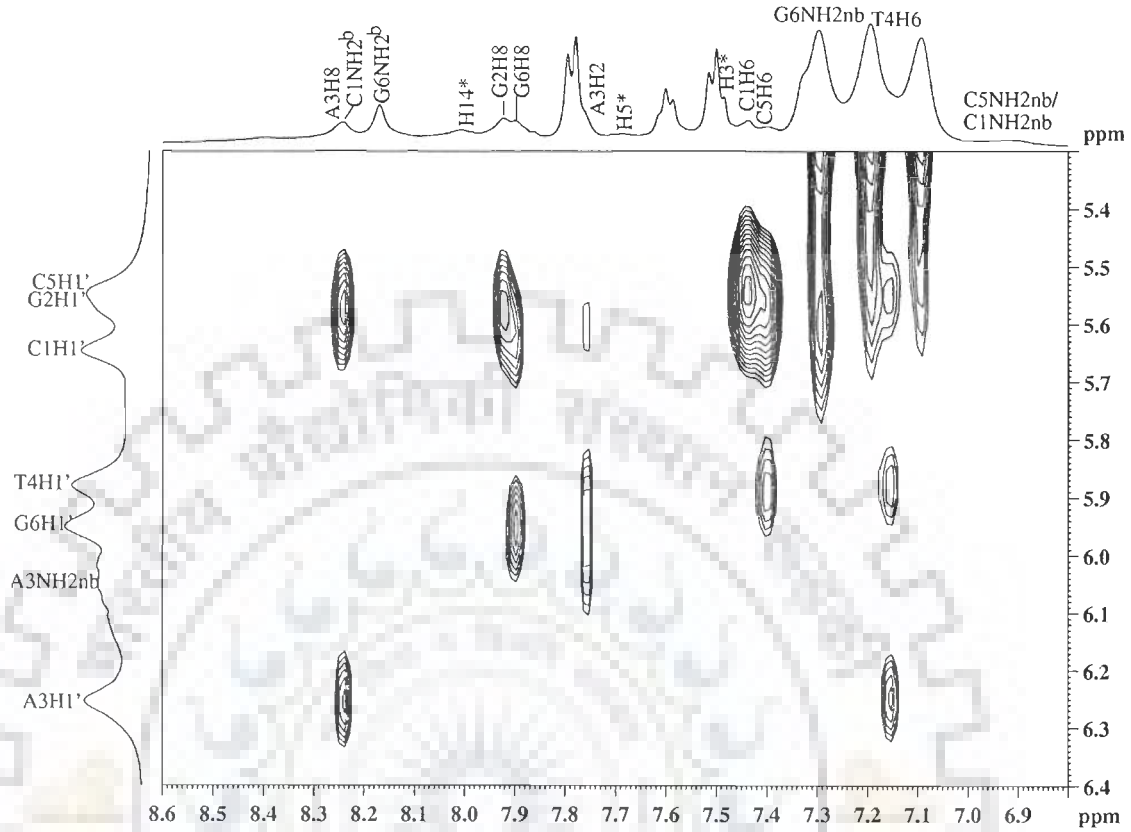

(Fig. 5.7a)

Fig. 5.7 (a-l): Expansions of the specific regions of NOESY spectra of palmatine complexed with d-(CGATCG)$_2$ to highlight specific connectivities (intramolcular peaks of palmatine: "#"present in uncomplexed palmatine; "(#)" absent in uncomplexed palmatine, "I" Intermolecular peaks in palmatine-d-(CGATCG)$_2$ complex).

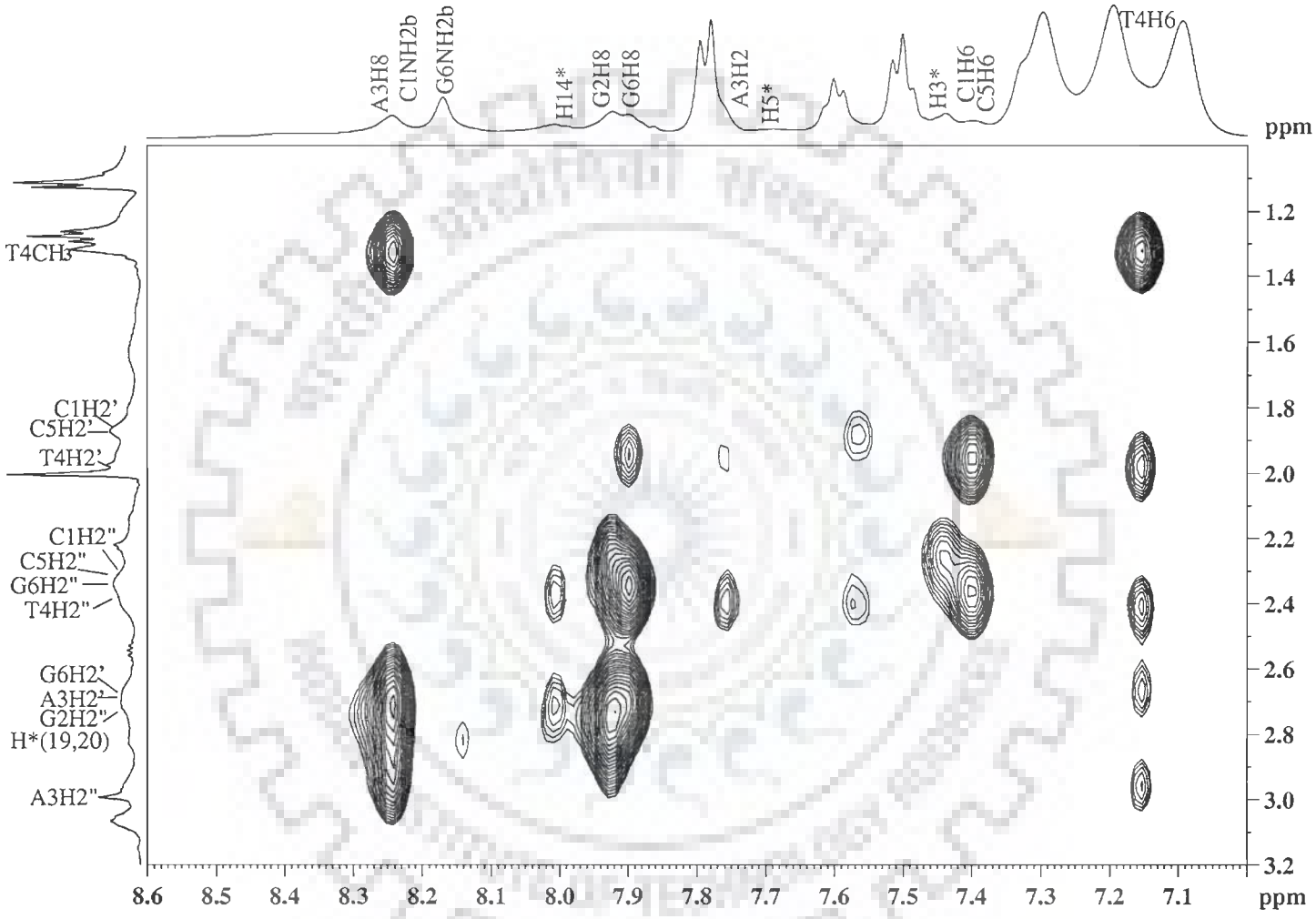
A3H8
C1NH2b
G6NH2b
H14*
G2H8
G6H8
A3H2
H5*
H3*
C1H6
C5H6
T4H6
ppm
T4CH3
C1H2'
C5H2'
T4H2'
C1H2"
C5H2"
G6H2"
T4H2"
G6H2'
A3H2'
G2H2'
H*(19,20)
A3H2"
1.2
1.4
1.6
1.8
2.0
2.2
2.4
2.6
2.8
3.0
3.2
8.6
8.5
8.4
8.3
8.2
8.1
8.0
7.9
7.8
7.7
7.6
7.5
7.4
7.3
7.2
7.1
ppm

(Fig. 5.7b)

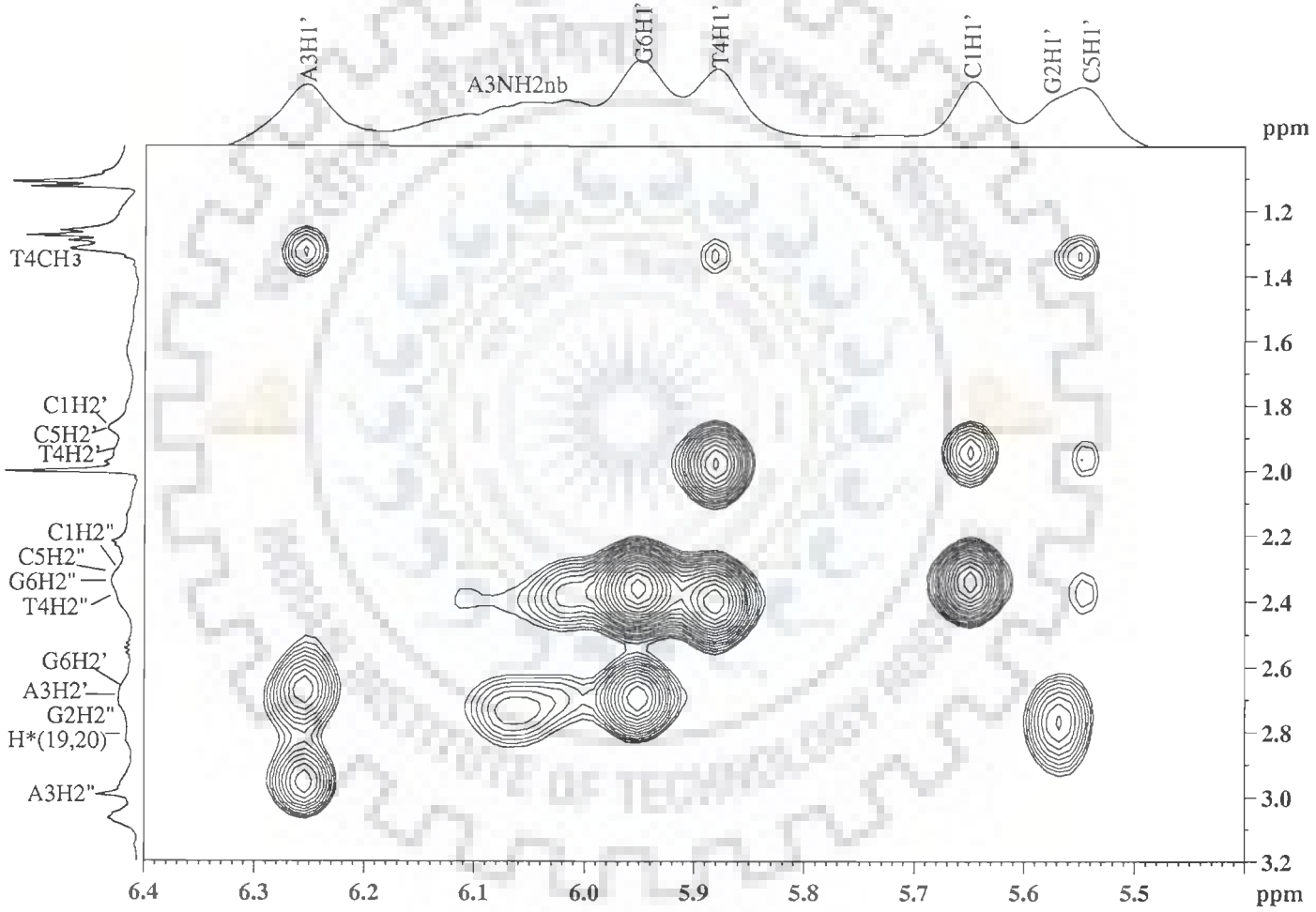
A3H1'
A3NH2nb
G6H1'
T4H1'
C1H1'
G2H1'
C5H1'
ppm
T4CH3
C1H2'
C5H2'
T4H2'
C1H2"
C5H2"
G6H2"
T4H2"
G6H2'
A3H2'
G2H2"
H*(19,20)
A3H2"
1.2
1.4
1.6
1.8
2.0
2.2
2.4
2.6
2.8
3.0
3.2
6.4
6.3
6.2
6.1
6.0
5.9
5.8
5.7
5.6
5.5
ppm

(Fig. 5.7c)

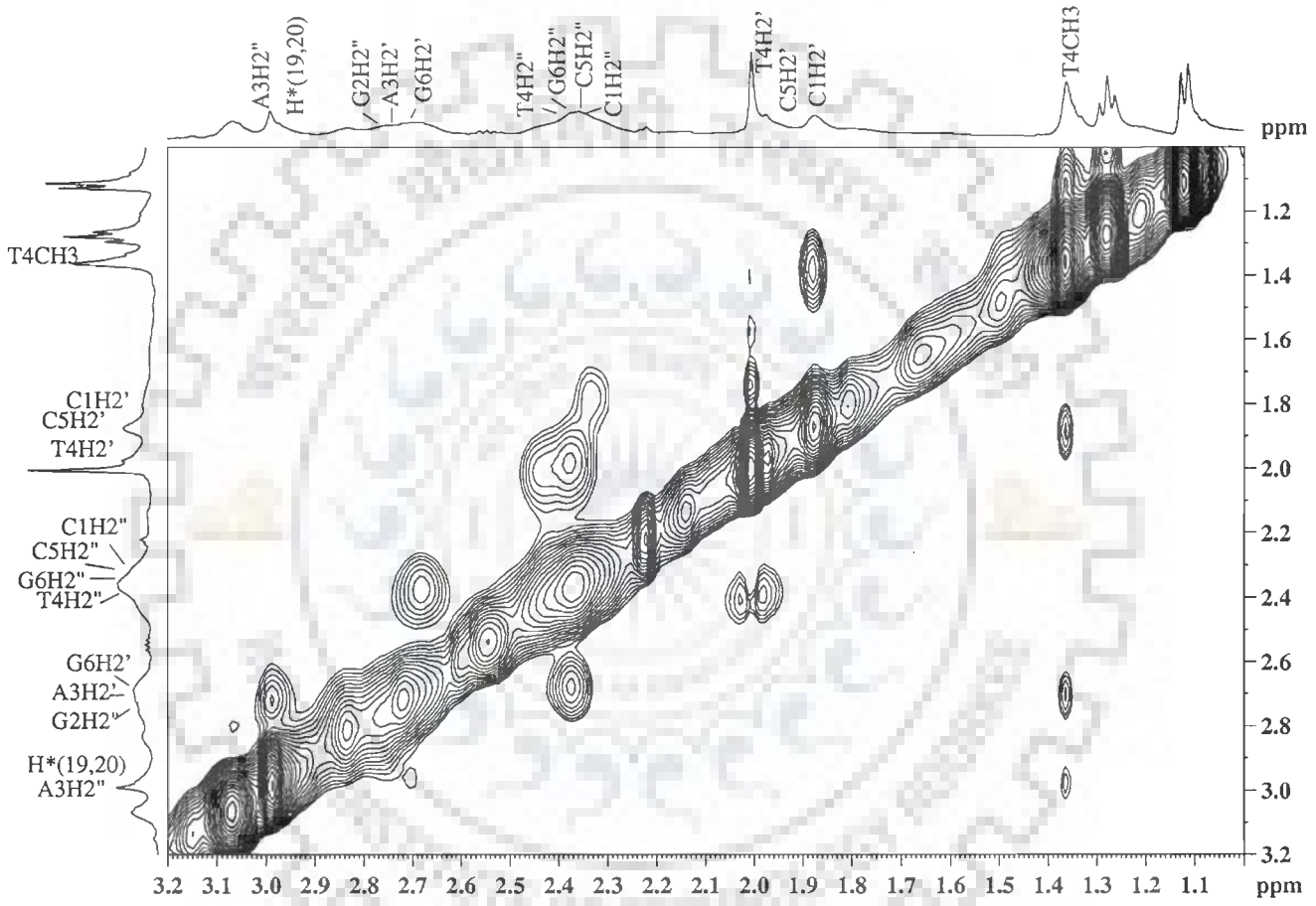
A3H2"
H*(19,20)
G2H2"
A3H2'
G6H2'
T4H2"
G6H2"
C5H2"
C1H2"
T4H2'
C5H2'
C1H2'
T4CH3
ppm
T4CH3
C1H2'
C5H2'
T4H2'
C1H2"
C5H2"
G6H2"
T4H2"
G6H2'
A3H2'
G2H2"
H*(19,20)
A3H2"
1.2
1.4
1.6
1.8
2.0
2.2
2.4
2.6
2.8
3.0
3.2
3.2 3.1 3.0 2.9 2.8 2.7 2.6 2.5 2.4 2.3 2.2 2.1 2.0 1.9 1.8 1.7 1.6 1.5 1.4 1.3 1.2 1.1
ppm

(Fig. 5.7d)

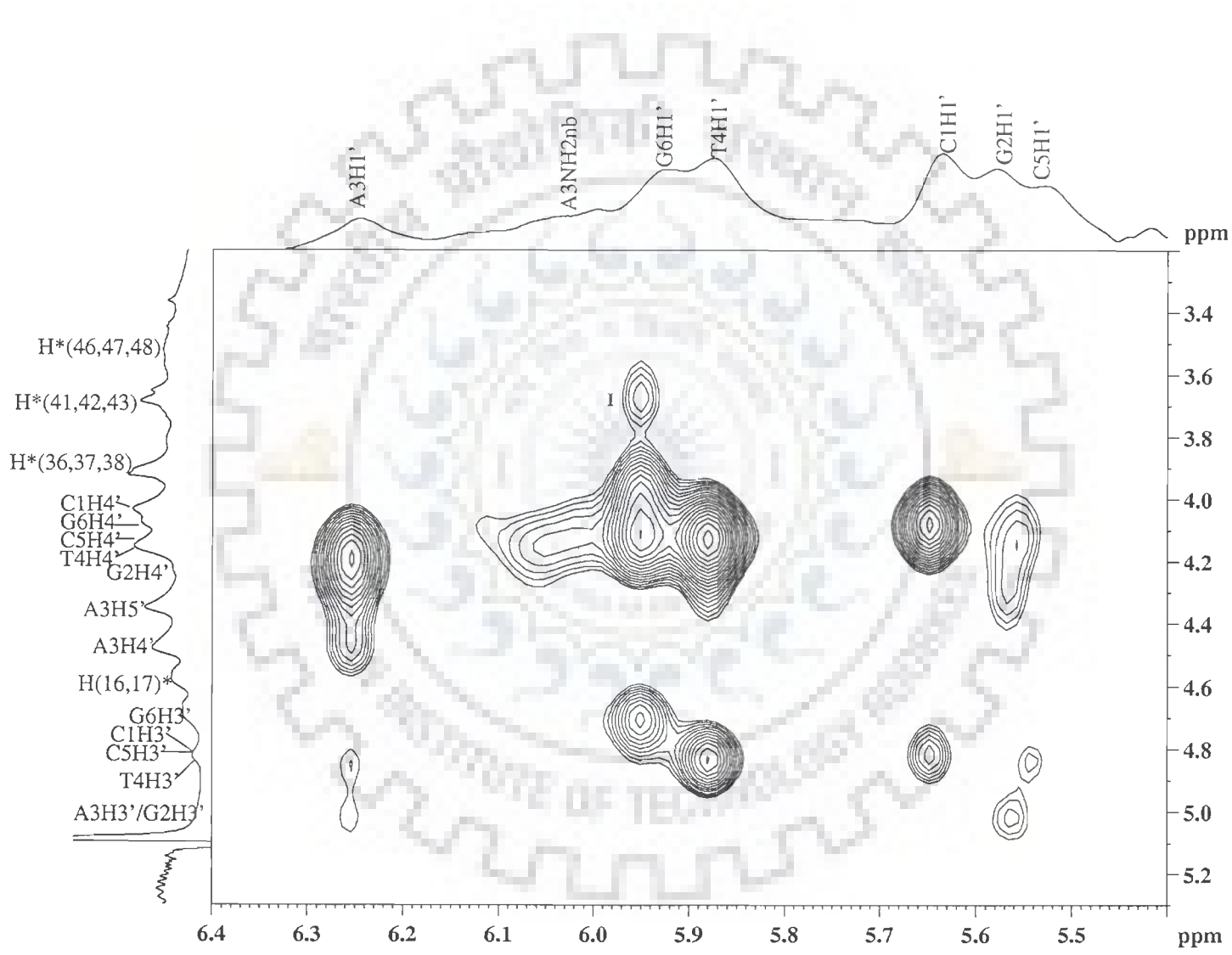
A3H1'
A3NH2nb
G6H1'
T4H1'
C1H1'
G2H1'
C5H1'
ppm
H*(46,47,48)
H*(41,42,43)
H*(36,37,38)
C1H4'
G6H4'
C5H4'
T4H4'
G2H4'
A3H5'
A3H4'
H(16,17)*
G6H3'
C1H3'
C5H3'
T4H3'
A3H3'/G2H3'
I
3.4
3.6
3.8
4.0
4.2
4.4
4.6
4.8
5.0
5.2
6.4
6.3
6.2
6.1
6.0
5.9
5.8
5.7
5.6
5.5
ppm

(Fig. 5.7e)

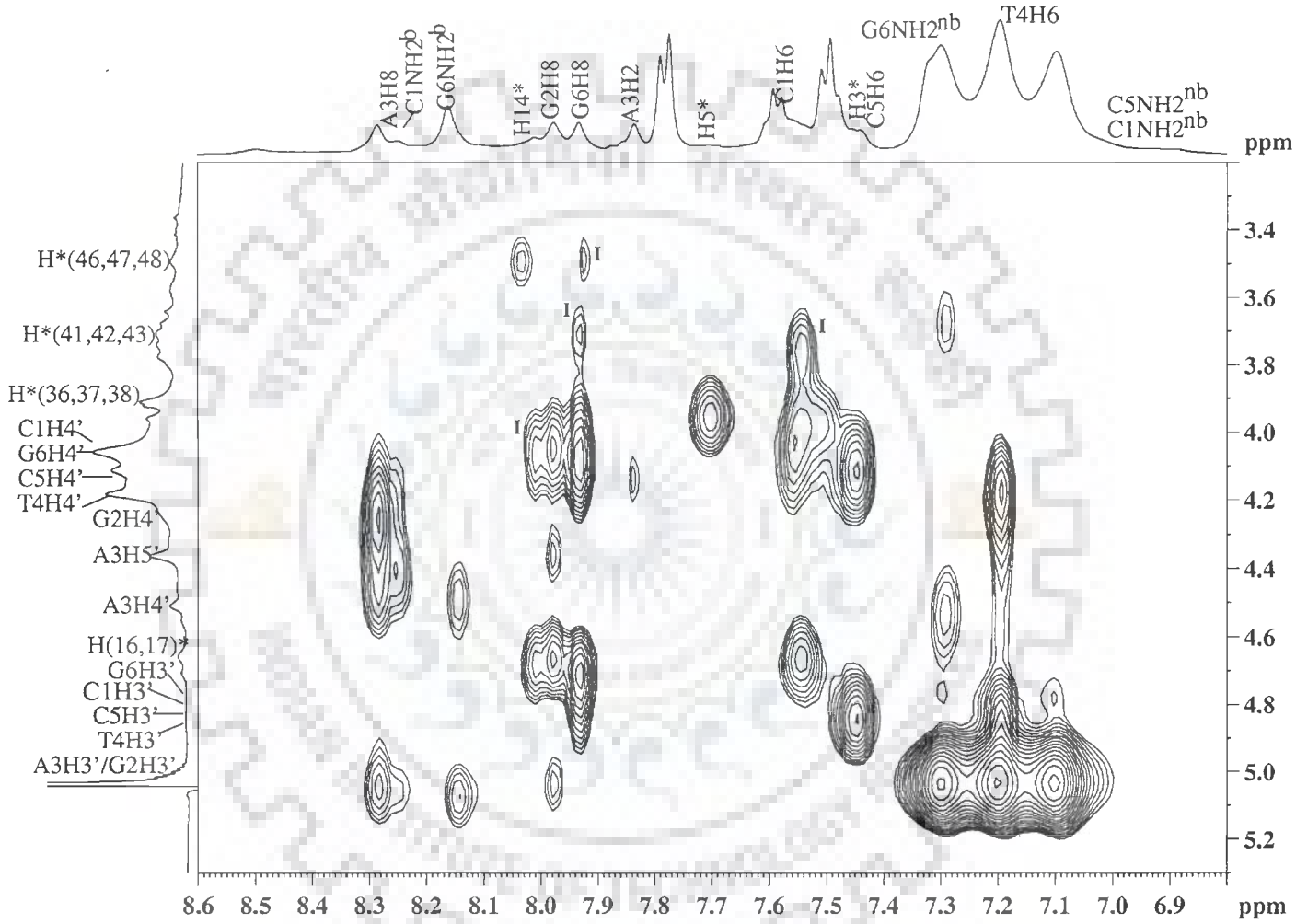
A3H8
C1NH2b
G6NH2b
H14*
G2H8
G6H8
A3H2
H5*
C1H6
H3*
C5H6
G6NH2nb
T4H6
C5NH2nb
C1NH2nb
ppm
H*(46,47,48)
H*(41,42,43)
H*(36,37,38)
C1H4'
G6H4'
C5H4'
T4H4'
G2H4'
A3H5'
A3H4'
H(16,17)*
G6H3'
C1H3'
C5H3'
T4H3'
A3H3'/G2H3'
I
3.4
3.6
3.8
4.0
4.2
4.4
4.6
4.8
5.0
5.2
8.6 8.5 8.4 8.3 8.2 8.1 8.0 7.9 7.8 7.7 7.6 7.5 7.4 7.3 7.2 7.1 7.0 6.9
ppm

(Fig. 5.7f)

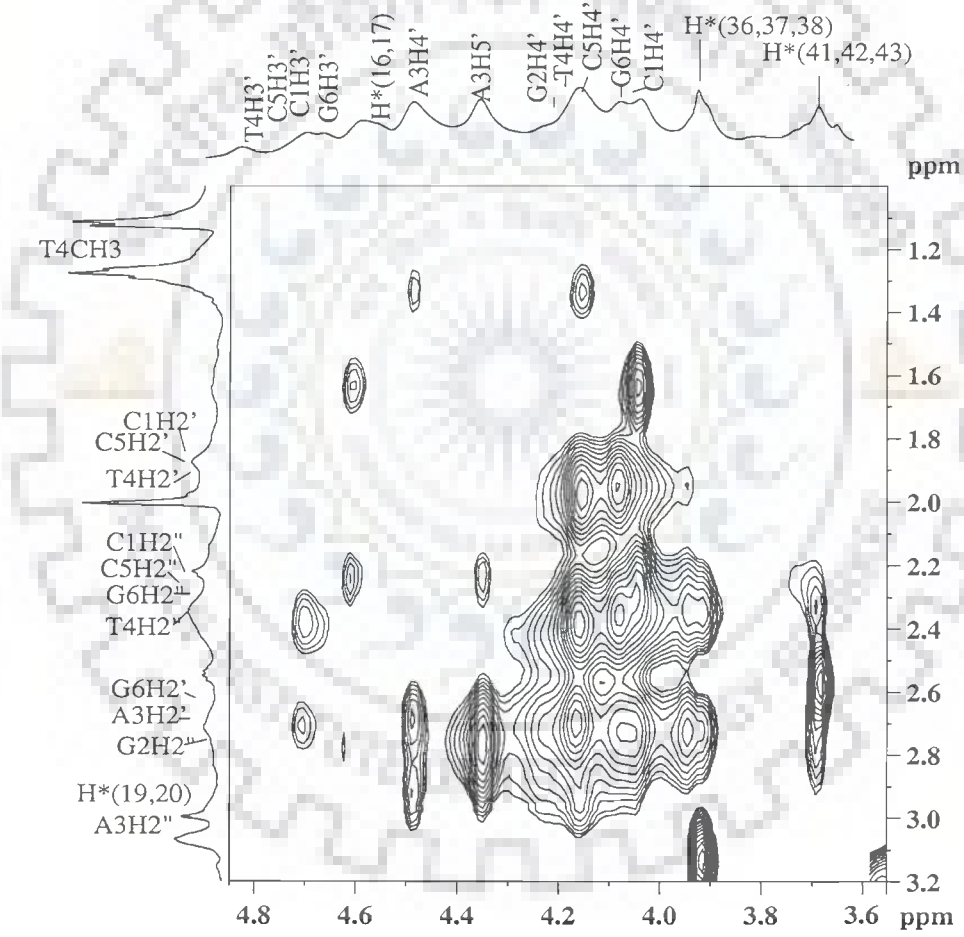
T4H3'
C5H3'
C1H3'
G6H3'
H*(16,17)
A3H4'
A3H5'
G2H4'
T4H4'
C5H4'
G6H4'
C1H4'
H*(36,37,38)
H*(41,42,43)
ppm
T4CH3
C1H2'
C5H2'
T4H2'
C1H2"
C5H2"
G6H2"
T4H2"
G6H2'
A3H2'
G2H2"
H*(19,20)
A3H2"
1.2
1.4
1.6
1.8
2.0
2.2
2.4
2.6
2.8
3.0
3.2
4.8
4.6
4.4
4.2
4.0
3.8
3.6
ppm

(Fig. 5.7g)

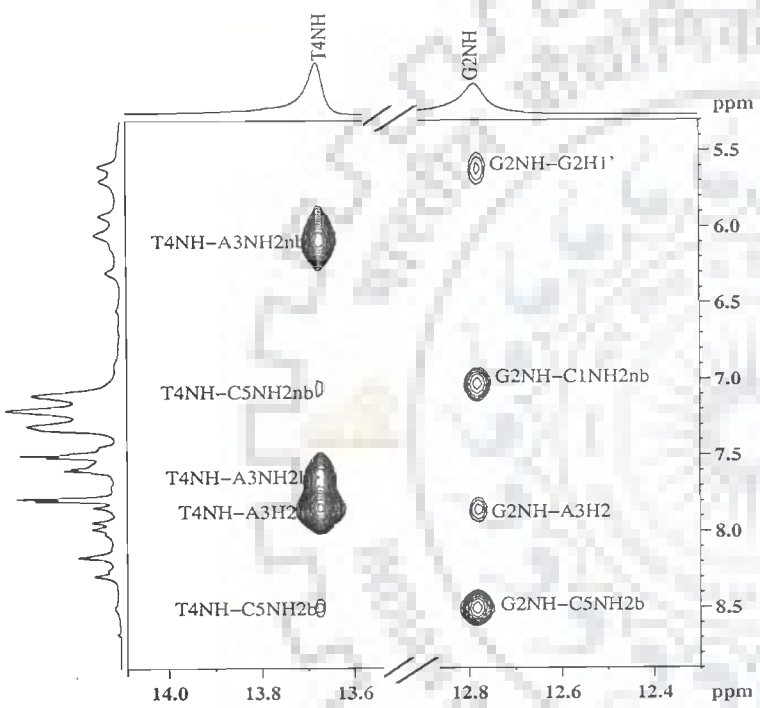

(Fig. 5.7h)

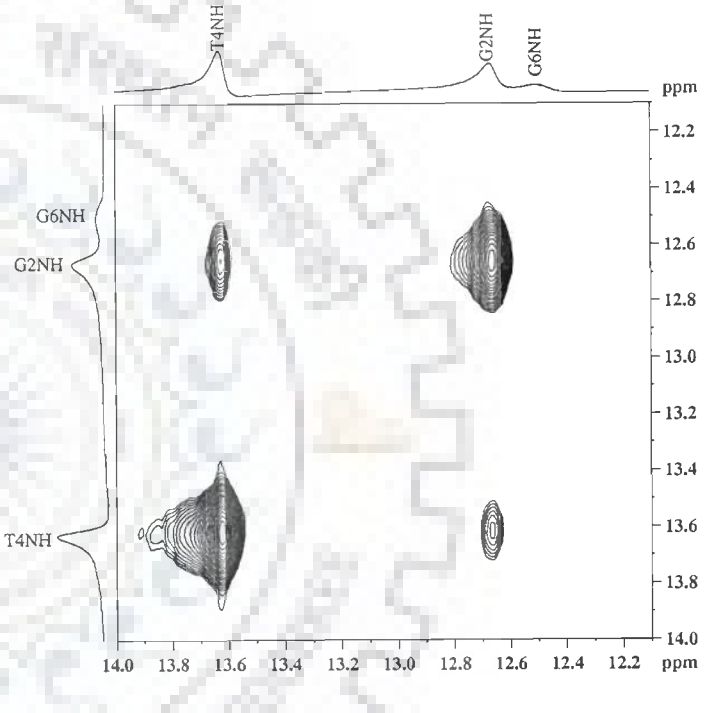

(Fig. 5.7i)

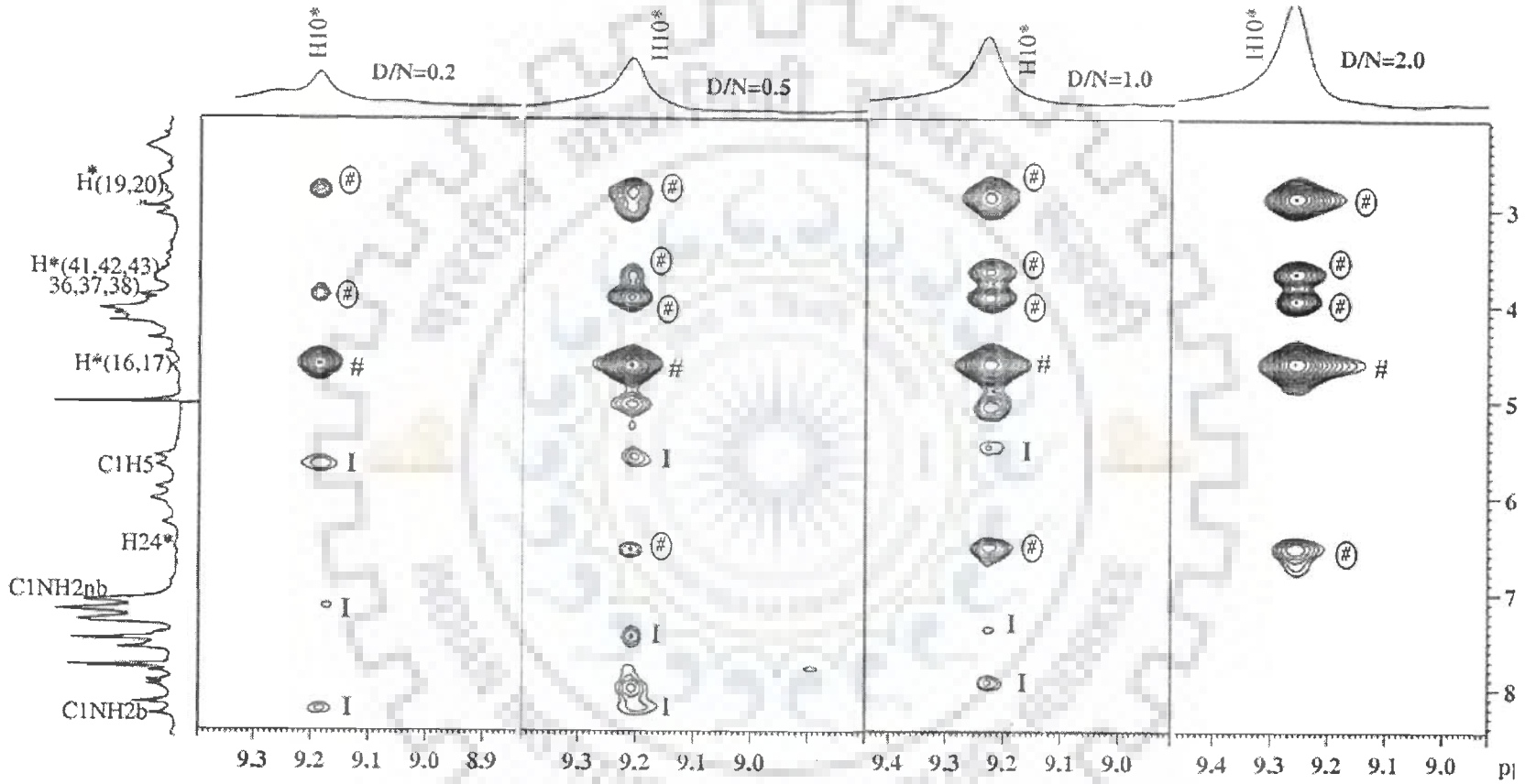
H10*
H10*
H10*
H10*
D/N=0.2
D/N=0.5
D/N=1.0
D/N=2.0
H*(19,20)
H*(41,42,43)
36,37,38)
H*(16,17)
C1H5
H24*
C1NH2nb
C1NH2b
9.3 9.2 9.1 9.0 8.9
9.3 9.2 9.1 9.0
9.4 9.3 9.2 9.1 9.0
9.4 9.3 9.2 9.1 9.0
3
4
5
6
7
8

Fig. 5.7j)

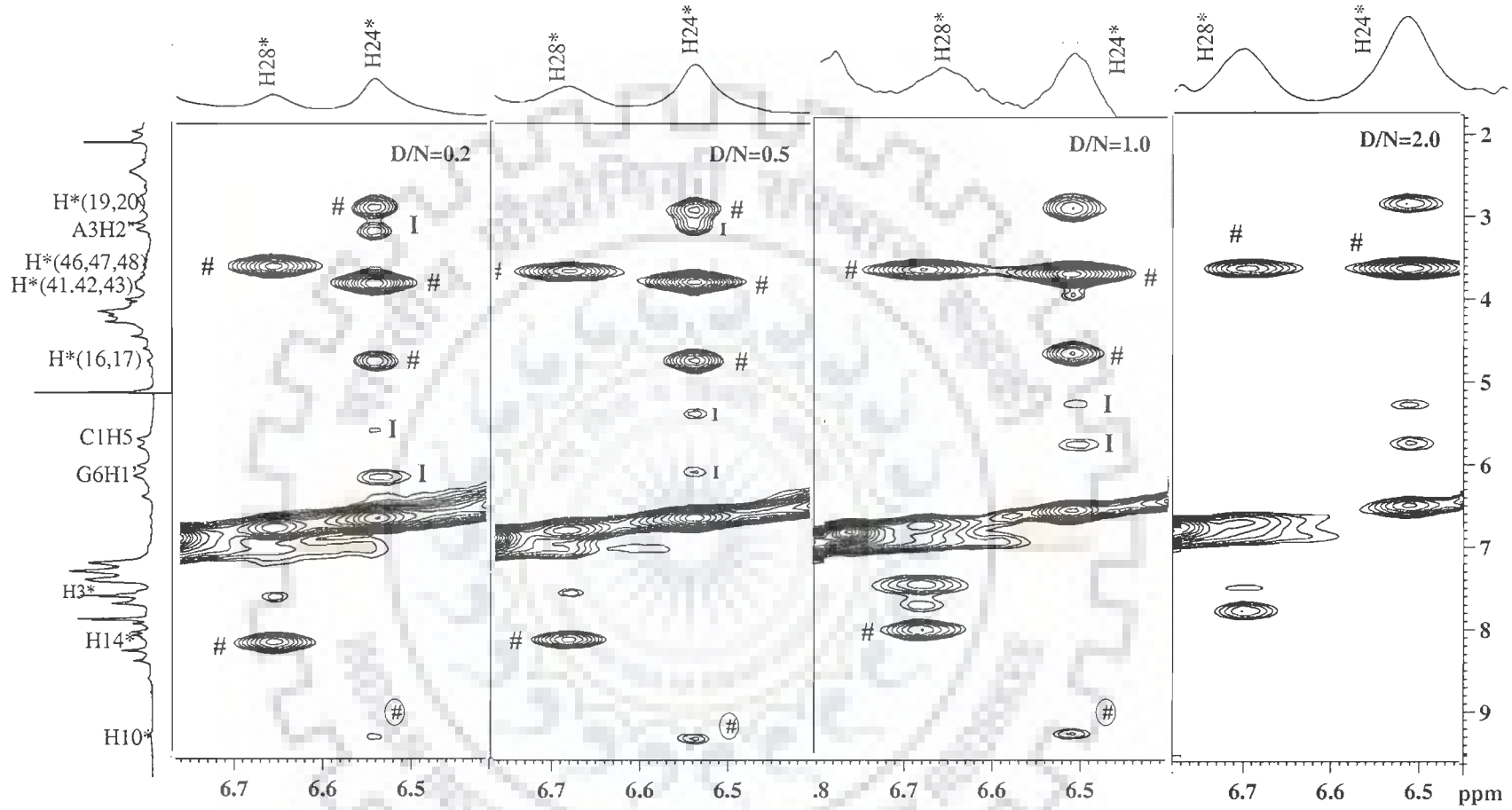
H28*
H24*
D/N=0.2
D/N=0.5
D/N=1.0
D/N=2.0
H*(19,20)
A3H2*
H*(46,47,48)
H*(41.42,43)
H*(16,17)
C1H5
G6H1
H3*
H14*
H10*
6.7
6.6
6.5
ppm
2
3
4
5
6
7
8
9

(Fig. 5.7k)

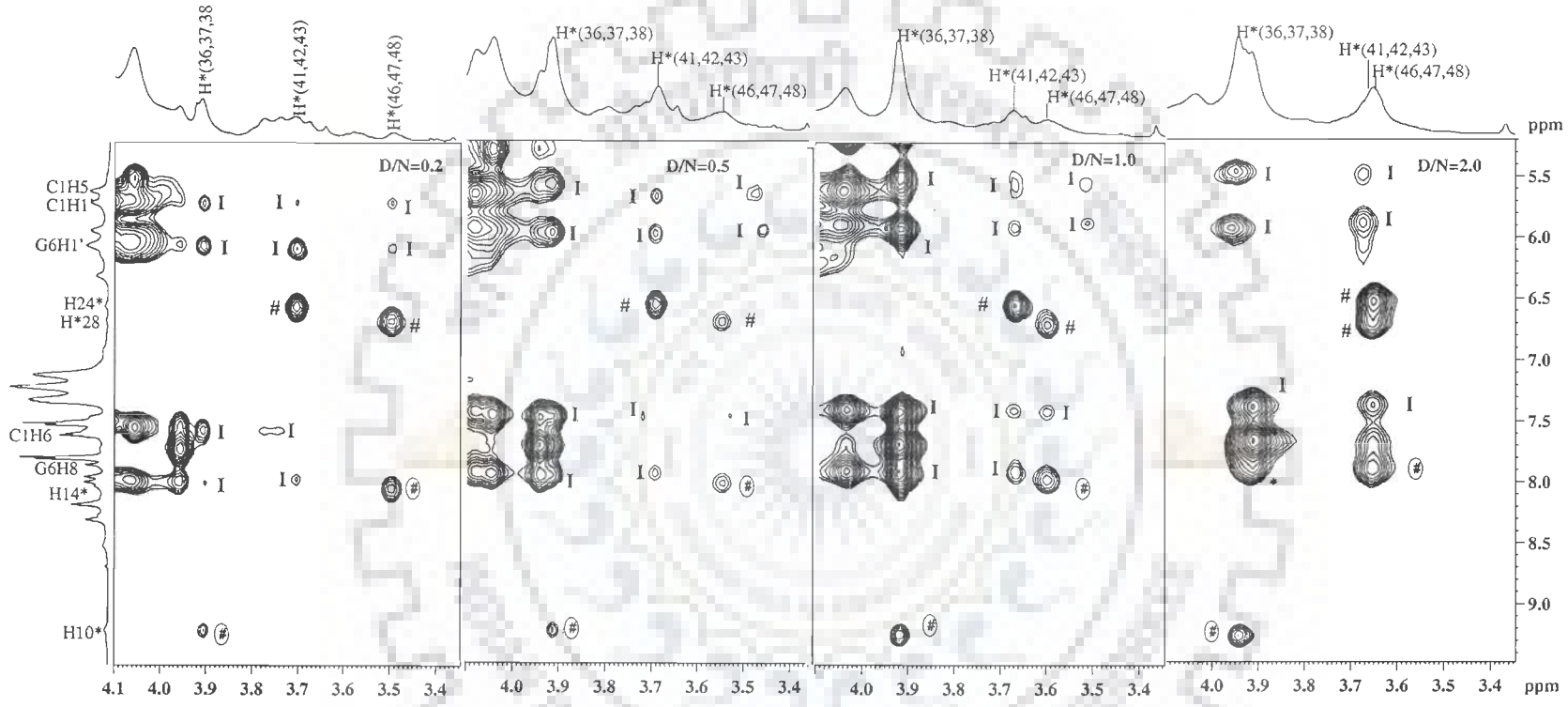
H*(36,37,38)
H*(41,42,43)
H*(46,47,48)
D/N=0.2
D/N=0.5
D/N=1.0
D/N=2.0
C1H5
C1H1
G6H1'
H24*
H*28
C1H6
G6H8
H14*
H10*
ppm

(Fig. 5.7l)

Table 5.5: Chemical shift (ppm) of d-(CGATCG)$_2$ protons in uncomplexed state (δ^f) and that bound to palmatine (δ^b) at drug (D) to nucleic acid duplex (N) ratio D/N=2.0 at 278 K. Also shown here is the change in chemical shift on binding, that is. $\Delta\delta = \delta^b_{(D/N=2.0)} - \delta^f_{(D/N=0.0}$.

Protons	C1			G2			A3			T4		
	δ_b	δ_f	$\Delta\delta$	δ_b	δ_f	$\Delta\delta$	δ_b	δ_f	$\Delta\delta$	δ_b	δ_f	$\Delta\delta$
H8/H6	7.34	7.65	-0.31	7.85	8.03	-0.18	8.20	8.34	-0.14	7.10	7.23	-0.13
H1'	5.58	5.73	-0.15	5.46	5.65	-0.19	6.20	6.34	-0.14	5.82	5.96	-0.14
H2'	1.88	1.98	-0.10	2.71	2.84	-0.13	2.64	2.73	-0.09	1.91	2.05	-0.14
H2"	2.26	2.40	-0.14	2.71	2.84	-0.13	2.88	3.01	-0.13	2.32	2.47	-0.15
H3'	4.77	4.86	-0.09	5.02	5.06	-0.04	5.00	5.06	-0.06	4.84	4.89	-0.02
H4'	4.00	4.12	-0.12	4.28	4.31	-0.03	4.45	4.52	-0.07	4.05	4.19	-0.14
H5/H2/CH$_3$	5.51	5.85	-0.34	-	-	-	7.72	7.89	-0.17	1.29	1.41	-0.12
NH$_2^b$	8.18	8.35	-0.17	-	-	-	7.56	7.72	-0.16	-	-	-
NH$_2^{nb}$	6.84	7.10	-0.26	-	-		6.00	6.14	-0.14	-	-	-
NH	-	-	-	12.60	12.91	-0.31	-	-	-	13.53	13.74	-0.21
	C5			G6								
	δ_b	δ_f	$\Delta\delta$	δ_b	δ_f	$\Delta\delta$						
H8/H6	7.32	7.50	-0.18	7.82	7.96	-0.14						
H1'	5.51	5.66	-0.15	5.85	6.14	-0.31						
H2'	1.88	2.03	-0.15	2.65	2.67	-0.02						
H2"	2.26	2.42	-0.16	2.32	2.38	-0.06						
H3'	4.79	4.89	-0.10	4.70	4.71	-0.01						
H4'	4.06	4.15	-0.09	3.99	4.18	-0.19						
H5/H2/CH$_3$	5.45	5.66	-0.21	-	-	-						
NH$_2^b$	8.28	8.62	-0.34	7.90	8.14	-0.24						
NH$_2^{nb}$	6.84	7.10	-0.26	7.30	7.31	-0.01						
NH	-	-	-	12.30	13.08	-0.78						

+ve $\Delta\delta$ indicates downfield shift

-ve $\Delta\delta$ indicates upfield shift

5.1.2.1 Effects of Titrimetric Addition of Palmatine

The titration of hexamer d-$(CGATCG)_2$ with palmatine is carried out at 278 and 298 K. Almost same pattern of changes were observed for all the protons of d-$(CGATCG)_2$ upon the addition of palmatine at both the temperatures. It is found that chemical shift for d-$(CGATCG)_2$ did not change significantly by adding a low amount of palmatine. Therefore, data recorded at D/N 0.1 interval and at 298 K is not been shown here. ^{1}H 1D NMR spectra of d-$(CGATCG)_2$ and change in spectra on successive addition of palmatine to DNA at D/N 0.0, 0.2, 0.5, 1.0, 1.5, 2.0 at 278 K is shown in Fig. 5.8a-d. On addition of palmatine to DNA, new resonance peaks pertaining to palmatine protons starts appearing which increase in intensity as D/N ratio increases.

There is only one set of DNA resonances and one set of bound palmatine resonances observed through out the titration indicating that free and bound species are in fast exchange regime on NMR time scale also at temperature of 278 K. Fig. 5.9 shows the change in proton chemical shift for palmatine as a function of D/N ratio. It shows that the difference in chemical shift between bound and alone palmatine protons is maximum at low D/N ratio and remain constant through out the titration, which indicates that maximum amount of palmatine added to duplex is in the bound form. The resonances of palmatine are considerably broad and shows maximum upfield shift of 0.31 ppm w.r.t to the free drug (Table 5.6). The palmatine protons H28 and H24, located on ring D exhibits the maximum upfield shift of 0.31 and 0.27 ppm, respectively (Fig. 3.1). The protons H10, H(16, 17) and H(19, 20) located on the concave side of the molecule shows upfield shift of 0.21, 0.09 and 0.20 ppm, respectively while the protons located on convex side i.e. H14, H5 shows upfield shift of 0.13 and 0.17 ppm, respectively.

Table 5.6: Chemical shift (ppm) of palmatine protons as a function of drug (D) to nucleic acid duplex (N) ratio, D/N, at 278 K. Also shown here is the maximum change in chemical shift due to binding, with respect to palmatine in free form. $\Delta\delta = \delta^{b}_{(D/N=2.0)} - \delta^{f}_{(D/N=0.0)}$.

Palmatine Proton	δ_f D/N 0.0	δ_b D/N 0.2	δ_b D/N 0.5	δ_b D/N 1.0	δ_b D/N 1.5	δ_b D/N 2.0	$\Delta\delta$ (Present work)	Berberine* Proton	$\Delta\delta^*$ (T5GA)	$\Delta\delta^*$ (A5)	$\Delta\delta^*$ (A2T2)	$\Delta\delta^*$ (GATC)	$\Delta\delta^*$ (TATA)	$\Delta\delta^*$ (TA)	$\Delta\delta^{\#}$ (HP14)
H10	9.45	9.19	9.21	9.22	9.24	9.24	-0.21	**H10**	-0.44	0.50	0.29	0.35	0.35	0.34	0.06
H14	8.04	8.03	8.01	7.97	7.97	7.96	-0. 13	**H14**	-0.67	0.69	0.55	0.62	0.49	0.49	0.11
H5	7.83	7.69	7.68	7.65	7.65	7.66	-0.17	**H5**	-0.65	0.51	0.38	0.41	0.40	0.38	0.05
H3	-	-	-	-	-	-	-	**H3**	-0.28	-	0.20	0.18	0.23	0.22	0.07
H28	7.00	6.66	6.68	6.68	6.68	6.69	-0.31	**H28**	-0.20	0.89	0.54	0.62	0.49	0.50	0.03
H24	6.78	6.54	6.54	6.52	6.51	6.51	-0.27	**H24**	-0.27	0.57	0.38	0.52	0.38	0.38	0.06
H16, 17	4.69	4.63	4.63	4.61	4.60	4.60	-0.09	**H16, 17**	-0.24	-	0.17	0.22	-	0.13	-
H41,42,43	3.79	3.70	3.69	3.67	3.67	3.67	-0.12	**H41,42,43**	-0.26	0.30	0.13	0.13	0.13	0.19	-
H36,37,38	4.07	3.90	3.91	3.92	3.93	3.94	-0.13	**H36,37,38**	-0.33	0.30	0.15	0.15	0.20	0.24	-
H19,20	3.06	2.80	2.80	2.86	2.86	2.86	-0.20	**H19,20**	-0.39	0.40	0.24	0.26	0.24	-	0.04
H46,47,48	3.84	3.50	3.51	3.59	3.68	3.65	-0.19	-	-	-	-	-	-	-	-

*-[Mazzini et al., 2003]
#- [Jeon et al., 2002]
+ve $\Delta\delta$ indicates downfield shift
-ve $\Delta\delta$ indicates upfield shift

The methoxy group protons of palmatine H(41, 42, 43), H(46, 47, 48) and H(36, 37, 38) showed an upfield shift of 0.12, 0.19 and 0.13 ppm, respectively. Anticancer drugs like camptothecin and topotecon which are proved as external binder of DNA by stacking at the terminal end of oligonucleoiteds also shows a chemical shift variation of < 0.50 for several oligonucleotides [Mazzini et al., 2004]. It is also worth mentioning that the shielding effect was more or less spread over the whole palmatine molecule, but the values were found to be more significant for aromatic protons. Hence, these results suggest that aromatic chromophore (ring C and D, Fig. 3.1) of palmatine might be stacked with base pairs of DNA. The chemical shift change of palmatine shows no specific trend. The shift variation effect on the drug moleclule is considered as the sum of specific and non specific interaction. The lack of specificity of upfield changes in chemical shift for the protons of palmatine upon binding indicates external non-specific ionic interaction of the positively charged palmatine molecule with negatively charged ionic surface of the hexamer d-$(CGATCG)_2$. Our results are in accordance with earlier structural studies done on protoberberines berberine and berberrubine by a few authors using NMR spectroscopy [Mazzini et al., 2003; Park et al., 2004a; Park et al., 2004b]. Mazzini et al has studied 1D spectra for berberine interaction with several oligonucleotides i.e., d-$(AAGAATTCTT)_2$ (A2T2), d-$(GCGATCGC)_2$ (GATC), d-$(CGTACG)_2$ (TA), d$(CGTATACG)_2$ (TATA), d-(ACATCAAAAAGGT) (ss-A5) and d-$(ACCTTTTTGATGT)_2$ (T5GA) (listed in Table 5.6) [Mazzini et al., 2003]. They have suggested external non specific ionic interactions of the positively charged berberine molecule with the negatively charged ionic surface of the oligonucleotide, which is shown by the shielding of berberine protons (0.2–0.7 ppm) observed with the single-

strand fragment, for which intercalation or groove binding processes are excluded. Park et al has also reported the chemical shift values for berberine on binding to oligonucleotide d-(GCCGTCGTTTTACA)$_2$ (HP14) which contains topoisomerase cleavage site. Overall very little shielding for berberine protons with a maximum value of 0.11 for H14 was observed on berberine binding with HP14 [Park et al., 2004a]. The aliphatic resonances of berberine showed a gradual line broadening effect as the drug to DNA ratio is increased. They suggested non specific interaction between berberine and DNA.

However, the chemical shift variation of the drug is cannot be used to obtain structural information. This is attributed to the following reasons: (i) the shift variation effects on the drug molecule must be interpreted as the sum of specific and non- specific interactions. (ii) The external non-specific ionic interactions of a positively charged drug with the negatively charged ionic surface of the oligonucleotide are the main factors responsible for such effects, as also reported for berberine [Mazzini et al., 2004]. (iii) Shift variation can also occur when a ligand intercalates between the base pairs or binds to the minor groove. Thus, ^{1}H chemical shift variation observed on the drug is risky to draw any conclusion about the type of interactions. The chemical shift variation of the ^{31}P resonances provides unique evidence of the binding process. Our ^{31}P studies has shown that the addition of palmatine did not induces significant chemical shift variation of the phosphate signals (<0.2). However, the binding of intercalating molecule is associated with a downfied shift of 1.0-1.5 ppm of the phosphorus resonances. Therefore, the intercalation as the binding mechanism of palmatine to the hexamer d-(CGATCG)$_2$ can be excluded. The ^{1}H upfield shifts observed for the palmatine molecule are not a

consequence of the drug intercalation into the base pairs of the double helix, but they are mainly due to external ionic interactions.

All the spectral lines for DNA are uniformly broadened on binding as the internal motions are affected and the protons are getting immobilized. The resonances of d-$(CGATCG)_2$ did not show any significant change during addition of increased amount of palmatine except the resonances of terminal C1:G6 imino, sugar and base protons. The $\Delta\delta$ increases with D/N ratio as more drug binds to DNA. The results are tabulated in table 5.8. DNA protons chemical shift change ($\Delta\delta$) versus D/N ratio are shown in Fig. 5.8a-d. The imino proton resonances of hexamer continuously shift upfield on titration. In uncomplexed d-$(CGATCG)_2$, T4NH, G2NH and G6NH resonances appeared at 13.74, 12.91 and 13.08 ppm, respectively. All the three imino protons broadened considerably with increasing ratio of palmatine, the broadening is found to be more significant at D/N ratio of 2.0. T4NH and G2NH resonances showed upfield shift of 0.21 and 0.31 whereas a significant upfield shift of 0.78 ppm is found in G6NH imino proton. The upfield shift (0.78 ppm) observed for the imino proton of the terminal CG base pair suggests that the ends of the palindromic oligomer d-$(CGATCG)_2$ is the site of interaction for palmatine. G6NH proton's more shielding (Fig 5.8d) due to binding of palmatine is in accordance with the results on other protoberberines from literature [Park et al., 2004a], which showed that the guanines imino protons are more effected due to binding with berberine and berberrubine. Park et al demonstrated that imino protons of HP14 showed line broadening effect and a gradual chemical shift change up to ~0.16 ppm when molar ratio of berberine to HP14 was increased. However, the up-field shift of imino protons in berberrubine - HP14 complex was most evident at molar ratio 1:1 but became less

pronounced as the ratio of the bound to free berberrubine decreased during titration with the berberine [Park et al., 2004a].

The non exchangeable proton resonances of d-$(CGATCG)_2$ exhibits upfield shift at all D/N ratios (Fig. 5.8a-c). The strongest chemical shift perturbation of DNA is observed in the protons belonging to C1 and G6. In particular C1H5, C1H6 and G6H1' exhibited upfield shift of 0.36, 0.31 and 0.31 ppm, respectively. This shift in the C1 and G6 base pair protons again support the interaction of palmatine with the terminal ends of the hexamer. The shielding observed for C1H3' and C5H3' protons is highest among protons in H3' region (Fig.5.8c). Among H2" protons, C5H2" proton showed maximum upfield shift of 0.16 ppm during titration. Overall the non exchangeable resonance of oligomer shows insignificant chemical shift change ($\Delta\delta = 0.01 - 0.31$) during the titration. The plots of change in chemical shift of d-$(CGATCG)_2$ protons complexed with palmatine as a function of drug to DNA (D/N) ratio are given (Figs. 5.10a-i). The variation in chemical shift is maximum for the terminal CG protons. The change in chemical shift is not the sufficient indicator of the interaction; instead the observed intermolecular short contacts are the direct proof of the structure of a specific drug-DNA complex.

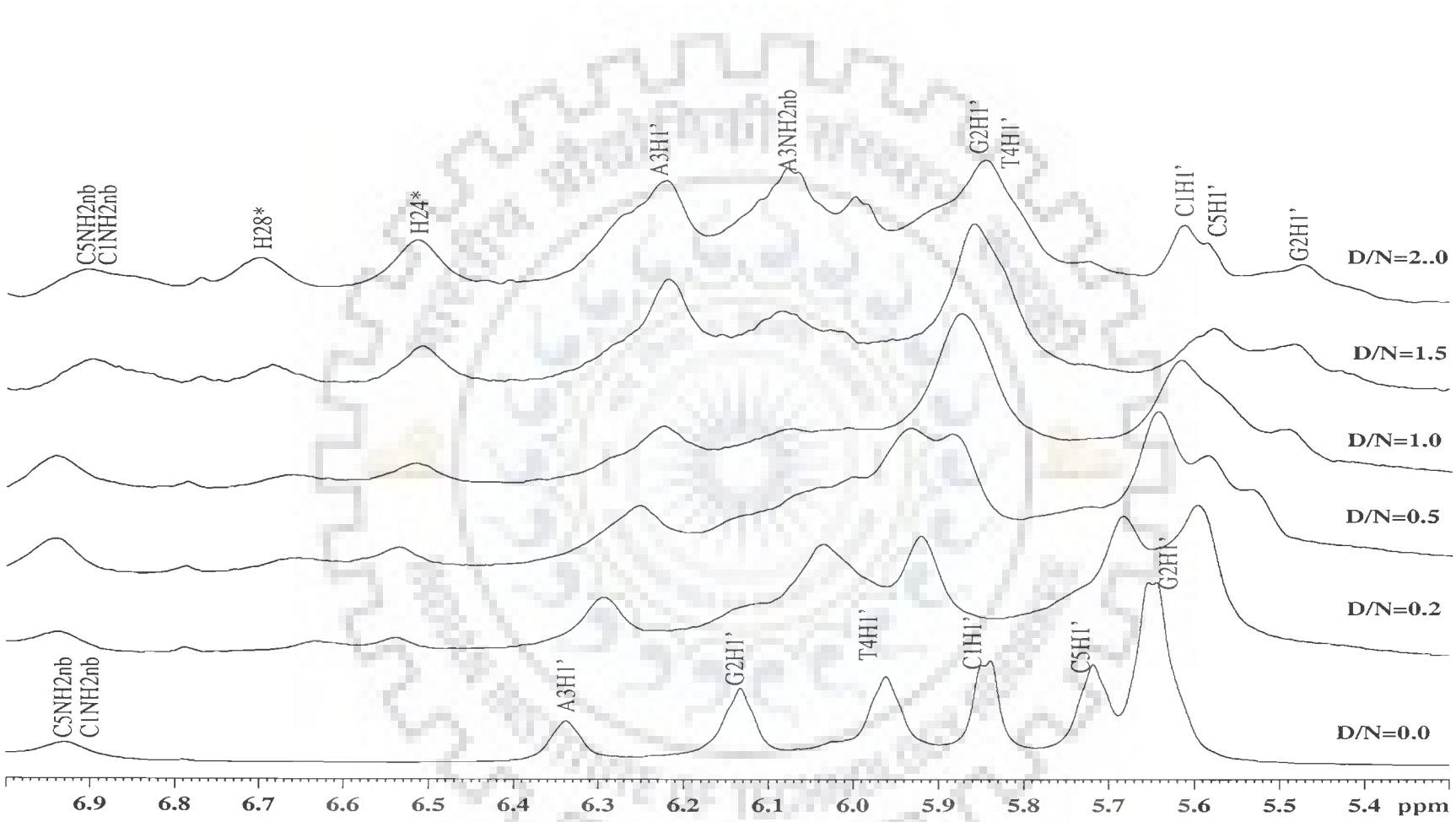
C5NH2nb
C1NH2nb
H28*
H24*
A3H1'
A3NH2nb
G2H1'
T4H1'
C1H1'
C5H1'
G2H1'
D/N=2..0
D/N=1.5
D/N=1.0
D/N=0.5
D/N=0.2
D/N=0.0
6.9
6.8
6.7
6.6
6.5
6.4
6.3
6.2
6.1
6.0
5.9
5.8
5.7
5.6
5.5
5.4
ppm

Fig. 5.8a

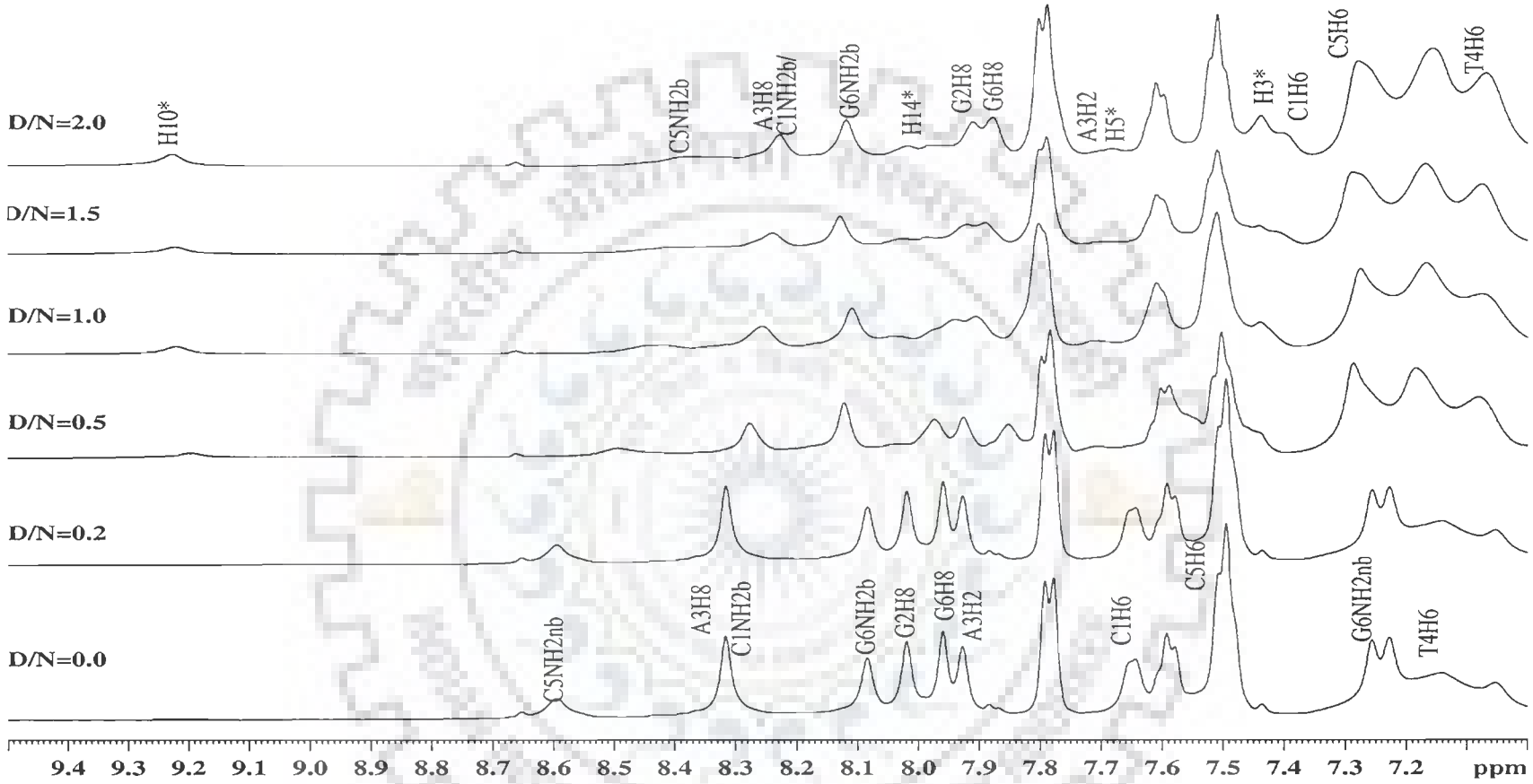
D/N=2.0
D/N=1.5
D/N=1.0
D/N=0.5
D/N=0.2
D/N=0.0
H10*
C5NH2b
A3H8
C1NH2b/
G6NH2b
H14*
G2H8
G6H8
A3H2
H5*
H3*
C1H6
C5H6
T4H6
C5NH2nb
A3H8
C1NH2b
G6NH2b
G2H8
G6H8
A3H2
C1H6
C5H6
G6NH2nb
T4H6
9.4 9.3 9.2 9.1 9.0 8.9 8.8 8.7 8.6 8.5 8.4 8.3 8.2 8.1 8.0 7.9 7.8 7.7 7.6 7.5 7.4 7.3 7.2 ppm

Fig. 5.8b

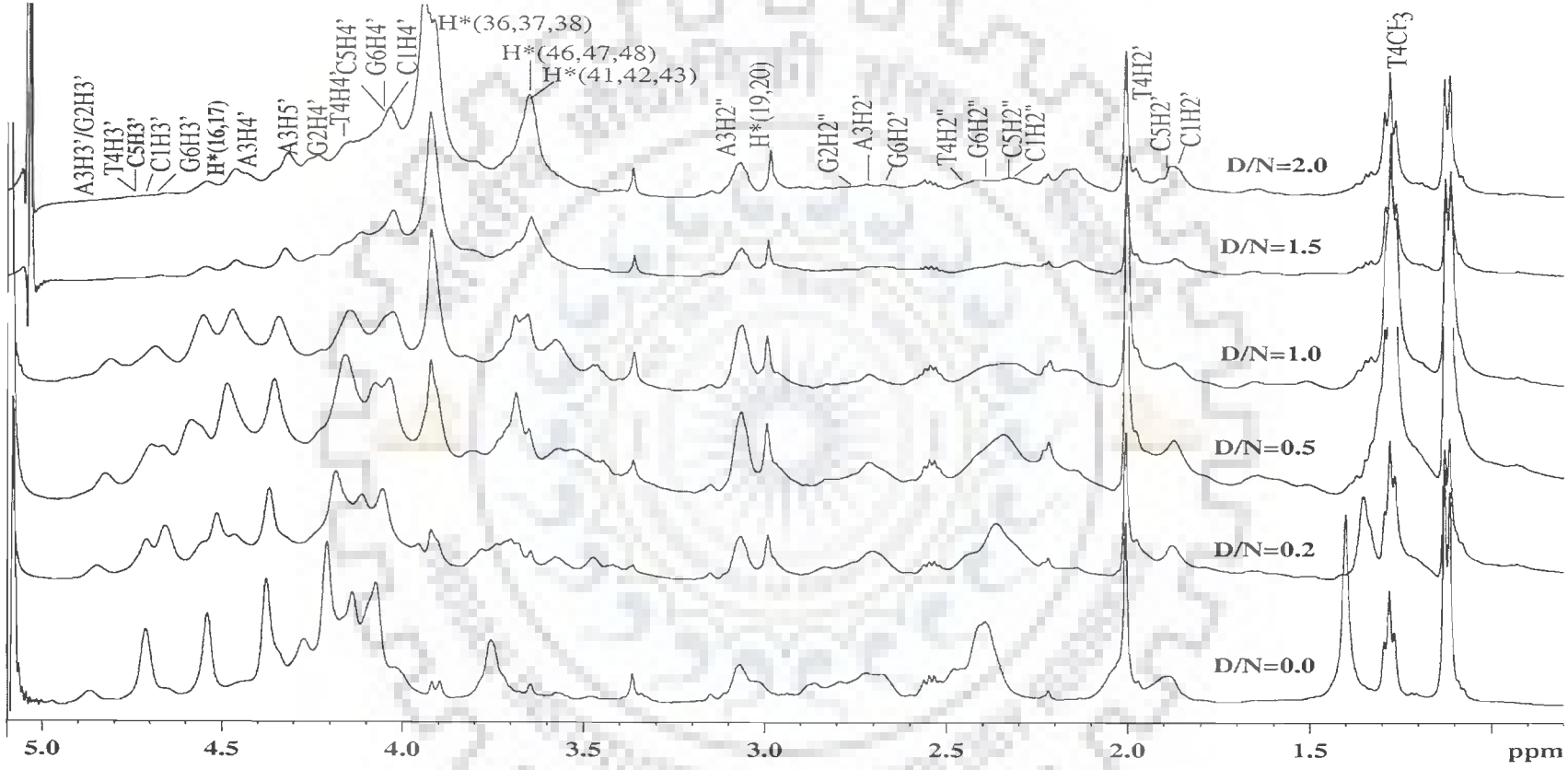
A3H3'/G2H3'
T4H3'
C5H3'
C1H3'
G6H3'
H*(16,17)
A3H4'
A3H5'
G2H4'
T4H4'C5H4'
G6H4'
C1H4'
H*(36,37,38)
H*(46,47,48)
H*(41,42,43)
A3H2"
H*(19,20)
G2H2"
A3H2'
G6H2'
T4H2"
G6H2"
C5H2"
C1H2"
T4H2'
C5H2'
C1H2'
T4CH3
D/N=2.0
D/N=1.5
D/N=1.0
D/N=0.5
D/N=0.2
D/N=0.0
5.0
4.5
4.0
3.5
3.0
2.5
2.0
1.5
ppm

Fig. 5.8c

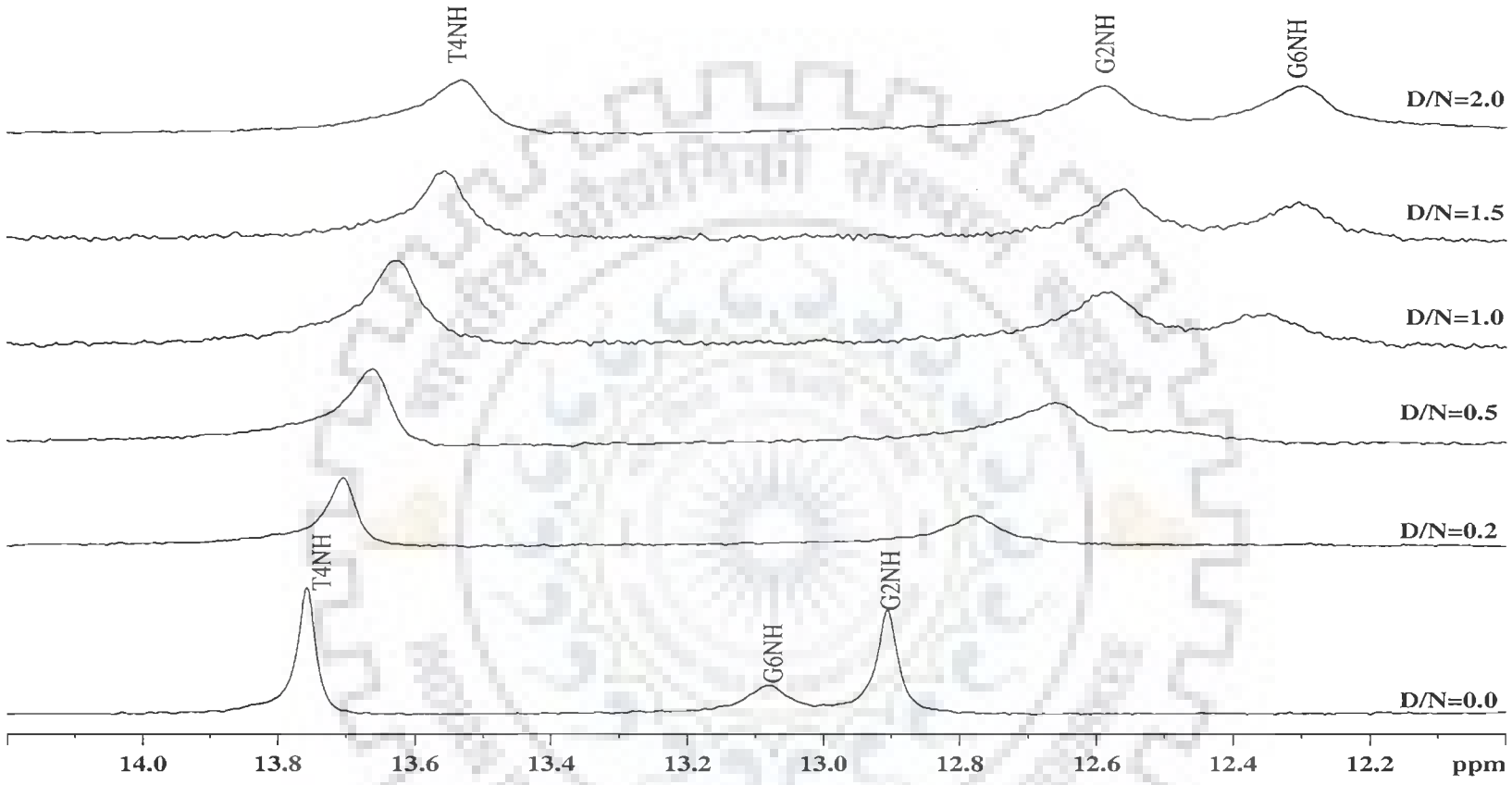

Fig. 5.8d

Fig. 5.8 a-d: Proton NMR spectra of complex of palmatine with d-$(CGATCG)_2$ as a function of D/N ratio at 278 K (* palmatine proton in palmatine -d-$(CGATCG)_2$ complex).

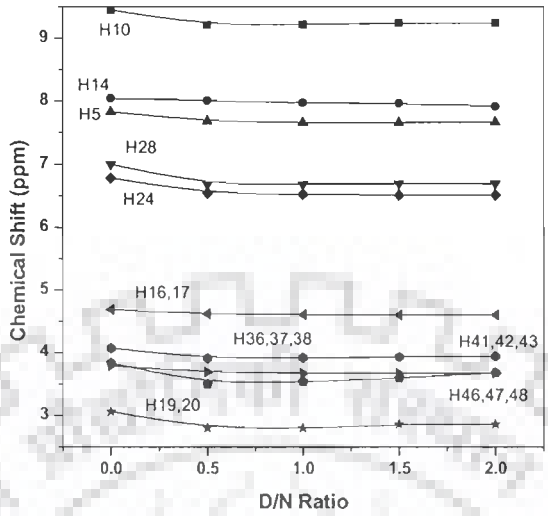

Fig. 5.9: Change in ^{1}H chemical shift of palmatine protons complexed with d $(CGATCG)_2$ at various D/N ratio, 278 K.

Table 5.7: Relative intensities of intramolecular NOE cross peaks within the palmatine molecule in the palmatine-d-$(CGATCG)_2$ complex at D/N = 2.0, at 278 K. The strong intense (ss), strong (s), medium (m), weak (w), very weakly (vw) intense cross peaks correspond to distances in the range ss 1.8 - 2.5 Å, s 2.5 - 3.0 Å, m 3.0 - 3.5 Å, w 3.5 - 4.0 Å, vw 4.0 - 5.0 Å, respectively in the NOESY spectra.

S. No.	Cross peak	Intensity	Distances (Å) from rMD
1.	H24-H(19,20)	w	3.51
2.	H24-H(41,42,43)	ss	2.59
3.	H24-H(16,17)	m	3.24
4.	H28-H(46,47,48)	ss	2.58
5.	H28-H3	vw	5.25
6.	H28-H14	m	3.21
7.	H3-H14	w	4.28
8.	H(16,17)-H(19,20)	m	3.02
9.	H10-H(19,20)	w	3.42
10.	H10-H(36,37,38)	m	3.30
11.	H10-H(16,17)	ss	2.62
12.	H10-H24	w	3.56
13.	H10-H(41,42,43)	w	3.89
14.	H(46,47,48)-H14	ss	2.78

Table 5.8: Chemical shift (ppm) of d-(CGATCG)$_2$ protons in palmatine -d-(CGATCG)$_2$ complex as a function of drug (D) to nucleic acid duplex (N) ratio, D/N, at 278 K. Also shown here is the change in chemical shift on binding, that is, $\Delta\delta = \delta$(D/ N=2.0) - δ(D/ N= 0.0) equivalent to δTotal = δ^b (D/ N=2.0)- δ^f.

D/N	C1H1'	G2H1'	A3H1'	T4H1'	C5H1'	G6H1'	C1H5	C5H5	T4CH$_3$	C1H6	G2H8	A3H8	T4H6	C5H6	G6H8
0.0	5.73	5.65	6.34	5.96	5.66	6.14	5.85	5.66	1.41	7.65	8.03	8.34	7.23	7.50	7.96
0.5	5.64	5.56	6.25	5.89	5.54	5.95	5.58	5.54	1.32	7.44	7.92	8.25	7.15	7.39	7.91
1.0	5.61	5.54	6.22	5.85	5.50	5.86	5.56	5.48	1.29	7.38	7.89	8.21	7.13	7.36	7.86
1.5	5.59	5.48	6.21	5.85	5.51	5.85	5.52	5.45	1.29	7.36	7.87	8.20	7.10	7.35	7.86
2.0	5.58	5.46	6.20	5.82	5.51	5.83	5.51	5.45	1.29	7.34	7.85	8.20	7.10	7.32	7.82
$\Delta\delta$	-0.15	-0.19	-0.14	-0.14	-0.15	-0.31	-0.34	-0.21	-0.12	-0.31	-0.18	-0.14	-0.13	-0.18	-0.14
D/N	A3H2	A3NH2nb	A3NH2b	G6NH2nb	G6NH2b	C5NH2nb	C5NH2b	C1NH2nb	C1NH2b	C1H3'	G2H3'	A3H3'	T4H3'	C5H3'	G6H3'
0.0	7.89	6.14	7.72	7.31	8.14	7.10	8.62	7.10	8.35	4.86	5.06	5.06	4.89	4.89	4.71
0.5	7.79	6.02	7.57	7.30	8.17	6.93	8.38	6.96	8.30	4.81	5.05	5.02	4.87	4.83	4.70
1.0	7.73	6.02	7.57	7.33	8.17	6.87	8.30	6.88	8.26	4.80	5.04	5.01	4.86	4.82	4.70
1.5	7.72	6.00	7.58	7.31	7.92	6.85	8.28	6.87	8.21	4.78	5.03	5.01	4.86	4.82	4.70
2.0	7.72	6.00	7.56	7.30	7.90	6.84	8.28	6.84	8.18	4.77	5.02	5.00	4.84	4.79	4.70
$\Delta\delta$	-0.17	-0.14	-0.26	-0.01	-0.24	-0.26	-0.34	-0.26	-0.17	-0.09	-0.04	-0.06	-0.05	-0.10	-0.01
D/N	C1H4'	G2H4'	A3H4'	T4H4'	C5H4'	G6H4'	A3H5'	C1H2'	C1H2"	G2H2'	G2H2"	A3H2'	A3H2"	T4H2'	T4H2"
0.0	4.12	4.31	4.52	4.19	4.19	4.18	4.27	1.98	2.40	2.83	2.84	2.73	3.01	2.05	2.47
0.5	4.08	4.30	4.45	4.12	4.14	4.11	4.25	1.94	2.34	2.76	2.77	2.67	2.96	1.99	2.39
1.0	4.04	4.31	4.44	4.12	4.10	4.08	4.19	1.91	2.30	2.73	2.74	2.64	2.93	1.94	2.37
1.5	3.96	4.32	4.46	4.11	4.10	4.02	4.19	1.91	2.25	2.72	2.72	2.64	2.91	1.94	2.34
2.0	4.00	4.28	4.45	4.06	4.05	3.99	4.18	1.88	2.26	2.70	2.71	2.64	2.88	1.91	2.32
$\Delta\delta$	-0.12	-0.03	-0.07	-0.13	-0.14	-0.19	-0.19	-0.10	-0.14	-0.12	-0.13	-0.09	-0.13	-0.14	-0.15

Contd....**Table-5.8**

D/N	C5H2'	C5H2"	G6H2'	G6H2"
0.0	2.03	2.42	2.67	2.38
0.5	1.96	2.38	2.69	2.36
1.0	1.93	2.35	2.69	2.35
1.5	1.92	2.32	2.65	2.34
2.0	1.88	2.26	2.65	2.32
$\Delta\delta$	-0.15	-0.16	-0.02	-0.06

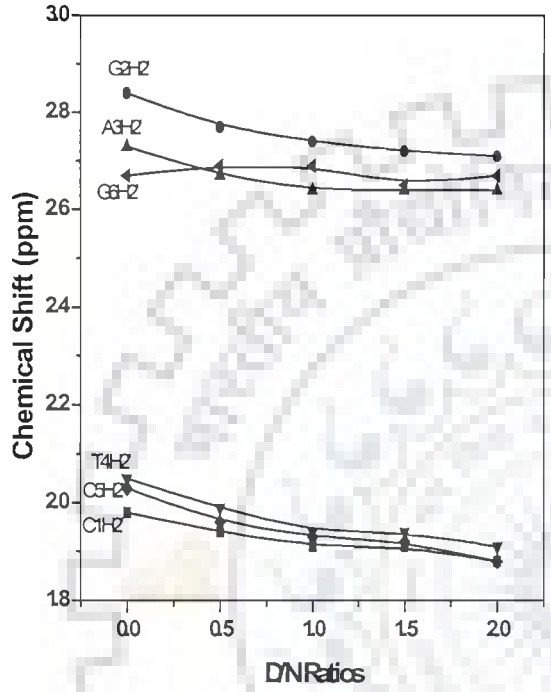

(Fig. 5.10a)

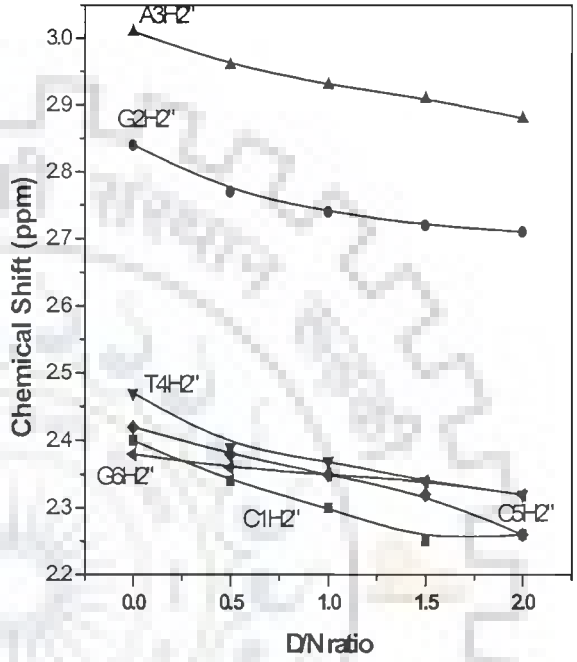

(Fig. 5.10b)

Fig. 5.10 (a-i): Change in chemical shift of d-$(CGATCG)_2$ protons complexed with palmatine as a function of drug to DNA (D/N) ratio, 278 K.

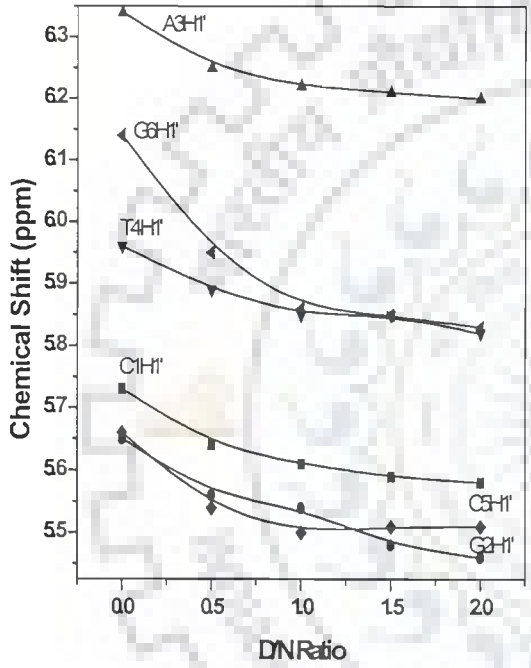

(Fig. 5.10c)

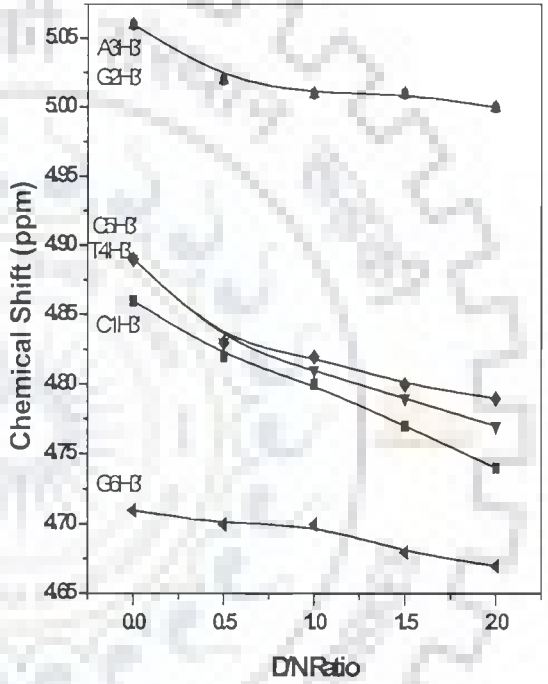

(Fig. 5.10d)

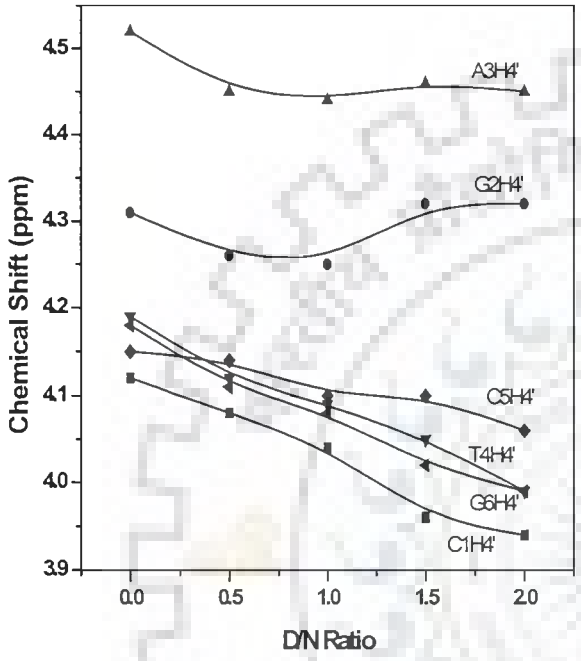

(Fig. 5.10e)

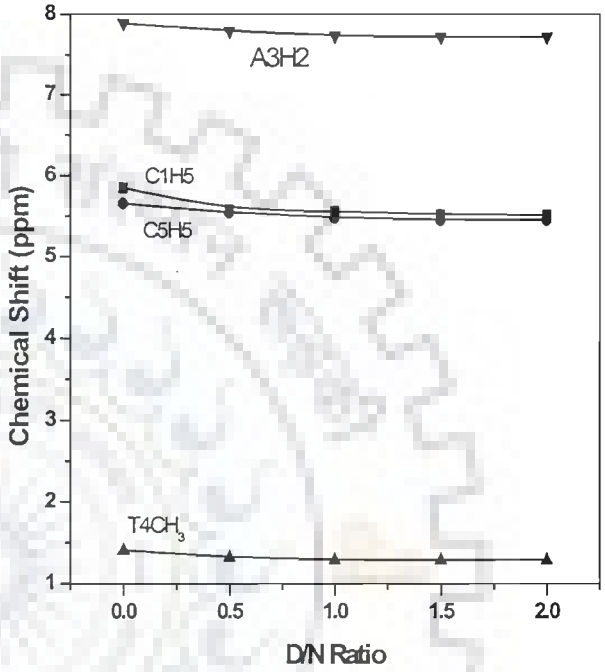

(Fig. 5.10f)

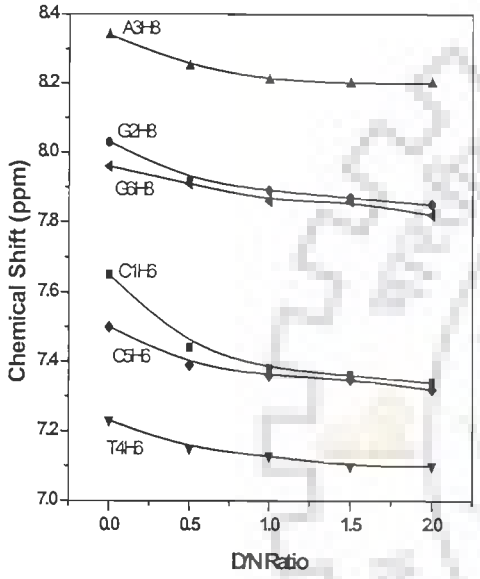

(Fig. 5.10g)

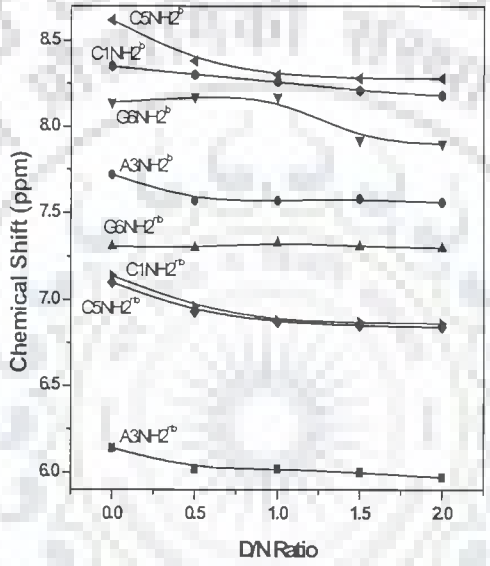

(Fig. 5.10h)

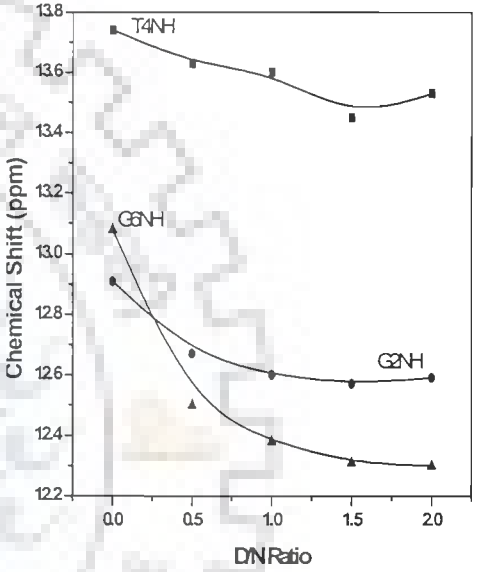

(Fig. 5.10i)

5.1.2.2 Temperature Dependence Studies

In order to monitor the duplex to single strand transition one dimensional NMR spectra are recorded in the temperature range 278-328 K. Binding of palmatine to d-$(CGATCG)_2$ gradually became weak with increase in temperature. Therefore, to spot the changes in resonances of drug and DNA protons due to dissociation of bound palmatine from d-$(CGATCG)_2$, 1D-^1H versus temperature studies are performed at D/N 0.0, 1.0 and 2.0. ^1H NMR spectra of the palmatine -d-$(CGATCG)_2$ complex at D/N=1.0 and 2.0, in the temperature range of 278-328 K are shown in Fig. 5.11a-g and Fig. 5.12a-g, respectively. The observation of the chemical shifts as a function of temperature further helped to resolve the overlapping resonance peaks. Palmatine resonances, which were broad and tough to identify in 1D ^1H spectrum of complex are identified at higher temperature due to signal sharpening with increase in temperature. It can be clearly seen from Fig. 5.11 and Fig.5.12 that palmatine resonances H10, H14, H28, H24 of palmatine-d-$(CGATCG)_2$ complex are broad at low temperature, whereas at high temperature the palmatine binding with d-$(CGATCG)_2$ weakened and resonances became sharp.

Resonances of palmatine protons in palmatine-d-$(CGATCG)_2$ complex shift downfield with increase in temperature while in alone palmatine no chemical shift change was observed with increase in temperature (Fig. 3.5). This clearly indicates that these palmatine protons are involved in binding with the hexamer d-$(CGATCG)_2$. Chemical shift value for these palmatine protons at different temperatures at D/N 1.0 and 2.0 are tabulated in Table 5.9. It is found that even at 328 K chemical shift value for H10, H28 and H24 protons of palmatine in the complex is found to be downfield shifted then their position in alone palmatine. These results clearly indicate that palmatine binds to

d(CGATCG)$_2$ at higher concentration and amount of palmatine is in the bound form even at higher temperature (328 K). The chemical shift for d-(CGATCG)$_2$ protons showed a linear dependence with temperature in the range of 278- 328 K (Fig. 5.11a-g and Fig. 5.12 a-g). It is observed that chemical shift of hexamer varied with temperature. Downfield shift was observed for all the DNA protons. All the DNA protons chemical shift values at different temperatures for D/N ratio 1.0 and 2.0 are listed in Table 5.10 and 5.11, respectively. The chemical shift values indicate that structurally only one complex is formed and the chemical shift at any one temperature is an average of bound and unbound d-(CGATCG)$_2$ the equilibrium of which was likely to shift with temperature. The resonances for imino protons of thymine and guanines were in fast exchange with water at higher than the melting temperature and hence imino protons disappeared at T_m. The spectra for imino protons as a function of temperature are shown in Fig. 5.11g and 5.12g and 5.13 for D/N 1.0, 2.0 and 0.0, respectively. It is known that thermal denaturation of DNA can be studied either by following the changes of chemical shift of the non- exchangeable protons [Braunlin and Bloomfield, 1991; pardi et al, 1981: Petersheim and Turner, 1981] or by the disappearance of the signals of the imino protons [Braunlin and Bloomfield, 1988]. Conformational changes associated with denaturation modify the local environment of the protons, leading to a change in their chemical shifts.

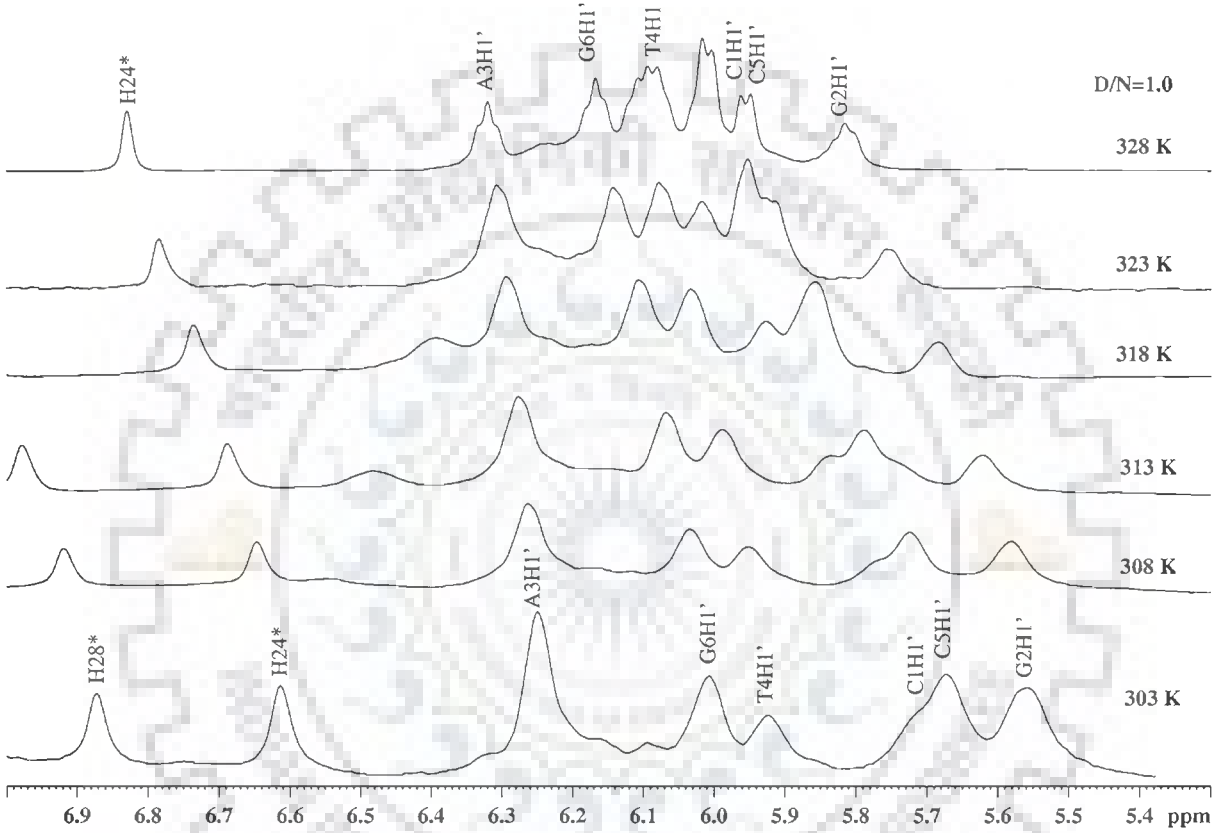
H24*
A3H1'
G6H1'
T4H1
C1H1'
C5H1'
G2H1'
D/N=1.0
328 K
323 K
318 K
313 K
308 K
303 K
H28*
H24*
A3H1'
G6H1'
T4H1'
C1H1'
C5H1'
G2H1'
6.9
6.8
6.7
6.6
6.5
6.4
6.3
6.2
6.1
6.0
5.9
5.8
5.7
5.6
5.5
5.4
ppm

Fig. 5.11a

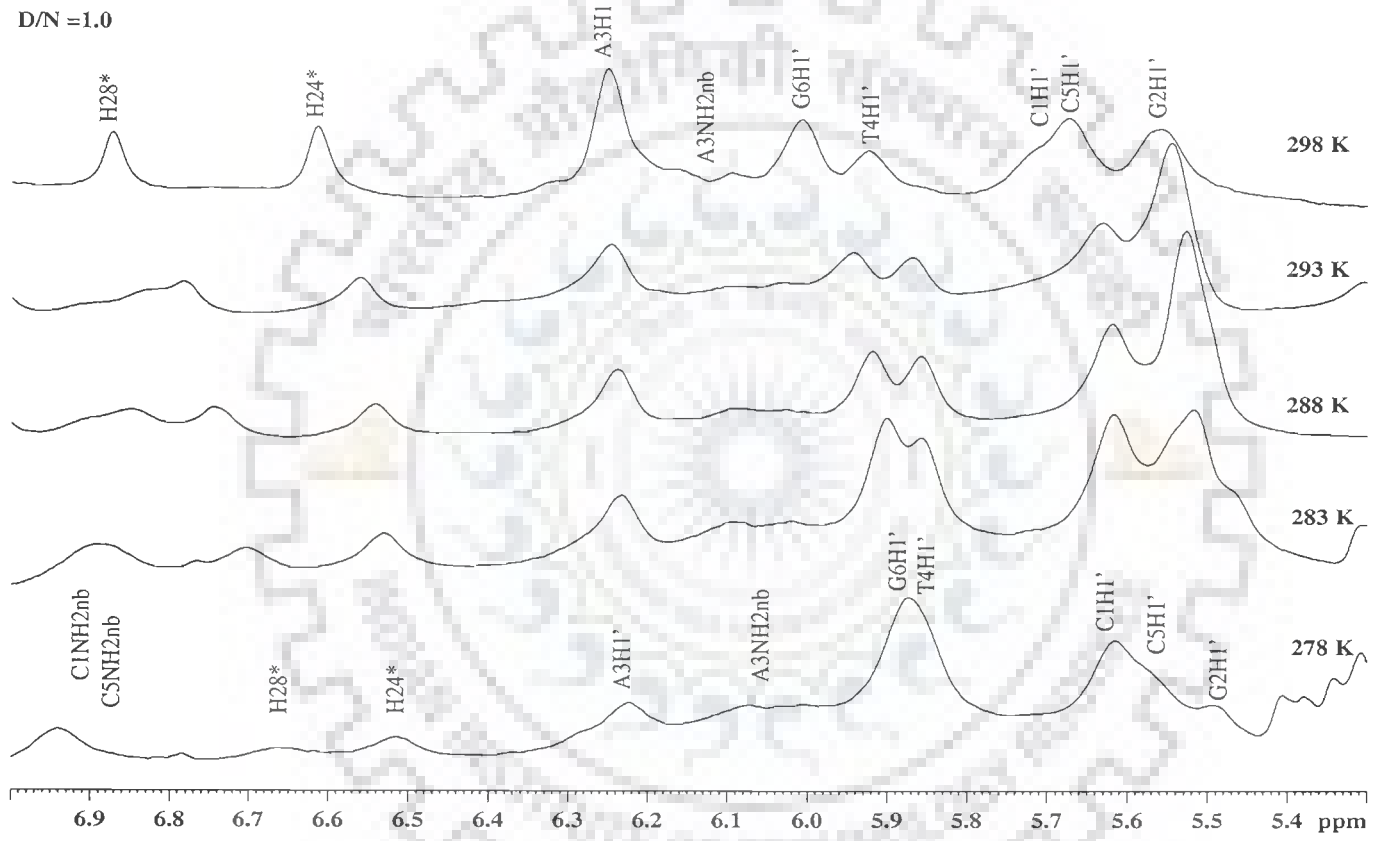
D/N =1.0
H28*
H24*
A3H1
A3NH2nb
G6H1'
T4H1'
C1H1'
C5H1'
G2H1'
298 K
293 K
288 K
283 K
278 K
C1NH2nb
C5NH2nb
H28*
H24*
A3H1'
A3NH2nb
G6H1'
T4H1'
C1H1'
C5H1'
G2H1'
6.9
6.8
6.7
6.6
6.5
6.4
6.3
6.2
6.1
6.0
5.9
5.8
5.7
5.6
5.5
5.4 ppm

Fig. 5.11b

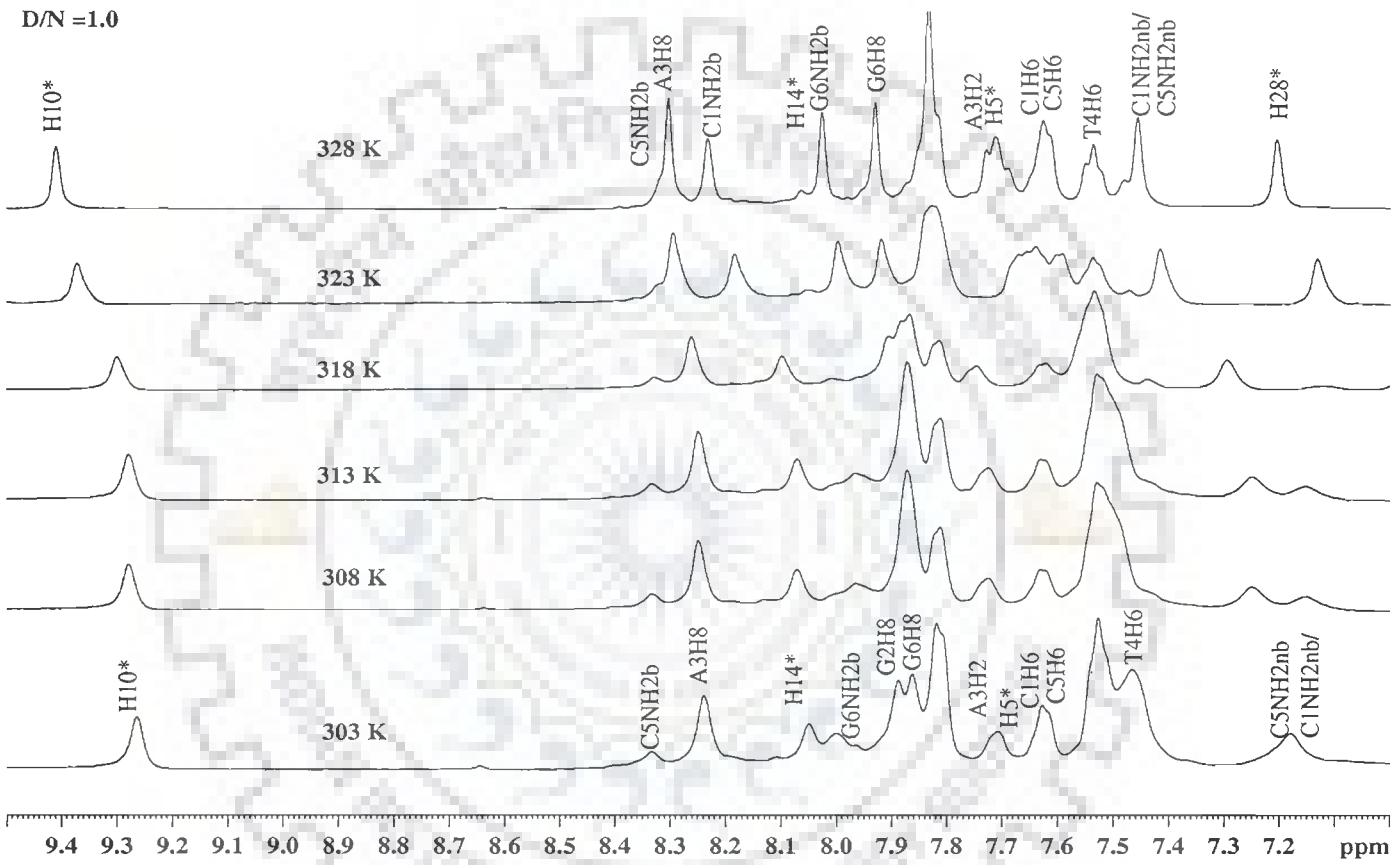
D/N =1.0
328 K
323 K
318 K
313 K
308 K
303 K
H10*
C5NH2b
A3H8
C1NH2b
H14*
G6NH2b
G6H8
A3H2
H5*
C1H6
C5H6
T4H6
C1NH2nb/
C5NH2nb
H28*
G2H8
C5NH2nb
C1NH2nb/
9.4 9.3 9.2 9.1 9.0 8.9 8.8 8.7 8.6 8.5 8.4 8.3 8.2 8.1 8.0 7.9 7.8 7.7 7.6 7.5 7.4 7.3 7.2
ppm

Fig. 5.11c

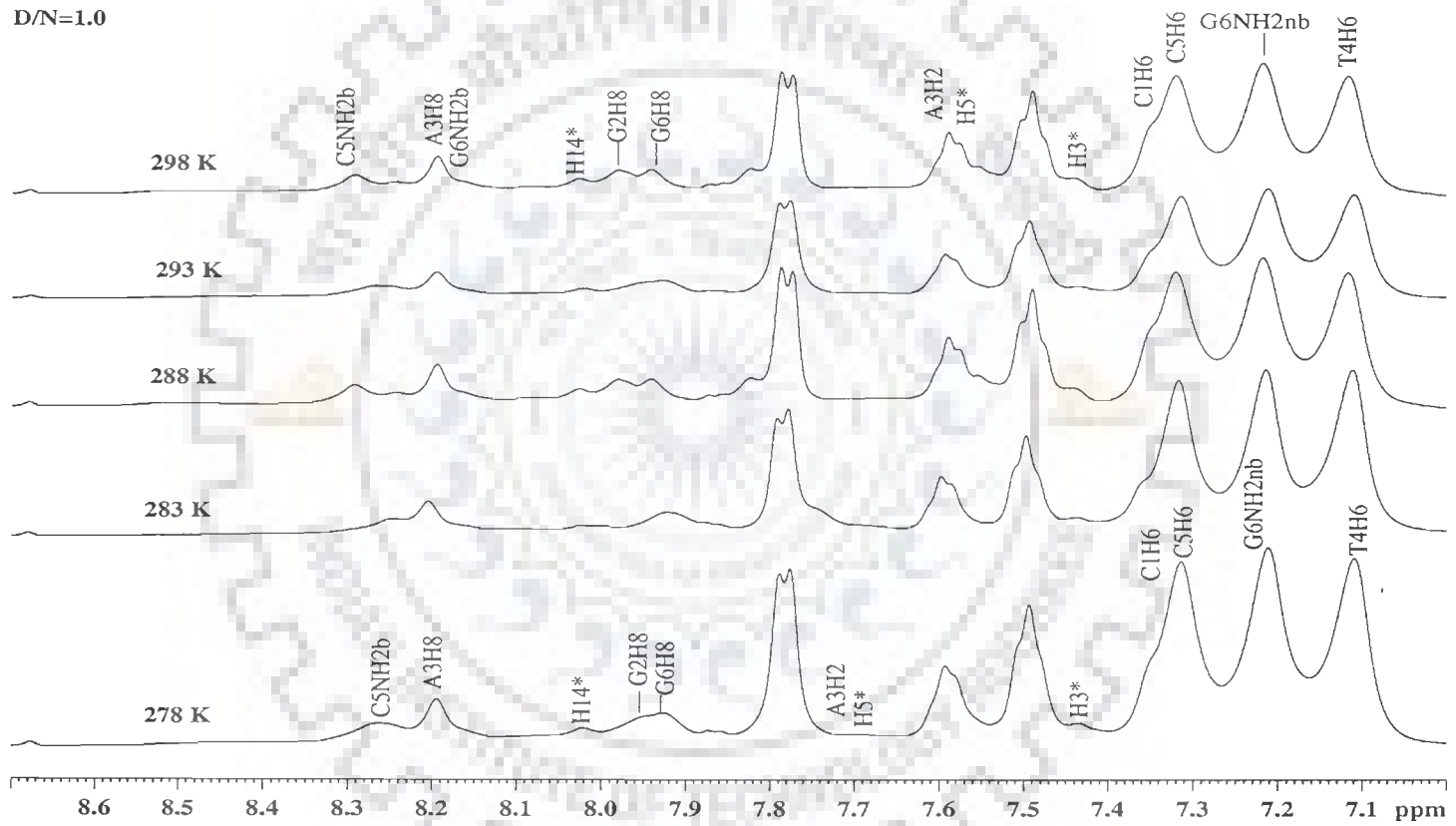
D/N=1.0
298 K
293 K
288 K
283 K
278 K
C5NH2b
A3H8
G6NH2b
H14*
G2H8
G6H8
A3H2
H5*
H3*
C1H6
C5H6
G6NH2nb
T4H6
8.6
8.5
8.4
8.3
8.2
8.1
8.0
7.9
7.8
7.7
7.6
7.5
7.4
7.3
7.2
7.1
ppm

Fig. 5.11d

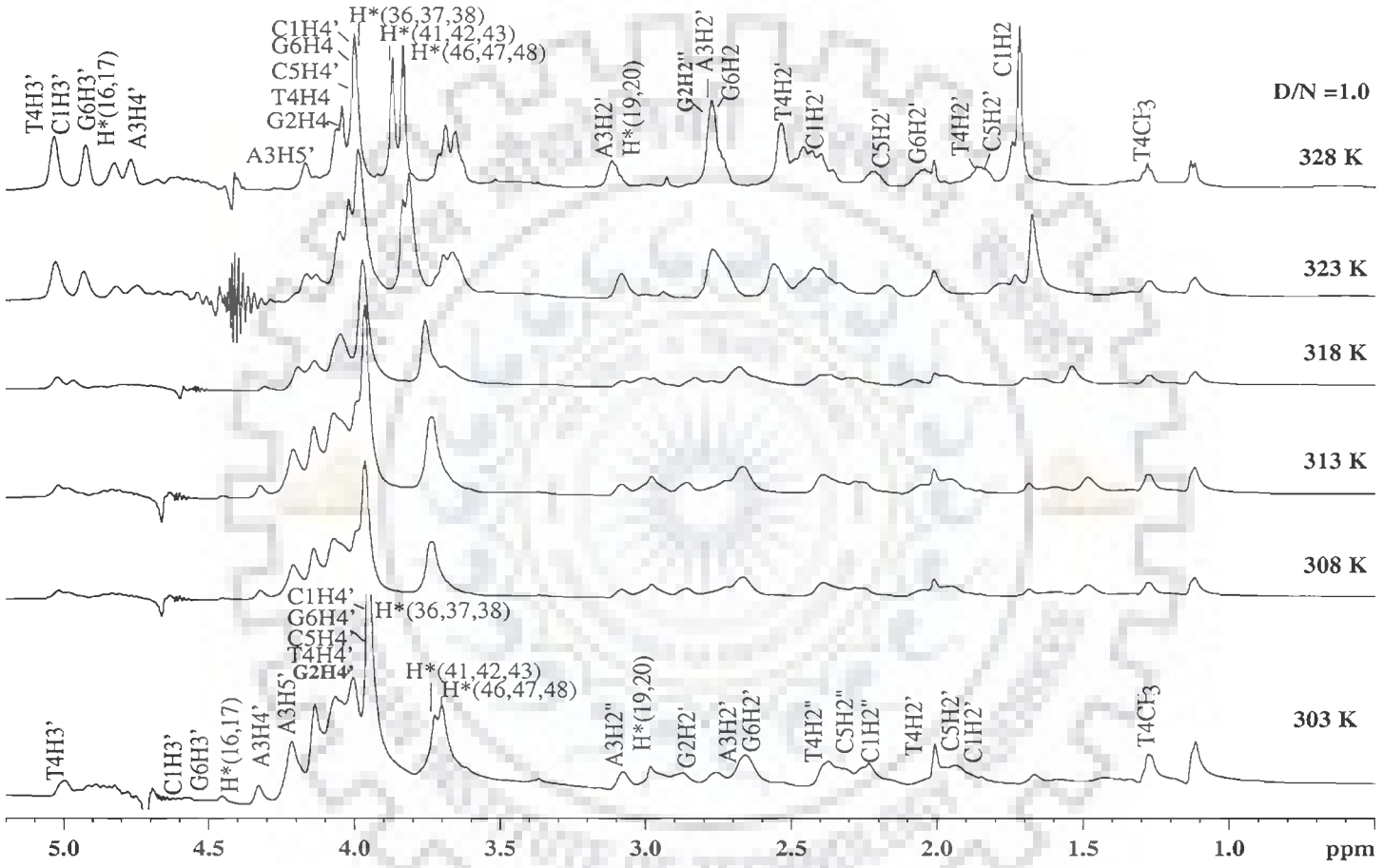
T4H3'
C1H3'
G6H3'
H*(16,17)
A3H4'
A3H5'
C1H4'
G6H4'
C5H4'
T4H4
G2H4
H*(36,37,38)
H*(41,42,43)
H*(46,47,48)
A3H2'
H*(19,20)
G2H2"
A3H2'
G6H2
T4H2'
C1H2'
C5H2'
G6H2'
T4H2'
C5H2'
C1H2
T4CH3
D/N =1.0
328 K
323 K
318 K
313 K
308 K
303 K
C1H4'
G6H4'
C5H4'
T4H4'
G2H4'
H*(36,37,38)
H*(41,42,43)
H*(46,47,48)
A3H2"
H*(19,20)
G2H2'
A3H2'
G6H2'
T4H2"
C5H2"
C1H2"
T4H2'
C5H2'
C1H2'
T4CH3
5.0
4.5
4.0
3.5
3.0
2.5
2.0
1.5
1.0
ppm

Fig. 5.11e

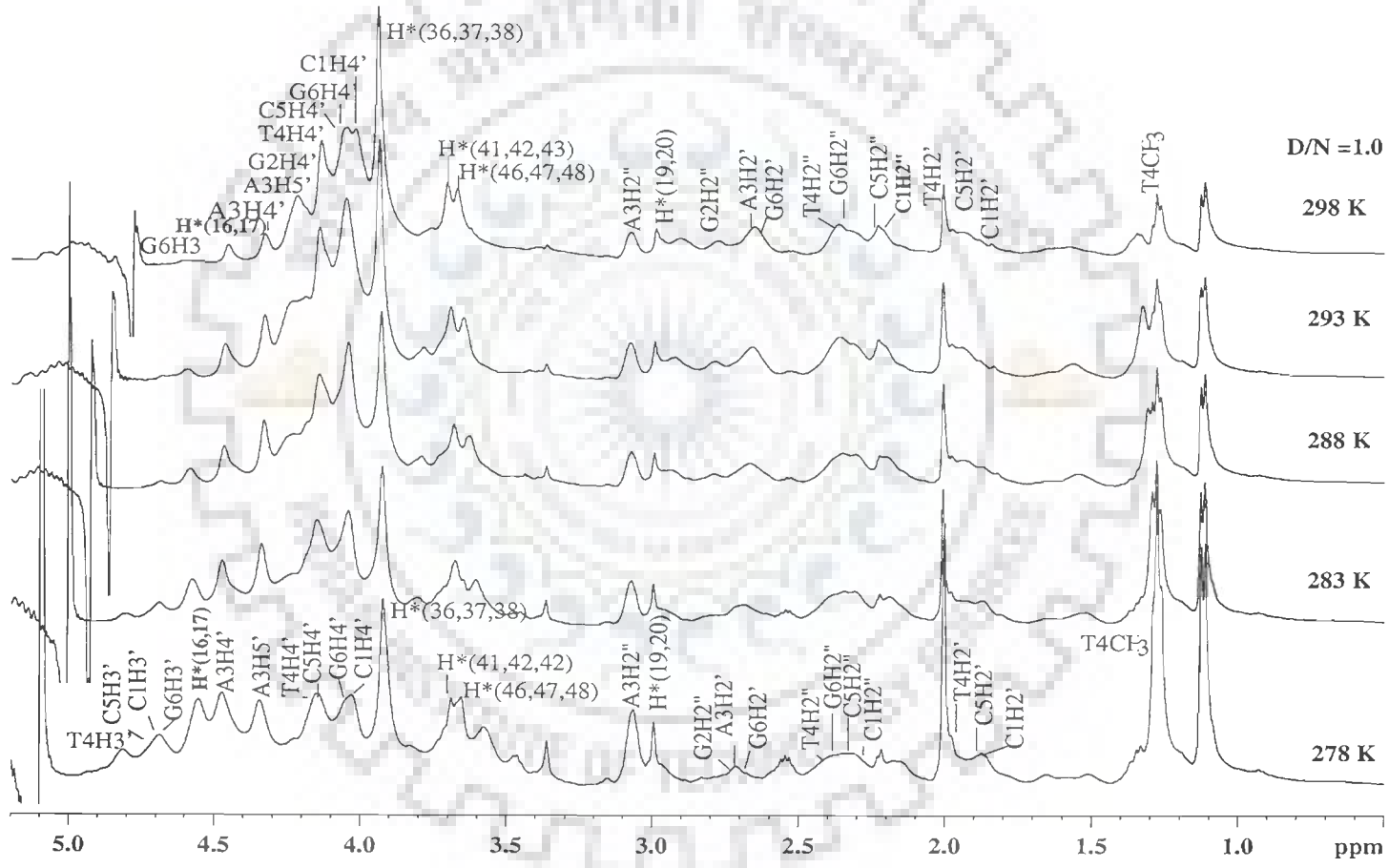
H*(36,37,38)
C1H4'
G6H4'
C5H4'
T4H4'
G2H4'
A3H5'
A3H4'
H*(16,17)
G6H3
H*(41,42,43)
H*(46,47,48)
A3H2"
H*(19,20)
G2H2"
A3H2'
G6H2'
T4H2"
G6H2"
C5H2"
C1H2"
T4H2'
C5H2'
C1H2'
T4CH3
D/N =1.0
298 K
293 K
288 K
283 K
278 K
C5H3'
C1H3'
T4H3'
G6H3'
H*(16,17)
A3H4'
A3H5'
T4H4'
C5H4'
G6H4'
C1H4'
H*(36,37,38)
H*(41,42,42)
H*(46,47,48)
A3H2"
H*(19,20)
G2H2"
A3H2'
G6H2'
T4H2"
G6H2"
C5H2"
C1H2"
T4H2'
C5H2'
C1H2'
T4CH3
5.0
4.5
4.0
3.5
3.0
2.5
2.0
1.5
1.0
ppm

Fig. 5.11f

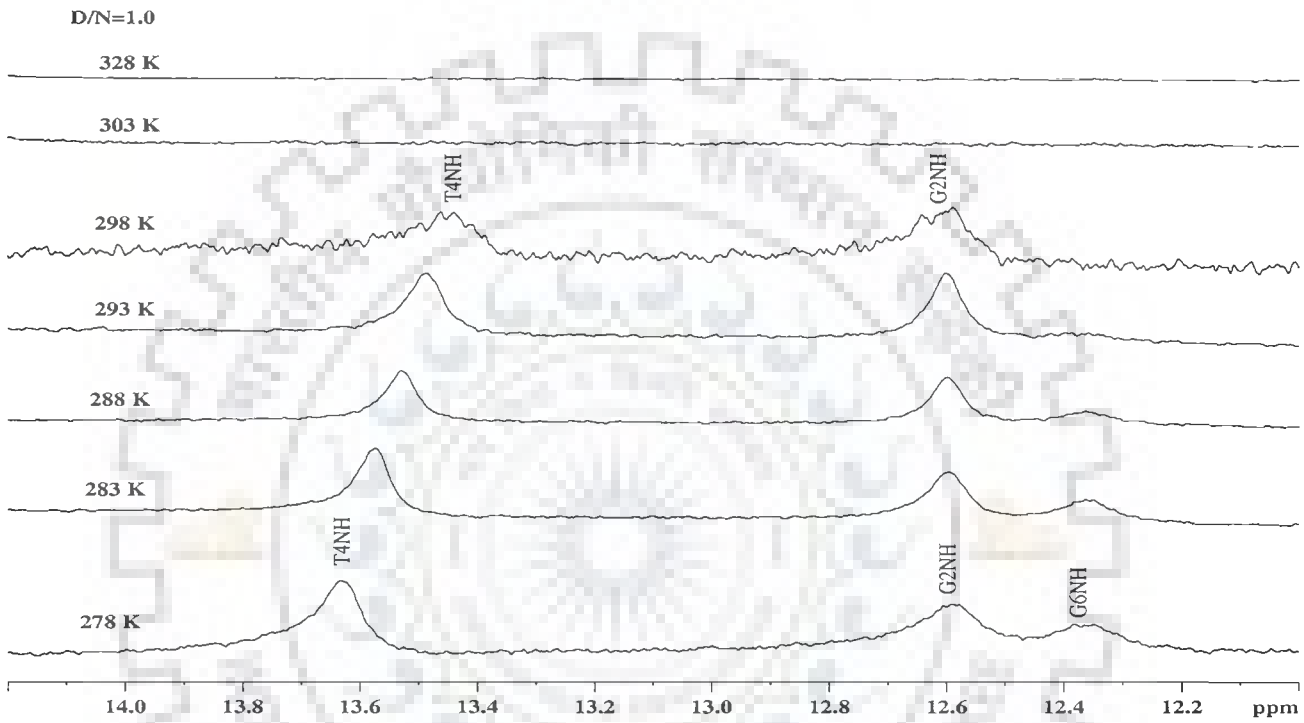

Fig. 5.11g

Fig. 5.11a-g: Proton NMR spectra of complex of palmatine with d-$(CGATCG)_2$ as a function of temperature at D/N = 1.0 (* palmatine proton in palmatine -d-$(CGATCG)_2$ complex

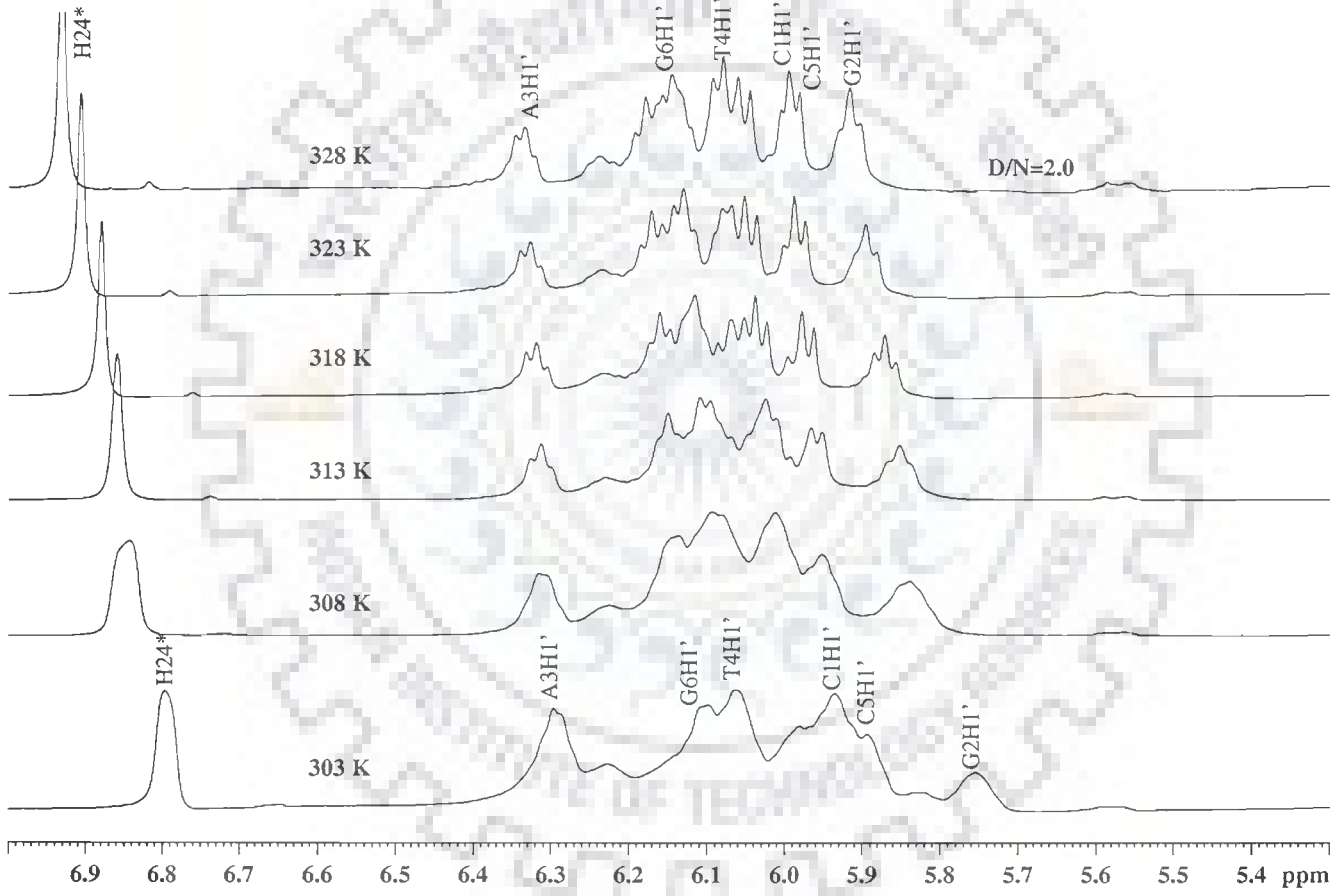
H24*
A3H1'
G6H1'
T4H1'
C1H1'
C5H1'
G2H1'
328 K
D/N=2.0
323 K
318 K
313 K
308 K
303 K
6.9
6.8
6.7
6.6
6.5
6.4
6.3
6.2
6.1
6.0
5.9
5.8
5.7
5.6
5.5
5.4 ppm

Fig. 5.12a

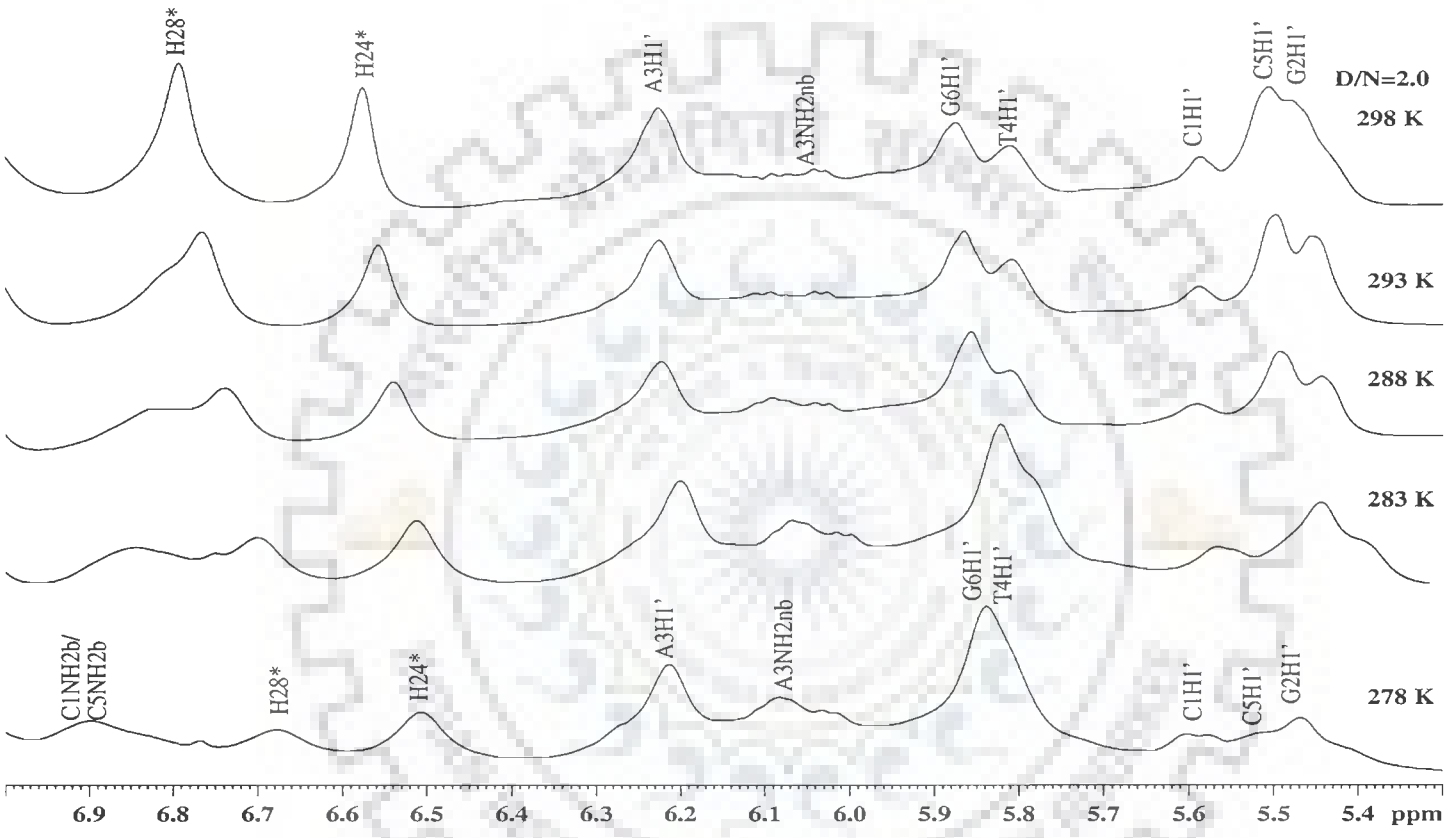
H28*
H24*
A3H1'
A3NH2nb
G6H1'
T4H1'
C1H1'
C5H1'
G2H1'
D/N=2.0
298 K
293 K
288 K
283 K
278 K
C1NH2b/
C5NH2b
6.9
6.8
6.7
6.6
6.5
6.4
6.3
6.2
6.1
6.0
5.9
5.8
5.7
5.6
5.5
5.4
ppm

Fig. 5.12b

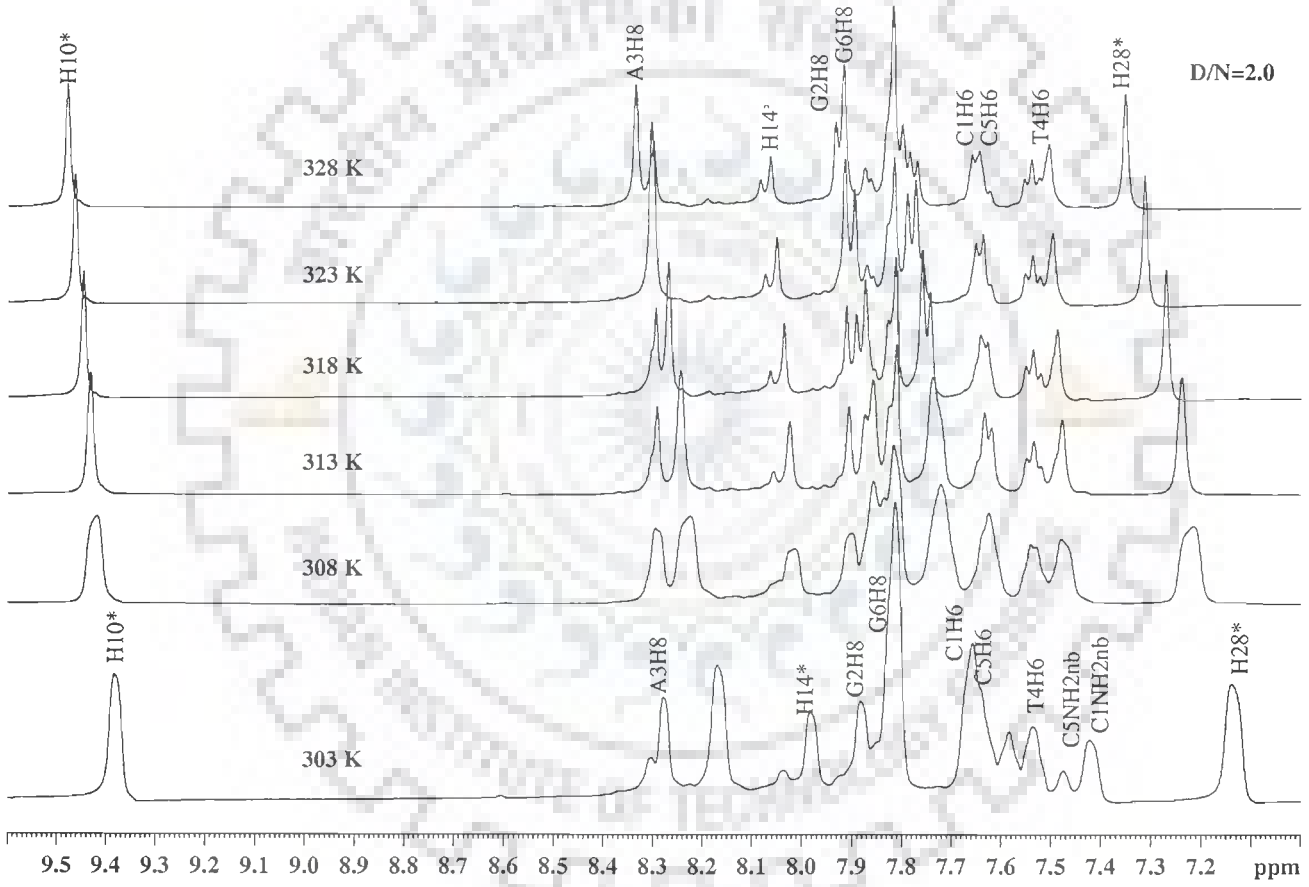
H10*
A3H8
H14'
G2H8
G6H8
C1H6
C5H6
T4H6
H28*
D/N=2.0
328 K
323 K
318 K
313 K
308 K
303 K
H10*
A3H8
H14*
G2H8
G6H8
C1H6
C5H6
T4H6
C5NH2nb
C1NH2nb
H28*
9.5 9.4 9.3 9.2 9.1 9.0 8.9 8.8 8.7 8.6 8.5 8.4 8.3 8.2 8.1 8.0 7.9 7.8 7.7 7.6 7.5 7.4 7.3 7.2
ppm

Fig. 5.12c

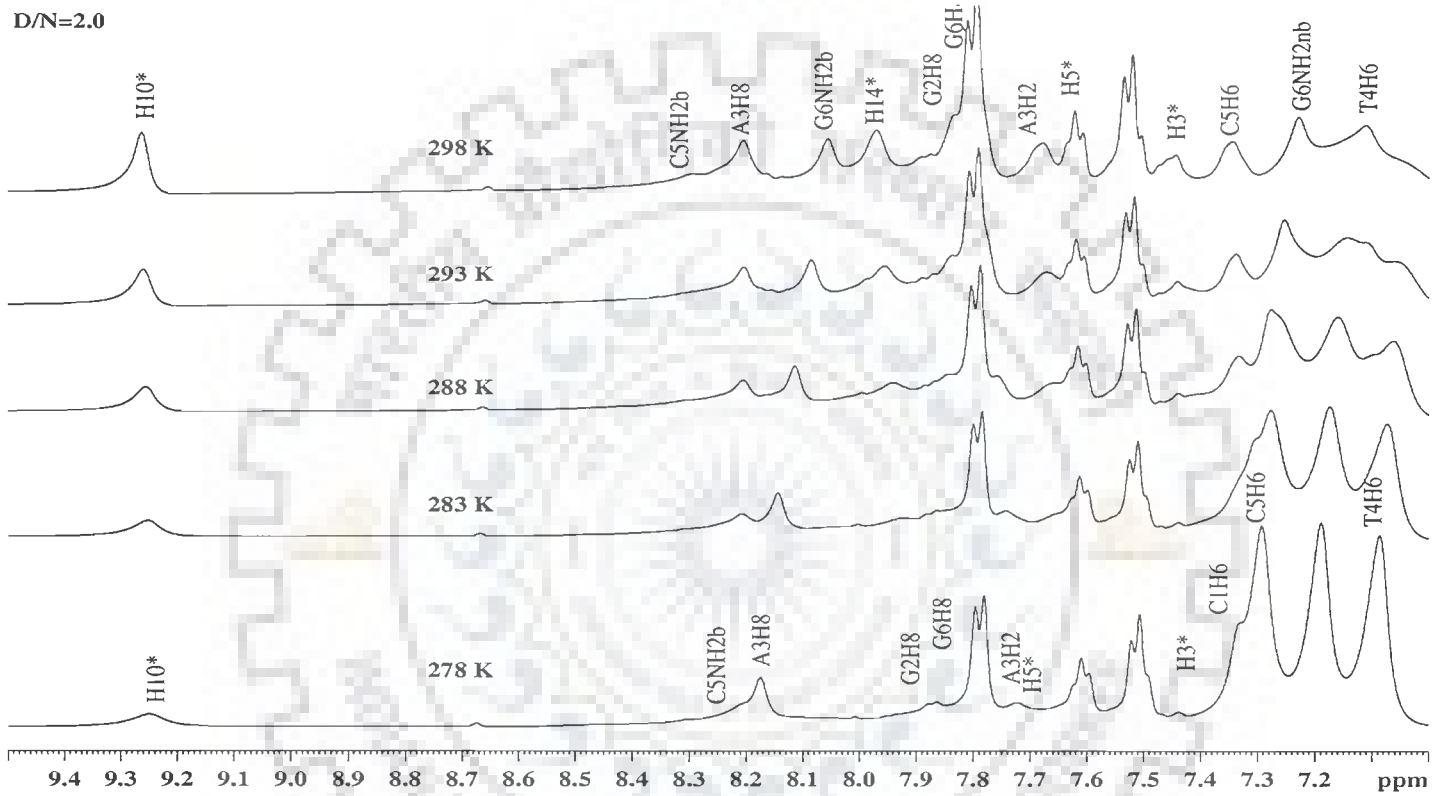
D/N=2.0
H10*
298 K
C5NH2b
A3H8
G6NH2b
H14*
G2H8
G6H8
A3H2
H5*
H3*
C5H6
G6NH2nb
T4H6
293 K
288 K
283 K
278 K
C5NH2b
A3H8
G2H8
G6H8
A3H2
H5*
H3*
C1H6
C5H6
T4H6
9.4 9.3 9.2 9.1 9.0 8.9 8.8 8.7 8.6 8.5 8.4 8.3 8.2 8.1 8.0 7.9 7.8 7.7 7.6 7.5 7.4 7.3 7.2 ppm

Fig. 5.12d

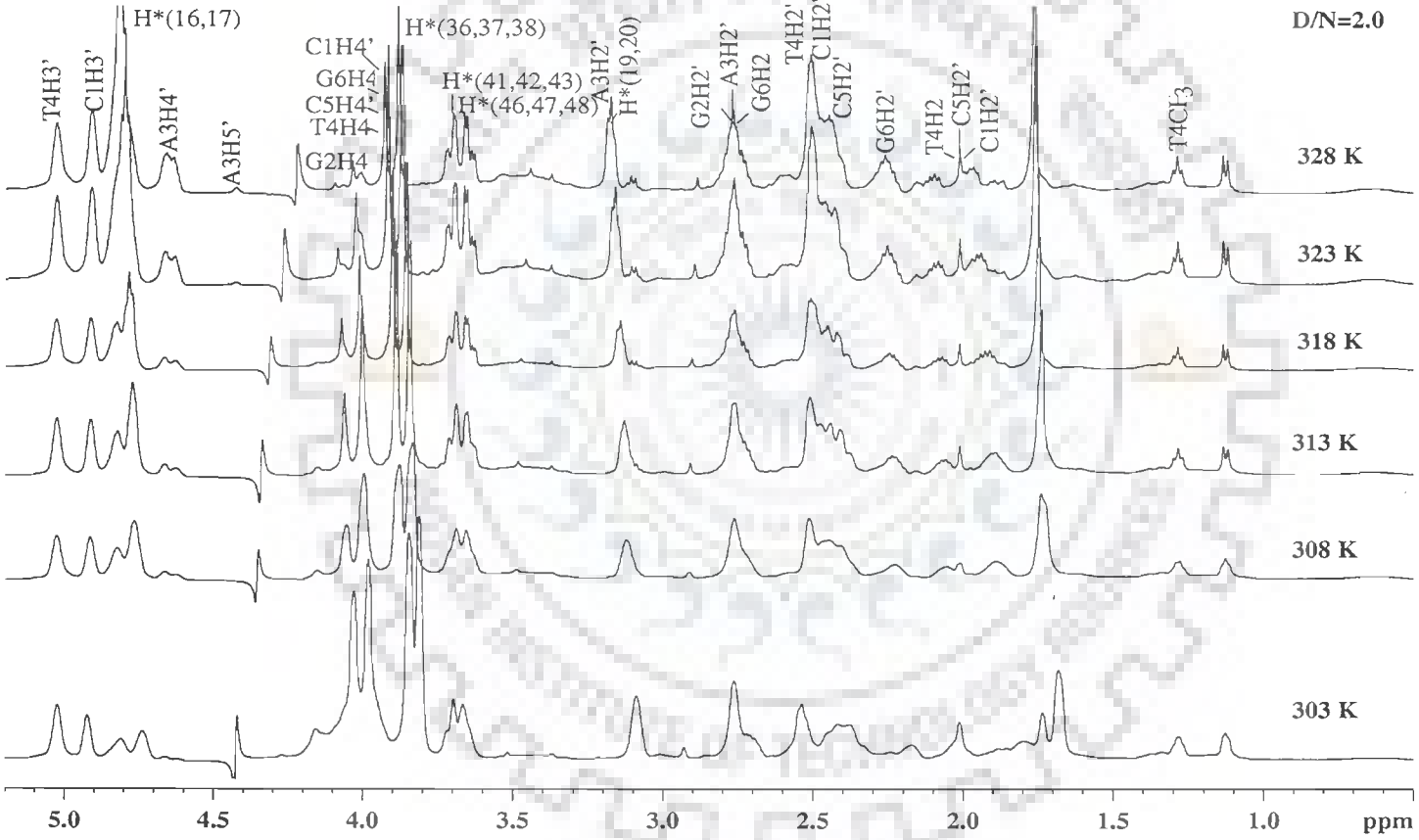
T4H3'
C1H3'
H*(16,17)
A3H4'
A3H5'
C1H4'
G6H4'
C5H4'
T4H4'
G2H4'
H*(36,37,38)
H*(41,42,43)
H*(46,47,48)
A3H2'
H*(19,20)
G2H2'
A3H2'
G6H2
T4H2'
C1H2'
C5H2'
G6H2'
T4H2
C5H2'
C1H2'
T4CH3
D/N=2.0
328 K
323 K
318 K
313 K
308 K
303 K
5.0
4.5
4.0
3.5
3.0
2.5
2.0
1.5
1.0
ppm

Fig. 5.12e

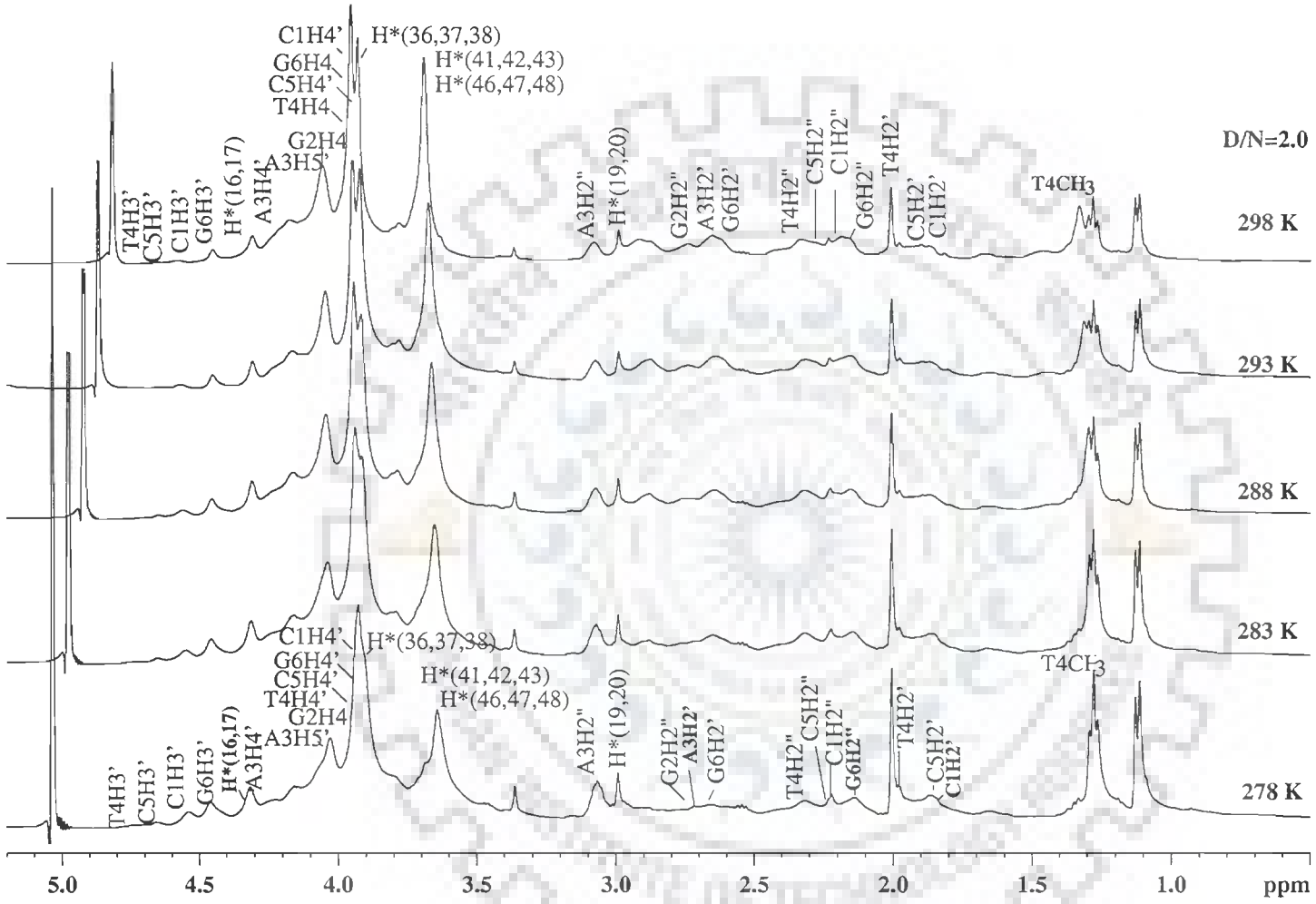
C1H4'
H*(36,37,38)
G6H4'
H*(41,42,43)
C5H4'
H*(46,47,48)
T4H4'
G2H4'
A3H5'
T4H3'
C5H3'
C1H3'
G6H3'
H*(16,17)
A3H4'
A3H2"
H*(19,20)
G2H2"
A3H2'
G6H2'
T4H2"
C5H2"
C1H2"
G6H2"
T4H2'
C5H2'
C1H2'
T4CH3
D/N=2.0
298 K
293 K
288 K
283 K
278 K
5.0
4.5
4.0
3.5
3.0
2.5
2.0
1.5
1.0
ppm

Fig. 5.12f

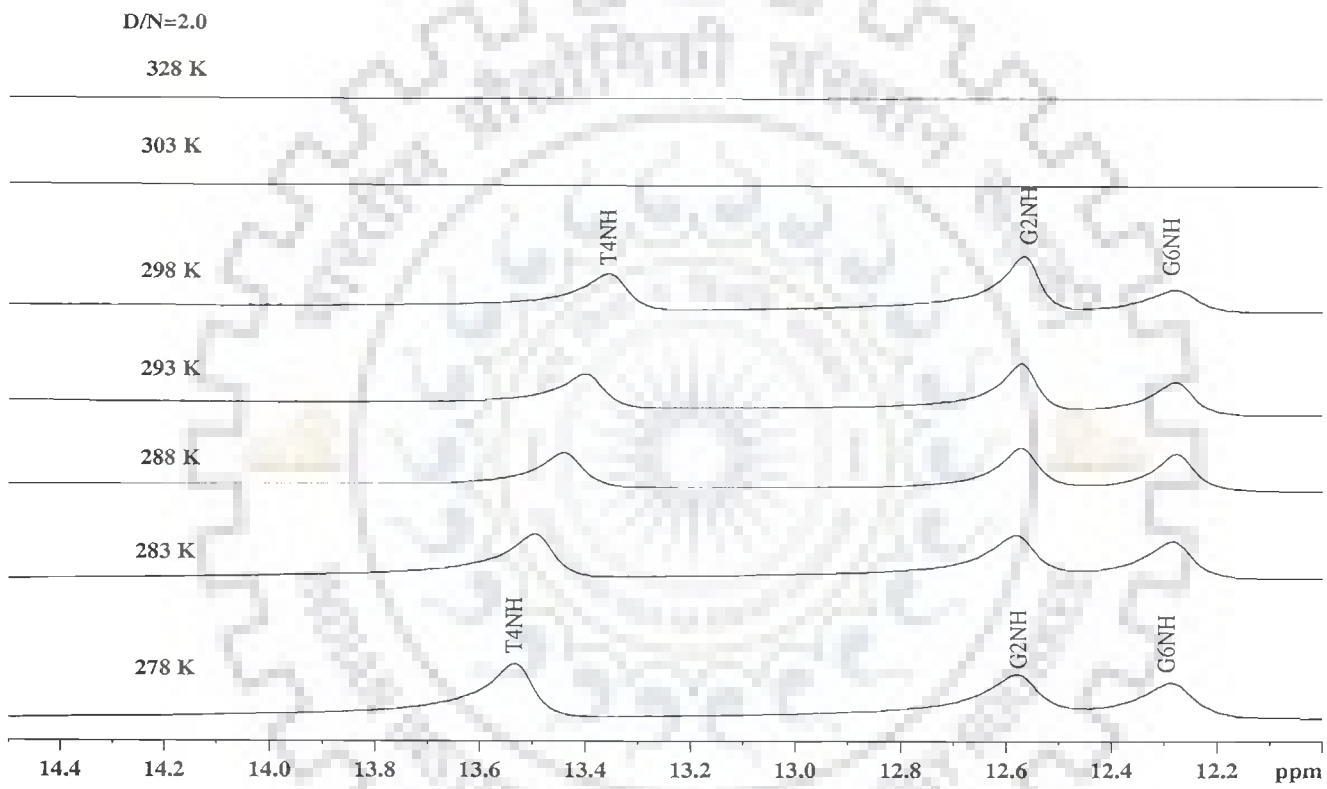

Fig. 5.12g

Fig. 5.12a-g: Proton NMR spectra of complex of palmatine with d-$(CGATCG)_2$ as a function of temperature at D/N = 2.0 (* palmatine proton in palmatine -d-$(CGATCG)_2$ complex).

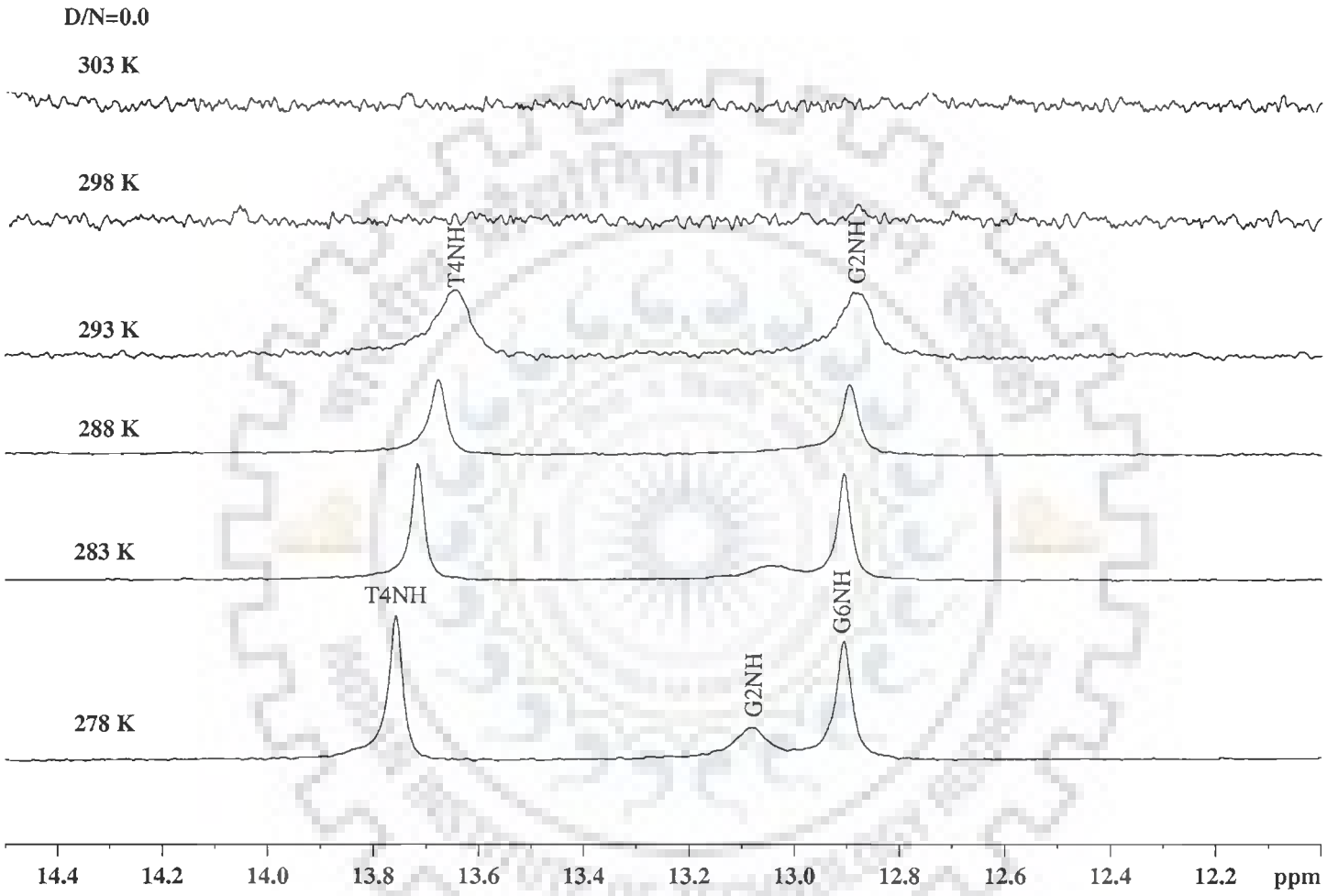

Fig. 5.13: Proton NMR spectra of imino region of uncomplexed d-$(CGATCG)_2$ as a function of temperature.

Table 5.9: Chemical shift (ppm) of some of the palmatine protons as a function of temperature at D/N= 1.0 and 2.0. Also shown here is the net change in chemical shift with temperature, that is, $\Delta\delta = \delta$ (328 K) - δ (278 K)

	D/N = 1.0				D/N = 2.0			
Temperature	**H10**	**H14**	**H28**	**H24**	**H10**	**H14**	**H28**	**H24**
278	9.22	7.97	6.68	6.51	9.24	7.95	6.69	6.51
283	9.23	7.97	6.69	6.52	9.26	7.93	6.70	6.52
288	9.23	7.99	6.74	6.53	9.26	7.94	6.73	6.54
293	9.25	8.01	6.78	6.56	9.27	7.96	6.76	6.55
298	9.26	8.03	6.79	6.58	9.26	7.97	6.79	6.58
303	9.27	8.05	6.81	6.62	9.38	7.98	7.13	6.79
308	9.38	8.08	6.91	6.65	9.42	8.02	7.22	6.84
313	9.30	8.10	6.97	6.68	9.43	8.02	7.24	6.86
318	9.33	8.13	7.05	6.73	9.44	8.04	7.27	6.87
323	9.37	8.19	7.13	6.79	9.46	8.05	7.31	6.90
328	9.41	8.23	7.20	6.82	9.48	8.06	7.35	6.93
$\Delta\delta$	+0.19	+0.26	+0.52	+0.31	+0.24	+0.11	+0.66	+0.42

-ve $\Delta\delta$ indicates upfield shift and
+ve $\Delta\delta$ indicates downfield shift.

The imino protons are involved in inter-strand hydrogen bonding and when accessible to water, they can exchange, which lead to broadening and disappearance of the imino peaks. As the temperature is increased the signals of the imino protons disappeared due to their fast exchange on the NMR time scale with the solvent protons. This occurs following denaturation or following the small scale opening of an individual or a few base pairs [Braunlin and Bloomfield, 1988]. The first signal to disappear is those corresponding to terminal G6NH, this peak was broad at 278 K, which indicates fraying of the last base pair. The imino protons T4NH and G2NH disappeared at 298 K in the palmatine-d$(CGATCG)_2$ complex, whereas in alone DNA they disappeared at 293 K (Fig. 5.13). At D/N 2.0 imino signals are sharp at 298 K as compared to broad imino signals at D/N 1.0 (Figs. 5.11g and 5.12g). This suggests that the binding of the alkaloid has increased the stability of DNA and the binding is tighter at D/N, 2.0. The binding of palmatine to the oligomer has increased its melting temperature by 5 K.

The difference between T_m calculated from the disappearance temperature for imino protons was increased due to binding of palmatine to d-$(CGATCG)_2$. These changes in chemical shift due to titrimetric and temperature dependent studies showed that palmatine binds to d-$(CGATCG)_2$ more firmly at D/N ratio 2.0. We know that the changes in chemical shift of DNA might result due to structural alterations on binding and not directly related to a specific structural parameter therefore one needs to look at the structure of the specific complex by alternate ways such as inter- proton contacts, which will be discussed further in this chapter. To confirm the binding of palmatine to d-$(CGATCG)_2$, DOSY studies were done.

Table 5.10: Chemical shift (ppm) of d-$(CGATCG)_2$ as a function of temperature at D/N 1.0. Also shown here is the net change in chemical shift with temperature, that is, $\Delta\delta = \delta$ (328 K) - δ (278 K).

Temp. (K)	C1H6	G2H8	A3H8	T4H6	C5H6	G6H8	C1H5	C5H5	A3H2	
278	7.48	7.89	8.21	7.13	7.36	7.86	5.56	5.48	7.73	
283	7.60	7.89	8.21	7.13	7.38	7.86	5.53	5.46	7.75	
288	7.61	7.89	8.21	7.13	7.39	7.87	5.54	5.52	7.74	
293	7.61	7.89	8.24	7.15	7.41	7.87	5.56	5.54	7.68	
298	7.62	7.89	8.25	7.18	7.42	7.90	5.58	5.56	7.71	
303	7.62	7.89	8.24	7.38	7.43	7.86	5.59	5.58	7.72	
308	7.63	7.89	8.25	7.39	7.44	7.87	5.63	5.61	7.74	
313	7.63	7.91	8.26	7.43	7.56	7.88	5.66	5.68	7.74	
318	7.64	7.95	8.28	7.49	7.57	7.90	5.76	5.75	7.75	
323	7.63	8.00	8.30	7.48	7.58	7.91	5.82	5.81	7.75	
328	7.64	8.02	8.31	7.48	7.59	7.93	5.83	5.81	7.76	
$\Delta\delta$	+0.15	+0.13	+0.10	+0.36	+0.22	+0.08	+0.31	+0.32	+0.04	
Temp. (K)	C1H1'	G2H1'	A3H1'	T4H1'	C5H1'	G6H1'	$T4CH_3$	T4NH	G2NH	G6NH
278	5.61	5.54	6.22	5.85	5.50	5.89	1.29	13.60	12.60	12.38
283	5.61	5.54	6.23	5.85	5.51	5.90	1.27	13.58	12.60	12.37
288	5.62	5.55	6.24	5.86	5.52	5.91	1.28	13.53	12.60	12.37
293	5.63	5.55	6.25	5.86	5.53	5.94	1.27	13.49	12.60	12.36
298	5.68	5.57	6.26	5.92	5.55	5.99	1.27	13.45	12.59	-
303	5.69	5.58	6.27	5.93	5.56	6.00	1.28			
308	5.73	5.59	6.28	5.95	5.58	6.04	1.28			
313	5.78	5.62	6.29	5.99	5.62	6.07	1.27			
318	5.87	5.69	6.30	6.03	5.69	6.11	1.27			
323	5.92	5.75	6.31	6.08	5.75	6.15	1.28			
328	6.00	5.82	6.32	6.09	5.85	6.17	1.28			
$\Delta\delta$	+0.39	+0.28	+0.10	+0.24	+0.35	+0.28	+0.02	-0.15	-0.01	-0.02

-ve $\Delta\delta$ indicates upfield shift
+ve $\Delta\delta$ indicates downfield shift

Table 5.11: Chemical shift (ppm) of d-$(CGATCG)_2$ as a function of temperature at D/N 2 .0. Also shown here is the net change in chemical shift with temperature, that is, $\Delta\delta = \delta$ (328 K) - δ (278 K) -ve $\Delta\delta$ indicates upfield shift and +ve $\Delta\delta$ indicates downfield shift

Temp. (K)	C1H6	G2H8	A3H8	T4H6	C5H6	G6H8	C1H5	C5H5	A3H2	
278	7.34	7.85	8.20	7.10	7.32	7.82	5.51	5.45	7.72	
283	7.40	7.87	8.20	7.08	7.31	7.84	5.52	5.48	7.74	
288	7.41	7.86	8.21	7.11	7.32	7.84	5.53	5.50	7.76	
293	7.43	7.85	8.22	7.15	7.34	7.83	5.55	5.53	7.67	
298	7.44	7.84	8.23	7.42	7.34	7.82	5.58	5.59	7.68	
303	7.46	7.88	8.24	7.43	7.42	7.86	5.61	5.62	7.69	
308	7.40	7.83	8.22	7.44	7.33	7.78	5.74	5.75	7.70	
313	7.49	7.87	8.26	7.46	7.48	7.87	5.78	5.83	7.75	
318	7.52	7.89	8.27	7.47	7.49	7.88	5.82	5.85	7.78	
323	7.53	7.90	8.28	7.48	7.51	7.89	5.85	5.88	7.80	
328	7.53	7.91	8.30	7.49	7.52	7.89	5.88	5.89	7.81	
$\Delta\delta$	+0.19	+0.06	+0.10	+0.39	+0.20	+0.07	+0.37	+0.44	+0.09	
Temp. (K)	C1H1'	G2H1'	A3H1'	T4H1'	C5H1'	G6H1'	$T4CH_3$	T4NH	G2NH	G6NH
278	5.58	5.46	6.20	5.82	5.51	5.83	1.29	13.53	12.60	12.30
283	5.48	5.43	6.22	5.81	5.48	5.85	1.28	13.49	12.58	12.28
288	5.49	5.44	6.22	5.81	5.49	5.85	1.28	13.44	12.57	12.28
293	5.49	5.44	6.22	5.81	5.49	5.86	1.28	13.40	12.57	12.28
298	5.51	5.47	6.22	5.81	5.51	5.88	1.28	13.46	12.57	12.28
303	5.52	5.75	6.29	6.05	5.52	6.10	1.28			
308	5.95	5.83	6.30	6.07	5.95	6.15	1.28			
313	5.96	5.86	6.31	6.08	5.96	6.15	1.29			
318	5.97	5.87	6.32	6.09	5.97	6.17	1.29			
323	5.98	5.89	6.33	6.10	5.98	6.17	1.29			
328	5.99	5.91	6.34	6.10	5.99	6.17	1.29			
$\Delta\delta$	+0.41	+0.45	+0.14	+0.28	+0.48	+0.34	+0.01	-0.18	-0.03	-0.02

-ve $\Delta\delta$ indicates upfield shift
+ve $\Delta\delta$ indicates downfield shift

5.1.2.3 Diffusion Ordered Spectroscopy (DOSY) studies on palmatine-d-$(CGATCG)_2$ complex

Complexed and noncomplexed forms in a mixture can be distinguished using Diffusion Ordered Spectroscopy (DOSY) due to differences in their relative diffusion

coefficient values. Diffusion observed for any interacting molecule in complexed state forms is an average of the populations of the diffusion of the molecule in free and complexed forms in equilibrium. A change in the chemical shift does not provide sufficient indication about the strength of interaction between the components which could be due to other effects influencing the chemical shift but DOSY plots can provide a better insight about the strength of such interactions which are clearly manifested in the diffusion dimension.

The NMR diffusion measurements for palmatine (5.01 mM) and palmatine-d-$(CGATCG)_2$-complex of D/N ratio 2.0 were done at 298 K in D_2O according to the following conditions: 16 spectra were acquired using stimulated echo sequence incorporating bipolar gradients. The gradient strengths were incremented as a square dependence in the range of 1 to 32 G cm^{-1}. The diffusion time (Δ) and the length of diffusion gradient (δ) used were 100 ms and 6 ms respectively. The data were processed by fitting the diffusion decays using the SimFit algorithm provided with Bruker processing software- Topspin (version 1.3) and verified by plotting -ln(I/Io) versus $\gamma_H^2\delta^2G_z^2(\Delta-\delta/3)$. The slope of the line provides the Diffusion coefficient according to the equation:

$$I / Io = -\exp[D\gamma_H^2\delta^2G_z^2(\Delta-\delta/3]$$

DOSY spectra of palmatine and palmatine-d-$(CGATCG)_2$ complex of 2:1 D/N ratio is shown in Fig. 5.14a-b. We found that palmatine alone has a diffusion coefficient (D) of ~ 3.0×10^{-10} m^2/s. However, in the presence of d-$(CGATCG)_2$, palmatine diffused with D = ~1.0×10^{-10} m^2/s, indicating a strong interaction. Accurate measurement of the diffusion was not possible for each proton except for H10, H8, H24 in the complex because the

signals broadened on palmatine binding with d-$(CGATCG)_2$ and merged with other proton signals of DNA. Diffusion constant for H10, H28, H24 resonances corresponding to free and complexed palmatine with d-$(CGATCG)_2$ is present in Table 5.12. It can be noted from Table 5.12 that protons H24, H10 located on one side (convex) while H28 located on the other side (concave) showed almost equal magnitude change in their respective diffusion constant for free palmatine on complexation, which indicate that both sides of palmatine are involved in the interaction with d-$(CGATCG)_2$, which is in accordance to our chemical shift analysis. The diffusion plots for H10, and H24 in alone palmatine and in complex with d-$(CGATCG)_2$ are given in Fig.5.15a-b. The diffusion plots clearly shows that on complex formation, the value of diffusion coefficient of the palmatine resonances decreases in the complex as compared to that in the palmatine alone.

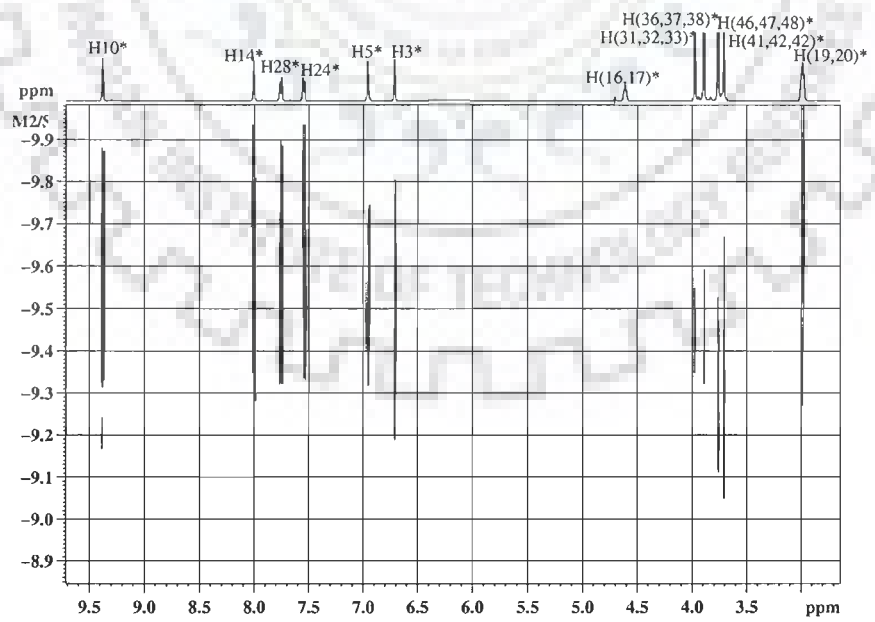

Fig. 5.14a

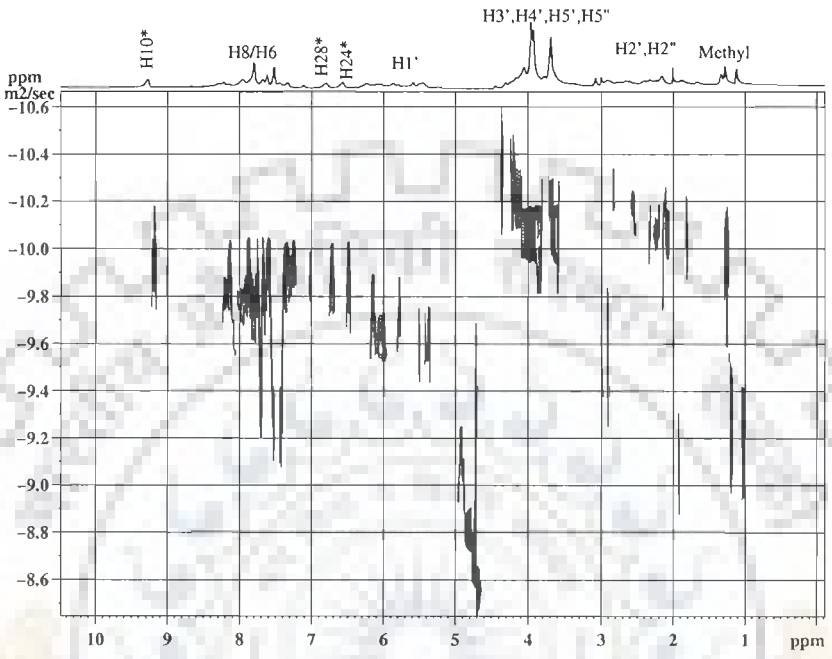

Fig. 5.14b

Fig. 5.14: DOSY spectra of (a) palmatine (b) palmatine- d-$(CGATCG)_2$ complex in D_2O at 298 K. (* palmatine proton in palmatine -d-$(CGATCG)_2$ complex).

This is because of the interaction of palmatine with d-$(CGATCG)_2$ which slows down the rate of diffusion. However, only one set of peaks are present, which is due to averaging of the diffusion coefficients for complexed and non-complexed resonances of palmatine. The diffusion measurements indicated that the majority of the ligand is associated with DNA even though it is present in 2-fold molar excess.

Table 5.12: Diffusion coefficients (10^{-10} m^2/s) of palmatine protons alone and in complex with d-$(CGATCG)_2$ at 298 K.

Proton	Palmatine (5mM) 298 K	Palmatine- $(CGATCG)_2$ (D/N =2.0)
H10	3.448	1.074
H28	3.343	1.410
H24	3.405	1.394

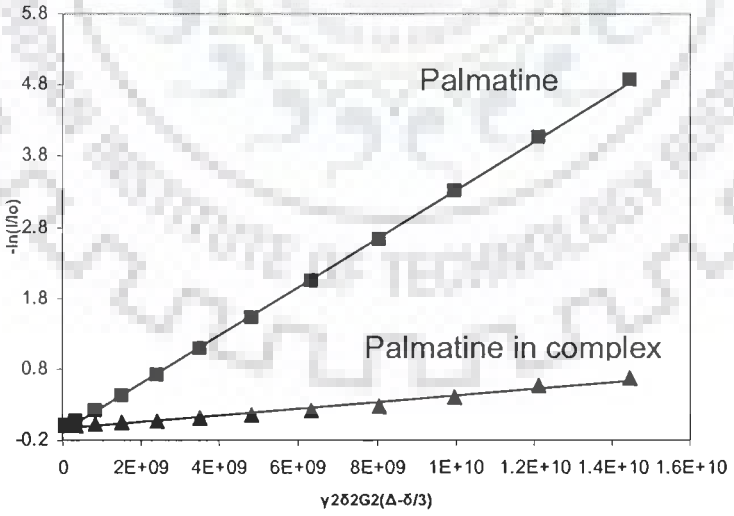

Fig.5.15a

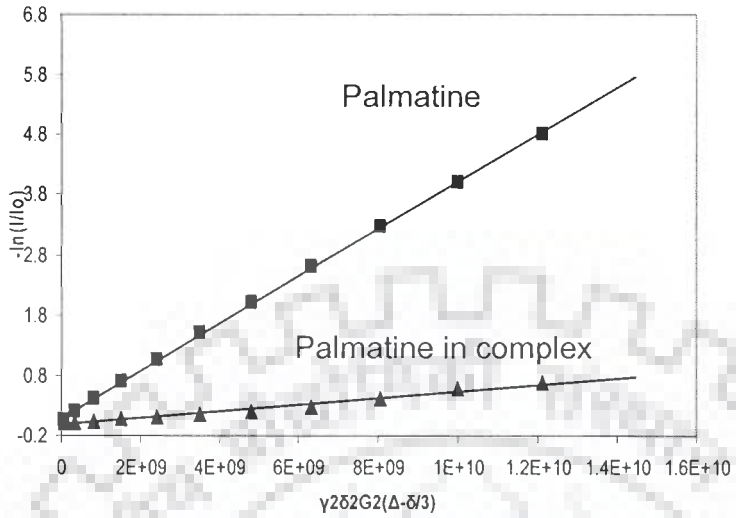

Fig. 5.15b

Fig. 5.15: NMR diffusion measurements at 298 K for palmatine protons (a) H10 and (b) H24 alone (▲) and in complex with d-(CGATCG)$_2$ (■). The diffusion coefficient is the slope of the plot -ln(I/Io) versus $\gamma_H^2\delta^2G_z^2(\Delta-\delta/3)$ in D_2O (* palmatine proton in palmatine -d-(CGATCG)$_2$ complex)

5.1.2.4 Conformational Features of DNA and drug in complex

The NOESY spectra of drug-DNA complex at stoichiometric D/N ratio of 1.0 and 2.0 have been investigated extensively at mixing time (τm) of 100, 200 and 300 ms. The intensities of cross peak have been estimated qualitatively as strong intense (ss), strong (s) medium (m) and weakly intense (w) and very weak (vw) for distances of about 1.8 - 2.5, 2.5 - 3.0, 3.0 - 3.5, 3.5 - 4.0, and 4.0 - 5.0 Å, respectively from the spectra recorded at τm = 200 ms. The inter-proton distances have also been evaluated by taking distance T4CH_3-H6 = 2.9 Å for τm = 200 ms as an internal standard. The observed NOEs

for (a) connectivities involving amino and imino protons of base pairs, (b) sequential connectivities (c) intranucleotide connectivities within sugar (d) intranucleotide base to sugar connectivities are given in Table 5.13a-d.

(a) Connectivities involving amino and imino protons of base pairs: The base sequence d-$(CGATCG)_2$ being self-complementary is responsible for a high symmetry in the NMR spectra. The observation of NOEs between the imino protons of guanine bases and the amino protons of the hydrogen bonded partner cytosine bases in NOESY spectra ($tC5N4H_2^b$, G2N1H) (Fig.5.7h) establish Watson–Crick base pairing at all dG–dC base pair in the duplex. Similarly the observation of NOEs between imino proton of thymine and H2 and amino protons of adenine residues (that is, pairs $T4NH^b$, A3H2; $T4NH^b$, $A3N6H_2$) (Fig.5.7h) establish Watson and Crick pairing at all dA–dT base pairs. Thus practically all sequential connectivities among adjacent base pairs, expected for a typical B–DNA structure, are observed (Table 5.13d). This clearly demonstrates that DNA duplex is intact, apparently with no opening of base pairs to accommodate drug chromophore as expected on binding of typical intercalator to DNA molecule. The base sequence d–$(CGATCG)_2$ being self–complementary is responsible for a high symmetry in the NMR spectra, which remains unbroken in the presence of drug.

(b) Sequential connectivities: The sequential connectivities base $(H6/H8)_n$ to $(H1')_{n-1}$, $(H2')_{n-1}$, $(H2'')_{n-1}$, base $(H6/H8)_{n-1}$ connectivities are observed at all base pair steps (Fig. 5.7a-b, Table 5.13a). This clearly demonstrates that DNA duplex is intact, apparently with no opening of base pairs to accommodate drug chromophore as expected on binding of typical intercalator to the DNA molecule. The base sequence d–

$(CGATCG)_2$ being self–complementary is responsible for a high symmetry in the NMR spectra, which remains unbroken in the presence of drug.

(c) Intranucleotide connectivities within sugar:

Sugar conformation can be determined from the intensities of cross peaks in NOESY spectra (Table 5.13b) at 278 K. The deoxyribose conformation can be estimated from intra-sugar distances of a nucleotide residue. Intra residue inter-proton distances H1'-H2', H1'-H2", H2'-H3', H2"-H3', H2'-H4' and H3'-H4' varied with P_S and χ_S in a narrow range while the H1'-H4' and H2"-H4' distances varied significantly with PS and χS, respectively [Wüthrich, 1986] and can be used for conformational analysis. The base H6/H8-H1' connectivity (Table 5.13c) suggests the residues to be more close to anti conformation. The deoxyribose conformations were estimated from intrasugar distances of a nucleotide residue [Wüthrich, 1986]. Strong intense cross peaks were observed for H1'-H2", H1'-H2', H1'-H3'. The presence of more intense intraresidue H6/H8-H2' than interresidue H6/H8-H2' (Fig. 5.7b) shows the predominance of S-conformation for the deoxyribose ring. The observed intense cross peaks corresponding to H2"-H3' (Figure 5.7e) and H3'-H4' showed that N-conformer might be present.

Table 5.13a Intensity of sequential NOE cross peaks (d_s) of nucleotide protons in the drug-DNA complex at D / N = 1.0 at 278 K. The very strong (ss), strong (s), medium (ws) and weak (w) and very weak (ww), intensities correspond to distances in the range 1.8 – 2.5 Å, 2.5 – 3.0 Å, 3.0 – 3.5 Å, 3.5 – 4.0 Å, 4 – 5 Å, respectively in the NOESY spectra, Fig.6.6 Overlap of cross peaks is indicated as o.

Connectivity	Intensity	Connectivity	Intensity
C1pG2 step		T4pC5 step	
C1H1'- G2H8	o	T4H1'- C5H6	m
C1H2'- G2H8	m	T4H2'- C5H6	o
C1H2"- G2H8	o	T4H2"- C5H6	o
C1H3'- G2H8	o	T4H3'- C5H6	o
C1H4'- G2H8	o	T4H1' - C5H5	
C1H6 - G2H8	vw	T4H8 - C5H5	
G2pA3 step		T4H6 - C5H6	vw
G2H1' – A3H8	s	C5pG6 step	
G2H2' - A3H8	o	C5H1'– G6H8	o
G2H2"- A3H8	o	C5H2'– G6H8	o
G2H3' - A3H8	m	C5H2" – G6H8	o
G2H8 - A3H8	vw	C5H3'– G6H8	o
A3pT4 step		C5H6– G6H8	vw
A3H1'- T4H6	m		
A3H2'- T4H6	w		
A3H2"- T4H6	m		
A3H3'- T4H6	o		
A3H8 - T4H3'	-		
A3H8 - T4H6	vw		

Table 5.13b Intensities of intra sugar NOE cross peaks (d_i) in the drug-DNA complex at D / N = 1.0 at 278 K. The very strong (ss), strong (s), medium (m) weak (w) and very weakly (vw) intense cross peaks refer to distances in the range 1.8 – 2.5 Å, 2.5 – 3.0 Å, 3.0 – 3.5 Å, 3.5 – 4.0 Å, 4 – 5 Å, respectively from the NOESY spectra. Overlap of peaks is indicated as o.

Connectivity	C1	G2	A3	T4	C5	G6
H1'-H2'	s	o	s	s	w	s
H1'-H2"	ss	o	s	s	w	ss
H1'-H3'	m	w	vw	m	vw	m
H1'-H4'	ss	vw	w	ss	vw	ss
H1'-H5'	-	s	s	-	-	o
H1'-H5''	w	m	m	-	o	o
H2'-H3'	O	o	-	o	m	Vw
H2''-H3'	O	o	w	O	o	w
H2'-H4'	s	o	w	w	w	Vw
H2''-H4'	s(o)	m	w	s	m	w
H3'-H4'	w	m	w	o	w	o

Table 5.13c: Intensities of intra nucleotide NOE connectivities (d_i) of base to sugar protons of nucleic acid in drug–DNA complex at D / N = 2.0 at 278 K. The very strong (ss), strong (s), medium (m), weak (w), very weakly (vw) intense cross peaks correspond to distances 1.8 – 2.5 Å, 2.5 – 3.0 Å, 3.0 – 3.5 Å, 3.5 – 4.0 Å, 4 – 5 Å, respectively from the NOESY spectra. Overlap of peaks is indicated as o.

Connectivity	C1	G2	A3	T4	C5	G6
H8 / H6-H1'	w	o	ss	w	s(o)	ss
``H8 / H6-H2'	w	o	o	m	s	s(o)
H8 / H6-H2''	w	o	o	m	s	s(o)
H8 / H6-H3'	m	w	m	o	m	m
H8 / H6-H4'	o	vw	vw	m	o	m
H8 / H6-H5'	-	-	o	o	o	o
H8 / H6-H5''	-	-		o	o	o

Table 5.13d NOE connnectivities observed in NOESY spectra for exchangeable protons of the palmatine - $(CGATCG)_2$ complex at Drug/DNA ratio (D/N) = 2.0 at 278 K. The strong intense (ss), strong (s), medium (m), weak (w), very weakly (ww) intense cross peaks correspond to distances in the range ss 1.8 - 2.5 Å, s 2.5 - 3.0 Å, m 3.0 - 3.5 Å, w 3.5 - 4.0 Å, vw 4.0 - 5.0 Å, respectively.

Cross peak	NOE Intensity	Cross peak	NOE Intensity
T4NH-A3NH2^{nb}	s	T4NH-G2NH	s
T4NH-C5NH2^{nb}	vw	A3NH2^{b}-A3NH2^{nb}	ss
T4NH-C5NH2^{b}	w		
T4NH-A3H2	s		
T4NH-A3NH2^{b}	m		
G2NH-C1NH2^{nb}	m		
G2NH-A3H2	w		
G2NH-C5NH2^{b}	m		

The presence of moderately intense intranucleotide base H6/H8-H3' connectivities (Fig. 5.7f) also confirms the presence of minor N-conformer [Barthwal et al., 2004]. The NOE connectivity corresponding to H1'- H4' for C5 and G2 residue is weakly intense as compared to C1, A3, G6 and T4 residues (Fig. 5.e and Table 5.13b) indicating that pseudo rotation phase angle for C5 and G2 residue is ~162-180° while for other residues it might be ≤ 162°. Among purines, the intensity of H8-H1' cross peak in Fig. 5.8a decreased in order G2~G6>A3 so that χ value for A3 is close to that of B DNA while that for G2 and G6 residues deviated from -105°. Among pyrimidines, H6-H1' cross peak intensity decreased T4> C5~C1 (Fig. 5.7a) so that corresponding χ of C1 and C5 is close to ~ -105° whereas, T4 deviated from this value.

(e) Conformation of palmatine

The intramolecular NOE connectivities within the palmatine molecule in palmatine-d-$(CGATCG)_2$ complex give information about the conformation of palmatine (Table 5.7). The intensities of palmatine protons increases with D/N ratio (Fig.5.8a-d), but are lesser than the expected intensity i.e. equal to the d-$(CGATCG)_2$ at 1:1 and double at 2:1. This is due to the broadening of peaks at higher ratios. Table 5.7 shows the intramolecular NOE connectivities observed within the palmatine molecule in the palmatine-d-$(CGATCG)_2$ complex at D/N= 2.0. It is observed that some new intramolecular cross peaks appeared in the NOESY spectrum of palmatine-d-$(CGATCG)_2$ complex (Fig. 5.7j-l) , which were absent in palmatine alone (Fig. 3.6 and Table 3.4). These new cross peaks which are observed on complex formation are shown as"Ⓗ" in Fig. 5.7j-l and are tabulated in Table 5.7. The H10 proton at ring C of palmatine give cross peaks with distantly placed protons H24, H(19,20) and H(41,42,43). Similarly, NOEs are observed between ring 'A' protons, H14 and H28 with H3 proton of ring 'D'. This is attributed to the conformation of palmatine. Palmatine shows deviation from planarity due to saturation at ring 'B', with atoms C15 and C18 deviating from the plane of aromatic rings 'A' and 'C' and lead to tilting of ring 'A' and fused rings C-D towards each other. The new intramolecular peaks indicates that the conformation of palmatine has changed due to binding and lead to the observation of new intramolecular cross peaks which were absent in drug alone.

(e) Intermolecular Interactions

Specific interactions between protons of palmatine and protons of d-$(CGATCG)_2$ were observed from proton 2D NOESY spectra recorded at D/N 0.0, 0.5, 1.0, 1.5 and 2.0. The results are shown in Fig. 5.7a-l. It is observed that palmatine interacts with d-$(CGATCG)_2$ even at low concentration and signals are sharp at lower D/N ratio. It is clear from fig. 5.7j-l that intermolecular interaction observed at D/N 2.0 are broad and merged as compared to separated signals in D/N 0.2, 0.5 and 1.0. All the intermolecular NOEs observed with their respective intensity is tabulated in Table 5.14. NOE data are used to determine and recognize the interaction site and to define the exact binding mode of palmatine to d-$(CGATCG)_2$. In the complex, NOEs are observed between the palmatine protons and d-$(CGATCG)_2$ with retention of symmetry of the hexamer. Table 5.14 gives a list of 19 intermolecular contacts observed between palmatine and DNA hexamer. 2D NOESY experiment allowed the detection of several contacts between the protons of palmatine molecule and those of the double helix, specifically with protons of the CG base pairs at the terminal end. The drug protons H(36,37, 38), H(41,42,43) and H(46,47,48) shows intermolecular contacts with G6H1', C1H1' and C1H6 of the hexamer d-$(CGATCG)_2$. H(36,37,38) and H(41,42,43) give close contacts with G6H8. Whereas, H10 proton show intermolecular peaks with C1H6, C1H5, $C1NH2^{nb}$ and $C1NH2^{b}$. H24 of the drug interacts with C1H5 and G6H1' of the hexamer. H14 of the drug molecule show intermolecular contacts with C1H4' and C1H3' of the hexamer. Zero intermolecular NOEs are found for imino residues and with the protons of the minor groove region of the hexamer. Thus, the observed intermolecular peaks exclude the minor groove binding mode of palmatine with the hexamer d-$(CGATCG)_2$.

Apparently drug is binding externally to the hexamer sequence in a specific orientation which gives rise to the observed NOEs. In contrast to the previous NMR characterized minor groove complex, the resonances of DNA protons located outside the minor groove binding site appear perturbed. The analysis of DNA chemical shift perturbation induced by palmatine suggests that the extremity of the hexamer is the site of binding. This is consistent with experimental intermolecular NOEs observed between palmatine protons and both minor groove and major groove protons of the last C1:G6 base pairs, which excludes the minor groove binding of palmatine in the hexamer d-$(CGATCG)_2$. Moreover the strong upfield shift of the G6NH imino resonance suggests an intercalation like binding of the ligand involving the last C1:G6 base pair according to the observed upfield shift of palmatine resonances. However, the absence of any intermolecular NOE, involving the G2 nucleotide together with the observation that the binding does not cause an increase on internucleotide sequential distances between C1 and G2 as well as C5 and G6 residues, indicates that intercalation of ligand between the last two base pairs can be excluded. Therefore based on intermolecular NOEs spectral changes and DNA structural perturbation, the minor groove and intercalation as the binding mode of palmatine-to hexamer d-$(CGATCG)_2$ is excluded. These results are consistent with a π, π-stacking interaction of palmatine molecule with the terminal C1:G6 base pairs on the outside of hexamer. Our detailed NMR analysis shows that all internucleotide sequential connectivities (Table 5.13a) exist. Further, the DNA hexamer in complexed state is expected to adopt a conformation close to that of canonical B–DNA structure. All the duplex pair peaks, including sequential intra and inter–strand peaks, exist. Thus it may be concluded that palmatine binds externally to the DNA duplex, being in close proximity to

C1.G6 base pair. All the spectral lines are somewhat uniformly broadened on binding as the internal motions are affected and the protons are getting immobilized. These results show that in the experimental condition examined, an intercalation between the base pairs as well as external binding in the minor groove or in the major groove, can be excluded, but indicate a stacking with the terminal bases. The significant upfield shift (0.78 ppm) for the imino NH protons of the terminal base pairs confirms these results.

Table 5.14 Relative intensities of intermolecular NOE connectivity's between d-$(CGATCG)_2$ and the palmatine molecule in the palmatine-d-$(CGATCG)_2$complex at drug to DNA ratio D / N =1.0 from NOESY spectra at 200 ms.

S.No	Sequence connectivity	Intensity	Distance from minimized model (Å)
1.	H(36,37,38)-C1H1'	m	3.35
2.	H(36,37,38)-C1H6	w	4.21
3.	H(36,37,38)-G6H1'	m	3.28
4.	H(36,37,38)-G6H8	w	4.28
5.	H(41,42,43)-G6H1'	m	3.42
6.	H(41,42,43)-G6H8	m	3.84
7.	H(41,42,43)-C1H1'	vw	4.01
8.	H(41,42,43)-C1H5	vw	4.68
9.	H(41,42,43)-C1H6	w	4.99
10.	H(46,47,48)-G6H1'	vw	5.41
11.	H(46,47,48)-C1H6	w	4.52
12.	H(46,47,48)-C1H1'	vw	5.21
13.	H24-C1H5	w	4.42
14.	H24-G6H1'	vw	4.82
15.	H10-C1H6	m	3.82
16.	H10- C1H5	m	3.91
17.	H10-C1NH2^{nb}	vw	5.32
18.	H10-C1NH2^{b}	w	5.10
19.	H14-C1H4'	w	4.24

5.1.3 Restrained Molecular Dynamics Studies

Restrained Molecular Dynamics (rMD) permits the system to undergo conformational and momentum change so that different parts of the phase space accessible to the molecule can be explored and stable conformations identified by energy minimization. Based on the observed intermolecular and intramolecular NOE data an initial model with two palmatine molecule located at the terminal ends of d-$(CGATCG)_2$ was considered. The schematic representation of the initial model used in rMD, is shown in Fig. 5.16. Distance restraints between atoms involved in the Watson-Crick hydrogen bonding pairs were imposed in the structure calculations based on the experimental evidence from NOESY spectra.

All other restrains for the intramolecular and intermolecular connectivities were also given. The front and side view of the final structure obtained after rMD is shown in Fig, 5.17. Table 5.15 indicates an assessment of refined structures after equilibration (at the end of 25 ps) in terms of energetics including restraint violations energies and root mean square derivative of energy with respect to atomic coordinates. The total potential energy of the final structure was 452 Kcal mol^{-1}, which is significantly lower than the corresponding energy of initial model B-DNA structure (3459 Kcal mol^{-1}). The forcing potential, which indicates contribution to potential energy due to violations of both experimental distances data, exhibits a decrease from 2048 to 336 kcal mol^{-1} after restrained energy minimization and restrained molecular dynamics simulations.

The palmatine -d-$(CGATCG)_2$ complex was stabilized via close contacts which involved specific Van der Waal's and electrostatic interactions and which is clearly shown in Fig. 5.18. Model obtained through rMD supports the results from the ^{31}P NMR, proton

chemical shift analysis, DOSY and intramolecular and intermolecular interaction obtained from 2D NOESY spectrum.

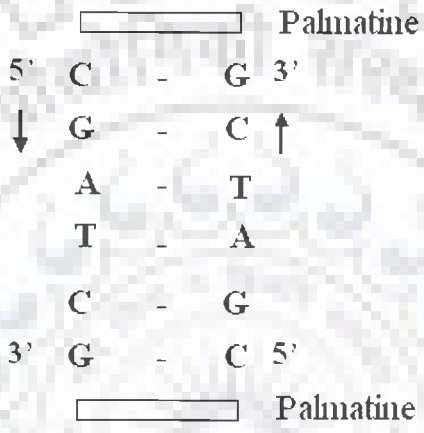

Fig. 5.16: Schematic Representation of palmatine in complex with d-$(CGATCG)_2$

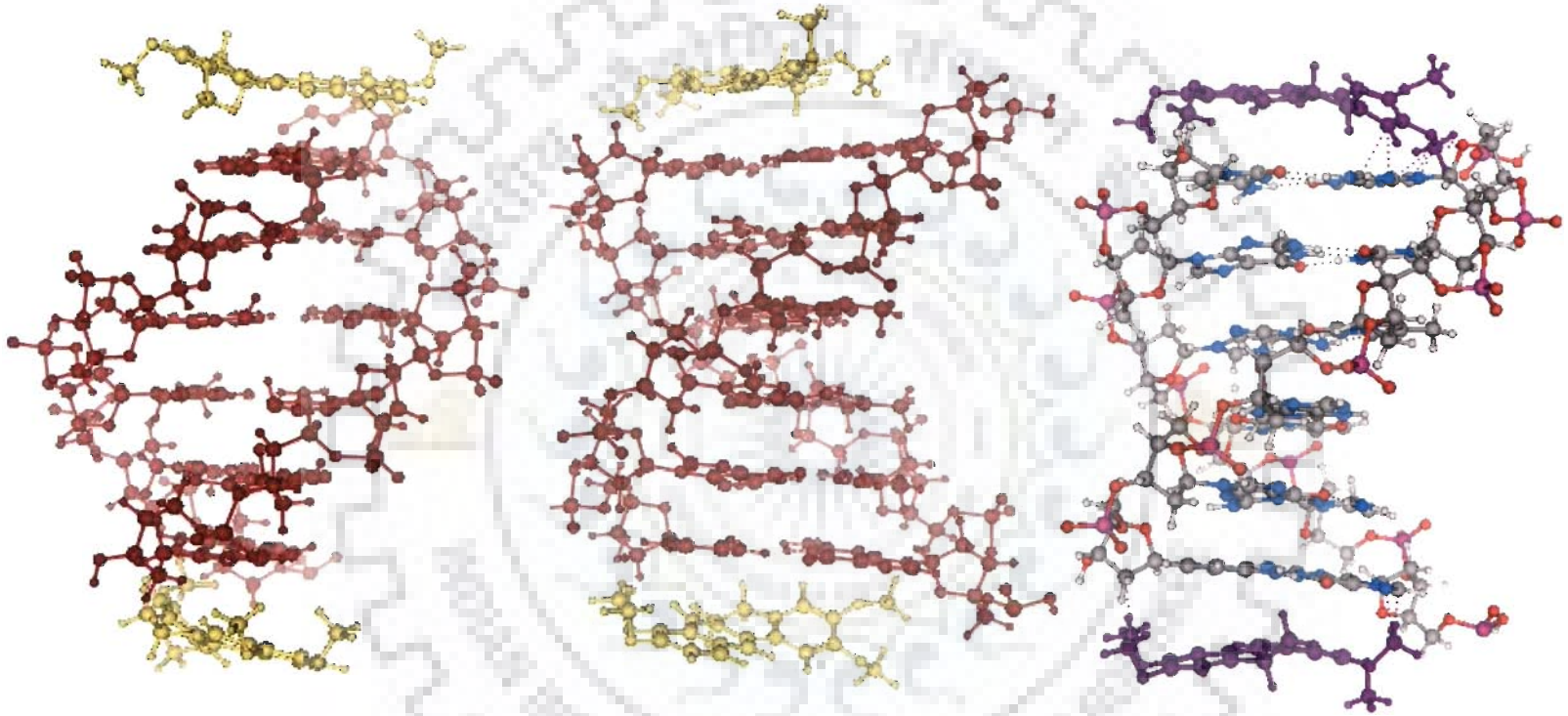

Fig. 5.17: Front view and Side view of the final structure of palmatine-d-$(CGATCG)_2$ complex obtained by restrained molecular dynamics simulations.

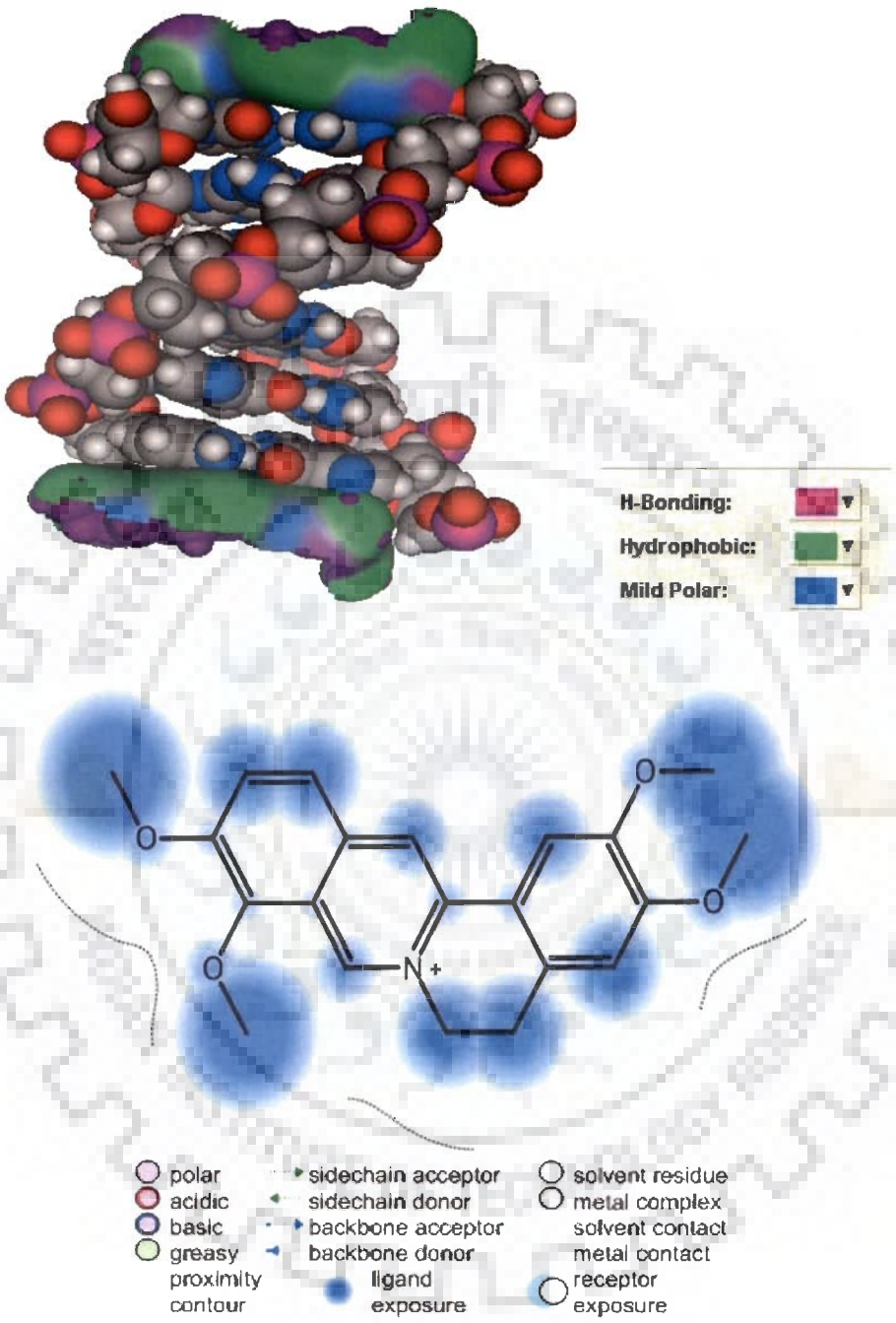

Fig. 5.18: Various Interactions present in 2:1 palmatine d-$(CGATCG)_2$ complex

Table 5.15a: Energy terms (Kcal mol^{-1}) for starting structure and final rMD structure.

Structure	Total	Bond	Angle	Dihedral
Initial	3459	493	512	448
Final	452	52	147	81
	Vdw	**Electrostatic**	**Restraint**	
Initial	505	-168	2048	
Final	171	-124	336	

Table 5.15b: Summary of experimental restraints and statistical analysis of final structure generated by restrained molecular dynamics (rMD)

Parameter	
	No. of Distance Restraints
Intra residue	132
Inter residue	28
Inter molecular	19
Average pairwise RMSD	Initial = 0 Final = 0.71
Average residuewise RMSD	C1=0.91, G2=0.80, A3=1.22 T4=1.10, C5=1.18, G6=0.98 Palmatine=0.92

All helical parameters, backbone torsional angles, and sugar conformations of the resulting rMD structures were thoroughly analyzed with the program CURVES, version 5.1 (Lavery et al, 1996; Lavery et al, 1989). Plot of the helicoidal parameters as a function of residue position in the duplex is shown in Fig. 5.19a-b, along with classical structures of A-DNA and BDNA. The overlap geometry at different base pair steps along the sequence in palmatine - d-$(CGATCG)_2$ is shown in Fig. 5.20. In the base pair-axis parameters, the average value of x-displacement is 0.81 Å. The average y-axis displacement (dy) is 0.0 Å. The rMD structure display inclination values of terminal C.G base pair deviating maximum from the average value of 7.74°. Among intra base parameters, the stagger (Sz) and stretch (Sy) values vary much from their ideal values for terminal residues. The shear (Sx) values lie within ±1.0 Å of the average. Base pair opening lies in the range 6 to 15 for all base pairs in all rMD structure. In regular A-DNA and B-DNA geometries, global values of the inter base pair parameters - shift (Dx), slide (Dy), roll (rho) and tilt (tau) are essentially zero. For rMD structures, the observed shift and slide values are small and do not show any significant variation with the base pair step. The rise per residue (Dz) approximately lies with in the range 3.2 - 3.7 Å that is standard for B-DNA. The variation of tilt value is ± 6° deviated from the ideal B-DNA value. The twist angle varies between 31° -43°. The backbone torsional angles and glycosidic bond rotation values (Table 5.16) show that the conformation of the structure obtained from rMD is close to that of the B-DNA. Thus d-$(CGATCG)_2$ on binding to palmatine has the global helical parameters near to standard B-DNA values, indicating that the drug is binding externally to DNA.

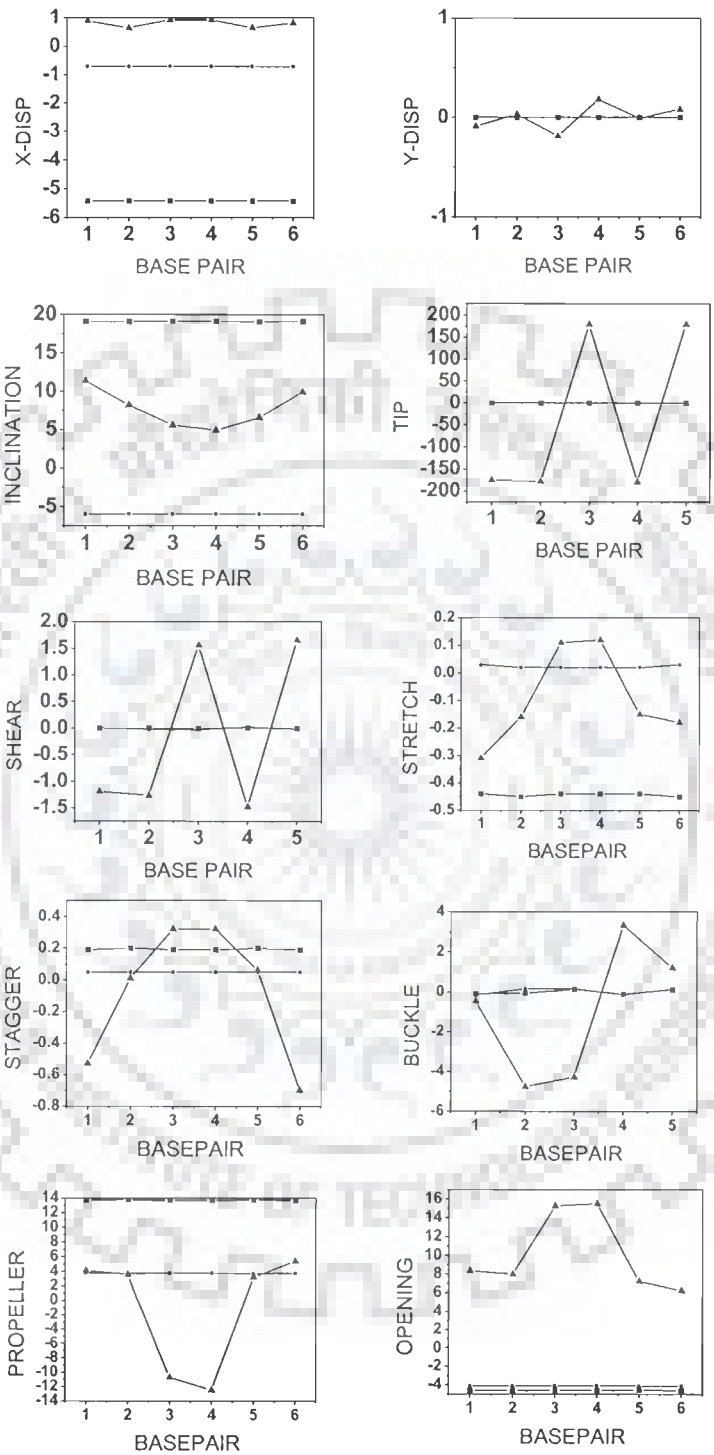
X-DISP
BASE PAIR
Y-DISP
BASE PAIR
INCLINATION
BASE PAIR
TIP
BASE PAIR
SHEAR
BASE PAIR
STRETCH
BASEPAIR
STAGGER
BASEPAIR
BUCKLE
BASEPAIR
PROPELLER
BASEPAIR
OPENING
BASEPAIR

(Fig. 5.19a)

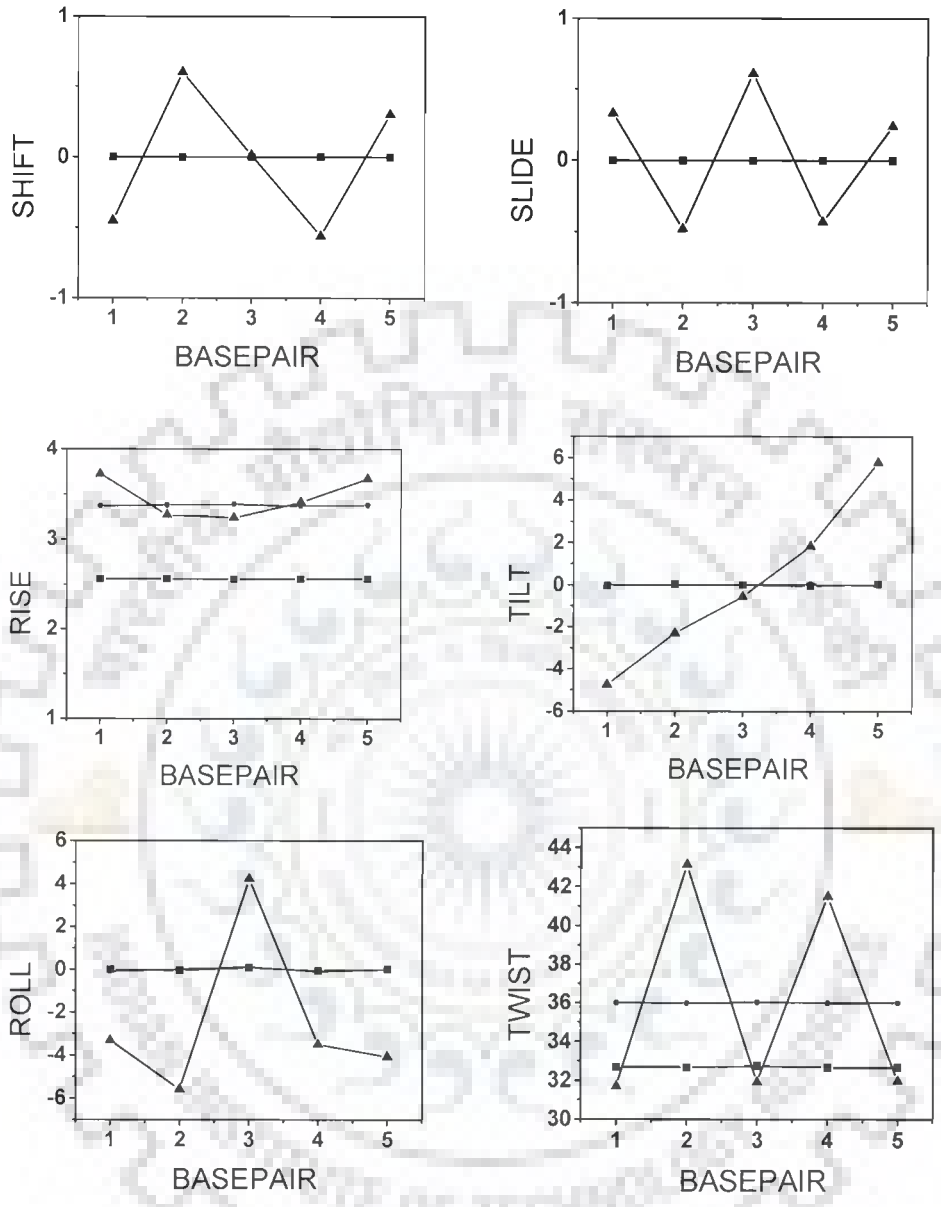

(Fig. 5.19b)

Fig. 5.19a: Helical parameters for d-(CGATCG)$_2$ complexed with palmatine calculated for structure obtained by restrained molecular dynamics simulations- ▲; d-(CGATCG)$_2$ + palmatine- (★) and that for canonical A-DNA (■) and B-DNA (●).

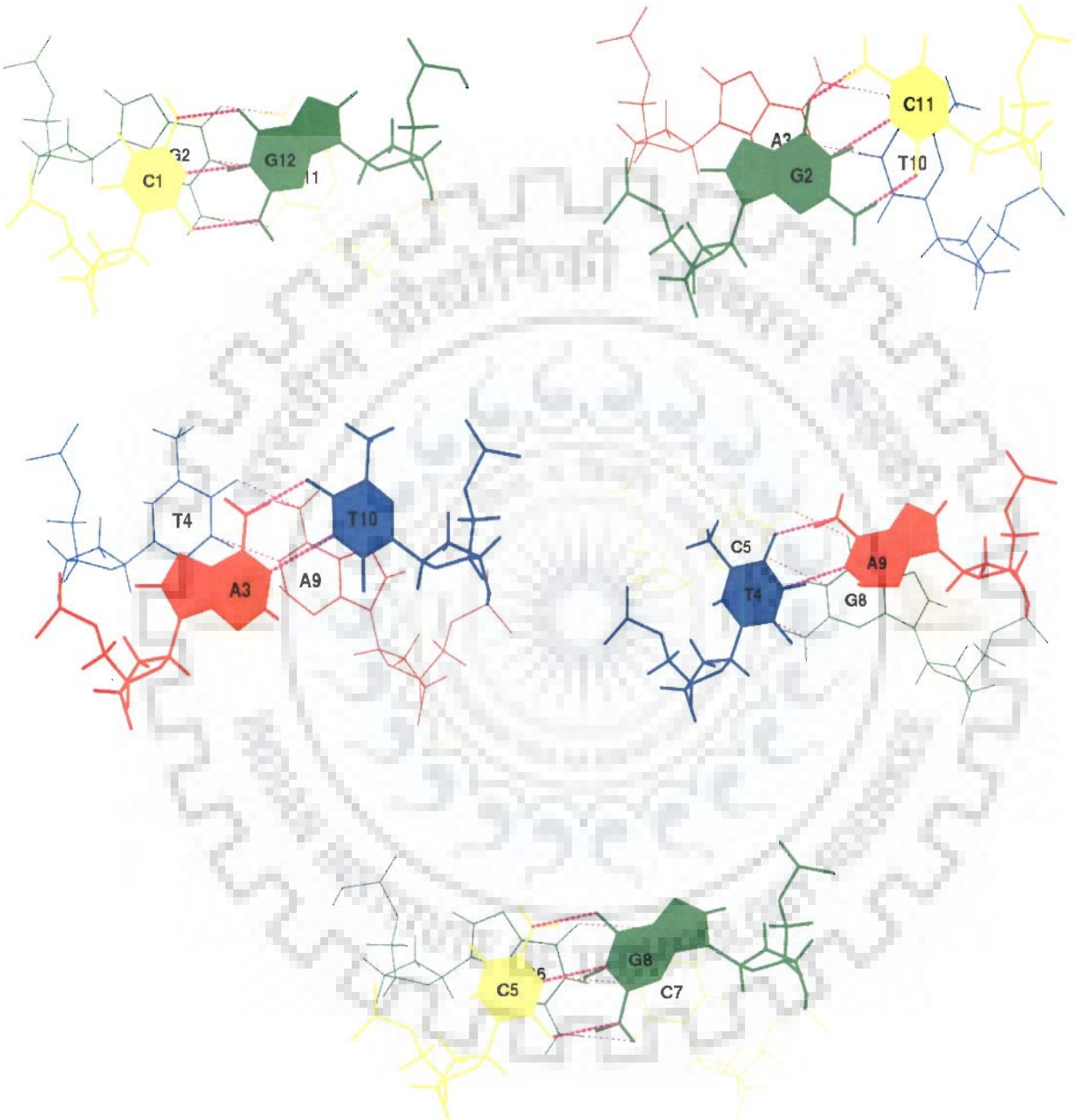

Fig. 5.20: Overlap geometry of base pairs in d-$(CGATCG)_2$ at different steps along the sequence in palmatine- d-$(CGATCG)_2$ complex.

Table 5.16: Backbone torsional angles, pseudoratation phase angle and glycosidic bond rotation of the final structure.

		α		β		γ		δ	
Strand I	Strand II	Strand I	Strand II	Strand I	Strand II	Strand I	Strand II	Strand I	Strand II
C1	G12	.....	....	.....	....	50.68	52.64	142.95	140.93
G2	C11	-57.32	-65.13	-177.81	160.35	52.60	5.036	149.58	136.63
A3	T10	-78.82	-64.83	-146.65	-172.68	54.58	51.28	143.58	143.79
T4	A9	-65.78	-79.07	-173.96	-141.01	52.27	54.28	142.79	141.91
C5	G8	-59.54	-56.34	160.65	-170.23	47.44	51.86	138.13	149.29
G6	C7	.....	.....	.....	.....	52.81	47.50	140.17	138.72
B-DNA		-63		136		54.0		123	

		ε		ζ		χ		P	
Strand I	Strand II	Strand I	Strand II	Strand I	Strand II	Strand I	Strand II	Strand I	Strand II
C1	G12	....	...	.....	.....	-127.95	-119.40	155.33	167.71
G2	C11	171.41	-141.34	-99.19	-137.50	-96.89	-118.24	188.33	138.86
A3	T10	175.59	178.70	-112.54	-94.39	-109.76	-112.42	153.55	168.32
T4	A9	-179.95	170.96	-94.70	-107.22	-112.97	-109.30	165.03	153.31
C5	G8	-151.03	168.44	-132.06	-97.58	-110.65	-95.19	143.58	188.92
G6	C7	....	...	.....	.....	-116.17	-121.50	167.84	153.68
B-DNA		-169		-108		-105		162	

5.2. Summary and Conclusions

The phosphates resonances of the hexamer in the complex show negligible chemical shift variation (0.01-0.14 ppm) as compared to the significant (1-1.5 ppm) low field shift by the intercalating molecules. This indicated that no deformation occurs at any level of the phosphodiester backbone. ^{31}P-^{31}P exchange spectrum of the d-$(CGATCG)_2$ - palmatine complex at various D/N ratios did not show any exchange peaks for free and bound resonances. These observations rule out intercalation and suggest the external binding mode of palmatine with d-$(CGATCG)_2$. Proton chemical shifts observed through titration showed that only one set of resonance signals were observed for both DNA and palmatine protons, with gradual change in chemical shift with increasing concentration of palmatine. It is suggested that the signals were in fast exchange regime and the observed resonances were considered to be an average of free and bound proton. Thermal melting temperature calculated by imino protons chemical shift change with temperature also proved that palmatine is stabilizing the oligomer d-$(CGATCG)_2$ on binding. Binding was also proved by DOSY which showed majority of the palmatine binding to DNA even at D/N ratio 2.0, which was further supported by NOESY data analysis. Presence of all internucleotide sequential connectivities suggests that the DNA did not open up to accommodate the palmatine chromophore as observed with intercalators. All the duplex pair peaks, sequential intra and inter-strand peaks exist. Zero NOEs were found with the imino, A3H2 and the protons in the central region of the duplex. This excludes the minor groove binding mode of palmatine. The detection of Intermolecular peaks between drug and the hexamer terminal CG base pairs and significant upfield shift of the terminal

guanine protons shows the interactions of palmatine at the terminal ends of the oligomer. These results shows that intercalation of palmatine between the base pairs, as well as its external binding in the minor or in the major groove of the hexamer d-$(CGATCG)_2$ can be excluded. Apparently drug is binding externally to the hexamer d-$(CGATCG)_2$ duplex which give rise to the observed NOEs. Major participation of Van der Waals interaction in the complex formation was also observed in the final rMD model. Conformational analysis showed that DNA hexamer in the complexed state adopted conformation close to that of canonical B-DNA structure.

CHAPTER 6

Summary and Conclusions

In designing novel chemotherapeutic agents, one of the major strategies is to develop novel DNA binding ligands that influence crucial cellular processes such as DNA topology, replication, transcription, and DNA repair. Systematic modifications of clinically effective chemotherapeutic agents have the potential for positively influencing their activity and delivery. Regulatory proteins that can repress or stimulate the flow of genetic information through DNA or RNA control gene expression throughout a cell's lifetime. If the binding specificity and strength of this regulatory protein can be mimicked by a small molecule, then DNA function can be artificially modulated, inhibited or activated by binding this molecule instead of the protein. Thus, synthetic/natural small molecule can act as drug when activation or inhibition of DNA function is required to cure or control a disease. These molecules can be isolated from natural sources or synthetically prepared. Palmatine is an isoquinoline alkaloid which belongs to the important class of protoberberine alkaloids. The cytotoxic activity of palmatine to HL-60 leukemic cells has also been well documented. Palmatine has been reported to be effective against experimental tumors by inhibiting the activity of reverse transcriptase. Its DNA binding affinity and sequence specificity is likely to be closely related to its biological activity. To better correrelate this structure-function relationship and to design better agents based on these correlations, it is useful to have a detailed view of how palmatine interact with DNA molecule. Several biophysical and structural studies were performed to obtain data on the conformational and structural features of palmatine and its interaction with DNA which help us to understand its mode of action.

We have obtained the structural and conformational features of palmatine using Nuclear Magnetic Resonance (NMR), restrained Molecular Dynamics (rMD) and quantum chemical calculations. All proton and carbon resonances were assigned using 1D-^{1}H and 2D-^{1}H NOESY, and 2D-^{1}H-^{13}C ; HSQC, HMBC experiments. Solution structure of palmatine has been determined for the first time by restrained Molecular Dynamics (rMD) using the distance constraints obtained from NOESY spectra of palmatine. The ^{1}H and ^{13}C chemical shifts of the molecule have been calculated using the Gauge-Invariant Atomic Orbital (GIAO) method. Tomasis's Polarizable Continuum Model (PCM) was used to evaluate the influence of solvent on the structural parameters and the chemical shift values. The structural and electronic properties of palmatine have been extensively studied using density functional theory employing B3LYP exchange correraltion in the gas phase and in the solvent phase. The effect of increasing size of basis set for STO-3G, 3-21G. 6-31G, 6-31G**, 6-311G** showed that the bigger basis set slowed down the calculations but gave more accurate results. Comparison of the calculated NMR chemical shifts with the experimental values revealed that DFT method produces good results for both proton and carbon chemical shifts. Further, it was also noticed that the solvent induced structural parameters are very similar to gas phase values but chemical shifts move in the right direction and improve the agreement between theoretical and experimental measurements.

An attempt was also made to elucidate the binding affinity of palmatine with DNA. To identify its preferred binding site, UV-visible and fluorescence spectroscopy was used. CT DNA, Poly dA-dT, Poly dG-dC and oligonucleotides: d-$(CGATCG)_2$, d-$(CGTACG)_2$, d-$(CGTACGCGTACG)_2$, d-$(CGATCGCGATCG)_2$, d-$(ATATATATAT)_2$, d-$(CGCGCGCGCG)_2$, d-$(CCAATTGG)_2$ having 6-12 base pairs

were used in this study. Palmatine-DNA interaction was investigated by observing the change in absorption intensity of 344 nm band of UV visible spectrum and of the 530 nm emission band of fluorescence spectrum when excited at 350 nm. Hypochromicity and sharp isobestic points in UV spectrum and enhancement in the fluorescence intensities were observed on successive addition of DNA to a fixed concentration of palmatine. The study showed the preferential binding of palmatine to AT rich sequences and showed base pair recognition to ApT then to TpA.

It is well established that palmatine inhibits the biosynthesis of DNA and RNA by interacting with DNA and hence shows anti cancer activity. In order to achieve exact mode for binding of palmatine to DNA; ^{31}P and ^{1}H Nuclear Magnetic Resonance spectroscopy followed by restrained Molecular Dynamics simulations studies were done for the first time on palmatine-d-$(CGATCG)_2$ complex. The ^{31}P NMR of d-$(CGATCG)_2$ in the complex showed negligible shift variation (< 0.14) of the phosphorus signals thus indicated no deformation at any level of the phosphorus backbone, which is generally found in case of intercalators associated with large down field shifts of 1.6-2.6 ppm [Gorenstein, 1992; Patel, 1974; Patel and Canuel, 1976; Patel et al., 1982]. ^{31}P-^{31}P NOESY exchange studies of complex showed single bound and free ^{31}P signals due to fast exchange on NMR time scale. These results obtained by ^{31}P NMR studies showed that palmatine do not intercalate into the double helix. ^{1}H NMR titrimatric analysis, temperature dependence studies, and DOSY studies also revealed the binding of palmatine to d-$(CGATCG)_2$ at higher concentration i.e. drug to nucleotide ratio (D/N) of 2.0. This was further supported by NOESY data analysis. The presence of intra base pair, sequential inter base pair and all sequential intramolecular NOE connectivities expected in standard B–DNA geometry confirmed that DNA duplex is intact in all three complexes with apparently

no opening of base pairs to accommodate drug chromophore as generally observed with drug intercalation. The NOESY spectra of the palmatine-d(CGATCG)$_2$ complex show several intermolecular contacts with CG base pairs at the terminal ends of the oligomer, whereas no NOEs were found with the imino, A3H2 and with the minor groove protons of the central region. These results show that, in the experimental condition examined, an intercalation between the base pairs as well as an external binding in the minor or major groove, can be excluded, and indicated the stacking of palmatine with the terminal CG base pair. The Conformational analysis of the final rMD structure showed d-(CGATCG)$_2$ in complex state adopted a conformation close to that of canonical B–DNA structure.

Present investigations explored the structure–activity basis for direct anticancer and topoisomerase inhibition activities of palmatine.

Bibliography

1. Abadi, B. E. A., Moss, D. S. and Palmer, R. A. Molecular-structure of an ancient folk medicine berberine hydrogen sulphate. J. Crystallogr. Spectrosc. Res., 1984, 14, 269–281.
2. Abraham, R. J., Mobil, M. and Smith, R. ^{1}H chemical shifts in NMR. Part 20-Anisotropic and steric effects in halogen substituent chemical shifts (SCS), a modelling and ab initio investigation. J. Magn. Reson. Chem., 2004, 42, 436 -444.
3. Aklank Jain, A. and Rajeswari, M. R. Binding studies on peptide–oligonucleotide complex: intercalation of tryptophan in GC-rich region of c-myc gene. BBA-General Subjects. 2003, 1622, 2, 73-81.
4. Altona, C. and Sundaralingam, M. Conformational analysis of the sugar ring in nucleotides and nucleosides. A new description using pseudo–rotation. J. Am. Chem. Soc., 1972, 94, 8205–8212.
5. Altona C. Conformational analysis of nucleic acids. Determination of backbone geometry of single-helical RNA and DNA in aqueous solution. Recl. Trav. Chim. Pays-Bas., 1982, 101, 413-433.
6. Amin, A.H., Subbahaiah, T.V. and Abbasi, K. M. Berberine sulfate: antimicrobial activity, bioassay, and mode of action. Can. J. Microbiol., 1969, 15, 1067–1076.
7. Barthwal, R., Monica., Awasthi, P., Srivastava, N., Sharma, U., Kaur, M. and Govil, G. Structure of DNA hexamer sequence d-CGATCG by two-dimensional Nuclear Magnetic Resonance Spectroscopy and Restrained Molecular Dynamics. J. Biomol. Struct. Dyn., 2003, 21, 407– 423
8. Barve, A. C., Ghosh, S., Kumbhar, A. A., Kumbhar, A. S. and Puranik, V. G. DNA-binding studies of mixed ligand cobalt (III) complexes. Transition Metal Chemistry, 2005, 30, 3, 312-316.
9. Basha, S. A., Mishra, R. K., Jha, R. N., Pandey, V. B. and Singh, U.P. Effect of berberine and (C/K)-bicuculline isolated from Corydalis

chaerophylla on spore germination of some fungi, Folia Microbiol., (Praha). 2002, 2, 161–165.

10. Becke, A.D., Perspective on "Density functional thermochemistry. III. The role of exact exchange. J. Chem Phys.,1993, 98, 5648-5652.
11. Bentley, K.W. b-Phenylethylamines and the isoquinoline alkaloids. Nat. Prod. Rep.,2000, 17, 247–268.
12. Bentley, K.W. b-Phenylethylamines and the isoquinoline alkaloids., Nat. Prod. Rep., 2001, 18, 148–170.
13. Bentley, K.W. b-Phenylethylamines and the isoquinoline alkaloids. Nat. Prod. Rep.,2002, 19, 332–356.
14. Bentley, K.W. b-Phenylethylamines and the isoquinoline alkaloids. Nat. Prod. Rep., 2003, 20, 342–365.
15. Bentley, K.W. b-Phenylethylamines and the isoquinoline alkaloids., Nat. Prod. Rep., 2004, 21, 395–424.
16. Bentley, K.W. b-Phenylethylamines and the isoquinoline alkaloids. Nat. Prod. Rep., 2005, 22, 249–268.
17. Bentley, K.W. b-Phenylethylamines and the isoquinoline alkaloids. Nat. Prod. Rep., 2006, 23, 444–463.
18. Bhadra, K., Maiti, M. and Kumar G. S. DNA-binding cytotoxic alkaloids: comparative study of the energetics of binding of berberine, palmatine, and coralyne. DNA Cell Biol., 2008b, 27, 12, 675-685.
19. Bhadra, K., Maiti, M. and Kumar, G.S. Berberine–DNA complexation: New insights into the cooperative binding and energetic aspects. Biochimica et Biophysica Acta., 2008a, 1780, 1054–1061.
20. Bhadra, K., Maiti, M. and Kumar, G.S. Molecular recognition of DNA by small molecules: AT base pair specific intercalative binding of cytototoxic plant alkaloid palmatine. Biochim. et Biophy. Acta., 2007, 1770, 1071-1080.
21. Bhakuni, D.S., and Jain, S. Protoberberine alkaloids. In: Manske, R.H.F. (Ed.) The Alkaloids, 28. Academic Press, New York, 1986, 95–181.

22. Blasko, G., Cordell, G.A., Bhamarapravati, S., Beecher and Ch.W.W. Carbon-13 NMR assignments of berberine and sanguinarine. Heterocycles, 1988, 911– 916.

23. Bodenhausen, G., Freeman, R. and Turner D.L. Suppression of artifacts in two-dimensional spectroscopy. J. Magn. Reson., 1977, 27, 511-514

24. Brezova, V., Dvoranova, D and Kost alova, D. Oxygen activation by photoexcited protoberberinium alkaloids from mahonia aquifolium. Phytother. Res., 2004, 18, 640-646.

25. Braunlin, W. H., Bloomfield V.A. 1H NMR study of the base-pairing reactions of d(GGAATTCC): salt and polyamine effects on the imino proton exchange. Biochemistry, 1988 ,4, 1184–1191.

26. Braunlin, W.H., Bloomfield, V,A. 1H NMR study of the base-pairing reactions of d(GGAATTCC): salt effects on the equilibria and kinetics of strand association., Biochemistry, 1991, 3, 754–758.

27. Calladine, C.R. Mechanics of sequence-dependent stacking of bases in B-DNA. J. Mol. Biol., 1982, 161, 2, 343-352.

28. Casanovas, J., Namba, A.M., Leon, S., Aquino, G.L., da Silva, G.V., and Aleman, C. Calculated and experimental NMR chemical shifts of p-menthane-3,9-diols. A combination of molecular dynamics and quantum mechanics to determine the structure and the solvent effects. J. Org. Chem., 2001, 66, 3775-3782.

29. Celda, V., Widmer, H., Leupin, W., Chazin, W., Denny, A. and Wuthrich K. Conformational studies of d-$(AAAAATTTTT)_2$ using constraints from nuclear overhauser effects and from quantitative analysis of the cross peak fine structures in two-dimensional ^1H Nuclear Magnetic Resonance spectra. Biochemistry, 1989, 28, 1462.

30. Chaires, J. B. and Waring, M. J. Drug-nucleic acid interactions, Academic Press, 2001.

31. Chaires, J. B. Drug--DNA interactions. Curr. Opin. Struct. Biol., 1998, 8, 3, 314-320.

32. Chang, D. K and Cheng S. F. On the importance of van der Waals interaction in the groove binding of DNA with ligands: restrained molecular dynamics study. Int. J. Biol Macromol., 1996, 19, 4, 279-285.

33. Chang, Y. Li., Usami, S., Hsieb, M.T. and Jiang M. J. Effects of palmatjne on isometric force and mtracellular calcium levels of arterial smooth muscle., Life sciences, 1999, 64, 597-606.

34. Chang, Z., R.K.Y and Cheng, C.C. Tetramethoxydibenzoquinolizinium Salts. Preparation and Antileukemic Activity of Some Positional and Structural Isomers of Coralyne., Journal of Med. Chem., 1976, 19, 882-886.

35. Chen, W.H., Chan, C. L., Cai, Z., Chan, C., Luo, G..A. and Jiang, Z.H., Study on noncovalent complexes protoberberine alkaloids with double-stranded DNA by using electrospray ionization mass spectrometry. Biorg. Med. Chem. Letts., 2004, 14, 4955- 4959.

36. Chen, W. H., Pang, J. Y., Qin Y., Peng, Q., Cai, Z. and Jiang, Z. H. Synthesis of linked berberine dimers and their remarkably enhanced DNA-binding affinities. Bioorg. Med. Chem. Lett., 2005a, 15, 10, 2689-2692.

37. Chen, W.H., Qin, Y., Cai, Z., Chan, C., Luo, G.A. and Jiang, Z.H., Spectroscopic studies of cytotoxic protoberberine alkaloids binding to double-stranded DNA., Bioorg. and Med. Chem., 2005b, 13, 1859-1866.

38. Cheng, K.Y.G., Paull, K.D. and Cheng C.C. Experimental Antileukemic Agents. Coralyne, Analogs, and related Compounds. Journal of Med. Chem., 1974, 17, 3, 347-351

39. Chuang, W.C., Young, D.S., Liu, L.K. and Sheu, S.J. Liquid chromatographic-electrospray mass spectrometric analysis of Coptidis rhizoma. J. Chromatogr. A., 1996, 755, 19–26.

40. Colombo, D., Ferraboschi, P., Ronchetti, F. and Toma, L. Stereochemical analysis of the 3α- and 3 β-hydroxy metabolites of tibolone through NMR and quantum-chemical investigations. An experimental test of GIAO calculations. Magn. Reson.Chem., 2002, 40, 581-588

41. Cragg, G. and Suffness, M. Metabolism of plant-derived anticancer agents. Pharmacol. Ther., 1988, 37, 3, 425-461.

42. Cragg, G.M., Newman, D.J. and Snader, K,M. Drug discovery and development from natural plant.11th NAPRECA Symposium Book of Proceedings, Antananarivo, Madagascar, 1999, 56-69.

43. Creasy, W.A. Biochemical effects of berberine. Biochem. Pharmacol., 1979, 28, 1081–1084.

44. Creemers, G.J., Bolis, G., Gore, M., Scarfone, G., Lacave, A.J., Guastalla, J.P., Despax, R., Favalli, G., Kreinberg, R., Van Belle, S., Hudson, I., Verweij, J. and Ten Bokkel Huinink, W.W. Topotecan, an active drug in the second-line treatment of epithelial ovarian cancer: results of a large European phase II study. J. Clin. Onco., 1996, 14, 12, 3056-3061.

45. Danilov, V.I., Dailidonis, V.V., Hovorun, D.M., Kurita, N., Murayama, Y., Natsume, T., Potopalsky, A. I. and Zaika, L.A. Berberine alkaloid: Quantum chemical study of different forms by the DFT and MP2 methods. Chem. Phys. Lett., 2006, 430, 409-413.

46. Das, S., Kumar, G.S., Ray, A. and Maiti, M. Spectroscopic and thermodynamic studies on the binding of sanguinarine and berberine to triple and double helical DNA and RNA structures. J. Biom. Struc. & Dyn., 2003, 703-711.

47. Davidson, M.W., Lopp, I., Alexander, S. and Wilson, W. D. The interaction of plant alkaloids with DNA. II. Berberinium chloride.,Nucleic Acids Res., 1977, 4, 8, 2697-2712.

48. Debnath, D., Kumar, G. S. and Maiti, M. Circular dichroism studies of the structure of DNA complex with berberine. J. Biomol. Struct. Dyn., 1991, 9, 1, 61-79.

49. Debnath, D., Kumar, G. S., Nandi, R. and Maiti, M. Interaction of berberine chloride with deoxyribonucleic acids: evidence for base and sequence specificity. Indian J. Biochem. Biophys., 1989, 26, 4, 201-208.

50. Derome, A.E., Modern NMR Techniques for Chemistry Research, Elsevier, Oxford. 1987, 6.

51. Dervan, P.B. Design of sequence-specific DNA binding molecules. Science, 1986, 232, 464

52. Dickerson, R. E., Bansal, M., Calladine, C. R., Diekmann, S., Hunter, W.N., Kennard, O., Kitzing von, E., Lavery, R., Nelson, H.C.M., Olson, W. K., Saenger, W., Shakked, Z., Sklenar, H., Soumpasis, D.M., Tung, C. S., Wang, A. H. J. and Zhurkin, V.B. Definitions and Nomenclature of Nucleic Acid Structure Parameters. J. Mol. Biol., 1989, 208, 787–791.

53. Dostal, J., Man, S., Seckarova, P., Hulova, D., Necas, M., Potacek, M., Tousek, J., Dommisse, R., Van Dongen, W. and Marek, R. Berberine and coptisine free bases. J. Mol. Struct., 2004, 687, 135–142.

54. Elford, B.C. L-Glutamine influx in malaria-infected erythrocytes: a target for antimalarials. Parasitol., 1986, 2, 309–312.

55. Farnsworth, N.R., Akerele, O., Bingel, A.S., Soejarto, D.D. and Guo, Z. Medicinal plants in therapy, Bulletin of the World Health Organization. 1985, 63, 6: 965-981.

56. Favier, A., Blackledge, M., Simorre, J.P., Crouzy, S., Dabouis, V., Gueiffier, A., Marion, D. and Debouzy, J.C. Solution Structure of 2-(Pyrido [1, 2-e] purin-4-yl) amino-ethanol Intercalated in the DNA Duplex d $(CGATCG)_2$, Biochemistry, 2001, 40, 30, 8717-8726.

57. Fox, K.R. Drug-DNA interaction protocols, Humana Press, 1997.

58. Frederick, C.A., Williams, L.D., Ughetto, G., Van der Marel, G.A., Van Boom, J.H., Rich, A. and Wang, A.H.J. Structural comparison of anticancer drug-DNA complexes: adriamycin and daunomycin. Biochemistry, 1990, 29, 10: 2538-2549.

59. Frisch, M.J., Trucks, G.W., Schlegel, H.B., Scuseria, G.E., Robb, M.A., Cheeseman, J.R., Zakrzewski, V.G., Montgomery Jr, J,A., Stratmann, R.E. and Burant, J.C.. 1998. Gaussian 98, Revision A. 7, Gaussian. Inc., Pittsburgh, *PA*.

60. Fukuda, K., Hibiya, Y., Mutoh, M., Koshiji, M., Akao, S. and Fujiwarw, H. Inhibition by berberine of cyclooxygenase-2 transcriptional activity in human colon cancer cells. J. Ethnopharmacol., 1999, 2 227–233.

61. Fukuda, K., Hibiya,Y., Mutoh, M., Koshiji, M., Akao, S. and Fujiwarw, H. Inhibition of activator protein 1 activity by berberine in human hepatoma cells. Planta. Med., 1999, 65 ,4, 381–383.

62. Gatto, B., Sanders, M. M., Yu, C., Wu, H. Y., Makhey, D., LaVoie, E. J. and Liu, L. Identification of topoisomerase I as the cytotoxic target of the protoberberine alkaloid coralyne. Cancer Res., 1996, 56, 12, 2795-2800.

63. Gharbo, S.A., Beal, J.L., Doskotch, W. and Mitscher, L.A. Alkaloids of Thalictrum. XIV. Isolation of alkaloids having antimicrobial activity from Thalictrum polygamum.. Lloydia., 1973, 36, 349–351.

64. Giri, P. and Kumar, G.S. Self-structure induction in single stranded poly(A) by small molecules: Studies on DNA intercalators, partial intercalators and groove binding molecules. Arch. Biochem & Biophy., 2008, 474, 183- 192.

65. Giri, P., Hossain M. and Kumar, G.S. Molecular aspects on the specific interaction of cytotoxic plant alkaloid palmatine to poly (A). Int. J. Bio. Macromol., 2006b, 39, 210-221.

66. Giri, P., Hossain M. and Kumar, G.S. RNA specific molecules: Cytotoxic plant alkaloid palmatine binds strongly to poly (A). Bioorg. and Med. Chem. Letts., 2006a, 16, 2364-2368.

67. Gochin, M., Zon, G. and James, T. L. Two dimensional COSY and two dimensional NOE spectroscopy of $d(AC)_4$, $d(GT)_4$: Extraction of structural constraints. Biochemistry, 1990, 29, 11161.

68. Gorenstein, D.G. and Kar, D. ^{31}P chemical shifts in phosphate diester monoanions. Bond angle and torsional angle effects. Biochem Biophys Res Commun., 1975, 65, 3, 1073-1080.

69. Gorenstein, D.G., Luxon, B.A. and Findlay, J.B. The torsional potential for phosphate diesters. The effect of geometry optimization in CNDO and ab initio molecular orbital calculations. Biochimica et biophysica acta., 1977, 475, 1, 184.

70. Gorenstein, D.G., Lai, K. and Shah, D.O. ^{31}P and two-dimensional $^{31}P/^{1}H$ correlated NMR spectra of Duplex d (Ap [17O] Gp [18O] Cp [16O] T) and assignment of ^{31}P signals in d $(ApGpCpT)_2$-actinomycin D complex. Biochemistry, 1984 23, 26, 6717-6723.

71. Gorenstein D. G. ^{31}P NMR of DNA. Methods in enzymology, 1992, 211, 254-286.

72. Gorenstein D. G. Conformation and dynamics of DNA and protein-DNA\ complexes by 31P NMR. Chem. Rev., 1994, 94, 5, 1315-1338.

73. Gronenborn A. M. and Clore G.M. Investigation of the solution structure of short nucleic acid fragments by means of nuclear overhauser enhancements measurements. Prog. NMR Spec.,1985, 17, 1.

74. Gunther U. L., Ludwig C. and Ruterjans H. NMRLAB-Advanced NMR data processing in MATLAB. J. Magn. Reson., 2000, 145, 201.

75. Haberlein, H., Meibner., O, and Halbsguth, C. Positive cooperation of protoberberine Type 2 Alkaloids from corydalis cava on the GABA Binding site. Planta Med., 2003, 69, 305-309.

76. Hayashi, K., Minod, K., Nagaoka, Y., Hayashia T. and Uesatob, S. Antiviral activity of berberine and related compounds against human cytomegalovirus. Bioorg. & Med. Chem. Lett.,2007, 1562–1564.

77. Kazutaka, H. and Toru, H. The microenvironment of DNA switches the activity of singlet oxygen generation photosensitized by berberine and palmatine. Photochemistry and photobiology, 2008, 84, 202-208.

78. Ho, Y.T., Yang, J.S., Lu, C.C., Chiang, J.H., Li, T.C., Lind, J. J. Lai, K.C., Liao, C.L., Lin, J.G and Chung, J.G. Berberine inhibits human tongue squamous carcinoma cancer tumor growth in a murine xenograft model. Phytomedicine, 2009.

79. Hosur R.V., Ravikumar M., Roy K.B., Tan-Zu-Kun, Miles H.T. and Govil G. In "Magnetic resonance in biology and medicine". (Eds. Govil G., Khetrapal C.L. and Saran A.) Tata Mcgraw Hill, New Delhi, 1985, 305.

80. Hosur, R.V., Ravikumar M., Chary K.V.R., Sheth A., Govil G., Tan-Zu-Kunn and Miles H.T. solution structure of d-GAATTCGCAATTC by 2D NMR: A new approach to determination of sugar geometries in DNA segments. FEBS Letts., 1986, 205, 71.

81. Hosur, R. V., Govil, G. and Miles, H. T. Application of two-dimensional NMR spectroscopy in the determination of solution conformation of nucleic acids. Magnetic Resonance in Chemistry, 1988, 26, 10.

82. Hsieh, M.T., Su, S.H., Tsai, H.Y., Peng, W.H., Hsieh, C.C and Chen, C.F. Effects of Palmatine on Motor Activity and the Concentration of Central

Monoamines and Its Metabolites in Rats. The Jap. J. Pharma., 1993, 61, 1-5.

83. Huang, J., Lee, K.S and Hurley, S. J., Nuclear magnetic resonance spectral analysis and molecular properties of berberine., Int. J. Quantum Chem., 2005, 105, 396.

84. Huang, W.M., Wu, Z.D. and Gan, Y.Q. Effects of berberine on ischemic ventricular arrhythmia, Zhonghua Xin Xue Guan Bing Za Zhi (Chinese Journal of Cardiovascular diseases)., 1989, 17,300–301, 319.

85. Hwang, B.Y., Roberts, S.K., Chadwick, L.R., Wu, C.D. and Kinghorn, A.D., Antimicrobial constituents from goldenseal (the Rhizomes of Hydrastis canadensis) against selected oral pathogens Planta Med., 2003, 7, 623–627.

86. Hwang, J.W., Kuo, H.C., Tseng, T.H., Liu, J. Y. and Chu, C.Y. Berberine induces apoptosis through a mitochondria/caspases pathway in human hepatoma cells. Arch. Toxicol., 2006, 80, 62-73.

87. Iizuka, N., Miyamoto, K., Okita, K., Tangoku, A., Hayashi, H., Yosino, S., Abe, T., Morioka, T., Hazama, S. and Oka, M. Inhibitory effect of Coptidis Rhizoma and berberine on the proliferation of human esophageal cancer cell lines. Cancer Lett., 2000,148, 1, 19-25.

88. Inbaraj, J. J., Kukielczak, B. M., Bilski, P., Sandvik, S. L. and Chignell, C. F. Photochemistry and Photocytotoxicity of Alkaloids from *Goldenseal* (*Hydrastis canadensis L.*) 1. Berberine. Chem. Res. Toxicol., 2001, 14, 1529-1534

89. Islam, M. M. and Kumar G. S. RNA targeting by small molecule alkaloids: Studies on the binding of berberine and palmatine to polyribonucleotides and comparison to ethidium. J. Mol. Structure., 2008, 875, 382-391

90. Islam, M. M., Sinha., R., and Kumar G. S. RNA binding small molecules: Studies on t-RNA binding by cytotoxic plant alkaloids berberine, palmatine and the comparison to ethidium. Biophysical Chemistry, 2007, 125, 508-520.

91. Iwasa, K., Kamigauchi, M., Sugiura, M., and Nanba, H., Antimicrobial activity of some 13-alkyl substituted protoberberinium salts. Planta Med., 1997, 63, 196–198.

92. Iwasa, K., Moriyasu, M., Nader, B. Fungicidal and herbicidal activities of berberine related alkaloids. Biosci. Biotechnol. Biochem., 2000, 64, 1998–2000.

93. Iwasa, K., Moriyasu, M., Tachibana, Y., Kim, H.S., Wataya, Y.S., Wiegrebe, W., Bastow, K.F., Cosentino, L.M., Kozukab M., and Leeb, K.H. Simple Isoquinoline and Benzylisoquinoline Alkaloids as Potential Antimicrobial, Antimalarial, Cytotoxic, and Anti-HIV Agents. Bioorg. & Med. Chem., 2001, 2871–2884

94. Iwasa, K., Nishiyama, Y., Ichimaru, M., Moriyasu, M., Kim, H.S., Wataya, Y., Yamori, T., Takashi, T., Lee, D.U. Structure-activity relationships of quaternary protoberberine alkaloids having an antimalarial activity. Eur. J. Med. Chem., 1999, 34, 1077–1083.

95. Iwasa, K., Kim, H. S., Wataya, Y. and Lee, D. U. 1998a. Antimalarial activity and structure–activity relationships of protoberberine alkaloids. Eur. J. Med.Chem., 1998, 33, 65.

96. Jain, A., Akanchha, S. and Rajeswari, M. R. Stabilization of purine motif DNA triplex by a tetrapeptide from the binding domain of HMGBI protein. Biochimie., 2005, 87, 8, 781-790.

97. Jansen, R.H.A.M., Lousberg, J.J.C., Wijkens, P., Kruk, C. and Theuns, H.G. Assigment of ^{1}H and ^{13}C NMR resonances of some isoquinoline alkaloids. Phytochemistry, 1989, 28, 2833–2839.

98. Jantova, S., Cipak L., Cernakova and M. Kostalova D. Effect of berberine on proliferation, cell cycle and apoptosis in HeLa and L1210 cells. J. Pharmacy & Pharmacology., 2003, 55, 1143-1149.

99. Jantova, S., Cipak, L. and Letasiova, S. Berberine induces apoptosis through a mitochondrial/caspase pathway in human promonocytic U937 cells. Toxicol In Vitro., 2007, 21, 25-31.

100. Jeener J. Paper presented at the AMPERE International summer school, Borsko,Polje, Yugoslavia, 1971.

101. Jeon, W.Y., Jung, W.J., Kang, M., Chung, K, I. and Lee, W. NMR studies on antitumor drug candidates berberine and berberrubin. Bull. Korean Chem. Soc.,2002, 23, 391-394.

102. Junfen, Li., Shuang, S., and Dong, C. Study on the phosphorescence characterizations of palmatine chloride on the solid substrate and its interaction with ctDNA. Talanta., 2009, 77,1043-1049

103. Kariuki, B.M. Five salts of berberine. Acta Crystallogr. Sect. C., 1995, 51, 1234- 1240.

104. Keeler. J., and Neuhaus, D. Comparison and evaluation of methods for two-dimensional NMR spectra with absorption mode line shape. J. Magn. Reson., 1985, 63, 454.

105. Kohn, W., and Sham, L., J. Phys. Rev., 1965, 140, 1133.

106. Kirby, J.D., G.C., Warhurst, D.C., and Schiff, P. L. In vitro antiplasmodial, antiamoebic, and cytotoxic activities of some monomeric isoquinoline alkaloids. J. Nat. Prod., 2000, 63, 1638–1640.

107. Keawpradub, N., Dej-adisai, S. and Yuenyongsawad, S. Antioxidant and cytotoxic activities of Thai medicinal plants named Khaminkhrues: *Arcangelisisa flave, coscinium blumeanum* and *fibraurea tinctoria*. J. Sci. Technol., 2005, 27, 455-467.

108. Kettmann, V., Kosfalova, D., Jantova, S., Cernakova, M. and Drimal, J. In vitro cytotoxicity of berberine against HeLa and L1210 cancer cell lines. Pharmazie.,2004, 59, 7, 548-551.

109. Kelland, L.R., Flavopiridol, the first cyclin-dependent kinase inhibitor to enter the clinic: current status. Expert Opin. Investig. Drugs., 2000, 9, 12, 2903-2911.

110. Khetrapal, C.L. and Diehl, P. Nuclear magnetic resonance studies in lyotropic liquid crystals, 1975, Springer.

111. Kim, E., Yoo, S., Yi, K.Y., Lee, S., Noh, J., Jung, Y.S., Kom, E. Neony,N. Design, syntheses and biological evaluations of nonpeptidic caspase 3 inhibitors. Bull. Kor. Chem. Soc., 2002, 23, 1003–1010.

112. Kim, S.A., Kwon, Y., Muller, M.T., Chung, I.K. Induction of topoisomerase II-mediated DNA cleavage by a protoberberine alkaloid, berberrubine. Biochemistry, 1998, 37, 16316–16324.

113. Kluza, J., Baldeyrou, B., Colson, P., Rasoanaivo, P., Mambu, L., Frappier, F and Bailly, C., Cytotoxicity and DNA binding properties of the plant alkaloid burasaine., European J. Pharma. Sci., 2003, 20, 383- 391.

114. Kotovych, G., Lown, J. W. and Tong, J. P. High-field 1H and 31P NMR studies on the binding of the anticancer agent mitoxantrone to d [CpGpApTpCpG] $_2$. J. of biomol. struc. & dynam., 1986, 4, 1 111.

115. Krishnan, P. and Bastow, K. F. The 9-position in berberine analogs is an important determinant of DNA topoisomerase II inhibition. Anticancer Drug Des., 2000, 15, 4, 255-264.

116. Kumar, C. V. and Asuncion. E.H. DNA binding studies and site selective fluorescence sensitization of an anthryl probe. J. Am. Chem. Soc., 1993, 115, 8547-8553.

117. Kumar, G.S., Das, S., Bhadra K., and Maiti, M. Protonated Forms of Poly[d(G-C)] and Poly(dG).poly(dC) and Their Interaction with Berberine. Bioorg. Med. Chem., 2003, 11, 4861-4870.

118. Kunwar, A.C. Spectroscopic Applications of Liquid Crystals. Liquid crystals: applications and uses. 1991, 225.

119. Kuo. C.L., Chou, C.C. and Yung, Y.M. B. Berberine complexes with DNA in the berberine-induced apoptosis inhuman leukemic HL- 60 cells. Cancer lett., 1995, 93, 193-200.

120. Kupka, T., Pasterna, G., Jaworska, M., Karali, A., and Dias, P. GIAO NMR calculations for carbazole and its *N*-methyl and *N*-ethyl derivatives. Comparison of theoretical and experimental 13 C chemical shifts. Magn. Reson. Chem., 2000, 38(3), 149-155.

121. Labauowski, J. and Andzeln, J. Density Functional Methods in Chemistry, Springer-Verlag, New york, 1991.

122. Lampert, H., Mikenda, W., Karpfen, A. and Kahlig, H. NMR shieldings in benzoyl and 2-hydroxybenzoyl compounds. Experimental versus GIAO calculated data. J. Phys. Chem. A., 1997, 101, 50: 9610-9617.

123. Lancelot G. and Paquet F. In: G.A. Webb, Editor, Annual Reports on NMR Spectroscopy, Elsevier Science Ltd., 2003, 170.

124. Langlois d'Estaintot, B., Gallois, B., Brown, T. and Hunter, W.N. The molecular structure of a 4'-epiadriamycin complex with d(TGATCA) at 1.7A resolution: comparison with the structure of 4'-epiadriamycin d(TGTACA) and d(CGATCG) complexes. Nucleic Acids Res .,1992. 20, 14: 3561-3566.

125. Lau, C.W., Yao, X. Q., Chen, Z. Y., Ko, W. H. and Huang, Y. Cardiovascular actions of berberine., Cardiovasc. Drug Rev., 2001, 3, 234–244.

126. Lavery, R. and Sklenar, J. Defining the Structure of Irregular Nucleic Acids: Conventions and Principles. J. Biomol. Struct. Dyn., 1989, 6, 655.

127. Lavery, R., Sklenar, H., Zakrzewska, K. and Pullman, B. The flexibility of the nucleic acids:(II). The calculation of internal energy and applications to mononucleotide repeat DNA. J. Biomol. Struct.Dyn., 1986, 3, 5: 989-1014.

128. Lee C., Yang W. and Parr R. G. Development of the Colle-Salvetti correlation-energy formula into a functional of the electron density. Phys. Rev. B., 1988, 37, 785-789.

129. Lee, J.S., Latimer, J.P.L and Hampel, K. J. Coralyne Binds Tightly to Both T.A.T and C.G.C+-Containing DNA Triplexes. Biochemistry, 1993, 32, 5591-5597.

130. Leonard, G.A., Brown, T. and Hunter, W.N. Anthracycline binding to DNA. High-resolution structure of d(TGTACA) complexed with 4'-epiadriamycin. Eur. J. Biochem ., 1992, 204, 1: 69-74.

131. Lerman L. S. Structural considerations in the interaction of DNA with acridines. J. Mol. Biol., 1961, 3, 18–30.

132. Letasiova , S., Jantova, S., Horvathova, M., and Lakatos, B. Toxicity and apoptosis induced by berberine – a potential anticancer drug. Biologia., 2005, 60, 97–100.

133. Letasiova, S., Jantova, S., Cipak, L. and Muckova, M . Berberine-antiproliferative activity in vitro and induction of apoptosis/necrosis of the U937 and B16 cells. Cancer Lett., 2006, 239, 2, 254-262.

134. Levitt, M., Hirshberg, M., Shraon, R. and Daggett, V. Potential energy function and parameters for simulations of the molecular dynamics of proteins and nucleic acids in solution. Comp. Phys. ommun., 1995, 91, 215.

135. Li T. K., Bathory E., LaVoie E. J., Srinivasan A. R., Olson W. K., Sauers R. R., Liu L. F. and Pilch D. S. Human topoisomerase I poisoning by protoberberines: potential roles for both drug-DNA and drug-enzyme interactions. Biochemistry, 2000, 39, 24: 7107-7116.

136. Li, C.Y., Lu, H.J., Lin, C.H. and Wu, T.S. A rapid and simple determination of protoberberine alkaloids in cortex phellodendri by 1H NMR and its application for quality control of commercial traditional Chinese medicine prescriptions. J. Pharm. Biomed. Anal,,2006, 40, 173-178.

137. Liu, L.F., Desai, S.D., Li, T.K., Mao, Y., Sun, M. and Sim, S.P. Mechanism of action of camptothecin. Ann. N. Y. Acad. Sci., 2000, 922: 1-10.

138. Lown, J.W. and Hanstock, C.C. High field 1H-NMR analysis of the 1: 1 intercalation complex of the antitumor agent mitoxantrone and the DNA duplex [d (CpGpCpG)]. J. Biomol. Struc.t Dyn., 1985 2, 6: 1097.

139. Long, Y,H., Bai, L,P., Qin, Y., Pang, J.Y., Chen, W.H., Cai, Z., Xu, Z.L. and Jiang, Z.H. Spacer length and attaching position-dependent binding of synthesized protoberberine dimers to double-stranded DNA. Bioorg. Med. Chem., 2006, 14, 13: 4670-4676.

140. Mahajan, V. M., Sharme, A. and Rattan, A. Antimycotic activity of berberine sulphate: an alkaloid from an Indian medicinal herb, Sabouraudia., 1982, 1, 79–81.

141. Maiti, M. and Chatterjee, A. Production of singlet oxygen by sanguinarine and Berberine. Current science,1995, 68, 7: 734-736.

142. Maiti, M. and Chaudhuri, K. Interaction of berberine chloride with naturally occurring deoxyribonucleic acids. Indian J. Biochem. Biophys., 1981, 8, 4: 245-250.

143. Maiti, M. and Kumar, G.S. Molecular aspects on the interaction of protoberberine, benzophenanthridine, and aristolochia group of alkaloids with nucleic acid structures and biological perspectives. Med. Res. Rev., 2007, 27, 5: 649-695.

144. Makhey, D., Gatto, B., Yu, C., Liu, A., Liu, L.F. and LaVoie, E.J. Coralyne and related compounds as mammalian topoisomerase I and topoisomerase II poisons. Bioorg. Med. Chem., 1996, 4, 6: 781-791.

145. Man, S., Dosta l, J., Necas, M., Z ak, Z., Potacek, M. Berberine and coptisine in liquid ammonia.. Heterocyclic Commun., 2001a., 7, 243–248.

146. Man, S., Potacek, M., Necas, M., Zak, Z., Dostal, J. Molecular and crystal structures of three berberine derivatives. Molecules., 2001b, 6, 433–441.

147. Marek, R., Seckarova, P., Hulova, D., Marek, J., Dostal J. and Sklenar, V. J. Palmatine and berberine isolation artifacts. J. Nat. Prod., 2003, 66, 481-486.

148. Marek, J., Hulova, D., Dostal, J., Marek, R. Berberine formate–succinic acid (1/1). Acta Crystallogr. Sect. C., 2003a, 59, 583–585

149. Marek, R., Humpa, O., Dostal, J., Slavık, J., Sklenar, V. 15N NMR study of isoquinoline alkaloids. Magn. Reson. Chem., 1999, 37, 195–202.

150. Marek, R., Lycka, A. 15N NMR spectroscopy in structural analysis. Curr. Org. Chem., 2002, 6, 35–66.

151. Marek, R., Marek, J., Dosta, J., Taborska, E., Slavık, J. Dommisse, R. Isoquinoline alkaloids: a 15N NMR and X-ray study. Part 2. Magn. Reson. Chem., 2002, 40, 687–692.

152. Marion, D. and Wuthrich, K. Application of phase sensitive two-dimensional correlated spectroscopy (COSY) for measurement of 1H-1H spin coupling constant in proteins. Biochem. Biophys. Res. Comm., 1983, 113, 967.

153. Mazzini, S., Mondelli, R. and Ragg, E. Structure and dynamics of intercalation complexes of anthracyclines with d $(CGATCG)_2$ and d

(CGTACG)$_2$. 2D-^{1}H and ^{31}P NMR investigations. J. Chem. Soc. Perkin Trans. 2, 1998, 9: 1983-1991.

154. Mazzini, S., Bellucci, C. M. and Mondelli, R. Mode of binding of the cytotoxic alkaloid berberine with the double helix oligonucleotide D(AAGAATTCTT)$_2$. Bioorg. Med. Chem., 2003, 11, 505-514.

155. Miertus, M., Scrocco, E. And Tomasi., J. Chem. Phys. 1981, 55, 117.

156. Miertus, S., Tomasi., J. Chem. Phys., 1982, 65, 239.

157. Nakamoto, K., Sadamori, S. and Hamada, T. Effects of crude drugs and berberine hydrochloride on the activities of fungi. J. Prosthet. Dent., 1990, 6, 691–694.

158. Nandi, R., Debnath, D. and Maiti, M. Interactions of berberine with poly(A) and tRNA. Biochim. Biophys. Acta., 1990, 1049, 3: 339-342.

159. Neidle, S., DNA minor-groove recognition by small molecules. Natural product reports, 2001, 18, 3: 291-309.

160. Noble, R,L. The discovery of the vinca alkaloids--chemotherapeutic agents against cancer. Biochem. Cell Biol., 1990, 68, 12: 1344-1351.

161. Nunn, C.M., Van Meervelt, L., Zhang, S., Moore, M.H. and Kennard, O. DNA-drug interactions: the crystal structures of d (TGTACA) and d (TGATCA) complexed with daunomycin. J. Mol. Biol., 1991, 222, 2: 167-177.

162. Okunade, A. L., Hufford, C. D., Richardson, M. D., Petterson, J.R. and Clark, A. M. Antimicrobial properties of alkaloids from Xanthoriza simplicissima. J. Pharm. Sci., 1994, 83, 404–406.

163. Orfila, L., Rodrı´guez, M., Colman, T., Hasegawa, M., Merentes, E. and Arvelo. F. Structural modification of berberine alkaloids in relation to cytotoxic activity in vitro. J. Ethnopharmacology. 2000, 71, 449-456.

164. Ott, J. and Eckstein, F. Phosphorus-31 NMR spectral analysis of the dodecamer d (CGCGAATTCGCG). Biochemistry, 1985, 24, 10: 2530-2535.

165. Pal, S., Kumar, G. S., Debnath, D. and Maiti, M. Interaction of the antitumour alkaloid coralyne with duplex deoxyribonucleic acid structures:

spectroscopic and viscometric studies. Indian J. Biochem. Biophys., 1998, 35, 6: 321-332.

166. Pang, J.Y., Qin, Y., Chen, W.H., Luo, G.A. and Jiang, Z.H. Synthesis and DNA-binding affinities of monomodified berberines. Bioorg. & Med. Chem., 2005, 13, 20, 5835-5840.

167. Parr R.G. and Yang W. Density functional theory of Atoms and molecules, Oxford University Press Inc., New York, 1989.

168. Pardi, A., Walker, R., Rapaport, H., Wider, G. and Wüthrich, K. Sequential assignments for the 1 H and 31 P atoms in the backbone of oligonucleotides by two-dimensional nuclear magnetic resonance. J. Am. Chem. Soc., 1983, 105: 1652–165

169. Park, H.S., Kim, E.H., Kang, M. R., Chung, I. K., Cheong, C. and Lee, W. Spectroscopic studies of protoberberines with the Deoxyoligonucleotide d(GCCGTCGTTTTACA)$_2$. Bull. Korean Chem. Soc., 2004a, 25, 1559-1563

170. Park, H.S., Kim, E.H., Sung, Y.H., Kang, M. R., Chung, I. K., Cheong, C. and Lee, W. DNA Binding Mode of the Isoquinoline Alkaloid Berberine with the deoxyoligonucleotide d(GCCGTCGTTTTACA)$_2$. Bull. Korean Chem. Soc., 2004b, 25, 539-544.

171. Patel, D.J. Peptide antibiotic-dinucleotide interactions. Nuclear magnetic resonance investigations of complex formation between actinomycin D and d-pGpC in aqueous solution. Biochemistry, 1974, 13, 11: 2388-2395.

172. Patel, D.J. and Canuel, L.L. Ethidium bromide-(dC-dG-dC-dG)$_2$ Complex in Solution: Intercalation and Sequence Specificity of Drug Binding at the Tetranucleotide Duplex Level. Proc. Na.t Acad. Sci. U.S.A., 1976, 73, 10: 3343-3347.

173. Patel, D.J. d-CpCpGpG and d-GpGpCpC self-complementary duplexes: NMR studies of the helix-coil transition. Biopolymers, 1977, 16, 8: 1635-1656.

174. Patel, D.J. Helix-coil transition of the dG-dC-dG-dC self-complementary duplex and complex formation with daunomycin in solution. Biopolymers, 1979, 18, 3: 553-569.

175. Patel, D.J., Kozlowski, S.A., Marky, L.A., Broka, C., Rice, J.A., Itakura, K. and Breslauer, K.J. Premelting and melting transitions in the d(CGCGAATTCGCG) self-complementary duplex in solution. Biochemistry, 1982, 21, 3: 428-436.

176. Pavelka, S., and Smeikal, E. The fluorescence properties of protoberberine and tetrahydroprotoberberine alkaloids. Collect.Czech.Chem. Commun., 1976, 41, 3157–3169.

177. Phillips, D.R. and Roberts, G.C.K. Proton nuclear magnetic resonance study of the self- complementary hexanucleotide d-$(pTpA)_3$ and its interaction with daunomycin. Biochemistry, 1980, 19, 4795.

178. Pilch, D.S., Yu, C., Makhey, D., La Voie, E.J., Srinivasan, A.R., Olson, W.K., Sauers, R.R., Breslauer, K.J., Geacintov, N. E and Liu, L.F. Minor gorrve-directed and intercalative ligand –DNA interactions in the poisoning of human DNA Topoisomerase I by protoberberine analogs. Biochemistry, 1997, 36, 12542-12553.

179. Piantini, U., Sorensen, O.W. and Ernst, R.R. Multiple quantum filters for elucidating NMR networks. J. Am. Chem. Soc., 1982, 104, 6800.

180. Petersheim, M., & Turner, D. H. Base-stacking and base-pairing contributions to helix stability: thermodynamics of double-helix formation with CCGG, CCGGp, CCGGAp, ACCGGp, CCGGUp, and ACCGGUp. Biochemistry, 1983, 22, 256-263.

181. Pullay, P. and Hinton, J. F. Encyclopedia of Nuclear Magnetic Resonance, Willey, New York., 1995, 4334.

182. Qin, Y., Pang, J.Y., Chen, W.H., Cai, Z. and Jiang, Z.H. Synthesis, DNA-binding affinities, and binding mode of berberine dimers. Bioorg. Med. Chem., 2006, 14, 1: 25-32.

183. Qin, Y., Pang, J.Y., Chen, W.H., Zhao, Z.Z., Liu, L. and Jiang, Z.H. Inhibition of DNA topoisomerase I by natural and synthetic mono- and dimeric protoberberine alkaloids. Chem. Biodivers., 2007b, 4, 3: 481-487.

184. Qin, Y., Chen, W.H., Pang, J., Zhaoa, Z.Z, Liu, L and Jiang, Z. H. DNA-Binding Affinities and Sequence Specificities of protoberberine alkaloids

and their demethylated derivatives: a comparative study. Chem. Biodivers., 2007, 4, 2, 145-153.

185. Qin, Y., Pang, J.Y., Chen, W.H., Cai, Z., Jiang, Z.H. Synthesis, DNA-binding affinities, and binding mode of berberine dimers. Bioorg. Med. Chem., 2006. 14, 25–32.

186. Ragg, E., Mondelli, R., Battistini, C., Garbesi, A. and Colonna, F,P. 31P NMR study of daunorubicin-d (CGTACG) complex in solution., Evidence of the intercalation sites. FEBS letters ., 1988, 236, 1: 231.

187. Rajeshwari, M. R. Tryptophan Intercalation in G, C containing Polynucleotides: Z to B conversion of Poly [d(G-5MC)] in low salt induced by a tetrapeptide. J. Biomol. Struct. & Dyn., 1996, 14, 25-30.

188. Redfield, A.G., Kunj, S. and Ralph, E.K. Quadrature fourier NMR detection, simple multiplex for dual detection and discussion. J. Magn. Reson., 1975, 19, 116.

189. Reid, B.R., Banks, K., Flynn, P. and Nerdal, W. NMR distance measurement in DNA duplex: Sugar and bases have the same correlation times. Biochemistry, 1989, 28, 10001–10007.

190. Roche C. J., Berkowitz D., Sulikowski, G.A., Danishefsky, S.J. and Crothers D.M. Binding affinity and site selectivity of daunomycin analogues. Biochemistry, 1994, 33, 936.

191. Sanders, M.M., Liu, A.A., Li, T.K., Wu, H.Y., Desai, S.D., Mao, Y., Rubin, E.H., Lavoie, E.J., Makhey, D. and Liu, L.F. Selective cytotoxicity of topoisomerase-directed protoberberines against glioblastoma cells. Biochemical pharmacology, 1998, 56, 1157-1166.

192. Saran, K. and Srivastava, S. 1H NMR investigation of the interaction of berberine and sanguinary with DNA. Indian J. Biochem. Biophys., 1995, 32, 74-77.

193. Szeto. S., Yow, C.M.N., Fung, K.W. Characterization of Berberine on Human Cancer Cells in Culture. Turk. J. Med. Sci., 2002, 32, 363-368.

194. Schmeller, T., Bruning, L.B. and Wink, M. Biochemical activities of berberine, palmatine, and sanguinarine mediating chemical defence against microorganism and herbivores. Phytochemistry, 1997, 44, 257-266.

195. Schroeder, S.A., Roongta, V., Fu, J,M., Jones, C.R. and Gorenstein, D.G. Sequence-dependent variations in the phosphorus-31 NMR spectra and backbone torsional angles of wild-type and mutant lac operator fragments. Biochemistry, 1989, 28, 21: 8292-8303.

196. Searle, M.S., Hall, J.G., Denny, W.A. and Wakelin, L.P.G. NMR studies of the interaction of the antibiotic nogalamycin with the hexadeoxyribonucleotide duplex d (5'-GCATGC) $_2$. Biochemistry, 1988, 27, 12: 4340-4349.

197. Sethi, M .L. Enzyme inhibition VI: inhibition of reverse transcriptase activity by protoberberine alkaloids and structure–activity relationships. J. Pharm. Sci., 1983, 72, 538–541.

198. Shafer, R.H. Spectroscopic studies of the interaction of daunomycin with transfer RNA. Biochemical pharmacology, 1977, 26, 18: 1729.

199. Shen, Y.J. Chinese Pharmacology, Shanghai Science and Technology Publishing Company, 1997, 50–52.

200. Shigeta, K., Ootaki, K., Tatemoto, H., Nakanishi, T., Inada, A. and Muto, N. Potentiation of nerver growth factor- induced neurite outgrowth in PC12 cells by a coptidis rhizome extract and protoberberine alkaloids. Biosci. Biotechnol. Biochem., 2002, 6(11), 2491-2494.

201. Letasiova, S., Jantova, S., Cipak, L. Muckova, M. Berberine—antiproliferative activity in vitro and induction of apoptosis/necrosis of the U937 and B16 cells. Cancer letts., 2006, 239, 254-262.

202. Singh, M.P., Joseph, T., Kumar S., Bathini, Y. and Lown, J. W. Synthesis and Sequence –Specific DNA binding of a Topoisomerase Inhibitory Analog of Hoechst 33258 designed for altered base and sequence recognition. Chem. Res. Toxicol., 1992, 5, 597-607.

203. Singh, J. and Kakkar, P. Antihyperglycemic and antioxidant effect of *Berberis aristata* root extract and its role in regulating carbohydrate metabolism in diabetic rats. J. Ethnopharmacology., 2009, 123, 22-26

204. Sinha, R., Islam, M.M., Bhadra, K., Kumar, G.S., Banerjee, A. and Maiti, M. The binding of DNA intercalating and non-intercalating compounds to

A-form and protonated form of poly(rC).poly(rG): Spectroscopic and viscometric study. Bioorg. and Med. Chem., 2006, 14, 800-814.

205. Slaninova, I., Taborska, E., Bochorakova, H., Slanina, J. Interaction of benzo[c]phenanthridine and protoberberine alkaloids with animal and yeast cells. Cell Biol. Toxicol., 2001, 17, 51–63.

206. Slobodnıkova, L., Kostalova, D., Labudova, D., Kotulova, D., Kettmann,V. Antimicrobial activity of Mahonia aquifolium crude extract and its major isolated alkaloids. Phytother. Res., 2004, 18, 674–676.

207. Sriwilaijareon, N., Petmitr, S., Mutirangura, A., Ponglikitmogkol, M., Wilairat, P. Stage specificity of Plasmodium falciparum telomerase and its inhibition by berberine. Parasitol. Int., 2002, 51, 99–103.

208. States, D.J., Haberkorn, R.A. and Reuben, D.J. A two-dimensional overhauser experiment with pure absorption phase in four quadrants. J. Magn. Reson., 1982, 48, 286.

209. Stratmann, J.C., Burant, S., Dapprich, J.M., Millam, A.D., Daniels, K.N., Kudin, M.C., Strain, O., Farkas, J., Tomasi, V., Barone, M., Cossi, R., Cammi, B., Mennucci, C., Pomelli, C., Adamo, S., Clifford, J.Ochterski, G.A. Petersson, P.Y. Ayala, Q. Cui, K. Morokuma, NRega, P. Salvador, J.J. Dannenberg, D.K. Malick, A.D. Rabuck, K. Raghavachari, J.B. Foresman, J. Cioslowski, J.V. Ortiz, A.G. Baboul, B.B. Stefanov, G. Liu, A. Liashenko, P. Piskorz, I. Komaromi, R.Gomperts, R.L. Martin, D.J. Fox, T. Keith, M.A. Al-Laham, C.Y. Peng, A. Nanayakkara, M. Challacombe, P.M. W. Gill, B. Johnson,W. Chen, M.W. Wong, J.L. Andres, C. Gonzalez, M. Head-Gordon, E.S. Replogle, J.A. Pople. Gaussian 98 Revision .Gaussian, Inc.,Pittsburgh, 1998, Revision 03.

210. Sundaralingam, M. Stereochemistry of nucleic acids and their constituents. Allowed and preferred conformations of nucleosides, nucleoside mono–, di–, tri–, tetraphosphates, nucleic acids and polynucleotides. Biopolymers, 1969, 7, 821– 860.

211. Sung-Won, Ha., Tetsuo, A. and Raghuvansh, K. Distinctive influence of two hexafluoro solvents on the structural stabilization of Bombyx mori silk

fibroin protein and its derived peptides: 13C NMR and CD studies. Biomacromolecules, 2006, 7(1):18-23.

212. Tabernero, L., Bella, J. and Aleman, C. Hydrogen bond geometry in DNA-minor groove binding drug complexes. Nucleic Acids Res., 1996,24, 17: 3458-3466.

213. Tai, Y.H., Feser, J. F., Marnane, W. G., and Desjeux, J. F. Antisecretory effects of berberine in rat ileum. Am. J. Physiol., 1981, 3 253–258.

214. Takase, H., Yamamoto, K., Ito, K. and Yumioka, E. Pharmacological studies on antidiarrheal effects of berberine and geranii herba. Nippon Yakurigaku Zasshi., 1993, 2, 101–112.

215. Tous˘ek, J., Dommisse, R., Van Dongen, W., Marek, R. Berberine and coptisine free bases. J. Mol. Struct., 2004, 687, 135–142

216. Vennerstrom, J.L., Klayman, D.L. Protoberberine alkaloids as antimalarials. J. Med. Chem., 1988, 31, 1084–1087.

217. Wafo, P., Nyasse, B. and Fontaine, C. A. 7,8-dihydro-8-hydroxypalmatine from *Enantia chlorantha.* Phytochemisty, 1999, 50, 279-281.

218. Wang, A. H. J., Ughetto, G., Quigley, G. J., and Rich, A. Interaction between anthracycline antibiotic and DNA: Molecular structure of daunomycin complexed to d–CpGpTpApCpG at 1.2 Å resolution. Biochemistry, 1987, 26, 1152–1153.

219. Wang, D., Liu, Z., Guo, M., Liu, S. Structural elucidation and identification of alkaloids in Rhizoma Coptidis by electrospray ionization tandem mass spectrometry. J. Mass Spectrom., 2004a., 39, 1356–1365.

220. Wang, F., Zhou, H.Y., Zhao, G., Fu, L.Y., Cheng, L., Chen, J.G., Yao, W. X. Inhibitory effects of berberine on ion channels of rat hepatocytes. World J. Gastroenterol., 2004b, 10, 2842–2845.

221. Wang, X. N., Han, X., Xu, L. N., Yin, L.H., Xu, Y.W., Qi, Y. and Peng, J.Y. Enhancement of apoptosis of human hepatocellularcarcinoma SMMC-7721 cells through synergy of berberine and evodiamine. Phytomedicine, 2008, 15, 1062-1068.

222. Zhang, W,Jin., Ou, T.M., Lu, Y.J., Huang, Y.Y., Wu, W.B., Huang, Z.S., Zhou, J.L., Wongc, K.Y., and Gua, L.Q. 9-Substituted berberine

derivatives as G-quadruplex stabilizing ligands in telomeric DNA. Bioorg. Med. Chem., 2007, 15, 5493-5501.

223. Wilson, W.D., Gough, A.N and Doyle, J.J. Coralyne Intercalation with DNA as a Possible Mechanism of Antileukemic Action. Journal of Med. Chem., 1976, 19, 1261-1263.

224. Wilson, W, D., and Jones, R. L. Interaction of actinomycin D, ethidium quinacrine daunorubicin, and tetralysine with DNA: ^{31}P NMR chemical shift and relaxation investigation. Nucleic Acids Res., 1982, 10, 4: 1399-1410.

225. Williams, S,D., Birch, R., Einhorn, L.H., Irwin, L., Greco, F.A. and Loehrer, P.J. Treatment of disseminated germ-cell tumors with cisplatin, bleomycin, and either vinblastine or etoposide. N Engl. J. Med., 1987, 316, 23: 1435-1440.

226. Wright, C.W., Marshall, S.J., Russell, P.F. Anderson and M.M., Phillips. In vitro antiplasmodial, antiamoebic, and cytotoxic activities of some monomeric isoquinoline alkaloids. J. Nat Prod., 2000, 63, 12: 1638-1640.

227. Wu, D. J., Yuan, J. Y., Shi, H. L and Hu, Z. B. Palmatine, a protoberberine alkaloid, inhibits both Ca^{2+}- and cAMP-activated Cl^- secretion in isolated rat distal colon. British J. Pharma., 2008, 153, 1203-1213.

228. Wüthrich, K. Resonance assignments and structure determination in nucleic acids. In "NMR of Proteins and Nucleic Acids". Wiley Interscience, New York., 1986.

229. Xu, Z., Li, T. K., Kim, J.S., LaVoie, E.J., Breslauer, K. J., Liu, L. F and Pilch, D.S. DNA binding Groove binding-directed poisoning of Human DNA Topoisomerase I by Terbenzimidazoles. Biochem., 1998, 37, 3558-3566.

230. Yadav, R. C., Kumar, G. S., Bhadra, K., Giri, P., Sinha, R., Pal, S. and Maiti, M. ,Berberine, a strong polyriboadenylic acid binding plant alkaloid: spectroscopic, viscometric, and thermodynamic study. Bioorg. & Med. Chem., 2005, 13, 165-174.

231. Yamamoto, K., Takase, H., Abe, K., Saito, K. and Suzuki, A.,. Pharmacological studies on antidiarrheal effects of a preparation

containing berberine and gerainin herba. Nippon Yakurigaku Zasshi, 1993, 101 169–175.

232. Yu, S., Pang, X., Deng, Y., Liu, L., Liang, Y., Liu, X., Xie, L., Wang, G. and Wang, X. A sensitive and specific liquid chromatography mass spectrometry method for simultaneous determination of berberine, palmatine, coptisine, epiberberine and jatrorrhinzine from *Copitdis Rhizoma* in rat plasma. Int. J. Mass Spect., 2007, 268, 30-37.